Synthesis and self-assembly of polysaccharide-b-elastin-like polypeptide bioconjugates

Ye Xiao

université de BORDEAUX

THÈSE PRÉSENTÉE

POUR OBTENIR LE GRADE DE

DOCTEUR DE

L'UNIVERSITÉ DE BORDEAUX

ÉCOLE DOCTORALE DES SCIENCES CHIMIQUES

SPÉCIALITÉ POLYMÈRES

Par **Ye XIAO**

Synthesis and self-assembly of polysaccharide-*b*-elastin-like polypeptide bioconjugates

Sous la direction de : Sébastien LECOMMANDOUX
co-encadrant : Elisabeth GARANGER

Soutenue le 14 Octobre 2019

Membres du jury :

M. Jean-François GOHY	Professeur, UCLouvain, Belgium	Rapporteur
M. Christophe TRIBET	Directeur de recherche, CNRS, ENS, Paris	Rapporteur
M. Sami HALILA	Chargé de recherche, CNRS, Cermav, Grenoble	Examinateur
M. Olivier SANDRE	Directeur de recherche, CNRS, LCPO, Bordeaux	Examinateur
M. Sébastien LECOMMANDOUX	Professeur, Bordeaux INP, LCPO, Bordeaux	Directeur de thèse
Mme Elisabeth GARANGER	Chargée de recherche, CNRS, LCPO, Bordeaux	Co-encadrante

ACKNOWLEDGEMENTS

First of all, I would like to thank my jury for accepting to participate to the evaluation of my work. Thank you to Prof. Jean-François Gohy, Dr. Christophe Tribet, Dr. Sami Halila and Dr. Olivier Sandre. I am very honored to count you among the members of my jury.

I would like to sincerely thank my supervisor Prof. Sébastien Lecommandoux and Dr. Elisabeth Garanger for accepting me in this CSC project, encouraging me to evolve myself, and for your endless advices and help for my PhD. You are always patient to lead me figure out a solution or a orientation.

I am very grateful to Dr. Olivier Sandre and Dr.Leonardo Chiappisi for SANS experiments and discussions. I have learned a lot of physical chemistry from you. Special thank to Prof. Bertrand Garbay for your kind help in biology.

I would also like to express my gratitude to technicians, Amélie, Anne-Laure, Gilles, Katell and Cédric, Loic for all your kind support during my PhD. My special acknowledgement to Zoeisha and Shusheng for helping me adjust to scientific life abroad, teaching me many experimental skills, giving me endless help and advices.

I want to thank all the LCPO families. Thank you administrative staffs, Henri, Dominique, Claude, Corinne. Thank all the scientific staffs and friends from N0, N1and B8. Grand thanks to team 3, Colin, Christophe, Jean-François, Angela, N2-19 labmates, Coralie, Vusala, Perdo, Marie (great efforts to our paper and always encouraging me), Tim sniper, Hang, Tingting, Martin, Evangelis, Esra, Michele, Manon, and former colleagues Cony, Tuyen, Rosine, Gaelle, Louis, Gauvin, Ariane, Jani, Marie, Monica, Julien, Laura, Sophie, Guillaume, Yunjie, Mirjam, Lucy. I really enjoy being here with you and I appreciate every lovely days that we have been go through. I also want to thank all my schoolmates since 2015, Yibiao, Nan, Zhen, Jianqiao, Weiya, Shuo, Yuxin, Xiaozhou, Qian, Wenjing, without your support, I could not solve all the problems.

Finally, I want to thank my parents and Jing. Thank my parents for endless support for every choice I made and you are always there when I need you. Mom's dishes are the best cure in the world. I am so grateful and I feel I am so blessed to meet you Jing. My heart is so full and rock because of you. I know our story has not been easy in different time zone, but the challenges we have overcome with time made our heart closer, bonding stronger and love grow deeper. Thank you for supporting me in the way that only you could. You are important to me and I will always remember us this way.

Ye Machine

Résumé

Synthèse et auto-assemblage de bioconjugués polysaccharide-*b*-polypeptide d'élastine

Les nanoparticules polymères (NP) résultant de l'auto-assemblage de copolymères à blocs amphiphiles en tant que supports nanostructurés ont fait l'objet d'une grande attention, en particulier dans les domaines de l'administration de médicaments et du biomimétisme. Une large gamme de polymères synthétiques a été étudiée et sélectionnée comme éléments constitutifs en raison de leur biocompatibilité et de leur faible (cyto)toxicité. De plus, les polymères d'origine biologique ou d'inspiration biologique, comme les polysaccharides et les polypeptides, présentent l'avantage d'être biodégradables, biocompatibles et potentiellement biofactifs, ce qui les rend particulièrement adaptés à la fabrication de copolymères à blocs pour des applications biomédicales. En ce qui concerne les systèmes de délivrance de principes actifs, l'un des principaux défis consiste à améliorer l'accumulation des actifs au niveau du tissu cible. A cet égard, les copolymères à blocs bioactifs à base de polysaccharides capables de reconnaître et de se lier à des récepteurs spécifiques présentent des intérêts particulièrement prometteurs.

Récemment, les nanosystèmes polymères sensibles aux stimuli ont été largement explorés en raison de leur capacité à s'auto-assembler ou à se désassembler *in vivo* en réponse à des "stimuli internes", tels que le pH, l'environnement réducteur-oxydant et les enzymes, ou à des "stimuli externes", tels que la température, le rayonnement lumineux ou le champ magnétique. Parmi eux, les polypeptides recombinants de type élastine (ELPs) ont suscité beaucoup d'intérêt en tant que polymères protéiques thermosensibles. Les ELPs sont codés génétiquement et biosynthétisés par les techniques de l'ADN recombinant et d'ingénierie des protéines, ce qui permet un parfait contrôle de leur séquence macromoléculaire (*i.e.*, structure primaire, longueur de chaine, masse molaire). En solution aqueuse, les ELPs présentent un caractère thermo-répondant, avec une température critique basse de solubilité et une transition inverse (T_t) qui correspond à la température du point de trouble à une certaine concentration. En dessous de la T_t, les ELPs sont solubles dans l'eau, tandis qu'en chauffant la solution au-dessus de la T_t, les ELPs s'aggrègent, cette transition de phase étant totalement réversible. La T_t peut être modulée soit en jouant avec des paramètres moléculaires (*e.g.*, composition en acides aminés, longueur de chaîne) ou environnementaux (*e.g.*, concentration, cosolutés). Les modifications chimiques post-traductionnelles des ELPs peuvent également être exploitées pour moduler la T_t. Les post-modifications chimiosélectives des ELPs ont été d'un intérêt particulier ces dernières années. Cependant, seulement deux stratégies synthétiques pour modifier sélectivement les ELPs recombinants contenant de la méthionine ont été reportées. Celles-ci

sont réalisées dans des conditions acides et conduisent à des dérivés polycationiques (dérivés sulfoniums) avec donc des T*t*s très élevées.

Dans ce projet, nous visions donc à tirer profit des propriétés biologiques des polysaccharides et du caractère thermo-répondant des ELPs. Nous avons émis l'hypothèse que la combinaison de polysaccharides et d'ELPs sous forme de copolymères à blocs pourrait conduire à des matériaux aux propriétés uniques particulièrement intéressantes pour des applications biomédicales. Afin de mieux fonctionnaliser les chaînes latérales des ELPs, d'introduire diverses fonctionnalités et d'affiner leurs propriétés, une stratégie de synthèse basée sur la réactivité redox de la méthionine utilisant des réactifs à base d'oxaziridine a été développée et s'est avérée être un outil efficace pour la post-modification des ELPs dans des conditions physiologiques. Après une présentation du contexte bibliographique permettant de positionner mon étude (Chapitre 1), les principales recherches et découvertes réalisées sont résumées ci-dessous pour chaque chapitre.

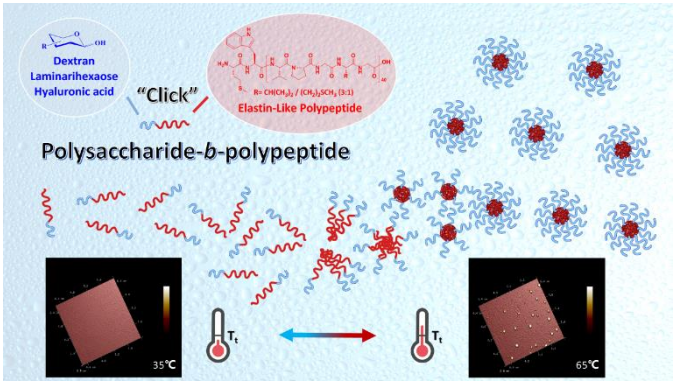

Chapitre 2. *Bioconjugués polysaccharide-b-polypeptide : vers des assemblages thermosensibles bioactifs.*

Les propriétés biologiques avantageuses des polysaccharides et la thermo-sensibilité des polypeptides de type élastine (ELPs) sont d'un grand intérêt pour la conception de copolymères à blocs amphiphiles pour des applications biomédicales. Le but de cette étude est de synthétiser et de caractériser une série de copolymères diblocs polysaccharide-*b*-ELP et d'étudier leur auto-assemblage en solution aqueuse sous forme de nanoparticules par chauffage au-dessus de la *T*t. Trois polysaccharides différents, àsavoir le dextran, le laminarihexaose et l'acide hyaluronique, ont été fonctionnalisés à leur extrémité réductrice avec un groupement azide, tandis que l'ELP a été modifié sur son extremité *N*-terminale avec un groupement alcyne. Trois bioconjugués polysaccharide-*b*-ELP ont alors pu être synthétisés par cycloaddition de Huigen, isolés et finenment caractérisés par Résonnance Magnétique Nucléaire (RMN), Chromatographie d'Exclusion Stérique (SEC), Spectroscopie Infra-Rouge à Transformée de Fourrier (FTIR), et Spectrométrie de Masse (MS). Leur température de transition à différentes concentrations ont été mesurées par Spectroscopie UltraViolet-Visible (UV-Vis) et leurs propriétés d'auto-assemblage ont ensuite été étudiées par diffusion dynamique de la lumière (DLS) et microscopie àforce atomique liquide à température contrôlée (AFM liquide). Les bioconjugués polysaccharide-*b*-ELP s'auto-assemblent en nano-objets de différentes tailles. Des objets stables de quelques centaines de nanomètres ont été mis en évidence, surtout lorsque le segment des polysaccharides hydrophiles était suffisamment grand. De plus, le processus d'auto-assemblage était entièrement réversible par le contrôle de la température, ce qui offre une perspective de bioconjugués polysaccharide-*b*-ELP pour des applications dans les biomatériaux, la libération de médicaments et la reconnaissance des récepteurs.

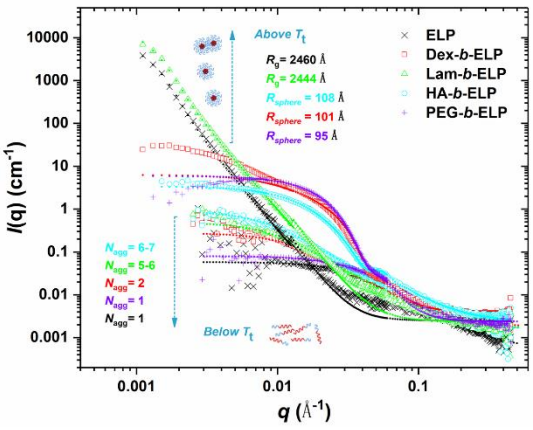

Chapitre 3. *Évolution structurelle des bioconjugués polysaccharide-b-ELP thermo-répondant : de l'unimère à la nanostructure auto-assemblée.*

La séquence précise des ELPs et leur caractère thermo-répondant permet d'envisager l'auto-assemblage spontané de copolymères à blocs à base d'ELPs sous forme de nanostructures induit par la température. Des travaux reportés dans la littérature ont montré que des copolymères à blocs d'ELPs, les fusions de protéines avec des segments ELPs ou encore des bioconjugués de type polymère synthétique-ELP peuvent s'auto-assembler sous forme de micelles sphériques, de micelles allongées ou de vésicules. Dans le cadre de l'étude de l'auto-assemblage des bioconjugués ELP-polymère, la flexibilité et la polyvalence des modifications synthétiques sur le squelette ELP permettent de moduler ses propriétés tout en conservant son caractère thermo-répondant. Dans le présent travail, l'impact du polysaccharide comme bloc hydrophile sur l'auto-assemblage des copolymères diblocs polysaccharide-*b*-ELP est exploré et discuté, en comparaison notamment avec un copolymère PEG-*b*-ELP porteur d'un segment poly(éthylène glycol) comme segment hydrophile. L'étude par diffusion dynamique de la lumière de ces bioconjugués a démontré un processus d'auto-assemblage et de désassemblage entièrement réversible en contrôlant la température au-dessus/en dessous de la température de transition (T_t) du dibloc. L'évolution structurale déclenchée thermiquement des chaines unimères vers des nanostructures auto-assemblés a été étudiée plus en détail par diffusion dynamique et statique de la lumière sous plusieurs angles (MALS) et par diffusion des neutrons aux petits angles (SANS). Sous la T_t, les chaînes polysaccharide-*b*-ELP se comportent comme unimères en solution avec peu d'agrégation. Au-dessus de la T_t, les segments ELPs des bioconjugués polysaccharide-*b*-ELP s'auto-assemblent par déshydratation et interaction hydrophobe, entraînant la formation de particules de taille sub-micrométrique. L'hydrophilie insuffisante du segment Laminarihexaose du bioconjugué Lam-*b*-ELP conduit en revanche à l'agrégation macroscopique et ne permet pas la stabilsation colloïdale de nanoparticules. Le mélange de plusieurs bionconjugués, en particulier Dex-*b*-ELP avec HA-*b*-ELP ou PEG-*b*-ELP, a également montré une évolution structurelle similaire. Des expériences supplémentaires sont toutefois nécessaires pour différencier la formation de micelles individuelles ou de micelles mixtes. Le mélange de HA/PEG-*b*-ELP a également indiqué un comportement plus complexe,

avec trois régimes de distribution des particules, qui pourrait être dû à l'interaction structurelle de ces deux bioconjugués. Encore une fois, d'autres expériences, utilisant des bioconjugués marqués par fluorescence ou des expériences en microscopie électronique, pourraient permettre de mieux comprendre ces phénomènes.

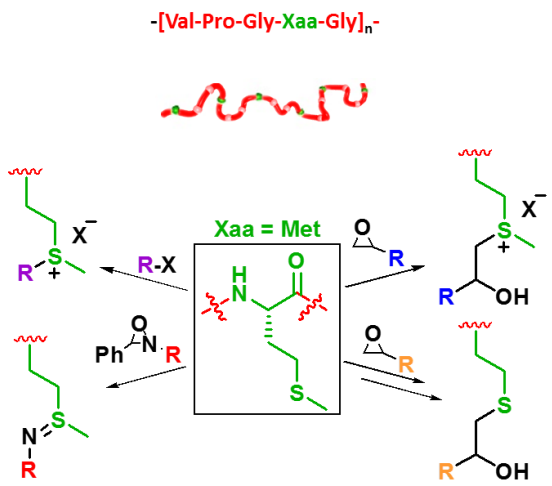

Chapitre 4. *Extension de la boîte à outils des modifications chimiosélectives des polypeptides de type élastine sur les résidus méthionine.*

Les modifications chimiosélectives des résidus méthionine dans les protéines ont fait l'objet d'une attention particulière ces dernières années. Les méthodes décrites précédemment pour modifier chimiosélectivement la chaîne latérale de la méthionine dans les polypeptides de type élastine (ELPs) impliquaient une addition nucléophile en utilisant des halogénures d'alkyle ou des époxydes conduisant à un groupement sulfonium avec une charge positive affectant fortement les propriétés physico-chimiques des ELPs, en particulier leur propriété de thermo-sensibilité. Nous avons exploré une nouvelle voie pour modifier chimiquement de façon sélective les ELPs contenant des résidus méthionine à l'aide d'une technique synthétique appelée ReACT (Redox-Activated Chemical Tagging) employant des réactifs à base de dérivés d'oxaziridine. Celle-ci vient élargir la variété des dérivés d'ELPs ainsi accessibles chimiquement par des liaisons sulfonium, thioéther ou sulfimide. Avec des réactifs disponibles dans le commerce, des temps de réaction raisonnables et une grande efficacité, la voie à base d'époxyde est très attrayante. La possibilité de récupérer une liaison thioéther, et donc un caractère thermo-répondant, par déméthylation du groupement sulfonium s'ajoute à la liste des avantages de cette voie synthétique. La stratégie ReACT s'est également avérée être une excellente alternative avec une grande efficacité, des temps de réaction courts et la possibilité de maintenir la thermo-sensiblité de l'ELP. Dans l'ensemble, cet ensemble de réactions ouvre toute une gamme de possibilités pour fonctionnaliser les ELPs avec une grande variété de molécules telles que des fragments bioactifs, des principes actifs ou des agents de contraste, pour la conception de nouveaux bioconjugués à base d'ELPs. D'une manière plus générale, les différentes stratégies étudiées dans ce travail peuvent facilement être étendues à d'autres polypeptides contenant des résidus méthionine.

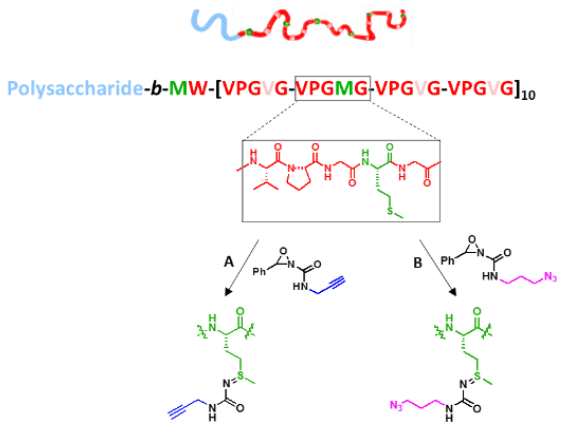

Chapitre 5. *Post-modifications chimiosélectives sur les résidus méthionine des bioconjugués polysaccharide-b-ELP.*

Le marquage chimique à base de dérivés d'oxaziridine (ReACT) constitue une stratégie intéressante pour la modification chimiosélective de la méthionine dans les protéines dans des conditions physiologiques. ReACT s'est révélé très sélectif à l'égard de la méthionine sur l'ensemble de la gamme des résidus canoniques d'acides aminés. Toutefois, la sélectivité et la compatibilité de ReACT en présence d'autres macromolécules naturelles telles que les polysaccharides sont encore inconnues. Nous avons exploré la possibilité d'appliquer ReACT sur nos bioconjugués polysaccharide-*b*-ELP décrits précédemment pour la modification sélective du bloc ELP aux résidus méthionine. Deux bioconjugués polysaccharide-*b*-ELP, Dex-*b*-ELP et HA-*b*-ELP, ont été fonctionnalisés de façon chimiosélective avec des groupes alcyne ou azide, en utilisant des réactifs appropriés à base d'oxaziridine, avec une conversion supérieure à 95% en 1 heure. Les dérivés polysaccharide-*b*-ELP bioconjugués résultants ont été caractérisés par RMN ^{1}H, COSY et HSQC, et l'effet des différentes modifications sur leur réponse thermique mesurée. En accord avec nos observations précédentes, la modification du Dex-*b*-ELP avec des dérivés de l'oxaziridine a considérablement augmenté leur T_t. Une petite molécule organique, à savoir la coumarine, a ensuite été greffée sur Dex-*b*-ELP^{ox}-N_3 par cycloaddition azide-alcyne catalysée au cuivre, ce qui a permis de détecter par fluorescence le bioconjugué ou les nanoparticules auto-assemblées obtenues, et permet d'envisager une réticulation interchaîne. Fait très important, la chimie à base d'oxaziridine sur Dex-*b*-ELP et HA-*b*-ELP n'a montré globalement aucune influence structurelle significative sur les blocs de dextran et d'acide hyaluronique, révélant la compatibilité de la méthode ReACT avec les bioconjugués contenant des polysaccharides.

TABLE OF CONTENTS

GENERAL INTRODUCTION

Polymeric nanoparticles (NPs) resulting from the self-assembly of amphiphilic block copolymers as nanostructured carriers have been receiving much attention especially in the fields of drug delivery and biomimetics. A broad range of synthetic polymers have been investigated and selected as building blocks due to their biocompatibility and low cytotoxicity. Additionally, biologically-derived or -inspired polymers, like polysaccharides and polypeptides, present the advantages of being biodegradable, biocompatible and potentially biofunctional, making them particularly suitable for the construction of block copolymers. Regarding the biomedical application of block copolymers as carriers, a key challenge is to enhance accumulation of the active components at the biological target. In this respect, bioactive polysaccharide-based block copolymers able to recognize and bind to specific receptors demonstrate particularly promising interests for potential biomedical applications.

Recently, stimuli-responsive polymer nanosystems have been extensively explored due to their ability to self-assemble or disassemble *in vivo* as a response to "internal stimuli", such as pH, reductive-oxidative environment, and enzymes, or "external stimuli", such as temperature, light irradiation and magnetic field. Among them, recombinant elastin-like polypeptides (ELPs) have gained significant attention as stimuli-responsive protein-like polymers. ELPs are genetically encoded and recombinantly biosynthesized, which offers an exquisite level of precision and tunability with regards to their molecular mass, sequence and monodispersity. In aqueous solution, ELPs display a thermoresponsive character, with an inverse transition temperature (T_t) that actually corresponds to the cloud point temperature at a certain concentration. Below the T_t, ELPs are water soluble, while upon heating the solution temperature above the T_t, ELPs aggregate into insoluble coacervates, this phase transition being fully reversible. The T_t can be highly tunable either by playing with molecular (*e.g.*, amino acid composition, chain length) or environmental (e.g., concentration, cosolutes) parameters. Post-translational chemical modifications of specific ELPs can also be exploited to modulate the *T*t. Chemoselective post-modifications in ELPs have been of particular interest in recent years. However only two synthetic strategies have been reported to selectively modify methionine-containing recombinant ELPs, both under acidic conditions and leading to polycationic derivatives with therefore high Tts. Selective methionine modification of ELPs under physiological conditions has been barely reported.

In this project, we were thus aiming at taking advantage of the biological properties of both polysaccharides and ELPs together with the precise stimuli-responsive character of ELPs. We hypothesized that the combination of polysaccharides and ELPs into block copolymers would lead to materials with unique properties especially interesting for biomedical applications. In order to further functionalize the ELP backbones and introduce various functionalities and tune their properties, a powerful strategy based on redox reactivity of methionine using oxaziridine-based reagents was developed and demonstrated to be a viable tool for highly efficient post-modifications of ELPs under physiological conditions.

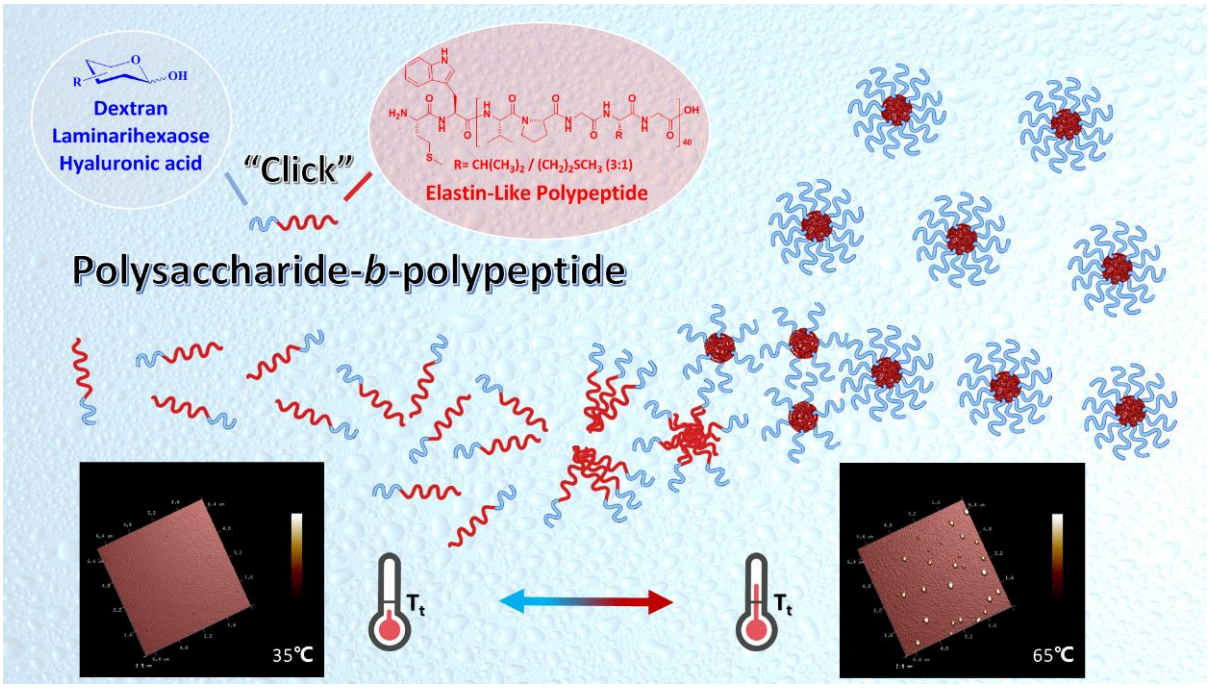

Figure 1. *Polysaccharide-b-polypeptide bioconjugates: towards bioactive thermo-responsive self-assemblies.*

Herein, the first chapter of this manuscript will be dedicated to a "state of art" bibliographic review of the field. In the second chapter, we will present a modular "click chemistry"-based approach to combine bioactive polysaccharides with a stimuli-responsive elastin-like polypeptide (ELP) into well-defined block copolymers (Figure 1). These bioconjugates were then fully characterized and their transition temperature behavior was studied through turbidity measurements by ultraviolet–visible (UV-Vis) spectroscopy and their temperature-induced self-assembly properties were subsequently investigated by temperature-varying dynamic light scattering and temperature-controlled liquid atomic force microscopy.

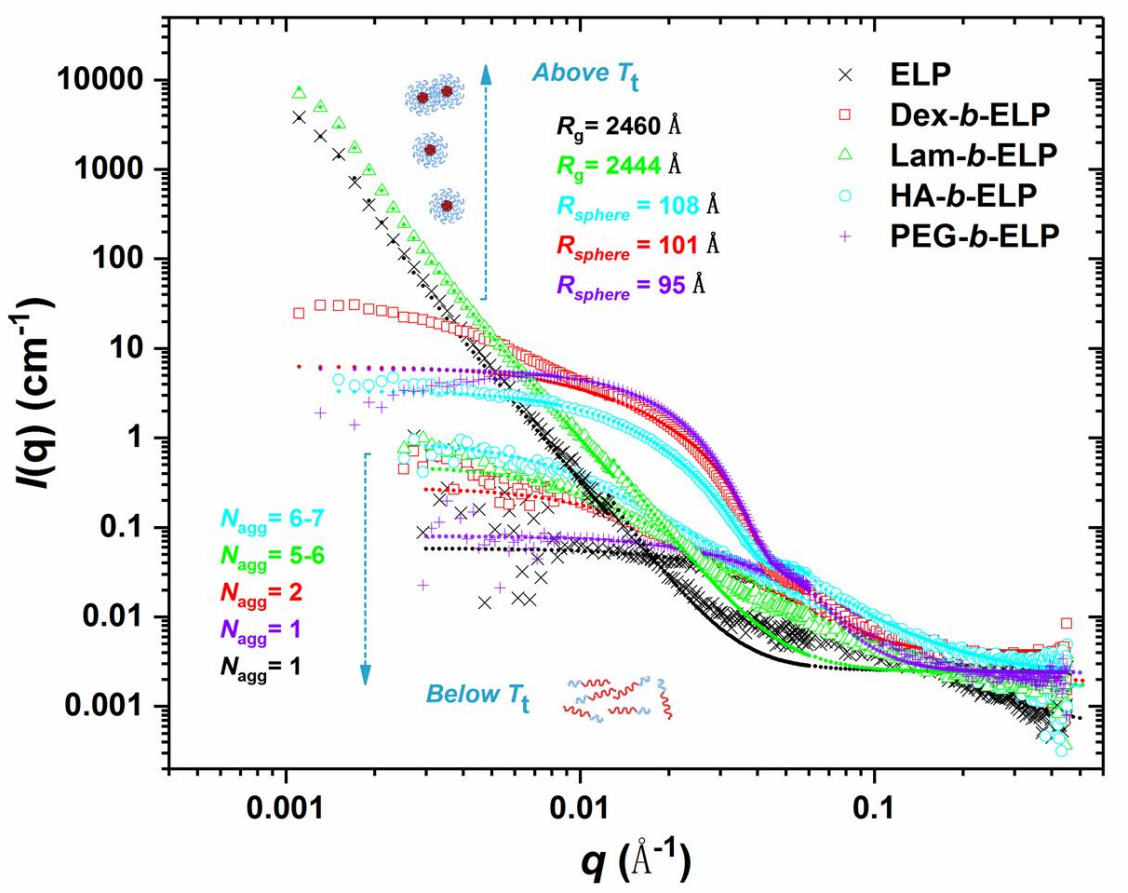

Figure 2. *Structural evolution of thermo-sensitive polysaccharide-b-ELP bioconjugates: from unimer to self-assembled nanostructure.*

Having a great interest in the temperature-induced self-assembly behavior of these polysaccharide-*b*-ELP bioconjugates, we will then in the third chapter, focus on exploring more details of their self-assembly behaviors by extensive dynamic and static light scattering as well as small angle neutron scattering (Figure 2). The stability, reversibility and thermodynamic equilibrium of the temperature-induced assemblies were investigated as well as the influence of different parameters in the self-assembly process, namely heating speed, concentration, hydrophilicity of the polysaccharide. Additionally physical mixture of polysaccharides, ELPs and diblock bioconjugates were also studied and will be discussed.

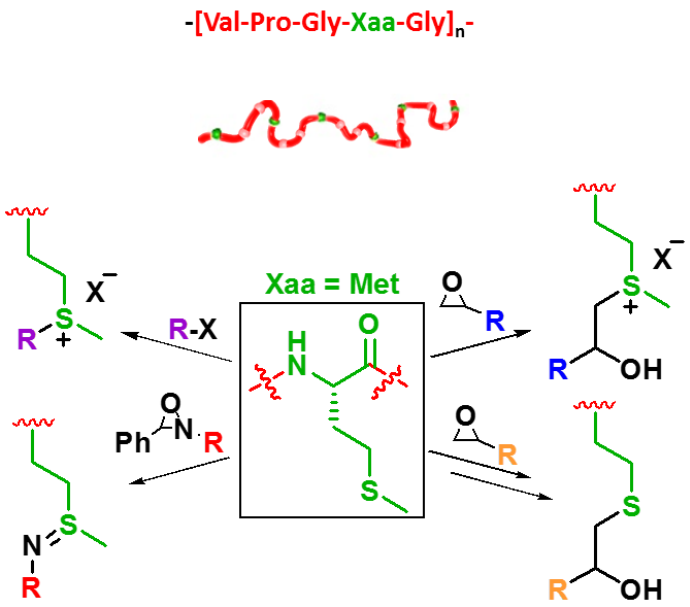

Figure 3. *Expanding the toolbox of chemoselective modifications of elastin-like polypeptides at methionine residues.*

In the fourth chapter, we will describe an innovative strategy to post-modify ELP-[V_3M_1-40] and therefore expand the toolbox of chemoselective modifications of ELP at methionine residues with recently reported redox alkylation through oxaziridine-based reagents. With four strategies in hand, we enlarged the scope of action to tune the thermoresponsive properties of elastin-like polymers giving access to either sulfonium, thioether or sulfimide derivatives. (Figure 3)

Taking advantage of the high selectivity and mild reaction conditions of oxaziridine-based modification, in the fifth chapter, we will explore the possibilities of applying oxaziridine chemistry on polysaccharide-*b*-ELP bioconjugates for further functionalization of the bioconjugates at methionine residues. Alkyne or azido groups were introduced allowing subsequent orthogonal biofunctionalization of polysaccharide-*b*-ELP bioconjugates with small molecules such as fluorescent dyes or inter-chain cross-linking. (Figure 4)

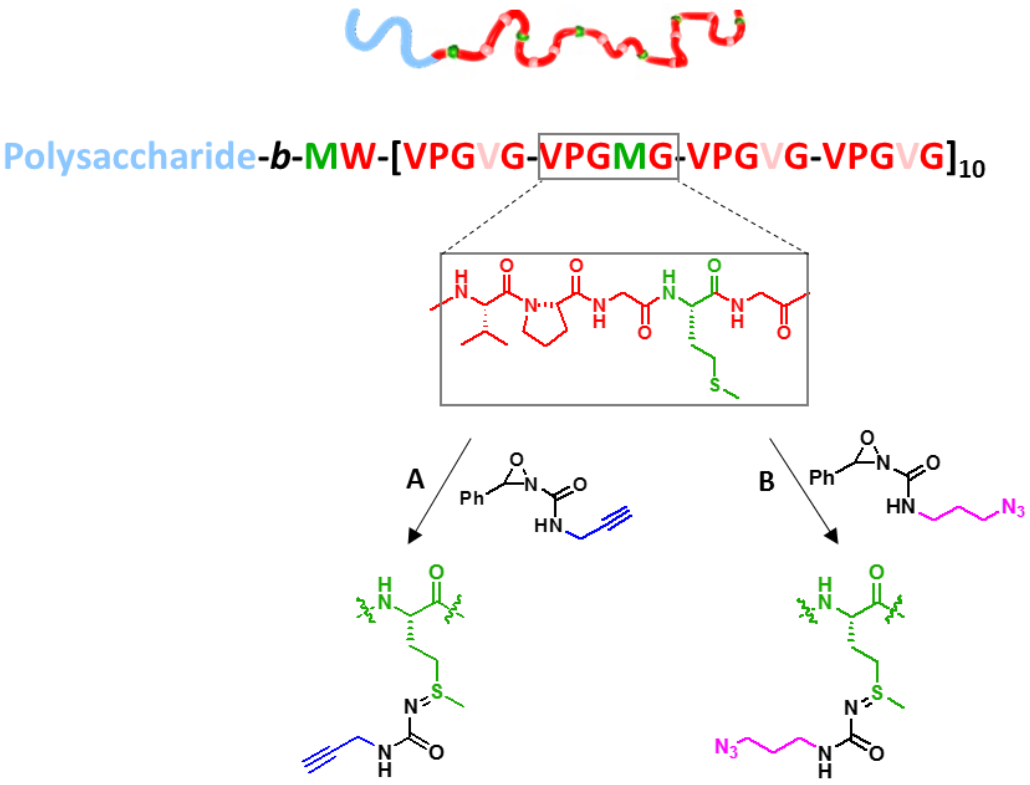

Figure 4. *Chemoselective post-modifications at methionine in polysaccharide-b-ELP bioconjugates.*

LIST OF ABBREVIATIONS

Ac-Dex	Acetal-modified dextran
AcOH	Acetic acid
AcONa	Sodium acetate
AFM	Atomic force microscopy
APDC	Ammonium pyrrolidinedithiocarbamate
BLG	γ-benzyl-L-glutamate
CD_{44}	Cluster determinant 44
CMT	Critical micelle temperature
COSY	Homonuclear correlation spectroscopy
CuAAC	Copper(I)-catalyzed azide-alkyne cycloaddition
$CuSO_4$	Copper(II) sulfate pentahydrate
DCR	Derived count rate
DDS	Drug delivery systems
DET	Diethylenetriamine
Dex	Dextran
DI	Deionized
DIPEA	Diisopropylethylamine
DLS	Dynamic ligt scattering
DMAP	4-Dimethylaminopyridine
DMF	Dimethylformamide
DMSO	Dimethyl sulfoxide
DOC	Docetaxel
Dox	Doxorubicin
DPA	3,3′-Dithiodipropionic acid
EAT	Ehrlich Ascites Tumor
ECM	Extracellular matrix
EDTA	Ethylenediaminetetraacetic acid
EPR	Enhanced permeation and retention effect
EtOAc	Ethyl acetate
FDA	U.S. Food and Drug Administration
FTIR	Fourier transform infrared spectroscopy
GlcNAc	*N*-acetylglucosamine

GlcUA	Glucuronic acid
GLUT	Glucose transporter proteins
GSH	Glutathione
HA	Hyaluronic acid
HARE	HA receptor for endocytosis
HCl	Hydrochloric acid
HFIP	hexafluoroisopropanol
HOBT	Hydroxybenzotriazole
HPMA	*N*-(2-hydroxypropyl) methacrylamide
HSQC	Heteronuclear single quantum coherence spectroscopy
IARC	International Agency for Research on Cancer
ITC	Inverse transition cycling
ITC	Inverse transition cycling
Lam	Laminarihexaose
LCST	Lower critical solution temperature
LRP	Living radical polymerization
LYVE-1	Lymphatic vessel endothelial hyaluronan receptor-1
MALDI	Matrix-assisted laser desorption/ionization
MALS	Muti-angel light scattering
MDR	Multidrug resistance effect
$MgSO_4$	Anhydrous magnesium sulfate
MWCO	Molecular weight cut off
NaAsc	Sodium ascorbate
$NaBH_3CN$	Sodium cyanoborohydride
$NaHCO_3$	Sodium bicarbonate
NHS	N-hydroxysuccinimide
NP	nanoparticle
NTP	*N*-transfer pathway
OTP	*O*-transfer pathway
PAsp	poly(L-aspartic acid)
PBLG	Poly(γ-benzyl-L-glutamate)
PCL	Poly(ε-caprolactone)
PDEAAM	poly(*N*,*N*-diethylacrylamide)

PDI	Polydispersity index
PEG	Poly(ethylene glycol)
PGlu	Poly(L-glutamic acid)
PLA	Polylactic acid
PLGA	Poly(lactic-co-glycolic acid)
PLL	poly(L-lysine)
PMDETA	*N,N,N′,N″,N″*- pentamethyldiethylenetriamine
PNIPAM	poly(N-isopropylacrylamide)
PPDSM	Poly(pyridyl disulfide methacrylate
PTX	paclitaxel
RAFT	Reversible addition fragmentation chain transfer polymerization
ReACT	Redox-activated chemical tagging
RHAMM	Hyaluronate-mediated motility receptor
ROP	Ring-opening polymerization
SCM	Shell crosslinked micelle
SEC	Size exclusion chromatography
SLS	Static light scattering
TBTA	Tris(benzyltriazolylmethyl)amine
TEA	Trimethylamine
TEM	Transmission electron microscopy
TOF	Time of flight
T_t	Transition temperature
UV-Vis	Ultraviolet–visible

LIST OF NATURAL AMINO ACIDS

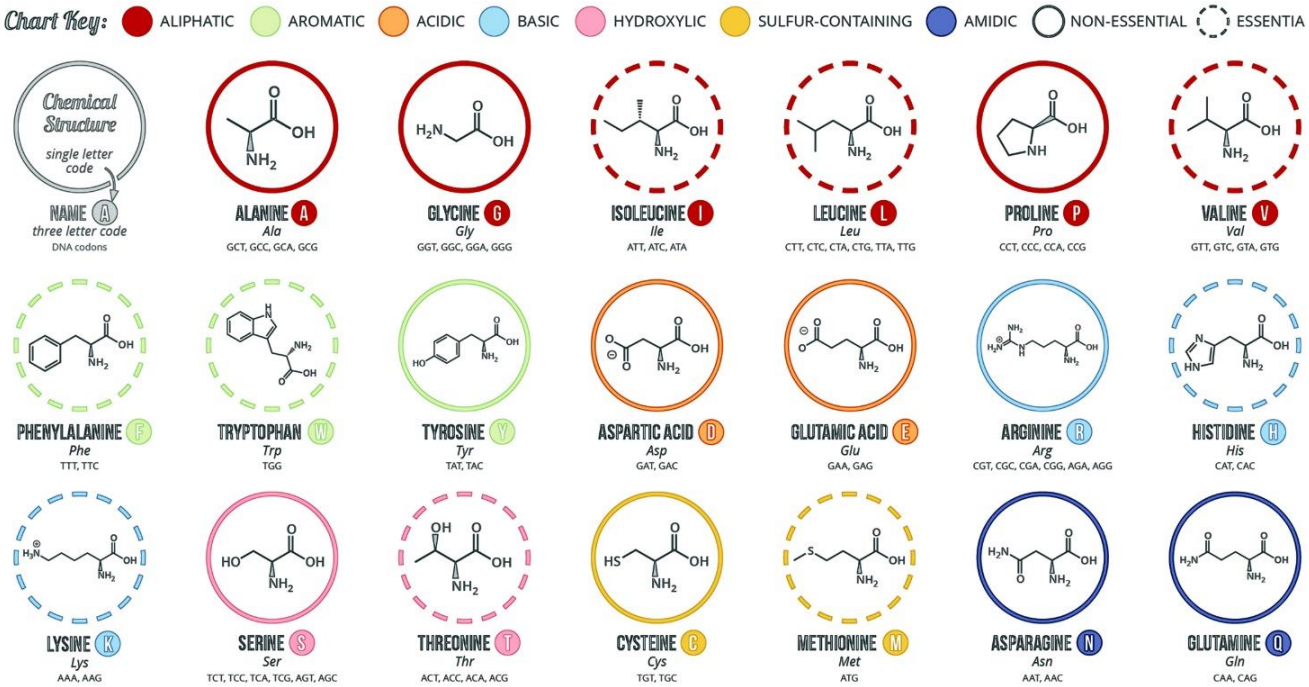

*Reproduced from: A Brief Guide to the Twenty Common Amino Acids. Compound Interest, September 16, **2014**.*

CHAPTER 1

BIBLIOGRAPHIC REVIEW

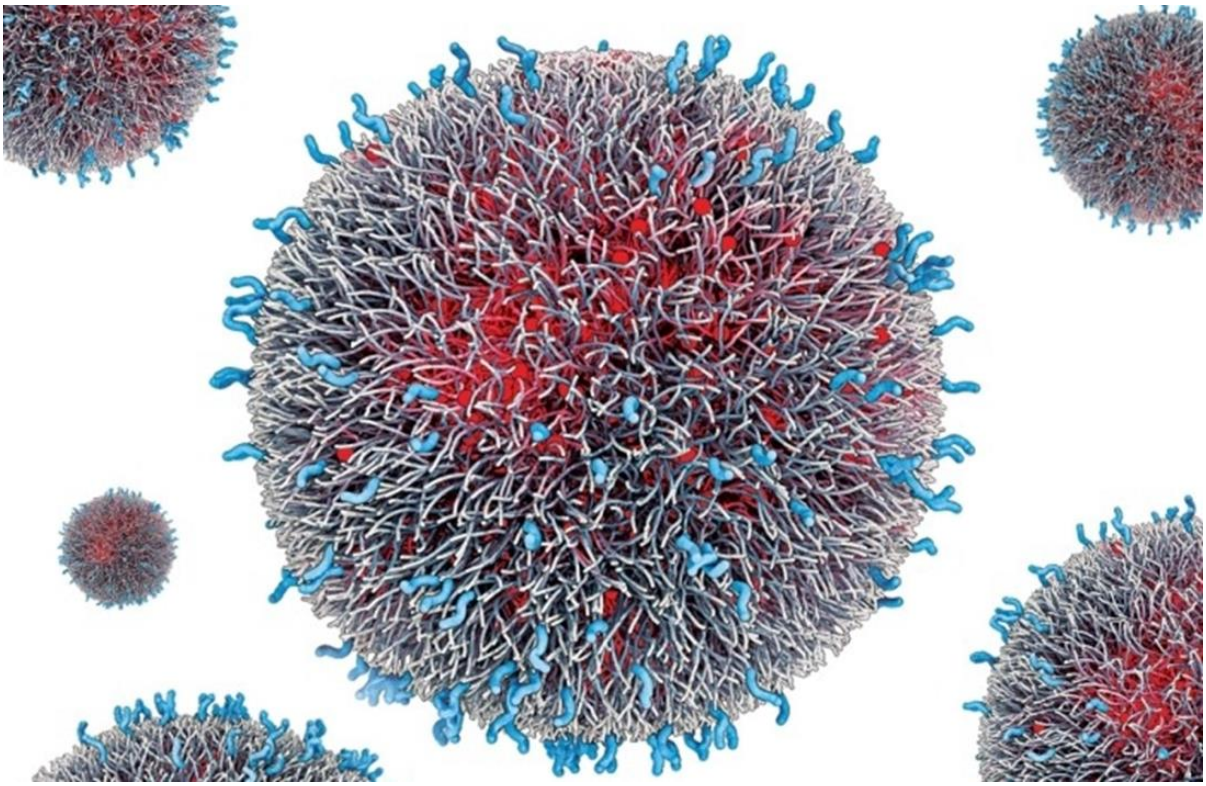

1. POLYMERIC NANOCARRIERS AS AN EMERGING PLATFORM FOR CANCER THERAPY

1.1 Introduction

Owing to the significant advantages over free drugs systemically administered, polymer-based nanocarriers as drug delivery systems (DDS) are emerging as ideal platforms for cancer therapy.[1–7] Not only that these nanocarriers can enhance the solubility, biocompatibility, bioavailability, and prolong the circulation time of the drugs, furthermore they can be designed in such a "smart" manner that they selectively release the drugs at the desired site of action.[8–11] Although the first attempt to load drugs onto polymers was reported in 1955 by Jatzkewitz,[12] the field of polymer therapeutics was promoted by the pioneering works of Ringsdorf,[13] Kopecek[14] and Duncan[1,4,6], among others, in the 1970s (Figure 1). After considerable efforts from scientists of various disciplines (polymer scientists, biologists, pharmoclogists, clinicians, among many others) for decades, the field of polymer therapeutics has experienced rapid growth. Advances in polymer chemistry and biomaterials science in particular have enlarged the scope of polymer classes, architectures and functionalities.

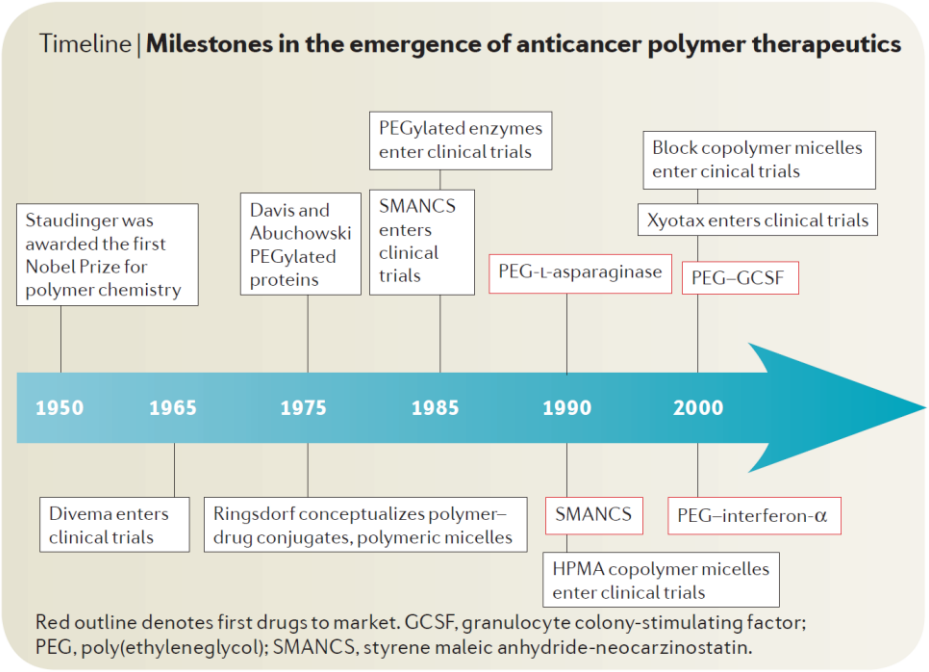

Figure 1. *Milestones in the emergence of anticancer polymer therapeutics. DIVEMA: 1:2 alternating cyclocopolymer of divinyl ether and maleic anhydride; XYOTAX: paclitaxel poliglumex (macromolecular conjugate of paclitaxel bound to poly-L-glutamic acid).*[1]

Block copolymers generally comprise two or more chemically distinct polymer chains linked together by covalent bonds. Owing to their amphiphilic character, block copolymers can self-assemble into particles of various morphologies and sizes, providing easy adjustability of their stability, permeability, functionality and surface chemistry.[15–19] Numerous polymers have been selected as building blocks due to their biocompatibility and low cytotoxicity, such as poly(ethylene glycol)[20–26], poly(L-glutamic acid)[27,28], poly(2-hydroxyethyl methacrylate),[29,30] polylactide,[31–33] polycaprolactone,[34,35] and poly(trimethylene carbonate),[36–38] and have been approved for biomedical applications by regulatory agencies. In the following, we will give a brief overview on the rational design of polymer-based nanocarriers for cancer therapy, with a main focus on FDA-approved polymers and polymer-based therapeutics, and introduce polymer classification, block copolymers and stimuli-responsive polymeric systems.

1.2 Rational design of nanocarriers for cancer therapy

1.2.1 Global statistics and therapeutic approaches for cancer

Nowadays, cancer remains one of the world's most devastating diseases. According to a report of the "Global Cancer Statistics 2018" released by the International Agency for Research on Cancer (IARC),[39] 9.6 million people died of cancer in 2018. Meanwhile the number of people around the world who have cancer is growing rapidly, with 18.1 million new cases in 2018. As mortality continues to rise, two approaches are bringing hope for improved therapies. On one hand, genomics and proteomics researches are identifying new tumor-specific signaling pathways and molecular targets as well as better understanding of tumor microenvironment.[40–42] On the other hand, innovative nanocarriers are being developed to deliver therapeutics more specifically to tumor tissues and away from sites of toxicity, and to maintain cure at a therapeutic concentration over long periods of time (Figure 2).[40,43]

1.2.2 Essential components for rational design of polymeric nanocarriers

Nevertheless, nanocarriers encounter many barriers en route to their target site, such as membrane barriers and non-specific uptake.[44–47] Nanocarriers with diameters 10-200 nm can extravasate into the tumor tissues *via* the leaky vessels by the enhanced permeability and retention (EPR) effect, a characteristic feature of tumor biology that allow nanocarriers to accumulate in some tumors by passive targeting.[48–50]

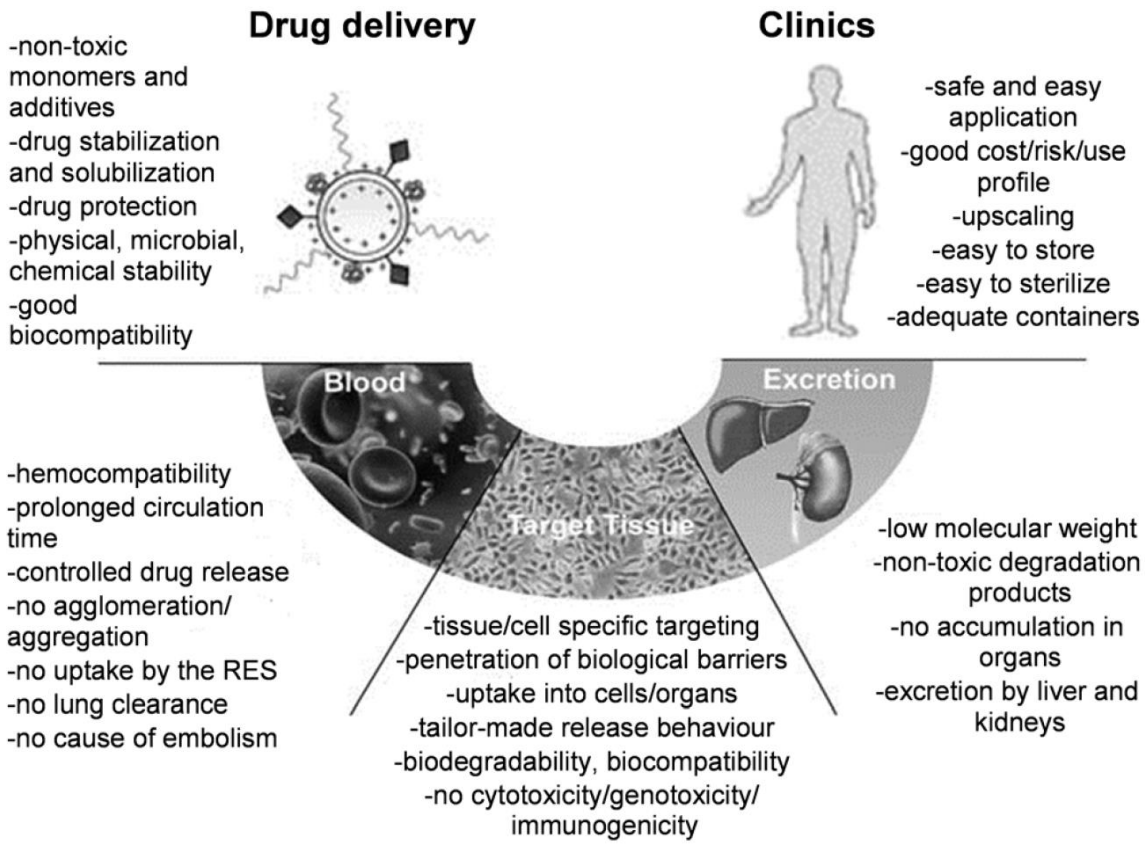

Figure 2. *Essential components for design of polymeric drug delivery systems. "RES" is the abbreviation of "Reticuloendothelial System".*[43]

Although passive targeting approaches form the basis of clinical therapy, they however suffer from several limitations such as high heterogeneity among patients in terms of EPR effect, lack of control and tumor specificity, as well as multiple-drug resistance mechanims.[49] One way to overcome these limitations is to attach targeting agents such as saccharides that bind to specific receptors on the cell surface to the surface or architecture of the nanocarrier by a variety of conjugation chemistry.[51,52] Nanocarriers can then recognize and bind to target cells through ligand–receptor interactions, and bound carriers are internalized before the drug is released inside the cell (Figure 3).[7,53] In general, when using a targeting agent to deliver nanocarriers to cancer cells, it is imperative that the targeting agent binds with high selectivity to markers or receptors that are mostly expressed on the cell surface. Thus for rapid and effective transition of polymeric therapeutics to clinical trials, it is essential to combine the fundamental understanding of tumor microenvironment with the rational design of polymeric nanocarriers.[47] The essential requirements for design of polymeric drug delivery systems are summarized by Fischer and his co-workers in Figure 2.[43] This emphasizes the necessariness of the

interdisciplinary work of polymer chemists with physicists, biologists as well as clinicians in the early stage of development of polymeric nanocarriers.

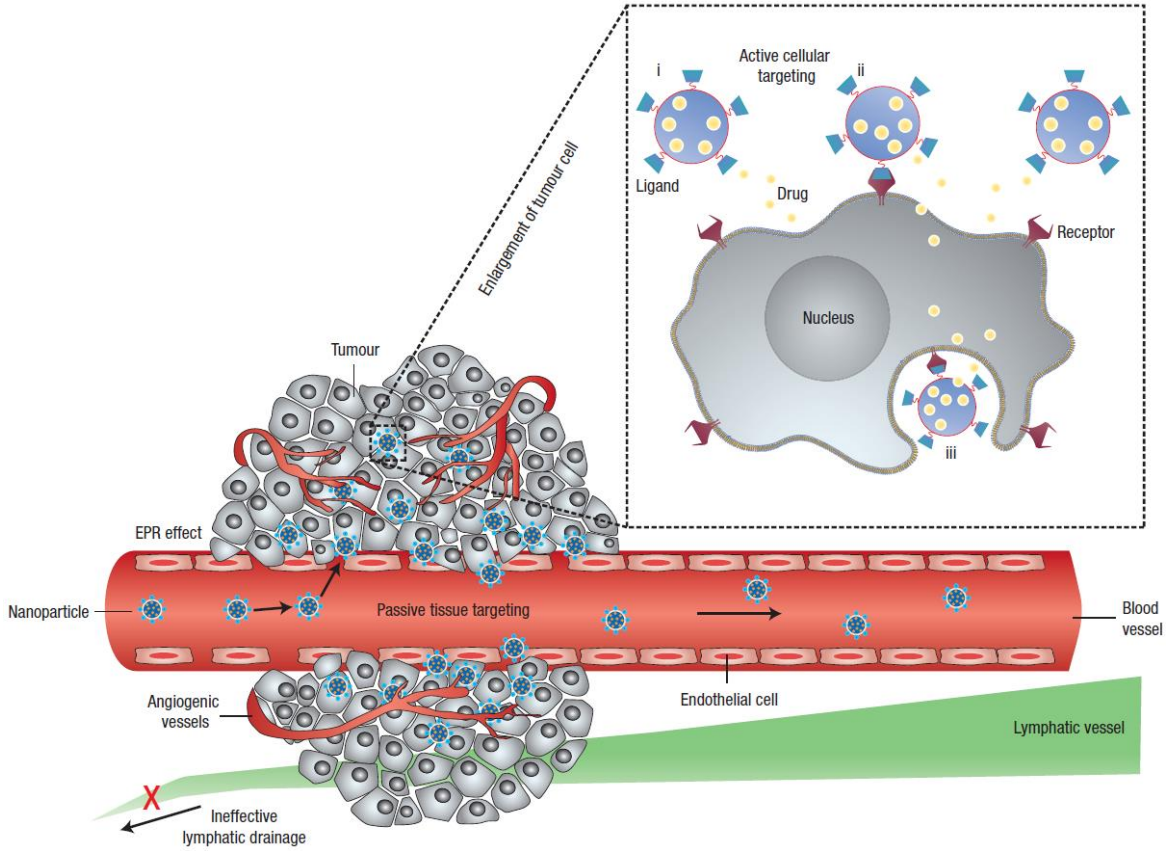

Figure 3. *Schematic representation of different mechanisms by which nanocarriers can deliver drugs to tumours. Polymeric nanoparticles are shown as representative nanocarriers (circles). Passive tissue targeting is achieved by extravasation of nanoparticles through increased permeability of the tumour vasculature and ineffective lymphatic drainage (EPR effect). Active cellular targeting can be achieved by functionalizing the surface of nanoparticles with ligands that promote cell-specific recognition and binding. The nanoparticles can (i) release their contents in close proximity to the target cells; (ii) attach to the membrane of the cell and act as an extracellular sustained-release drug depot; or (iii) internalize into the cell.*[53]

1.2.3 Polymeric nanocarrier formulations

After considerable effort by polymer scientists for decades, there is an increasing number of nanocarrier formulations progress from the laboratory to routine clinical use as nanocarriers (Figure 4). The emerging family of nanocarriers including polymer-based carriers such as polymer-drug conjugates,[54–57] block copolymer micelles,[16,58] polymersome[11,59–63] and polymeric nanoparticles,[18,64–67] lipid-based carriers such as liposomes,[68,69] and dendrimers,[70,71] carbon nanotubes,[72–74] inorganic particle based nanoshells and nanocages[75–77] (Figure 4). These nanocarriers have been explored for a variety of applications for cancer therapy, ranging from

prediagnosis, drug delivery to tumor imaging and detection, representing an emerging platform for cancer therapy.

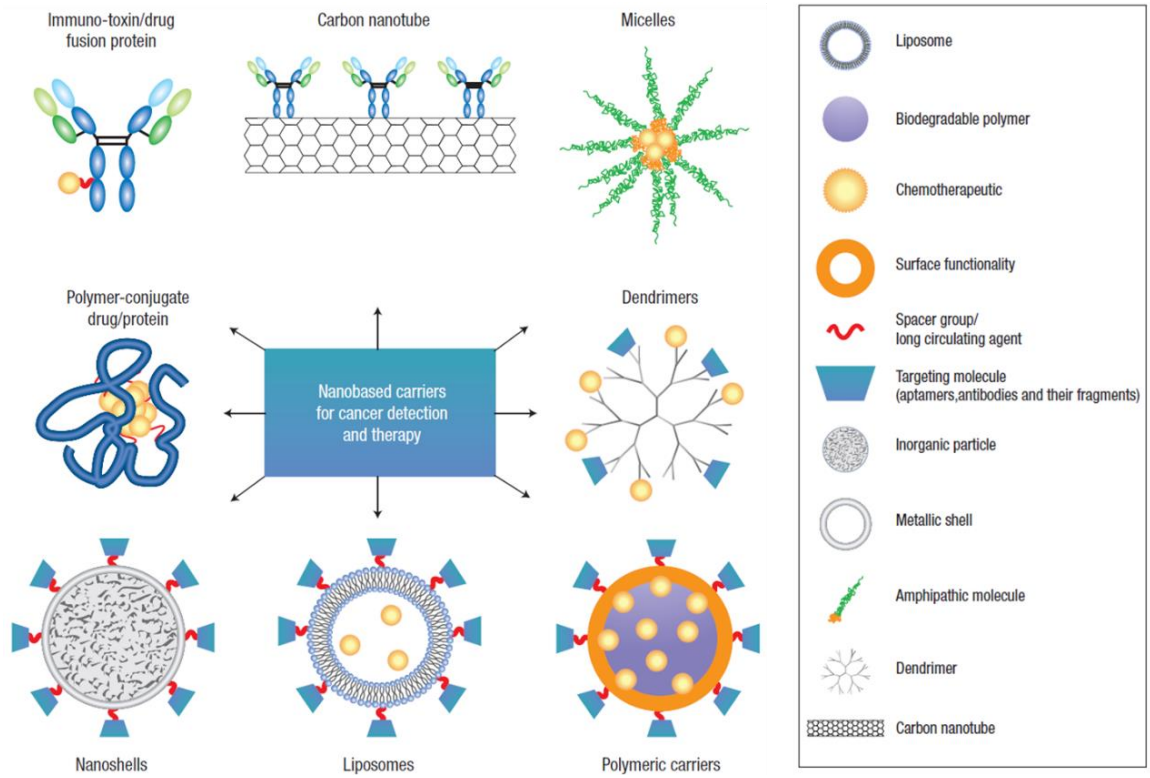

Figure 4. *Schematic representation of nanocarriers for cancer therapy. A whole range of delivery agents are possible but the main components typically include a nanocarrier, a cargo (such as the desired chemotherapeutic drugs) and a targeting moiety conjugated to the nanocarrier.*[53]

1.3 FDA-approved polymeric therapeutics

1.3.1 FDA regulatory process of nanomedicine

The regulatory and approval process for nanomedicines, as well as other drugs or devices for humans are regulated by the Food and Drug Administration (FDA) in USA. In terms of every new FDA approved drug, the entire process cost about 10-15 years including the discovery of the drug, the pre-clinical phase involves in vitro and in vivo studies to demonstrate efficacy, safety, toxicity profile, and to identify appropriate dose ranges, and finally 5 clinical trial phases 0- IV to assess if treatments are safe for and work in human.

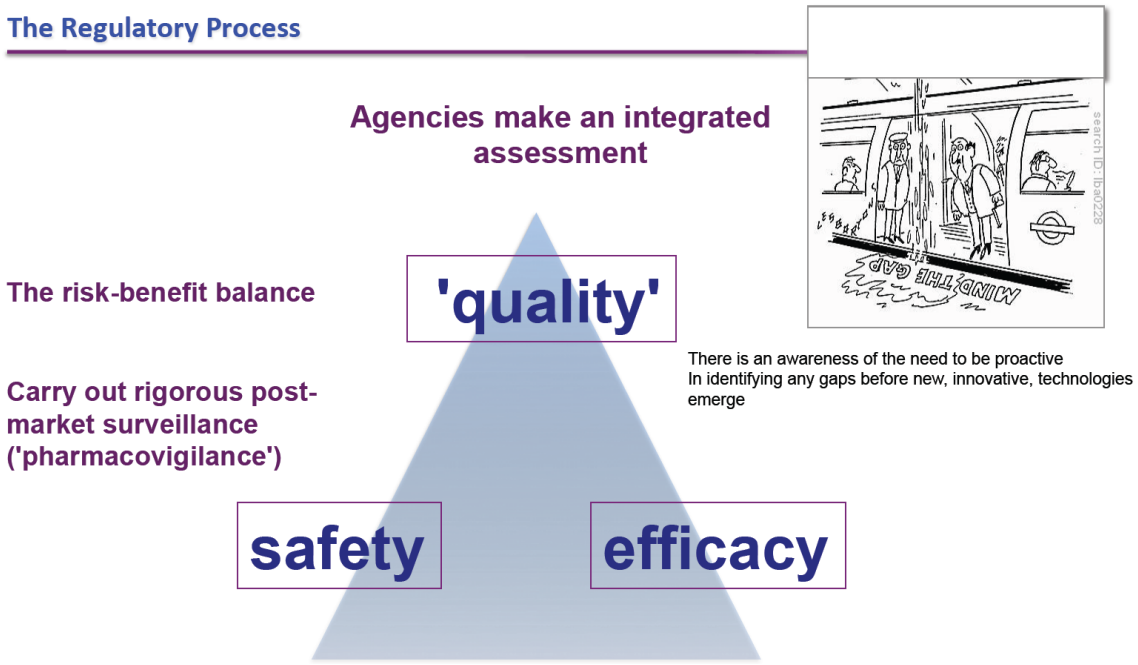

Figure 5. *The regulatory process of polymeric therapeutics. Agencies make an integrated assessment of the tisk-benefit balance.*[78]

Nanomedicine, as an emerging interdisciplinary field that combines nanotechnology with pharmaceutical chemistry and biomedical science, shows plenty differences in comparison to traditional drugs.[2,79,80] The behavior of nanomedicine under biological conditions (at the level of molecules, proteins, cells, tissues, etc.) is highly dependent on the physicochemical properties of the nanomedicine, such as particle morphology, size and surface chemistry.[81,82] Thus, there is a need to have a comprehensive understanding of the physicochemical parameters of the polymeric therapeutics, and the reproducibility and scalability of the manufacturing process. In the past several years, the "quality" of nanomedicine characterization is also the important part of several guidance documents issued by the FDA, hence it is a particularly key aspect in terms of drug research and transition. Therefore, the efficacy, safety, and physicochemical "quality" of polymeric therapeutic are compiled into an investigational new drug application for FDA consideration (Figure 5).

1.3.2 Trends in the development of nanomedicines

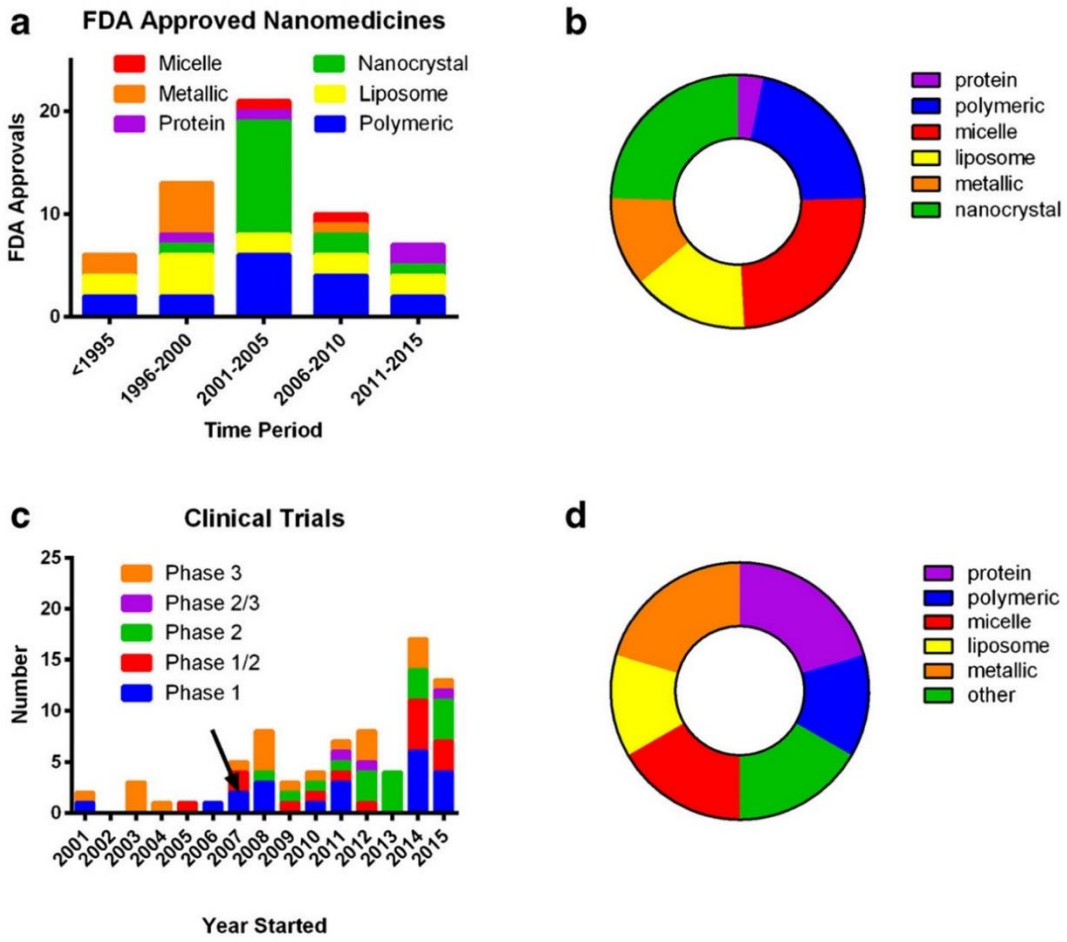

Figure 6. *Trends in the development of nanomedicines. (a) FDA approved nanomedicines stratified by category; (b) FDA-approved nanomedicines stratified by category overall; (c) clinical trials identified in clinicaltrials.gov from 2001 to 2015 with arrow indicating approximate start date of US law (FDAAA 801) requiring reporting to FDA database; (d) nanomedicines under clinical trial investigation stratified by category overall.*[66]

Based on the data extracted from the clinicaltrials.gov website in February 2016 using search terms centered on "nano", Simon and his co-workers provide a "snapshot" of the nanomedicines that have been approved by FDA.[66] As reproduced in Figure 6, approvals appeared to peak during 2001-2005 time period meanwhile the number of nanomedicines which have been advanced to clinical trials has increased steadily since 2007 and 2014-2015 are the best years. In terms of the category of nanomedicine, there are significantly more metallic and protein-based particles being submit to clinical trial in contrast to what has previously been approved (Figure 6). Although the overall proportion of polymeric particles has not increased, polymers are still necessarily essential component since most of the micelle and liposome systems being developed incorporate polymers as building blocks, while the protein-based systems may also have a polymer composition.

1.3.3 Polymeric therapeutics in the market and clinical development

With the rapid development of polymer science, there are increasing types and structures of polymer-based therapeutics have been approved by FDA. Typical examples of polymeric therapeutics in the market and clinical development are listed in Table 1, including polymeric drugs, polymer sequenstrants, polymer-drug/protein conjugates, PEGylated-protein/aptamer, block copolymer micelles and self-assembled polymer conjugate nanoparticles.[80] As the most well established polymer, poly (ethylene glycol) (PEG) are extremely popular and employed in various cases such as polymer-drug conjugates, PEGylated proteins or aptamers, and block copolymers.[23,25,26,83] Other synthetic polymers, for example *N*-(2-hydroxypropyl) methacrylamide (HPMA),[14] poly (glycolic acid),[84] poly(lactide-co-glycolide) (PLGA),[24] poly(lactic acid) (PLA)[32,33] and polycaprolactone (PCL),[34,35] have also been approved for clinical utilization from decades. Additionally, some biologically derived or inspired polymers, like polysaccharide (hyaluronic acid)[85–94] and polypeptide (polyglutamic acid)[84,95,96], are also approved by FDA for biomedical researches since they are naturally biodegradable, biocompatible and are potentially biofunctional.

Sub class	Examples	Composition	Status
Polymeric drugs	Copaxone	Glu, Ala, Tyr copolymer	Market
	Vivagel	Lysine-based dendrimer	Phase III
	Hyaluronic acid	Hyalgal, Synvisc	Market
Polymeric sequestrants	Renagel	Phosphate binding polymer cholesterol binding	Market
	Welchol		Market
Polymer–protein conjugates	Zinostatin Stimaler	Styrene maleic anhydride-neocarzinostatin, (SMANCS)	Market (Japan)
	SuliXen	Polysialylated insulin	Phase I/II
PEGylated proteins	Cimzia	PEG-anti-TNF Fab	Market
	Mircera	PEG-EPO	Market
	Peg-intron	PEG-Interferon alpha 2b	Market
	Pegasys	PEG-Interferon alpha 2a	Market
	Neulasta	PEG-hrGCSF	Market
	Uricase-PEG 20	PEG-uricase	Market
	ADI-PEG 20	PEG-arginine deaminase	Phase II
PEGylated-aptamer	Macugen	PEG-aptamer (apatanib)	Market
	E10030	PEG-anti-PDGF aptamer	Phase II
	ARC1779	PEG-anti-platelet-binding function of von Willebrand Factor	Phase II
Polymer–drug conjugate	CT-2103; Xyotax; Opaxio	Poly-glutamic acid (PGA)-paclitaxel	Phase II/III
	Prolindac	HPMA–copolymer–DACH platinate	Phase II
	PEG-SN38	Multiarm PEG-camptothecin derivative	Phase II
	XMT-1001	Polyacetal-camptothecin conjugate	Phase I
	NKTR-118	PEG-naloxone	Phase III
Block copolymer micelles	SP1049C	Doxorubicin block copolymer micelle	Phase I/II
	NK 105	Paclitaxel block copolymer micelle	Phase II
	NK-6004	Cisplatin block copolymer micelle	Phase II
Self assembled polymer conjugate nanoparticles	IT-101	Polymer conjugated-cyclodextrin nanoparticle-camptothecin	Phase II
	CALAA 01	Polymer-conjugated cyclodextrin-nanoparticle-siRNA	Phase I

Table 1. *Examples of polymeric therapeutics in the market and clinical development.*[4]

1.4 Block copolymers: construction, preparation and self-assembly

1.4.1 Rational design of block copolymer

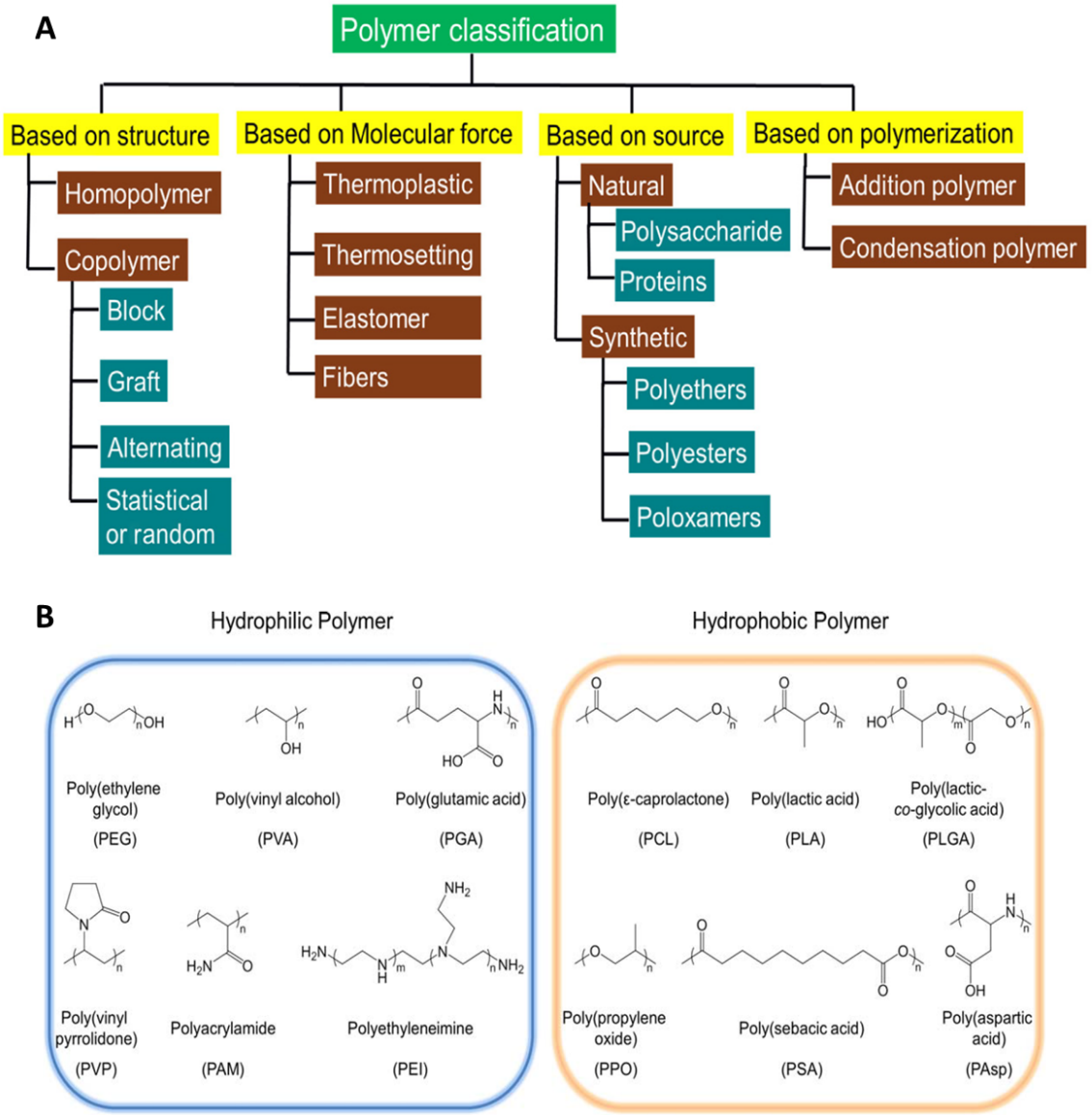

Figure 7. *(A) Classification of different types of available polymer based on their structure, molecular force, source, and polymerization. (B) Commonly used hydrophilic polymer and hydrophobic polymer.*[5]

Over recent decades, the aspects of polymer chemistry are emerging in nearly all of the advancement of drug delivery technologies by providing various possibilities of structures and morphologies. As shown in Figure 7A, polymer can be classified based on structures, molecular forces, sources or polymerization ways.[15] Block copolymers are a class of polymer consisting of two or more distinct polymer components that are chemically connected. Various nanoformulations resulting from the self-assembly of amphiphilic block copolymers, such as micelle, polymersome and hydrogel, have been extensively applied in drug delivery systems (Figure 8).[17] The vast biomedical application of amphiphilic block copolymers is primarily the result of the chemical flexibility of their structure results from their unique chemical

composition, characterized by a hydrophilic block conjugated to a hydrophobic block. Figure 7B summarized chemical structures of most commonly used hydrophilic polymers and hydrophobic polymers.[5]

In order to achieve a system of required hydrophilic-lipophilic balance for assemblies, the hydrophilic and the hydrophobic segments of the block copolymer can be flexibly varied in terms of their structure, molecular weight and length.[16,58] With the rational considerations, it is possible to choose appropriate architecture of block copolymers for desired purposes, for example, select PEG for prolonging the circulation time, select bioactive polysaccharide for specific receptor targeting and select stimuli-responsive polymer to improve the drug release profile of the delivery systems such as micelles or polymersomes.

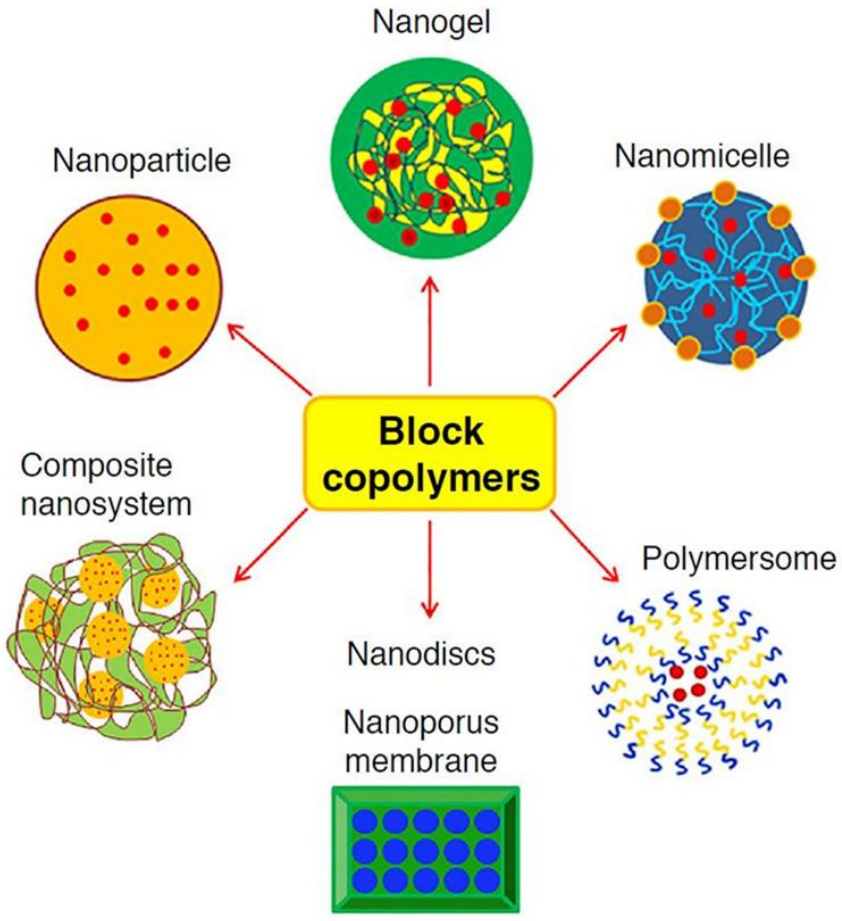

Figure 8. *Schematic presentation of block-copolymer-based nanoformulation assemblies.*[17]

1.4.2 Strategies to prepare block copolymers

A variety of synthetic methods of block copolymer maintain this flexibility in their original design. In general, the three principal ways to prepare the block copolymer : (i) living

polymerization of monomers by sequential addition or using of end-functional groups on one original polymer chain to initiate another living polymerization, such as ring opening polymerization (ROP)[97–100] and reversible addition fragmentation chain transfer (RAFT) polymerization;[101–104] (ii) coupling reaction between polymers through highly reactive functional groups, such as copper(I)-catalyzed azide-alkyne cycloaddition (CuAAC);[105–108] (iii) biosynthesis of protein-like polymers by recombinant DNA technology and protein engineering techniques, for example, biosynthesis of elastin-like polypeptide diblock copolymers[109–112] (Figure 9). The versatility of these synthesis methods have advanced enormously to enhanced the applicability of block copolymers especially in drug delivery approaches.

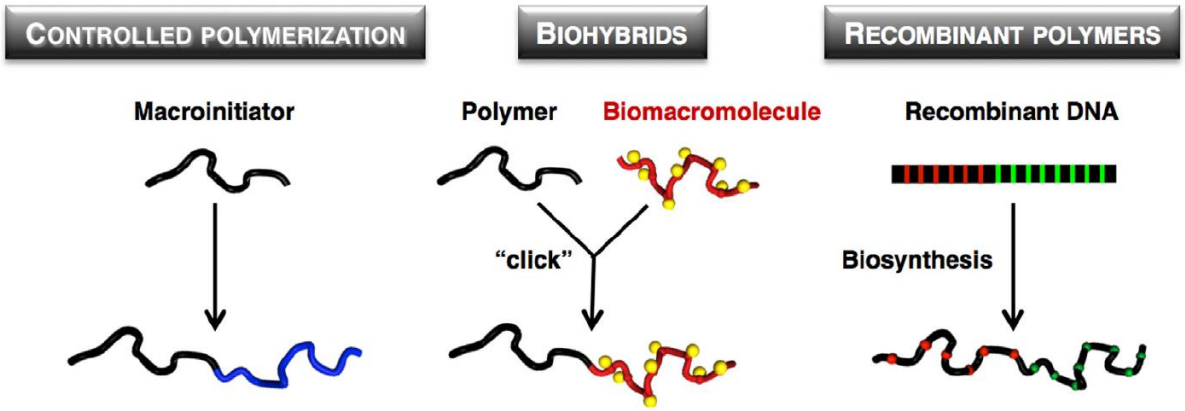

Figure 9. *Strategies to prepare block copolymers*

1.4.3 Block copolymer based self-assemblies

In the past decade, research on block copolymer self-assemblies has focused on the variations in their amphiphilicity, block length ratios, solubility, physicochemical properties, self-assembly behavior, or bioactive blocks of desired properties. Owing to the amphiphilic characteristics, block copolymers can assemble into various supramolecular structures (e.g. nanoparticles,[18,19,113] micelles,[16,58,114,115] polymersomes[11,59–63,96]), providing easy adjustability of their size, shape, stability and surface chemistry. The advantages of block copolymer self-assemblies for drug delivery include tunable amphiphilicity, controlled drug release, prolonged blood circulation time and improved therapeutic effectiveness. In the following subsections, block copolymer based polymersomes and micelles are briefly introduced.

Polymersomes

Polymersomes are a class of artificial vesicles made of amphiphilic block copolymers and contain a hollow core surrounded by a bilayer membrane.[96] The bilayer membrane is composed of hydrated hydrophilic coronas (e.g. PEG) both at the outer and inner side of the hydrophobic part of the membrane. Due to the relatively thick of the membrane, polymersomes are usually more stable compared with liposomes. Hydrophilic drugs can be encapsulated into the aqueous core and the membrane can integrate hydrophobic drugs within its hydrophobic part.[59,60] Owing to their significant properties, polymersomes have attracted massive interest for targeting and stimuli-responsive drug delivery approaches.[11] The presence of a PEG on the surface of polymersomes will reduce the protein adsorption during the blood circulation. Stimuli-responsiveness, rate of disruption and permeability of the membranes can be acheived by utilizing various stimuli-responsive and/or biodegradable block copolymers to control the release of encapsulated drugs. Functional groups on the block copolymers can be used to introduce targeting moieties like antibodies or saccharides,[62] which are able to recognize target receptors or cells. All these advantages make polymersomes one of the most interesting supramolecular structures for potential applications in delivery of drugs, proteins and genes.

Block copolymer micelles

Unlike polymersomes, polymeric micelles are characterised by the core–shell architecture. The hydrophobic blocks of micelle are segregated from the external to form an inner core, whereas the outer shell comprises the hydrophilic segments of the copolymer. In general, there are three major methods for loading drugs into micelles: physical encapsulation (e.g. co-solvent evaporation)[116], drug conjugation and polyionic complexation (e.g. ionic binding)[117,118]. The pharmacokinetics and pharmacodynamics of drug-loaded micelles can be influenced by a variety of factors including size, critical micelle concentration, morphology, interaction with external environment and the chemical nature of the block copolymers. By shaping these parameters, polymeric micelles have been developed as nanomedicines capable of delivering a wide range of therapeutics through effective accumulation on targets in the body, adjustment of their stabilities in response to particular stimuli and controlling the release of the loaded drugs at the targeted sites.[16,119]

1.5 “Smart” Stimuli-Responsive Polymeric Systems

1.5.1 Design of stimuli-responsive system

Clinical efficacy of therapeutics is limited by its poor water solubility and low bioavailability. The utility of polymeric nanocarriers to transport therapeutics like small-molecular drugs, peptides, or nucleic acids has gained increasing attention throughout the field of pharmaceutical sciences. In contrast to conventional drugs, polymeric nanocarriers improve the solubility, bioavailability of already existing drugs, thus enhance therapy efficacy. Additionally, these nanocarriers can be tailor-made in such a manner that they are triggered to release their cargo at the site of action, what so-called "smart" stimuli-responsive systems (Figure 10).[9] Endogenous stimuli like pH, enzymes, glucose, redox environment and exogenous stimuli like temperature, magnetic field, light, and ultrasound have employed solely or combinedly to advance the development of stimuli-responsive systems.[8,10,120]

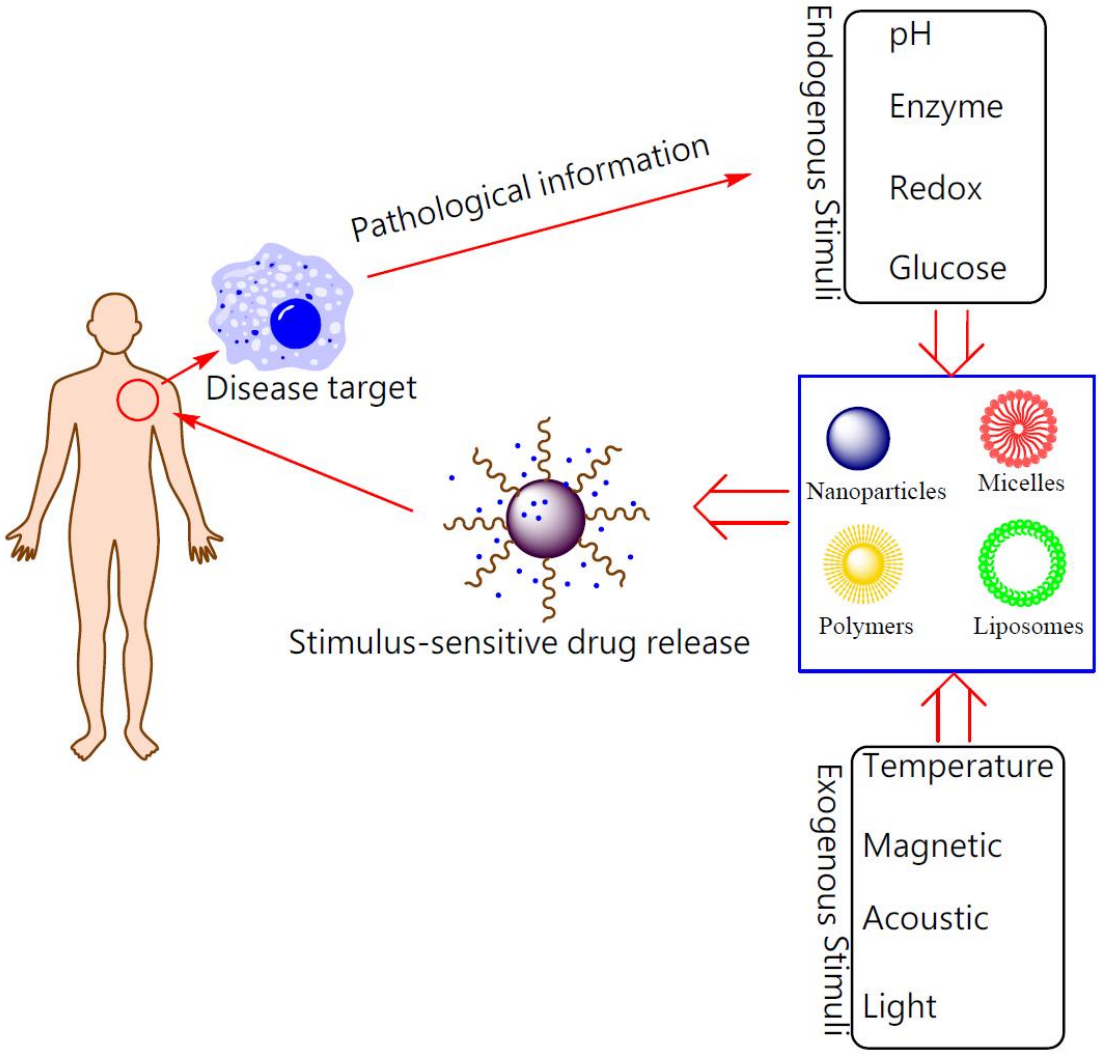

Figure 10. *Schematic illustration for stimuli-responsive DDSs.*[9]

Stimulus	Examples of responses
Endogenous	
pH gradients	Direct activation, expansion, gatekeeping, disassembly, assembly, morphology switch
Redox process	Gatekeeping, disassembly
Enzymes or proteins	Direct activation, gatekeeping, disassembly, assembly, morphology switch, motion
Nucleic acids or small molecules	Gatekeeping, disassembly, assembly, morphology switch, motion
Exogenous	
Temperature	Expansion, disassembly, assembly, morphology switch
Light	Direct activation, gatekeeping, disassembly, assembly, morphology switch
Ultrasound	Motion
Magnetic field	Motion

Table 2*. Highlights of stimuli example responses. Associated references broached in this reference.*[120]

To design such stimuli-responsive system for biomedical application, the mandatory principle of "smart" lies on the fact that a specific endogenous/exogenou stimulus of chemical, biochemical, or physical can trigger the response of the nanocarriers, thereby promoting structural changes in composition or conformation to release the cargo in specific biological environment. These structural changes mainly include activation, expansion, gatekeeping, disassembly, assembly, morphology switch and motion (Table 2).

1.5.2 Tumor microenvironmental stimulus

Indeed, biological stimuli-responsive are also naturally occurring in human body, such as the variation of pH in different cellular compartments. However, most variations in physiological parameters exist at the cell, tissue and organ levels, are usually associated closely with various pathological phenomenon, such as cancer, diabetes, cardiovascular disease and chronic inflammations (Figure 11).[121]

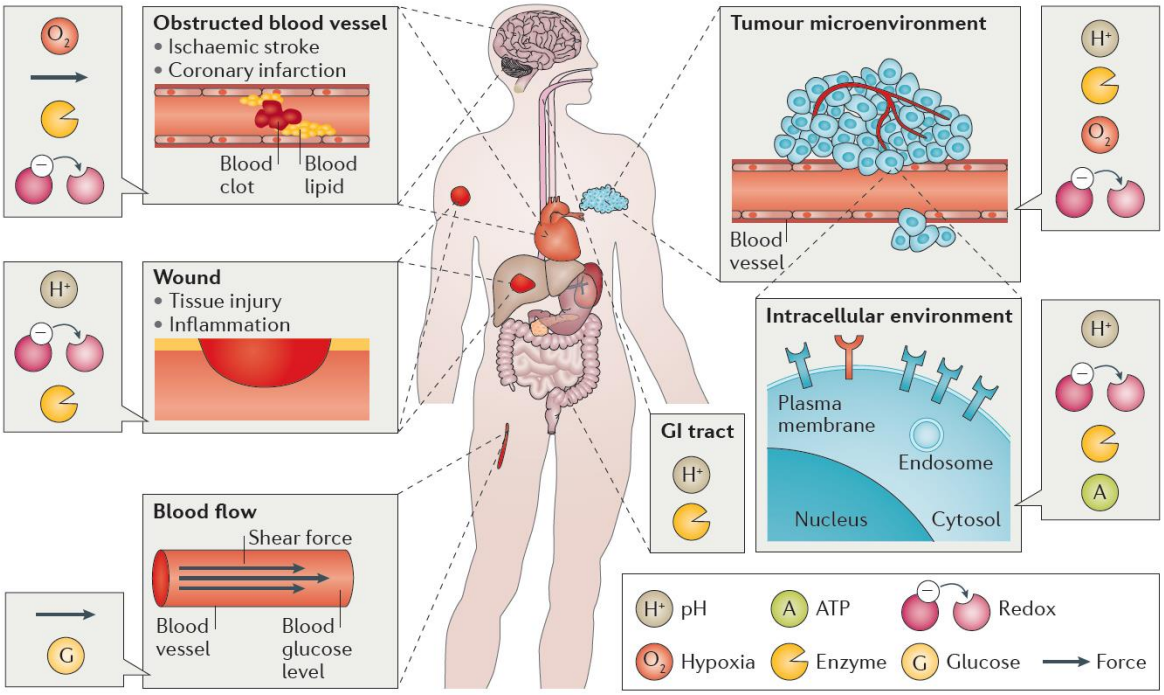

Figure 11. *Typical physiological environments with associated biological stimuli. ATP, adenosine triphosphate; GI, gastrointestinal.*[121]

It is widely known that the microenvironment of tumors presents unique physiological features as compared to healthy tissues, including acidic pH[122] due to the aerobic glycolysis and lactic acid production (Warburg effect)[123,124], hypoxia[125] owing to the aberrant vascular network, redox potential,[126] and overexpression of particular enzymes and molecules[127] such as matrix metalloproteinases[128] that are involved in tumor progression. These endogenous stimuli provide great opportunities for the development of "smart" polymeric nanocarriers for tumor-targeted delivery and activation of therapeutic or imaging agents. Additionally, the application of exogenous triggers, such as temperature, light irradiation, and ultrasound, to targeted tissues has also been used for developing pinpoint therapies. By merging such environmental responsive function with polymeric nanocarriers, "smart" polymeric system promoted the effective accumulation of anticancer drug at tumor site, thus to maintain anticancer therapies with high selectivity.

1.5.3 Design of "smart" polymeric nanocarriers

Block copolymer based assemblies, like polymersomes or polymeric micelles, are frequently designed to respond to various endogenous and exogenous stimuli for achieving desired needs. For example, polymeric micelles can incorporate various functions to sense the subtle changes

in the surroundings by fine-tuning their multicomponent and compartmentalized structure (Figure 12).

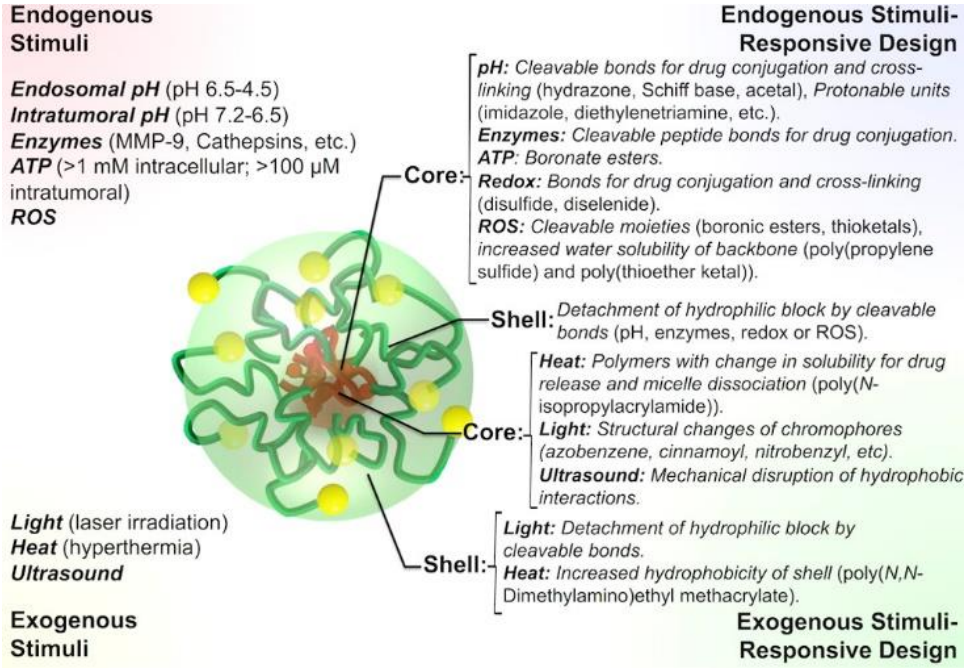

Figure 12. *Design of polymeric micelles responding to various endogenous and exogenous stimuli.*[16]

pH-sensitive

As mentioned above, pH in tumor tissues is usually slight acidic. There are usually two route to design pH-responsive polymeric nanocarrier for cancer therapy.[129] First, nanocarriers can be prepared with pH-sensitive linkages that are stable at physiological pH 7.4, but cleave under tumor pH, resulting the cargo release intratumorally or intracellularly. Typical examples of acid-sensitive linkages including *N*-cis-aconityl, hydrazone, acetal and imine.[130] The group of Kataoka used poly(ethylene glycol)-block-poly(aspartate) (PEG-*b*-PAsp) block copolymer to load doxorubicin via hydrazone bond.[131] Zhang and co-workers also used the same linkage but to deliver cisplatin by PEG-*b*-PLLA block copolymer.[132] Both drug release profiles were enhanced at acidic pH. Nanocarriers can be also equipped with ionizable groups, such as amines, histidines[133] and carboxylic acids, which stay neutral at pH 7.4, but rapidly protonate at acidic pH. The group of Lecommandoux prepared polypeptide diblock copolymers poly(L-glutamic acid)-*b*-poly(L-lysine) (PGA-PLL) which reversibly had one block or the other as the corona depending on the pH gradient.[134]

Enzyme-sensitive

Besides the pH variations, the variation of enzymes in healthy and tumor tissues can be used for drug delivery systems with high activation selectivity.[135] The design of enzyme-responsive nanocarriers mainly rely on the hydrolysis of esters or peptide sequences by esters or proteases. One of the most frequently studied peptide sequence is Gly-Phe-Leu-Gly.[136] The group of Duncan used *N*-(2-hydroxypropyl) methacrylamide (HPMA) as polymer backbone and Gly-Phe-Leu-Gly as linker for attaching chemotherapeutics like doxorubicin had been advanced to clinical studies.[137]

Light-sensitive

External stimuli are useful for directing the action of polymeric nanocarriers at target sites, although their application in some diseases might be restricted. The response to light of polymers is usually rely on the polymer-conjugated chromophores, such as azobenzene,[138] coumarin,[139] cinnamoyl,[140] or nitrobenzyl groups[141,142], which can be cleaved upon light irradiation at a defined wavelength or undergo light-mediated structural changes, resulting the disassembly of the nanocarrier and the release of the cargo.

Thermo-sensitive

Heating is usually applied in cancer therapy as local hyperthermia by raising the temperature of tumor tissues to about 43 ℃, which leads to cellular damage.[143] Thus, thermo-responsive polymers such as poly(N-isopropylacrylamide) (PNIPAM)[144] and poly(*N*,*N*-diethylacrylamide) (PDEAAM),[145] are advantageous for constructing block copolymers which respond to temperature changes within a narrow and sharp range. PNIPAM had been copolymerized with PEG[146] and poly(acrylic acid)[147] to form thermos-sensitive block copolymer micelles. Du et al. designed thermo-sensitive nanoparticles self-assembled from poly(*N*,*N*-diethylacrylamide- co-acrylamide)-block-poly(γ-benzyl L-glutamate) for paclitaxel (PTX) delivery in localized hyperthermia.[148] The lower critical solution temperature (LCST) of nanoparticles was adjusted to a level between physiological body temperature (37 °C) and that used local hyperthermia (about 43 °C) as a trigger. The release of PTX showed a thermo-sensitive controlled behavior and the cytotoxicity of PTX loaded nanoparticles increased with tumor cells compared to origin PTX when heating was performed.

Dual and multi-stimuli responsive

In addition, in an effort to further improve drug release profiles, dual and multi-stimuli responsive polymeric nanaocarriers that respond to a combination of two or more stimulus such as pH/temperature,[130] pH/reduction,[149] pH/magnetic field,[150] temperature/redox,[151] temperature/pH/redox,[152] temperature/pH/magnetic,[153] and pH/redox/magnetic,[154] have been developed and reviewed.[155,156] (Figure 13).

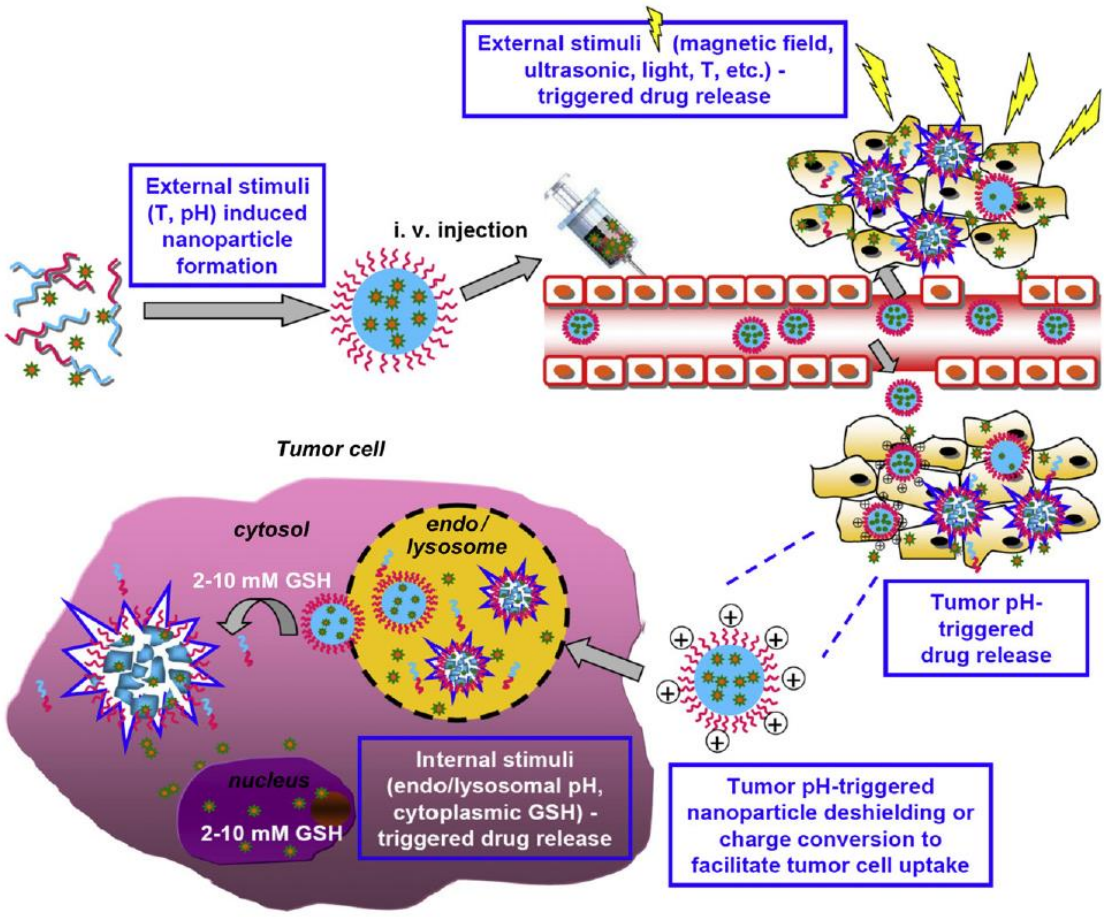

Figure 13. *Dual and multi-stimuli (e.g., T (temperature), pH, magnetic field, ultrasound, and light) smart polymeric materials used for smart drugs in solid tumors. The two and more stimuli are applied as following: (i) application of an external stimulus such as temperature and pH to facilitate formation of nanoparticles; (ii) application of an external stimulus such as magnetic field, ultrasonic, light, and temperature to trigger drug release, which allows precision spatial, temporal as well as dose control over drug release at will through a remote apparatus; (iii) acidic tumor pH (6.57.2) is utilized to trigger drug release and/or reverse shielding of nanoparticles at tumor site thereby enhancing tumor cell uptake of nanoparticulate drugs; and (iv) intracellular environments such as low pH in endo/lysosomal compartments and high redox potential in cytoplasm are utilized to improve intracellular drug release inside tumor cells.*

2. ELASTIN-LIKE POLYPEPTIDE: FROM NATURE TO BIOMEDICAL APPLICATIONS

2.1 Introduction

Stimuli-responsive polymers are promising candidates for biomedical applications, such as controlled drug delivery.[10,120,157] Recently, elastin-like polypeptides (ELPs) have attracted increasing interest as stimuli-responsive protein-like polymers and serve as an attractive alternative to synthetic polypeptides obtained by conventional polymerization.[109,110,158–160] ELPs are a biomimetic class of polymers inspired from a repeat motif VPGXG of human tropoelastin. X is a guest residue that can be any amino acid except proline.[161,162] Genetically encoded and recombinant synthesis of ELPs allows precise defined of the sequence and molecular weight of polymer, which is unmatched by conventional synthetic polymers. In aqueous solution ELPs exhibit a reversible phase transition behavior whereby ELPs remain soluble below a transition temperature (T_t) but form coacervates about T_t.[163] Their phase transition behavior and biocompatibility make ELPs interesting stimulus-responsive materials for various applications in drug delivery field including as soluble polypeptide carriers, thermally self-assembled micelles, cross-linked hydrogels or coacervated protein depots.[109,159,164,165] This part aims to give a general review of the definition, protein expression and properties of ELPs as well as their post-modification methods and biological applications in the field of nanomedicine.

2.2 Definition, protein expression and properties of ELP

2.2.1 ELP inspired from nature elastin

Elastin is an natural extracellular matrix (ECM) proteins that is plentifully exist in various tissues, such as elastin ligaments, blood vessels, lungs, tendons and skins, supporting them with indefinite cycles of stress and relaxation.[166–168] Mature elastin is generated by the self-assembly and crosslinking of the precursor protein, tropoelastin. Tropoelastin is a 72 kDa molecule comprising highly repetitive amino acid sequences.[169] As shown in Figure 14, there are three kinds of domains of tropoelastin: proline-rich hydrophobic, glycine rich hydrophobic, and crosslinking domains. Despite its unique self-assembly and physiological properties, the usage of natural elastin as biomaterials are remain under explored due to its intrinsic insolubility issues.[170] Accordingly, researchers attempted to “dissect” the elastin domains to determine the

key sequences that corresponding to its characteristics. In 1974, Urry et al. revealed that a repeat sequence $(VPGVG)_n$, which represent one of the most frequently sequences found in proline-rich domain of tropoelastin, could undergo a reversible phase transition in aqueous solvents identical to the native elastin.[171] Based on this breakthrough finding, Urry's group further generalized this approach to ELPs comprised of the pentapeptide VPGXG- where X can be any amino acid except proline.[172] Following this systematic studies, other motifs that are minor variations of the VPGXG, such as VPAVG, IPGXG and LPGXG, have also been investigated.[173,174] Along with rapid progress in recombinant DNA and protein engineering techniques, plenty of functional protein-like polymers containing elastin-derived sequences, namely elastin-like polypeptides, have been constructed and applied for various biomedical applications.[159,175,176]

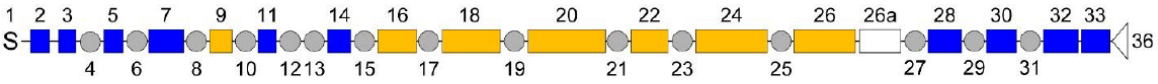

Domain name	Exon number	Peptide sequnce
Proline-rich hydrophobic domain	18	GAAAGLVPGGPGFGPGVVGVPGAGVPGVGVPGAGIPVVPGAGIPGAAVP
	20	GARPGVGVGGIPTYGVGAGGFPGFGVGVGGIPGVAGVPSVGGVPGVGGVPGVGIS
	24	ALLNLAGLVPGVGVAPGVGVAPGVGVAPGVGLAPGVGVAPGVGVAPGVGVAPGI
Glycine-rich hydrophobic domain	28	GAAVPGVLGGLGALGGVGIPGGVV
	30	GLVGAAGLGGLGVGGLGVPGVGGLG
	32	GAAGLGGVLGGAGQFPLG
Crosslinking domain	8	GAVVPQPGAGVKPGKVP
	25	GPGGVAAAAKSAAKVAAKAQL

Figure 14. *Domain structure encoded by human tropoelastin gene and the peptide sequences of several representative exons from each domain.*[177] *S stands for the signal sequence. Human tropoelastin lacks exons 34 and 35.*[178]

2.2.2 ELP production and purification

ELPs can be produced in different hosts from a recombinant gene that encodes the amino acid sequence of the ELP. The most frequently used protein expression system is *Escherichia coli*,[179–183] though others have also been used including yeast,[184] plants,[160,185] fungi,[186] and cell-free expression systems.[187] After the culture of designed bacteria clone, the bacteria was subject to cell lysis and the cell lysate was centrifuged at low temperature in order to collected the soluble ELP in the supernatant and to discard the cell residues in the pellet (Figure 15).

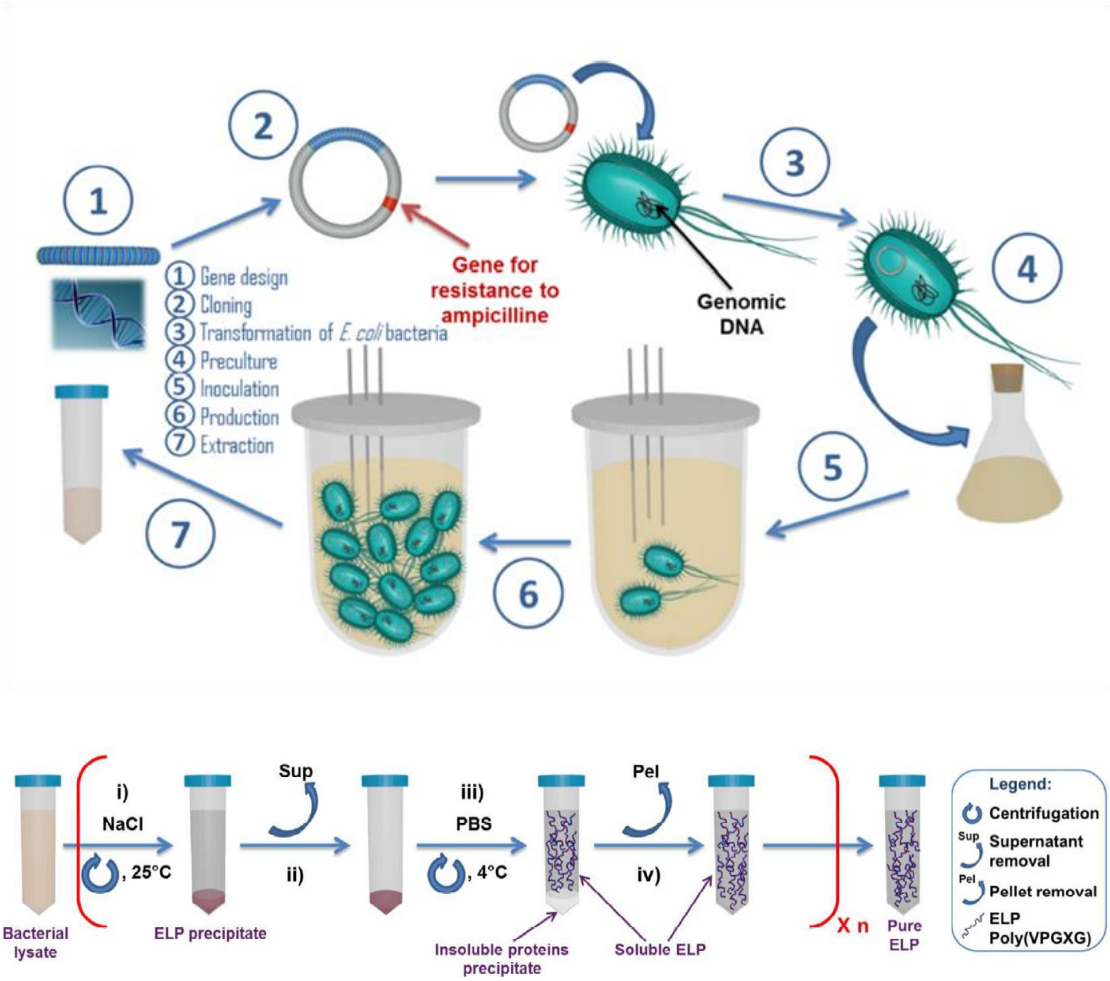

Figure 15. *Generalized schematic of recombinant ELPs biosynthesis and purification. (Illustration from R. Petitdemange PhD thesis).*

Purifying ELPs is cost-efficient due to a simple purification strategy, known as inverse transition cycling (ITC), that exploits the inverse phase separation property that can be triggered by a change in solution temperature or salt concentration.[188,189] The basic steps of ITC procedure are as follows: (i) the supernatant of cell lysate is heated above the T_t and/or the addition of salts such as sodium chloride, to trigger the ELP phase transition, and the suspension is centrifuged at a higher temperature leading to the formation of an ELP-rich precipitate; (ii) Soluble byproducts in the supernatant is discarded; (iii) the ELP in pellet is dissolved by reversing the phase transition with the addition of cold, low-salt buffer so that the solution temperature is now below the T_t; (iv) finally the suspension is centrifuged at a lower temperature to remove additional insoluble proteins precipitate while the soluble ELP stay in the supernatant. ITC steps are repeated several times until a purified product is obtained (Figure 15).

2.2.3 General biophysical properties of ELP

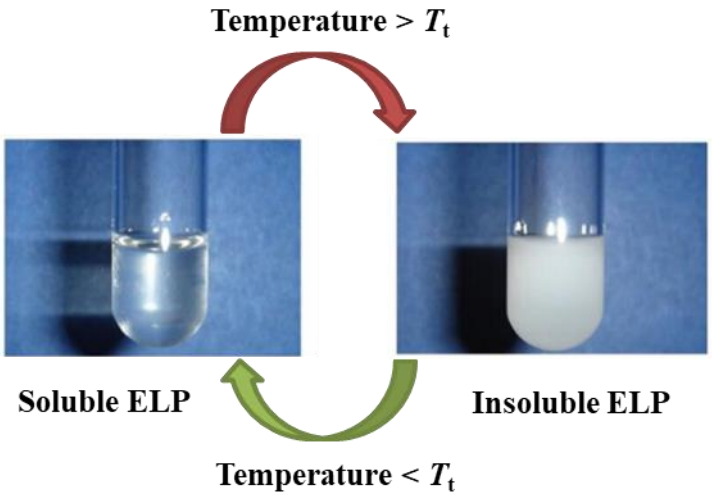

Figure 16. *Reversible phase transition of ELP*

As ELPs originate from human tropoelastin, they are non-injurious, non-immunogenic and are compatible with living systems.[190,191] ELPs exhibit a fast and reversible phase transition behavior at a specific temperature referred to as the lower critical solution temperature (LCST), commonly known as the inverse transition temperature (T_t).[188,192] When temperature below T_t, ELP chains assume a close-to-random coil conformation and highly soluble in aqueous solution.[193,194] When rising the solution temperature above the T_t, ELPs become insoluble and form large aggregates.[195,196] This transition is entirely reversible, such that the aggregated ELPs become totally resoluble when the temperature is lowered below the T_t of ELP (Figure 16). When fused with other proteins, ELPs retain its phase transition property, which highly facilitate the purification of fusion ELP-proteins.[197] The T_t can be highly tune by ionic strength, concentration, pH and polymer length.[198,199] The nature of the guest residue also affects the T_t, as more hydrophobic amino acid residues lower the T_t and vice versa. Chilkoti and coworkers established an empirical model that correlates T_t values to the ELP composition, concentration and chain length in a single equation[200]:

$$T_t = T_{t,c} + \frac{k}{L} ln(\frac{C_c}{C})$$

Where $T_{t,c}$ is the critical temperature, k is a constant, L is the number of pentapeptide units, C_c is the critical concentration, C is the concentration. This equation allows predicting the T_t of well-defined ELP sequence at specific concentration.

ELPs are degradable by proteolysis which reduces their adverse side effect due to long-term accumulation in the body.[201] The group of Mackay have extensively studied the biodegradability of ELPs in different physiological microenvironments.[202] They elaborated that the rate of biodegradation controls the accumulation of ELPs at the target site as well as clearance from the body and suggested a detailed mechanism for the degradation of ELPs. ELPs are internalized by cells pinocytosis, co-localized in low pH compartments, namely lysosomes and are eliminated over a period of 2–24 h after proteolytic cleavage by elastase and collagenase endopeptidases.[202] Due to its biocompatibility, biodegradability and non-immunogenic properties, ELPs are emerging as a new class of polymer appropriate for *in vivo* applications.[109,110,159,163]

2.3 Post-modification of ELPs

Post-translational modifications of proteins, involving chemical changes after proteins translation, play a fundamental role in the regulation of protein's structures and functions.[203–207] The modifications range from amino acid changes through to the addition of macromolecules, such as lipid, carbohydrate or protein. The major class of modification, however, is represented by glycosylation, *N*-linked, *O*-linked, or glycosylphosphatidylinositol (GPI)-linked. Such modifications have roles in protein stability and folding, targeting and recognition.[203]

In terms of ELPs, post-modified ELPs can adapted to various purpose, such as tuning the T_t, subsequent conjugation with drugs, polymers or other functional moieties. The main methodology has focused on selective chemical modification of amino acids either at ELP backbone chains or at the *N*- or *C*-terminus. Among various amino acids in ELP sequence, cysteine, lysine and tyrosine are the most commonly modified amino acids.[208] For example, Van Hest and coworkers selective converted the α-amine at the *N*-terminus or all amines to azide group by varying pH 8.5 to pH 10 using diazotransfer reaction. The modified ELPs were subsequently conjugated with one or two PEG moiety.[209] Brian et.al reported high-efficiency, high-specificity reactions focusing on diazonium coupling chemistry for the mass modification of tyrosine moieties in ELPs which can also preserve cysteine oligomerization. Multistep conjugations utilizing copper(I) catalyzed alkyne–azide cycloaddition (CuAAC) as a second step are also demonstrated to expand ELPs functional diversity.[205] ELPs were also post-modified at lysine residues by *N*-hydroxysuccinimide ester or tri-Boc hydrazinoacetic acid for subsequent drug loading or crosslinking.[210,211] Recently, selective post-modification of ELPs

on methionine residues, including by oxidation and/or alkylation, are emerging as a versatile pathways to tune the properties and/or to endue ELPs with functions.[212–214]

2.4 ELP-based nanomaterials and their applications

Due to its biocompatibility, biodegradability, non-immunogenic and stimuli-responsive properties, ELPs-based nanomaterial have generated significant interest in various biomedical applications, ranging from drug delivery to tissue engineering. Herein, ELP-based materials, typically, ELP block copolymer, ELP-based hybrid system and ELP-drug conjugates are briefly introduced.

2.4.1 ELP diblock copolymer

Advances in genetic engineering allow *de novo* designs and synthesis of tailor-made ELP block copolymers that self-assemble into nanoscale structure for drug delivery application.[215] In order to create temperature-triggered amphiphiles, ELP diblocks are designed such that the two blocks have a significantly different hydrophobicity by varying the guest residue. Below a critical temperature, both blocks are soluble. As the temperature is raised, the more hydrophobic block is selectively dehydrate while the hydrophilic block remains solvated. When reaching a critical temperature, that is, defined as the critical micelle temperature (CMT), the diblock ELP gains sufficient amphiphilicity to trigger its self-assembly into micelles.[216] This means that hydrophobic drugs can be entrapped in the micell core, whereas the hydrophilic surface can decorate with bioactive molecules.[217,218] Upon heating the solution temperatures further, the more hydrophilic block begins to dehydrate, and at another critical temperature, defined as aggregation temperature ($T_{\text{aggregation}}$), triggered the aggregation of micelles into polydisperse micro-sized aggregates. Cooling reverses the process, in which the aggregate disassembles to return to the unimer form (Figure 17). By rationally selecting appropriate ELP sequences, self-assembly properties of ELP block copolymer including CMTs, diameters, and aggregation numbers (ELP chains per one particle) can be finely tuned.

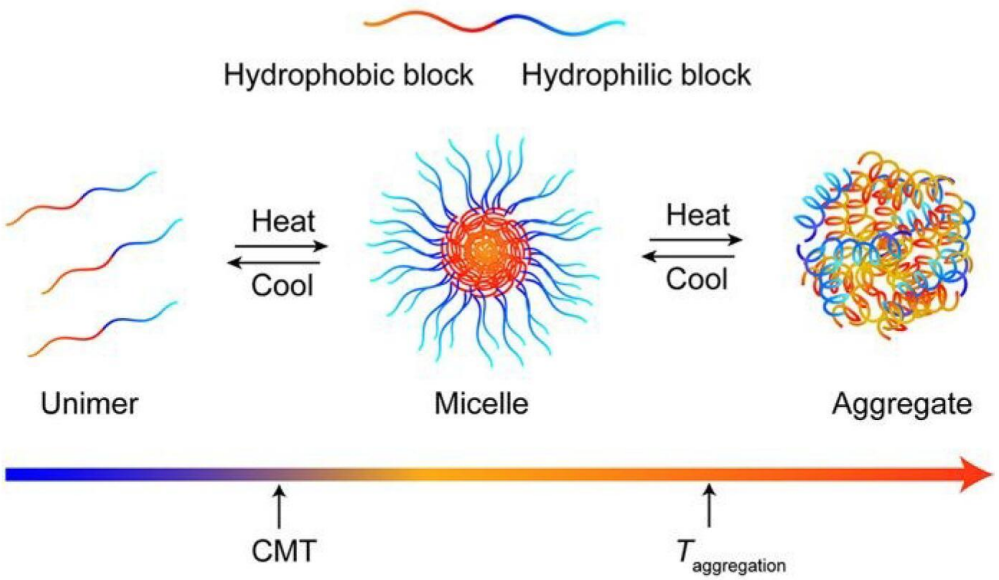

Figure 17. *Schematic of an amphiphilic block ELP assembling into nanoparticles upon thermal triggers. The amphiphilic ELP contains a hydrophobic block with a lower T_t and a hydrophilic block with a higher T_t. At temperatures above the CMT, micelles are formed by the association of the hydrophobic block while the hydrophilic block forms the micelle corona. Heating to temperatures higher than $T_{aggregation}$, the block ELP becomes completely hydrophobic and thus polydisperse micro-sized aggregates are formed. Cooling reverses the process, in which the aggregate disassembles to return to the unimer form.*[178]

The group of Chilkoti systematically investigated the behavior of ELP diblock copolymers by constructing a library of ten distinct ELP block copolymers based on the sequence $[VPGVG(VPGGG)_7(VPGAG)_8]_n$-$(VPGVG)_m$ with different molecular weights and hydrophilic-to-hydrophobic block ratios.[219] They revealed that the CMT is controlled by the length of the hydrophobic block, while the size of the micelles is controlled by the total copolymer length and hydrophobic/hydrophilic block ratio. Hassouneh et al. further physically characterized these micelles as having dense cores and "unstretched" coronas, a characteristic not observed with synthetic diblock copolymers.[111]

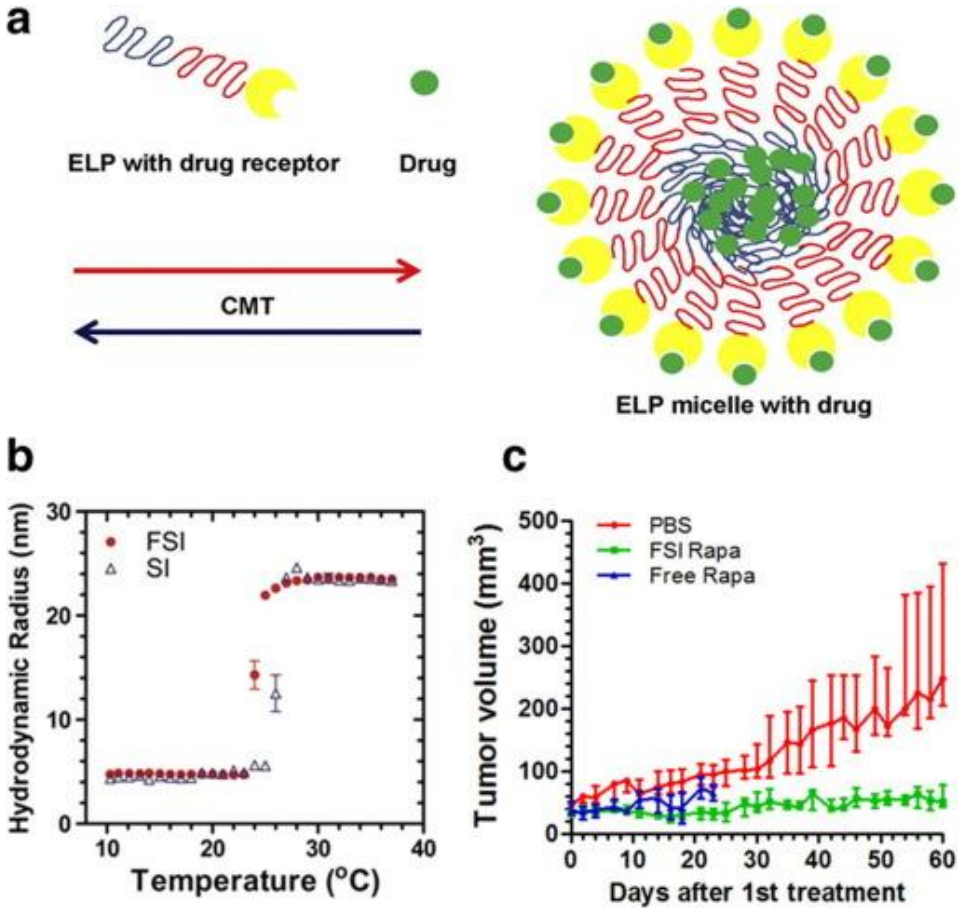

Figure 18. *Design of elastin-like polypeptide (ELP) nanoparticles that carry an anti-proliferative drug at both their core and corona. (a) High-avidity interaction between a small molecule drug (rapamycin) and its cognate target protein (FKBP) decorated at surface of an ELP nanoparticle. The nanoparticles assemble nanoparticles above a critical micelle temperature (CMT). (b) Dynamic light scattering of FKBP-decorated FSI and plain SI nanoparticles shows that protein modification minimally affects CMT or hydrodynamic radius. (c) Tumor growth inhibition by FSI-rapamycin versus free rapamycin (0.75 mg/kg BW). Free rapamycin mice were sacrificed at day 24 due to toxicity.*[220]

In terms of ELPs for drug delivery, the basic principle is to best exploit the relationship between the characteristic T_t of the ELP and body temperature (T_b). When the T_t is lower than T_b, ELP micelle can maintain stable at T_b. Interesting example could be found in ELP micelle with drug loaded in both core and corona (Figure 18). As shown in Figure 18b, T_t of drug loaded FKBP-decorated FSI and plain SI nanoparticles was 24 and 26 ℃, respectively. To determine if this stable nanoparticles has potential applications in vivo, FSI/Rapa was administered to mice bearing a human breast cancer model. Compared to free drug, FSI encapsulation significantly decreased gross toxicity and enhanced the anti-cancer activity as shown in Figure 18c.[220]

2.4.2 ELP triblock copolymer

ELP triblocks were also studied by serveral groups.[221,222] Sallach et al. have developed ELP triblock copolymer containing a central hydrophilic block and two hydrophobic. Below the T_t, dilute solutions of this amphiphilic triblock formed monodispersed micelles in a narrow range of R_h of 100 nm. When the temperature was raised above T_t, an abrupt increase in micelle internal density was observed with a concomitant reduction in micelle size from 122 to 88 nm.[223]

2.4.3 ELP-based hybrid systems

ELP-based hybrid systems, in which ELP as a building block is combined with other blocks, have also been reported. These conjugation partner includes proteins like collagen-like polypeptides,[224] silk-like polypeptides,[224,225] resilin-like polypeptides,[226] or mcherry proteins.[227] However, only a few examples of ELP hybrid systems containing synthetic polymers have been reported in the literature. For example, ELP conjugate with poly(ethylene glycol) by click chemistry, in which control of the assembled structures was described by Van Hest's group.[209] The encapsulation of a hydrophobic fluorescent dye was shown to exemplify the potential of the ELP-PEG micelles to serve as nanocarriers for hydrophobic drugs, with the PEG corona providing stealth and steric protection of encapsulated materials. Apart from direct conjugation method for preparation of ELP hybrid system, other strategies, for example, by ring opening polymerization (ROP) is reported recently.[228] Le Fer et.al used ELP as a macroinitiator for the ROP of γ-benzyl-L-glutamate (γ-BLG NCA). Diblock copolypeptides were obtained with an excellent control of the polymerization highlighted by the dispersity below 1.04.[228] Acid deprotection of BLG units leads to well-defined poly(L-glutamic acid)-*b*-ELP (PGlu-*b*-ELP) hybrid diblock copolypeptides.[229] Unexpected salt-dependent behavior of this series of diblock copolypeptides was found and they suggested that this temperature-responsive self-assembly behavior of diblock copolypeptides in PBS occurred *via* a mechanism involving both conformational changes due to a dehydration process and densification of micelle-like structure thanks to the presence of salt ensuring both micellar core compaction and screening effect between negatively charged Glu units in the shell.

Additionally, lipid-ELP conjugates were also reported. For example, Park et al. developed thermosensitive liposome by introducing fatty acid conjugated ELP to convey a high thermoresponsive property.[230] Very recently, Chilkoti's group constructed lipid-ELP conjugate using post-translational modification methods.[231,232] Fatty acid[231] and cholesterol[232] were

incorporated at the *N*- and *C*-terminal of an ELP, respectively, and the effects of the conjugation on self-assembly properties were studied and discussed.

2.4.4 ELP-drug conjugate

ELPs are often exploited to increase drug delivery efficiency due to the biodegradability and temperature sensitivity of ELP and ability to self-assemble. The conjugation of Dox to ELPs via acid-labile hydrazine linker had been proven to be highly efficient.[211] Once the ELP-drug conjugates had been internalized into the cells, the resulting systems were able to trigger the release of drug in the acidic environment of lysosomes while negligible amounts of drug being released into the external medium of the cell. They also found conjugates with longer linkers exhibited slower transition kinetics compared to those with shorter linkers. The highest release profile provided by the shortest linker of the ELP-Dox conjugate was nearly 80 % at pH 4 over 72 h.[233] In another study, ELP was flanked with a Tat cell penetrating peptide at the *N*-terminus and a GFLGC cathepsin cleavage sequence by cassette mutagenesis. Dox was attached to the *C*-terminus cysteine and the resulted ELP-drug conjugates (Tat-ELP-GFLG-Dox) showed equally cytotoxic in both sensitive and resistant cell lines (MES-SA/Dx5) while free Dox was rapidly pumped out by the P-glycoprotein.[234] This study provide a means to overcome drug resistance in cancer cells. Another ELP-Dox conjugate SynB1–ELP–Dox consisting of a cell-penetrating peptide at the *N*-terminus and the 6-maleimidocaproyl hydrazone derivative of Dox at the *C*-terminus of the ELR was reported by Shama Moktan et al. Preclinical study of this ELP-Dox conjugate showed complete inhibition of tumor growth and a substantially higher therapeutic benefit in an animal model with breast cancer.[235]

2.4.5 Targeting by local hyperthermia in tumor

When T_t of ELPs were between body temperature T_b and the temperature of a local hyperthermia (42 ℃ for tumor therapy), ELPs can thermally targeted drug delivery to solid tumors by triggering ELP coacervation with mild hyperthermia at the tumor site.[236] Meyer et al. synthesized a thermally responsive ELP with a T_t of 41 ℃. [237] By radiolabel distribution studies and *in vivo* fluorescence video microscopy, they demonstrated that hyperthermia targeting of the thermally responsive ELP for 1 h shows about 2-fold increase in tumor localization compared to the same polypeptide without hyperthermia, which reveals that the phase transition of the thermally responsive ELP carriers can be engineered to occur *in vivo* at a specific temperature.[237] Liu et al. further investigated this link between mild hyperthermia

and tumor penetration by studying the degradation, pharmacokinetics, tumor localization, and tumor spatial distribution of a radiolabeled ELPs using FaDu tumor grafts in nude mice models. Once the tumors were heated to 42 ℃, the thermally responsive ELP (T_t = 40 ℃) exhibited a 1.5 fold increase in accumulation rates over a thermally unresponsive ELP control.[238] These findings provide a promising pathway for applying ELP-based carriers for the targeted delivery of cancer therapeutics to solid tumors.[239]

2.4.6 Tissue engineering

The field of tissue engineering aims to restore or replace native tissue. One of the main approach towards achieving this goal is the injection or implantion of a temporary, degradable scaffold that is seeded with cells or that attract the appropriate cells and lead to native tissue regeneration. Majority work on developing scaffolds for tissue regeneration has focused on biomimetic synthetic polymers or decellularized natural extracellular matrix (ECM). Since ELPs are inspired from tropoelastin, a natural ECM protein, they are attractive as interesting intermediates between these two types.[165,240] Biosynthesis of genetically encoded ELPs from a synthetic gene provides precise control over the amino acid sequence and MW while retaining part of the biocompatible characteristics of decellularized matrices. Besides, due to the thermally responsive behavior, ELPs are also attractive materials for the formation of scaffolds in situ,[237] and as injectable cell scaffolds for liver regeneration,[241] cartilage,[242,243] ocular,[244] cell sheet engineering[245] and vascular grafts.[246,247] Hybrid biopolymers, such as silk-ELPs fusions, have also employed the behavior for tissue engineering.[237]

3. POLYSACCHARIDE-BASED BLOCK COPOLYMERS FOR BIOMEDICAL APPLICATION

3.1 Introduction

Polysaccharides (PSs) are a complex class of polymers isolated from animal origin (chitosan, chondroitin), algal origin (e.g. alginate), plant origin (e.g. pectin, guar gum), and microbial origin (e.g. dextran), and that are built from monosaccharides linked by O-glycosidic linkages. Generally PSs are in high abundance and easily processed and so provide relatively low cost biopolymers. Additionally, due to their natural properties, PSs are well adapted to cellular physiology, making them excellently biodegradable, biocompatible, low toxic, non-immunogenic, and specifically bioactive. Their diverse structures also let them easily chemical modified and functionalized. This varied range of properties provides advantages for PSs extensively used in life science (Figure 19). Here in this part, we pay attention to give a general overview of most widely used PSs, rational design of PSs-based nanocompositions and their synthetic strategies, and finally we focus on polysaccharide-*b*-polypeptide block copolymers and their biomedical applications.

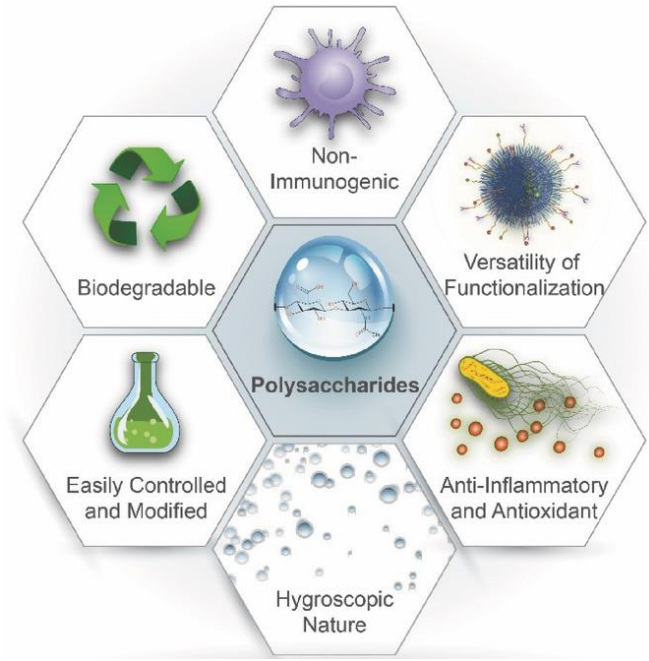

Figure 19. *Schematic illustration of unique physiochemical and biological properties of polysaccarides.*[248]

3.2 Most widely used polysaccharides for biomedical application

3.2.1 Hyaluronic acid

Hyaluronic acid (HA) is a non-sulfated glycosaminoglycan that is abundant in the skin, lung, intestine and extracellular matrix (ECM), playing an essential role in the human body.[249] HA is composed of glucuronic acid (GlcUA) and *N*-acetylglucosamine (GlcNAc), which are repeated by β-1,3 and β-1,4 glycosidic linkages. The biological function of HA has been widely investigated for the regulation of cell behaviors.[249,250] A strong correlation between the presence of HA, and cell migration and proliferation has been demonstrated.[251] There have been many reports on HA receptors that play important biological roles such as endocytosis, degradation and signal transduction. Receptors including cluster determinant 44 (CD_{44}),[252] receptor for hyaluronate-mediated motility (RHAMM),[253,254] HA receptor for endocytosis (HARE),[255,256] and lymphatic vessel endothelial hyaluronan receptor-1 (LYVE-1)[257], have been identified as HA receptors for various biological functions.

Taking advantage of these biological functions and excellent physicochemical properties of HA, HA and its derivatives have been used as delivery vehicles for polypeptides and proteins, steroid drugs, anticancer chemotherapeutics as well as nucleic acids.[258–261] HA-based nanocarriers such as nanoparticles, block copolymer micelles and polymersomes, demonstrate various advantages.[261–264] Firstly, the ease of chemical modification on HA or its derivative, allowing drug loading either directly or through a nanocarrier, meanwhile solving solubility problems of hydrophobic drugs. Secondly, HA-based nanoassemblies was reported to improve pharmacokinetic properties of drugs, for example extending blood plasma half-life, slowing the clearance mechanism, and thus presenting a similar stealth effect to PEG.[248] Regarding anticancer therapy HA has attracted significant attention due to the possibility of active tumor targeting.[263–265] Thanks to the well-known enhanced permeation and retention (EPR) effect, nanosized polymeric assemblies can improve drug distribution at tumor site. Furthermore, since CD_{44} receptor is overexpressed in tumor cells, active delivery of drug to targeted tumor cells may be improved by CD_{44} mediated endocytosis, thus enhanced cellular uptake of HA-based nanocarriers. This CD_{44} receptor-mediated endocytosis also might attribute to overcome the multidrug resistance (MDR) effect by modulating the activity of P-glycoprotein (a class of transporter relate to the efflux transmembrane).[266]

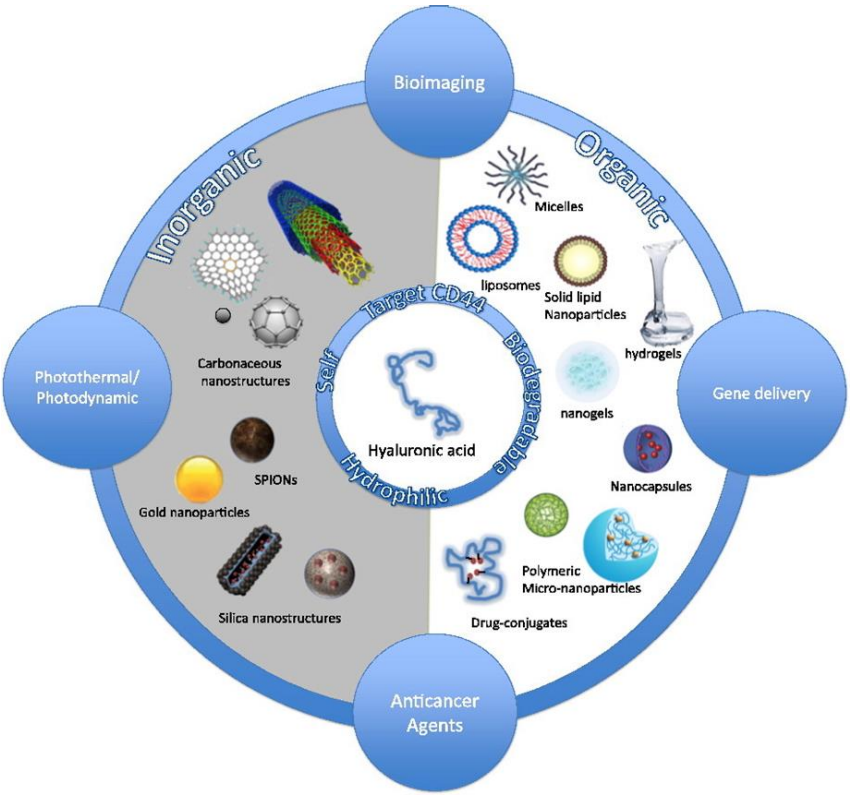

Figure 20. *Applications of organic or inorganic HA-based nanoformations.*[259]

Thanks to the structural versatility of HA, a variety of examples of modified HA derivatives have been reported for developing HA-based self-assemblies and hydrogels.[267,268] As an attractive material for the construction of hydrogels, HA-based hydrogels with diverse architecture, tunable viscoelasticity, unique anisotropy and desired bioactivity have been synthesized and characterized. Physical entrapment or covalent integration of hydrogels in a secondary HA network give rise to hybrid networks that are hierarchically structured and mechanically robust, capable of deliver cells and therapeutic agents for tissue repair and regeneration.[269–271]

3.2.2 Dextran

Dextran is a branched PS consisting of glucose units, which in the main chain are connected through α-1,6-glycosidic bonds, while all branches begin with α-1,3 linkages. Dextran have been used for more than 50 years for plasma volume expansion, peripheral flow promotion, and as antithrombolytic agents. Beside, dextran also have been investigated as starting material for the construction of drug delivery nanocarriers.[272] As a non-ionic PS, dextran can not only dissolve in water but also in organic solvents like DMSO, making it easier to select compatible solvent for both dextran and hydrophobic molecules when synthesizing amphiphilic dextran

derivatives.[87,273] Also, dextran has showed particularly resistant to some protein adsorptions, thus prolonged half life time.[272]

3.2.3 Chitosan

Chitosan is derived from chitin by a process of deacetylation, comprising of β-1,4 linked d-glucosamine and *N*-acetyl-d-glucosamine units.[274,275] As a unique alkaline polysaccharide in nature, cationic chitosan exerts advantages as a desirable nanocarrier due to the enhanced adhesion to the negatively charged mucosal surface by electrostatic interaction, resulting in the improvement on drug internalization into cells.[276,277] On the other hand, this cationic property of chitosan also makes chitosan suitable carrier for complexing and condensing negatively charged anionic nucleic acids, protecting from degradation by nuclease in serum, therefore achieving efficient gene therapy.[278,279] The major obstacle for its application is chitosan only soluble in an aqueous acidic medium but not at neutral pH, which may lead to aggregation or precipitation when chitosan is not sufficiently protonated.[280] To solve this problem, chitosan has been hydrophilically modified, for example, glycol chitosan[281] and PEG-chitosan,[282] which can also be further attached with hydrophobic moieties to yield amphiphiles.[283]

3.3 Synthesis of polysaccharide-based amphiphiles

Regarding to the synthesis of PSs-based amphiphiles, which is typically based on the conjugation of hydrophobic moieties to PSs, can be also classified into three approaches: (i) polysaccharide-drug complex; (ii) polysaccharide-based graft copolymer; (iii) polysaccharide-based block copolymers.

3.3.1 Polysaccharide-drug complex

Small drug molecules can be directly grafted to PS backbones *via* coupling reactions, as long as they are reactive towards the functional groups (hydroxyl, amine, carboxylic acid groups) on PS chains.[284] If not, linkers are required onto either the PS or the drug.

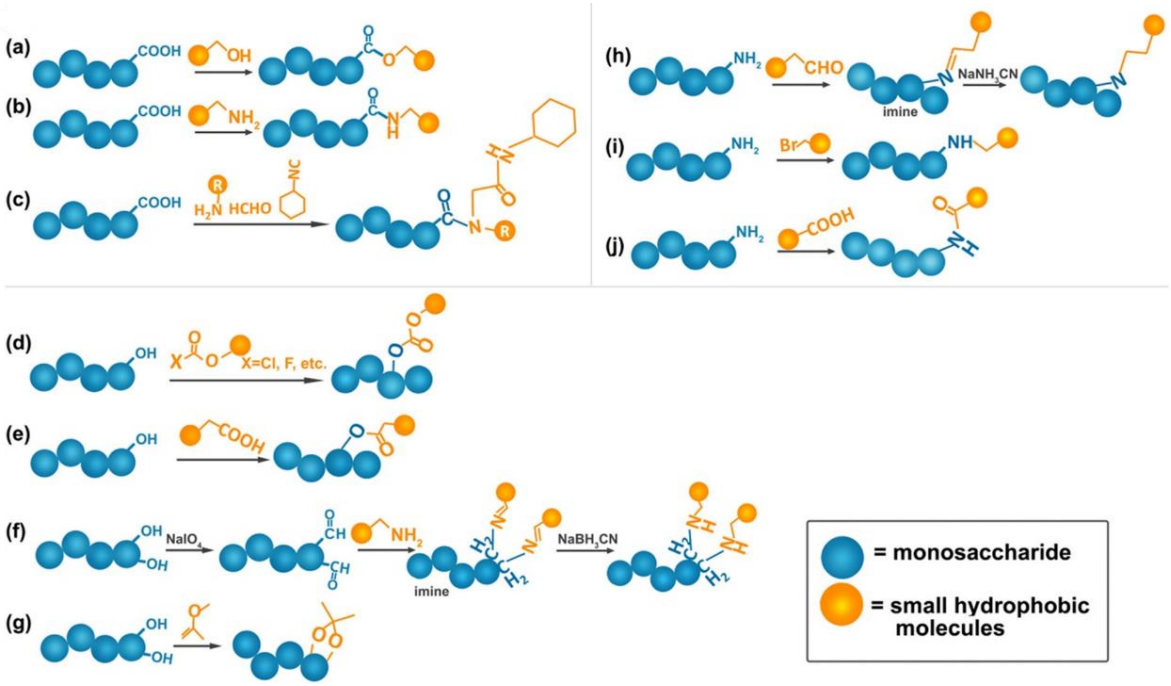

Figure 21. *Methodologies of grafting different small hydrophobic molecules to PS backbones. Representative reactions for grafting small hydrophobic molecules to PS chains based on carboxyl (a–c), hydroxyl (d–g) and amine groups (h–j).*[285]

Typical reactions of hydroxyl groups mainly include esterification and etherification in the presence of carboxylates, alcohols or chloroformate agents (Figure 21d-g). For example, Elschner et al. applied different type of chloroformate to synthesize dextran alkyl carbonates.[286] Chen's group developed pH-sensitive prodrug dextran-graft-Dox via esterification of hydroxyl groups of dextran with the carboxylic groups of cis-aconitic anhydride-modified Dox, using EDC/DMAP as coupling agents.[287] Another reported strategy for hydroxyl modification is the oxidation of vicinal hydroxyl groups of PSs with $NaIO_4$ or peroxides, which can generate two aldehyde groups. Adopting this method, a wide variety of amines can be introduced by imine formation or reductive-amination onto PSs.[94] Generally, the amine groups in PSs also can be alkylated or acylated by reductive amination or amidation *via* a nucleophilic substitution mechanism (Figure 21h-j). The carboxylic groups on certain PS backbones (e.g., HA, and heparin) provide opportunities for esterification and amidation in the presence of coupling agents, for example carbodiimides/DMAP and *N*-hydroxysuccinimide/HOBT (Figure 21a-c). Besides, Ugi condensation has been utilized to form a bis-amide from carboxylic group of PSs together with a ketone (or aldehyde), an amine, and an isocyanide.[287]

3.3.2 Polysaccharide-based graft copolymers

Polymer-grafted polysaccharides with controllable functions were reported to be well-suited for different kinds of biomedical applications. Versatile functionalization of polysaccharides *via* polymer grafts has been well-reviewed.[288] Briefly, there are mainly three strategies for preparing polymer-grafted polysaccharides with satisfactory biocharacteristics. Firstly, functionalized polysaccharides with diverse grafts can be flexibly and effectively achieved by living radical polymerization (LRP).[289,290] The introduced grafts include cationic components for nuclei acid delivery, PEGylated and zwitterionic moieties for shielding effects, and functional species for bioimaging applications as well as bioresponsive drug release applications. Secondly, biodegradable polymer-grafted polysaccharides can prepared by ring-opening polymerization (ROP).[291] The amine-functionalized polysaccharides was applied to trigger ROP of amino acids.[292,293] A series of poly(amino acid)-grafted polysaccharides with advanced structures (including linear, star-shaped, and comb-shaped copolymers) were developed to study and optimize the structural effects. Besides, biodegradable polyester-grafted polysaccharides were prepared and utilized for drug delivery.[294,295] Another emerging strategy was to conjugate of preformed polymers onto PS backbones. A variety of synthesized polymers (e.g., PLA, PCL, PLGA)[296–299] can be grafted to PS chains *via* condensation or "click" reactions.[300,301]

3.3.3 Polysaccharide-based block copolymers

The preparation of PS-based amphiphilic block copolymers emerge as an efficient and facile avenue to a wide variety of PSs-based amphiphiles. Compared with grafted PS derivatives, these PS-containing hybrid block copolymers may fully preserve the integrity of the two blocks.[302] To obtain blocks of synthetic polymers in combination with those of PS, there are typically two routes: (i) polymerizing monomers at the functional end of a PS block; (ii) "end-to-end coupling" of PS blocks with preformed polymer. To apply the first approach, the functional end of PS needs to firstly functionalized with monomers, for example, ε-caprolactone[303] and styrene[304,305] have been polymerized *via* ROP or LRP.

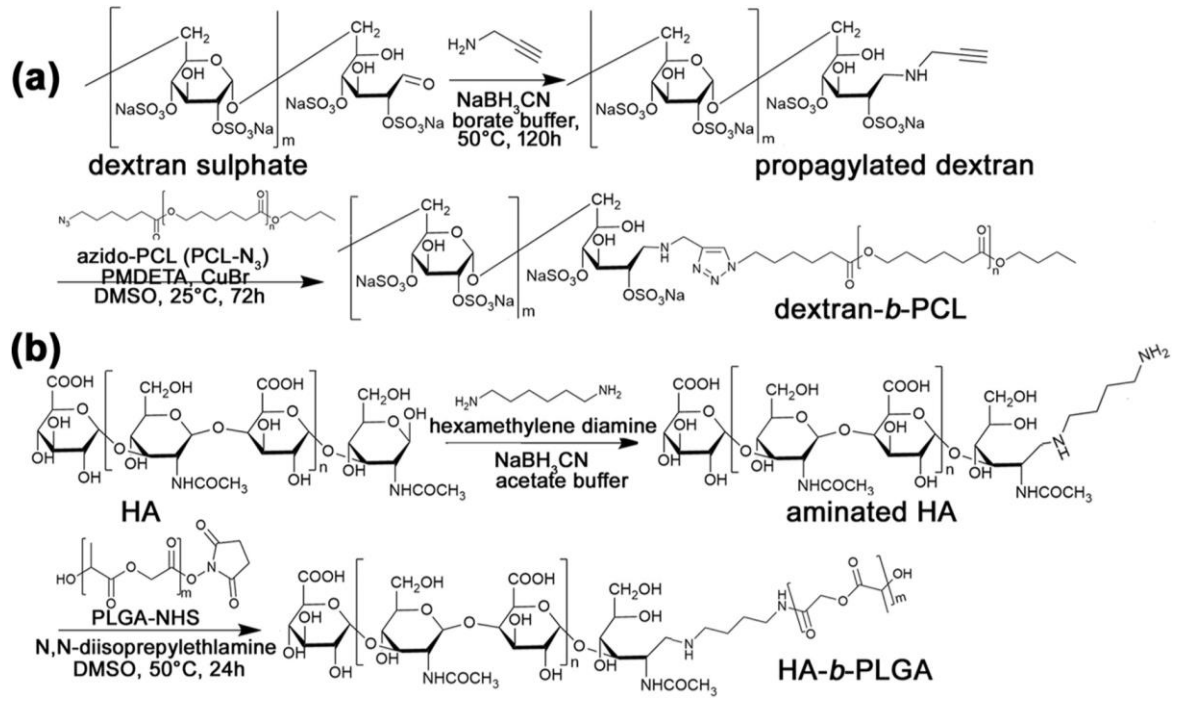

Figure 22. *Block copolymers via "end-to-end" coupling strategy (a) click reaction*[306]*; (b) reductive amination.*[307]

The reducing end of PSs can be useful sites for chemoselective functionalization with azide and alkyne moieties. The end-functionalization methods basically based on small molecular conjugation which is discussed in the previous section. Azido- or alkynyl terminated PSs enable constructing PS-based block copolymer with a variety of hydrophobic blocks like PCL,[265,306,308,309] PLA,[310,311] PBLG[312–314] and PPDSM (poly(pyridyl disulfide methacrylate)[265] *via* click chemistry (Figure 22a).[301] Additionally, diamine linkers has been used to construct aminated PSs at the reducing end by reductive amination, thus allow further conjugation of hydrophobic block to the other end of the linker (Figure 22b).[113,307,315]

3.4 Self-assembly of polysaccharide-based amphiphiles

PSs-based amphiphiles can self-assemble into a variety of NPs with different structures (e.g., block copolymer micelles, polymersomes and nanogels), which can be classified into three categories depending on their nanostructures: (A) NPs with core-shell structure, (B) NPs with mixed hydrophilic and hydrophobic domains and (C) NPs with bi-layer capsule structure (Figure 23).[316]

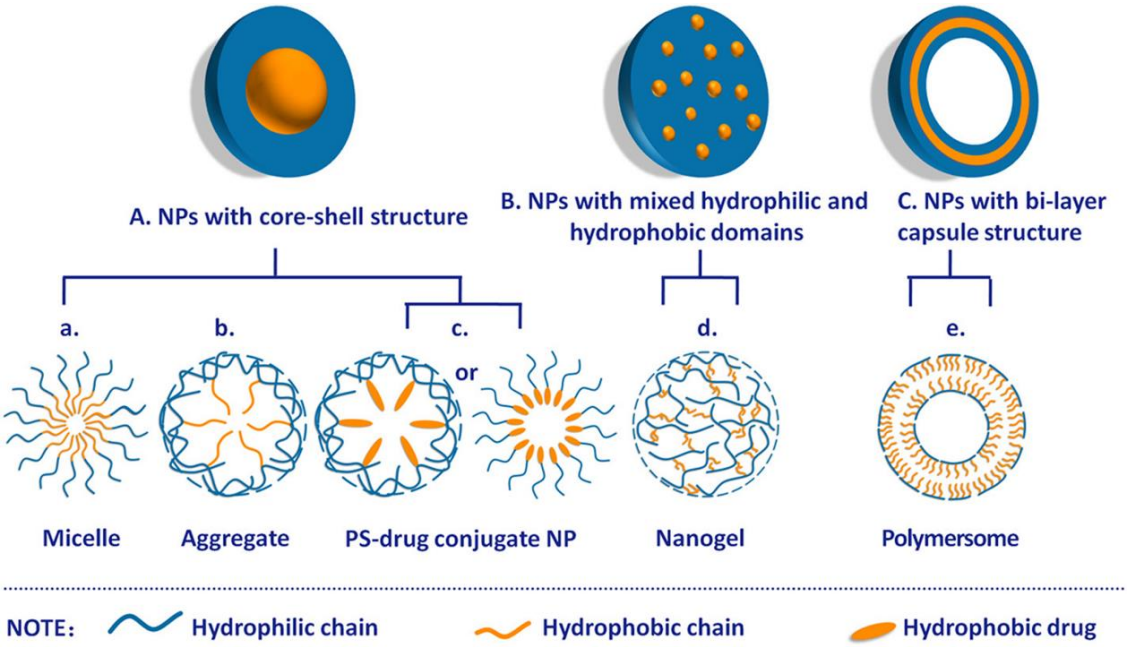

Figure 23. *Self-assembled NPs based on amphiphilic polysaccharide derivatives with different nanostructure.*[316]

A variety of methods have been adopted to facilitate the self-assembly of PS-based assemblies. Apparently, the efficiency of the process depends on the nature of the NPs. To prepare core-shell structured NPs (Figure 23A), the simple strategy is direct dispersion of the amphiphile in aqueous medium, or water-organic cosolvents followed by evaporation, sonication or dialysis to get rid of the organic solvent.[265,317,318] Other alternative process including emulsion[319,320] or double emulsion,[321] film casting,[322] also give core-shell structures. For polymersomes (Figure 23C), a solvent nanoprecipitation method has been commonly utilized.[323,324] Regading nanogels (Figure 23B), direct dissolution and dialysis have been most frequently employed.[325,326] Recently, microfluidic techniques are emerging as a promising tool to produce polysaccharide NPs in a well-controlled, reproducible, and high-throughput manner.[327]

3.5 Active targeting with polysaccharide-based carriers

Active targeting with polysaccharide-based carriers has gained significant attention as an attractive approach to deliver bioactives to specific cell or tissues. Specific saccharide molecules, such as lactose, galactose and mannose, are recognized by a vast array of receptors (e.g. lectins) present on a variety of cell surfaces (Figure 24A).[328] These interactions between saccharide and receptors can be utilized for PSs-mediated targeting by constructing the carrier surface with PSs, known as glycosylation.[329–331] Once glycosylated particles are bound to the

lectins or vice versa, receptor-mediated endocytosis occurs, thereafter the carriers are internalized by the cell.[332]

Glycosylation can also enable alternative dosage forms by adhering to tissues for localized delivery (Figure 24B).[333] PSs-mediated mucoadhesion and cytoadhesion allows for enhanced bioavailability, local accumulation, and efficacy.[334] Since there are relatively permeable membrane structures on site, drug delivery to the oral, nasal, or pulmonary mucosa is widely investigated.[335–337]

Due to the Warburg effect, glucose transporter proteins (GLUT) are overexpressed on human cancer cells and glucose and glucose substrate are internalized by GLUT.[338,339] Taking advantage of this aspect, glycan-conjugated prodrugs has been designed and applied to target cancer cell uptake *via* GLUT and release drug upon hydrolysis or triggers (Figure 24C).[340,341] As cancer cells rapidly internalize glucose, the glucosylated carriers promote malignant cell apoptosis by upregulating GLUT in a positive feedback mechanism, causing an increased uptake of the glycan-prodrug polymer.[342]

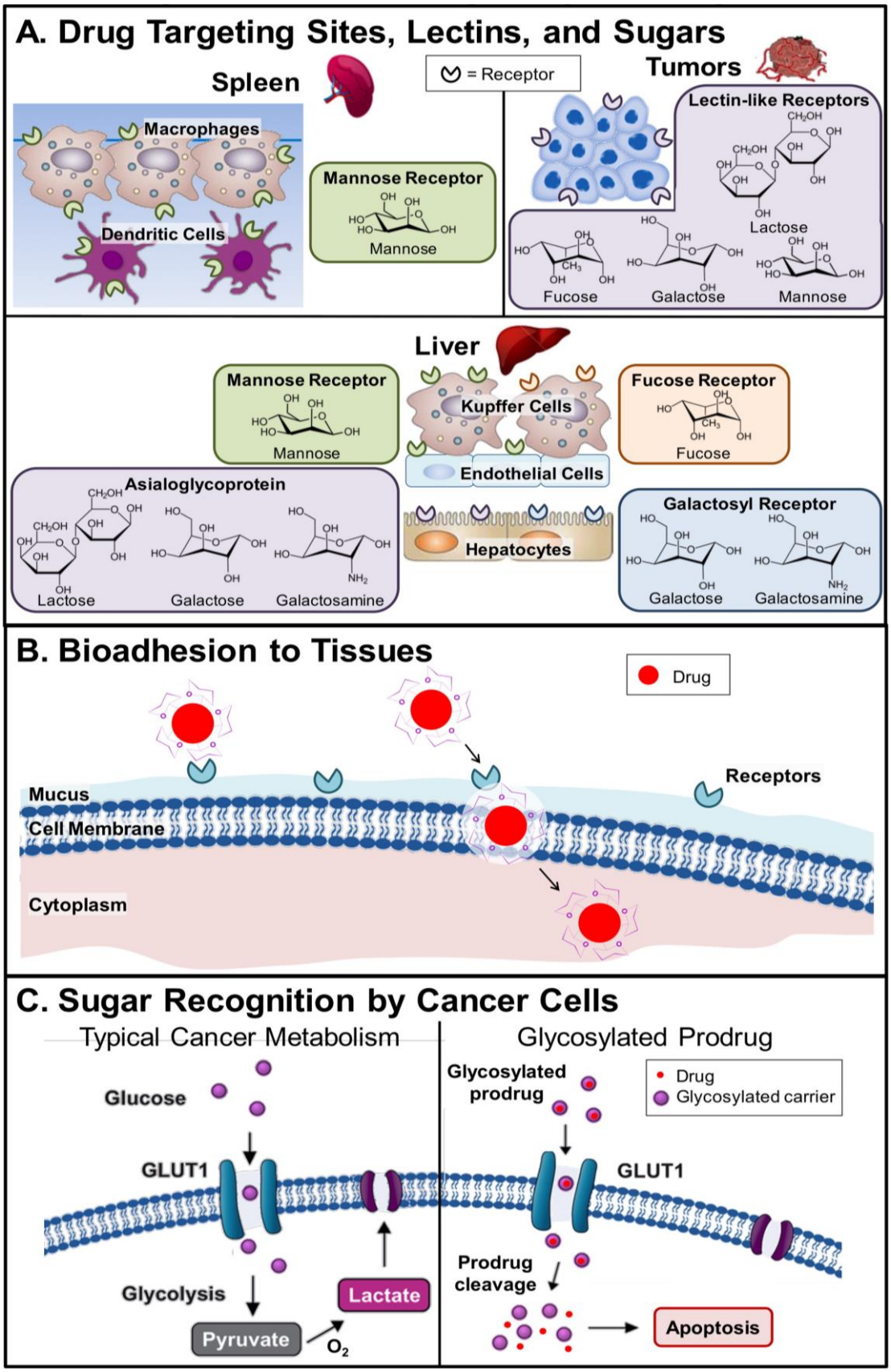

Figure 24. *Glycosylation enables a range of targeting strategies including (A)glycosylated drug carriers for tissue- and cell-specific interactions; (B) bioadhesion and/or mucoadhesion to tissues; (C) recognition as nutrients for cancer cell internalization.*[343]

3.6 Polysaccharide-*block*-polypeptide block copolymers and their biomedical applications

As a class of bio-inspired polymers like polysaccharides, polypeptides show considerable promise as building blocks for block copolymer. Polypeptides comprise a backbone which is inherently biocompatible and degradable, can exhibit different secondary structures. Containing two biocompatible and biodegradable polymers, polysaccharide-*block*-polypeptide block copolymers have attract special attention toward biomimetic and bioactive nanoparticles.

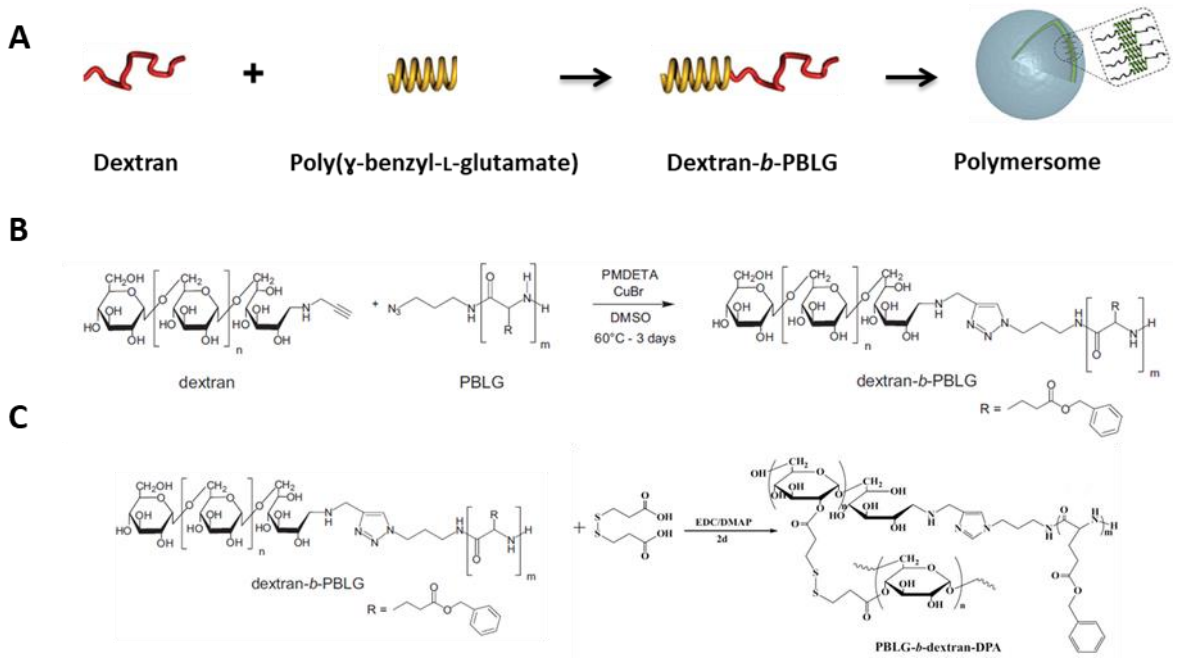

Figure 25. *(A) Schematic representation of preparation of dextran-b-PBLG polymersome; (B)Synthesis of dextran-b-PBLG; (C) Synthesis of redox-sensitive PBLG-b-dextran-DPA.*[87]

For instance, Lecommandoux's group synthesized amphiphilic polysaccharide-*block*-polypeptide copolymers by click chemistry from dextran end-functionalized with an alkyne group and poly(γ-benzyl-L-glutamate) end-functionalized with an azide group (Figure 25B). [87] The resulting dextran-*b*-PBLG block copolymers were able to self-assemble into small vesicles that mimic the structure of the viral capsid made of glycoproteins (Figure 25A). Accordingly, they further prepared hyaluronan-*block*-poly(γ-benzyl-L-glutamate) block copolymer (HA-*b*-PBLG), in which the α-helical structure of the PBLG was used to favor the formation of lamellar morphologies and HA displayed at the surface of the nanoparticles used to target specifically cancer cells overexpressing the CD_{44} receptors.[344]

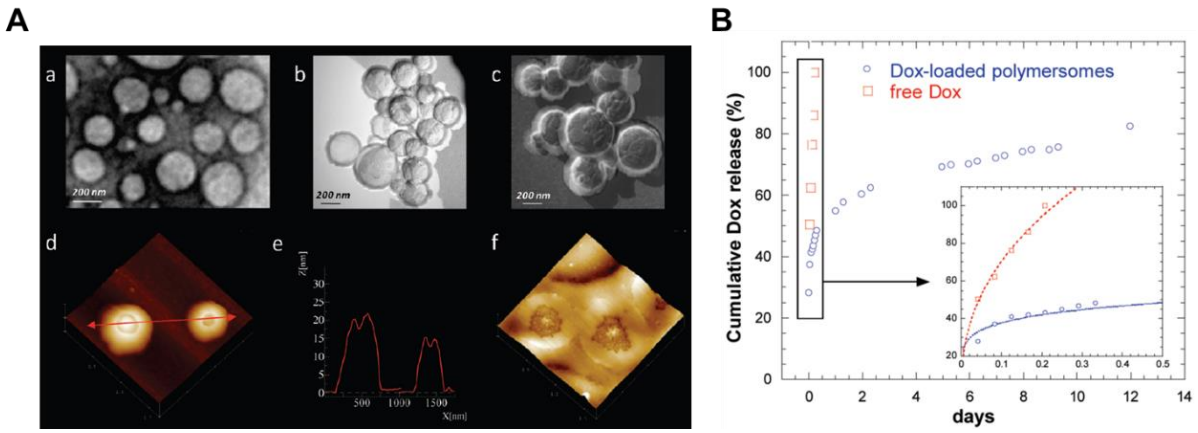

Figure 26. *(A) PBLG$_{23}$-b-HA$_{10}$ polymersomes imaging from (a) TEM, (b) freeze-fracture TEM, and (d) AFM. (e) Section from AFM image d. Doxoburicin loaded polymersomes observed by (c) freeze-fracture TEM and (f) AFM. (B) Release profile of free Dox and Dox-loaded polymersomes using a dialysis procedure. The same drug concentration was used (100 μg/mL) as free Dox or in Dox-loaded polymersomes (with an loading content of 12 wt %).*[323]

HA-*b*-PBLG can self-assemble into polymersomes and doxorubicin (Dox) was successfully loaded into polymersome (PolyDox) using nanoprecipitation method (Figure 25A). Flow cytometry data suggested high accumulation was found in high (MCF-7) than low (U87 cells) CD_{44} expressing cancer cell models, revealing that intracellular delivery of PolyDox was depended on the CD_{44} expression level in cells due to presence of HA on the surface of polymersomes.[324]. Subsequent in vivo study further demonstrated PolyDox enhanced intracellular uptake of doxorubicin in a murine model of Ehrlich Ascites Tumor (EAT) through CD_{44} receptor mediated endocytosis, resulting in prolonged Tumor Doubling Time and increase in life span of mice.[345] Another anticancer drug docetaxel (DOC) loaded HA-*b*-PBLG polymersome was also found uptake in Ehrlich Ascites Tumor (EAT) tumor bearing mice was larger at each time point compared to free drug.[346]

Interestingly, Zhang et al. developed shell crosslinked dextran-*b*-PBLG redox-responsive micelles by crosslinking of dextran with 3,3′-dithiodipropionic acid (DPA) (Figure 27C). Cytometry study of this shell crosslinked micelle (SCM) exhibit a faster drug release behavior in glutathione pretreated HeLa cells (Figure 27).[314] In another example, Li et al. synthesized a pH-sensitive, biodegradable, and biocompatible polysaccharide-*block*-polypeptide copolymer derivative Ac-Dex-*b*-PAsp(DET) is synthetized from acetal-modified dextran (Ac-Dex) and diethylenetriamine (DET) grafted poly(L-aspartic acid) PAsp(DET) by using click and aminolysis reaction. Acetal-modified dextran herein acted as a pH-sensitive hydrophobic block. This polysaccharide-*block*-polypeptide block copolymer can self-assemble into cationic

nanopaticles and did not result in significantly cytotoxicity to the cells, exhibited Ac-Dex-*b*-PAsp(DET) an ideal candidate for co-delivery of plasmid DNA and anticancer drug (Dox).[347]

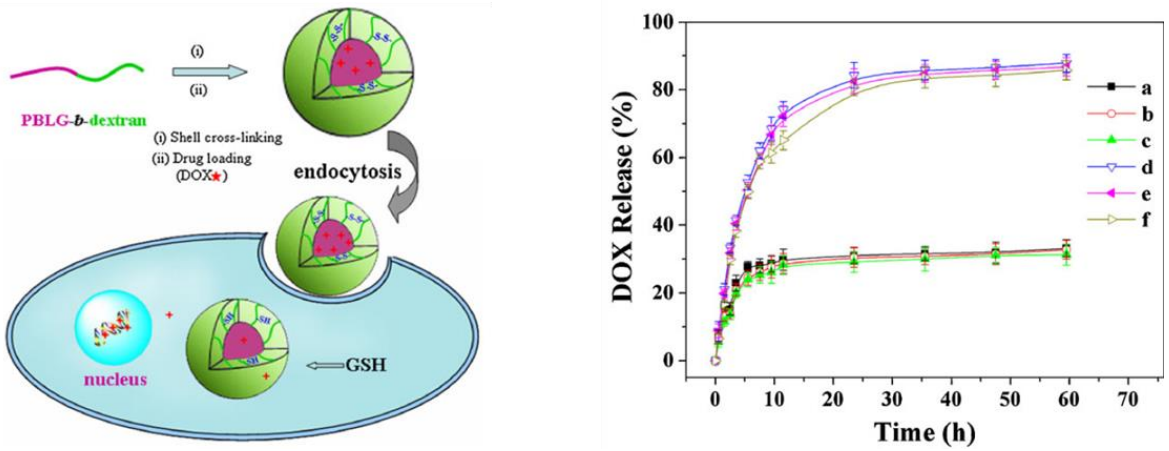

Figure 27. *In vitro Dox release from Dox-loaded SCM-1 (a), -2 (b), and -3 (c) without GSH, and SCM-1 (d), -2 (e), and -3 (f) with 0.010 M glutathione in PBS at pH = 7.4, 37 °C. Data are presented as mean ± standard deviation (n = 3).*[314]

CONCLUSION

With the rapid development of polymer science, nanotechnology and biochemistry, polymers have gained a worldwide interest in biomedical applications as the most versatile class of materials. A broad range of polymeric nanocarriers with various nanoformulations have been developed towards improving cancer therapy and some of them have already been approved by regulatory agency. Owing to the limitation of passive targeting *via* EPR effect, active targeting are one key consideration in the design of nanocarriers as tumor-targeted drug delivery systems. Polysaccharide-based block copolymers with originally bioactive properties emerge as a promising approach for targeted drug delivery.

Elastin-like polypeptides represent a class of well-defined biopolymers with very interesting features towards biomedical applications. Their thermos-responsive properties not only facilitate isolation and purification of ELPs, but also as a tool to control self-assembly behavior with tunable transition temperature. Post-translational chemical modifications of ELPs can be exploited to modulate T_t and enable further functionalization of ELPs. However, only a few studies have reported. Thus, there is still a need to develop chemoselective modification methods on ELPs, especially under physiological conditions.

Combining polysaccharides and ELPs into block copolymers would take advantage of the biological properties of both polysaccharides and ELPs, which may give rise to materials with bioactive and stimuli-responsive properties especially interesting for biomedical applications.

REFERENCES

(1) Duncan, R. The Dawning Era of Polymer Therapeutics. *Nat. Rev. Drug Discov.* **2003**, *2* (5), 347–360. https://doi.org/10.1038/nrd1088.

(2) Ventola, C. L. Progress in Nanomedicine: Approved and Investigational Nanodrugs. *P T* **2017**, *42* (12), 742–755.

(3) Park, J. H.; Lee, S.; Kim, J. H.; Park, K.; Kim, K.; Kwon, I. C. Polymeric Nanomedicine for Cancer Therapy. *Prog. Polym. Sci.* **2008**, *33* (1), 113–137. https://doi.org/10.1016/j.progpolymsci.2007.09.003.

(4) Duncan, R.; Vicent, M. J. Polymer Therapeutics-Prospects for 21st Century: The End of the Beginning. *Adv. Drug Deliv. Rev.* **2013**, *65* (1), 60–70. https://doi.org/10.1016/j.addr.2012.08.012.

(5) Guo, X.; Wang, L.; Wei, X.; Zhou, S. Polymer-Based Drug Delivery Systems for Cancer Treatment. *J. Polym. Sci. Part A Polym. Chem.* **2016**, *54* (22), 3525–3550. https://doi.org/10.1002/pola.28252.

(6) Duncan, R. Polymer Therapeutics: Top 10 Selling Pharmaceuticals - What Next? *J. Control. Release* **2014**, *190*, 371–380. https://doi.org/10.1016/j.jconrel.2014.05.001.

(7) Kumari, P.; Ghosh, B.; Biswas, S. Nanocarriers for Cancer-Targeted Drug Delivery. *J. Drug Target.* **2016**, *24* (3), 179–191. https://doi.org/10.3109/1061186X.2015.1051049.

(8) Fleige, E.; Quadir, M. A.; Haag, R. Stimuli-Responsive Polymeric Nanocarriers for the Controlled Transport of Active Compounds: Concepts and Applications. *Adv. Drug Deliv. Rev.* **2012**, *64* (9), 866–884. https://doi.org/10.1016/j.addr.2012.01.020.

(9) Liu, D.; Yang, F.; Xiong, F.; Gu, N. The Smart Drug Delivery System and Its Clinical Potential. *Theranostics* **2016**, *6* (9), 1306–1323. https://doi.org/10.7150/thno.14858.

(10) Cabane, E.; Zhang, X.; Langowska, K.; Palivan, C. G.; Meier, W. Stimuli-Responsive Polymers and Their Applications in Nanomedicine. *Biointerphases* **2012**, *7* (1), 9. https://doi.org/10.1007/s13758-011-0009-3.

(11) Hu, X.; Zhang, Y.; Xie, Z.; Jing, X.; Bellotti, A.; Gu, Z. Stimuli-Responsive Polymersomes for Biomedical Applications. *Biomacromolecules* **2017**, *18* (3), 649–673. https://doi.org/10.1021/acs.biomac.6b01704.

(12) Jatzkewitz, H. Peptamin (Glycyl-L-Leucyl-Mescaline) Bound to Blood Plasma Expander (Polyvinylpyrrolidone) as a New Depot Form of a Biologically Active Primary Amine (Mescaline). *Z. Naturforsch.* **1955**, *10* (b), 27–31.

(13) Ringsdorf, H. Structure and Properties of Pharmacologically Active Polymers. *J. Polym. Sci. Polym. Symp.* **2007**, *51* (1), 135–153. https://doi.org/10.1002/polc.5070510111.

(14) Kopeček, J.; Kopečková, P. HPMA Copolymers: Origins, Early Developments, Present, and Future☆. *Adv. Drug Deliv. Rev.* **2010**, *62* (2), 122–149. https://doi.org/10.1016/j.addr.2009.10.004.

(15) Raval, N.; Kalyane, D.; Maheshwari, R.; Tekade, R. K. Copolymers and Block Copolymers in Drug Delivery and Therapy. In *Basic Fundamentals of Drug Delivery*; Elsevier, 2019; pp 173–201. https://doi.org/10.1016/B978-0-12-817909-3.00005-4.

(16) Cabral, H.; Miyata, K.; Osada, K.; Kataoka, K. Block Copolymer Micelles in Nanomedicine Applications. *Chem. Rev.* **2018**, *118* (14), 6844–6892. https://doi.org/10.1021/acs.chemrev.8b00199.

(17) Meng, J.; Agrahari, V.; Youm, I. Advances in Targeted Drug Delivery Approaches for the Central Nervous System Tumors: The Inspiration of Nanobiotechnology. *J. Neuroimmune Pharmacol.* **2017**, *12* (1), 84–98. https://doi.org/10.1007/s11481-016-9698-1.

(18) Sarkar, B.; Alexandridis, P. Block Copolymer-Nanoparticle Composites: Structure, Functional Properties, and Processing. *Prog. Polym. Sci.* **2015**, *40* (1), 33–62. https://doi.org/10.1016/j.progpolymsci.2014.10.009.

(19) Hoheisel, T. N.; Hur, K.; Wiesner, U. B. Block Copolymer-Nanoparticle Hybrid Self-Assembly. *Prog. Polym. Sci.* **2015**, *40* (1), 3–32. https://doi.org/10.1016/j.progpolymsci.2014.10.002.

(20) Kutikov, A. B.; Song, J. Biodegradable PEG-Based Amphiphilic Block Copolymers for Tissue Engineering Applications. *ACS Biomater. Sci. Eng.* **2015**, *1* (7), 463–480. https://doi.org/10.1021/acsbiomaterials.5b00122.

(21) Wang, J.-Z.; You, M.-L.; Ding, Z.-Q.; Ye, W.-B. A Review of Emerging Bone Tissue Engineering via PEG Conjugated Biodegradable Amphiphilic Copolymers. *Mater. Sci. Eng. C* **2019**, *97*, 1021–1035. https://doi.org/10.1016/j.msec.2019.01.057.

(22) Grossen, P.; Witzigmann, D.; Sieber, S.; Huwyler, J. PEG-PCL-Based Nanomedicines: A Biodegradable Drug Delivery System and Its Application. *J. Control. Release* **2017**, *260*, 46–60. https://doi.org/10.1016/j.jconrel.2017.05.028.

(23) Kolate, A.; Baradia, D.; Patil, S.; Vhora, I.; Kore, G.; Misra, A. PEG — A Versatile Conjugating Ligand for Drugs and Drug Delivery Systems. *J. Control. Release* **2014**, *192*, 67–81. https://doi.org/10.1016/j.jconrel.2014.06.046.

(24) Zhang, K.; Tang, X.; Zhang, J.; Lu, W.; Lin, X.; Zhang, Y.; Tian, B.; Yang, H.; He, H. PEG–PLGA Copolymers: Their Structure and Structure-Influenced Drug Delivery Applications. *J. Control. Release* **2014**, *183*, 77–86. https://doi.org/10.1016/j.jconrel.2014.03.026.

(25) Pasut, G.; Veronese, F. M. PEG Conjugates in Clinical Development or Use as Anticancer Agents: An Overview. *Adv. Drug Deliv. Rev.* **2009**, *61* (13), 1177–1188. https://doi.org/10.1016/j.addr.2009.02.010.

(26) Roberts, M. J.; Bentley, M. D.; Harris, J. M. Chemistry for Peptide and Protein PEGylation. *Adv. Drug Deliv. Rev.* **2012**, *64*, 116–127. https://doi.org/10.1016/j.addr.2012.09.025.

(27) Li, C. Poly(l-Glutamic Acid)–Anticancer Drug Conjugates. *Adv. Drug Deliv. Rev.* **2002**, *54* (5), 695–713. https://doi.org/10.1016/S0169-409X(02)00045-5.

(28) Bajaj, I.; Singhal, R. Poly (Glutamic Acid) – An Emerging Biopolymer of Commercial Interest. *Bioresour. Technol.* **2011**, *102* (10), 5551–5561. https://doi.org/10.1016/j.biortech.2011.02.047.

(29) Schöttner, S.; Schaffrath, H.-J.; Gallei, M. Poly(2-Hydroxyethyl Methacrylate)-Based Amphiphilic Block Copolymers for High Water Flux Membranes and Ceramic Templates. *Macromolecules* **2016**, *49* (19), 7286–7295. https://doi.org/10.1021/acs.macromol.6b01803.

(30) Weaver, J. V. M.; Bannister, I.; Robinson, K. L.; Bories-Azeau, X.; Armes, S. P.; Smallridge, M.; McKenna, P. Stimulus-Responsive Water-Soluble Polymers Based on 2-Hydroxyethyl Methacrylate. *Macromolecules* **2004**, *37* (7), 2395–2403. https://doi.org/10.1021/ma0356358.

(31) Basu, A.; Kunduru, K. R.; Doppalapudi, S.; Domb, A. J.; Khan, W. Poly(Lactic Acid) Based Hydrogels. *Adv. Drug Deliv. Rev.* **2016**, *107*, 192–205. https://doi.org/10.1016/j.addr.2016.07.004.

(32) Raquez, J.-M.; Habibi, Y.; Murariu, M.; Dubois, P. Polylactide (PLA)-Based Nanocomposites. *Prog. Polym. Sci.* **2013**, *38* (10–11), 1504–1542. https://doi.org/10.1016/j.progpolymsci.2013.05.014.

(33) James, R.; Manoukian, O. S.; Kumbar, S. G. Poly(Lactic Acid) for Delivery of Bioactive Macromolecules. *Adv. Drug Deliv. Rev.* **2016**, *107*, 277–288. https://doi.org/10.1016/j.addr.2016.06.009.

(34) Woodruff, M. A.; Hutmacher, D. W. The Return of a Forgotten Polymer—Polycaprolactone in the 21st Century. *Prog. Polym. Sci.* **2010**, *35* (10), 1217–1256. https://doi.org/10.1016/j.progpolymsci.2010.04.002.

(35) Dash, T. K.; Konkimalla, V. B. Polymeric Modification and Its Implication in Drug Delivery: Poly-ε-Caprolactone (PCL) as a Model Polymer. *Mol. Pharm.* **2012**, *9* (9), 2365–2379. https://doi.org/10.1021/mp3001952.

(36) Dargaville, B. L.; Vaquette, C.; Peng, H.; Rasoul, F.; Chau, Y. Q.; Cooper-White, J. J.; Campbell, J. H.; Whittaker, A. K. Cross-Linked Poly(Trimethylene Carbonate- Co - l -Lactide) as a Biodegradable, Elastomeric Scaffold for Vascular Engineering Applications. *Biomacromolecules* **2011**, *12* (11), 3856–3869. https://doi.org/10.1021/bm201291e.

(37) Li, X.; Mignard, N.; Taha, M.; Prochazka, F.; Chen, J.; Zhang, S.; Becquart, F. Thermoreversible Supramolecular Networks from Poly(Trimethylene Carbonate) Synthesized by Condensation with Triuret and Tetrauret. *Macromolecules* **2019**, acs.macromol.9b00585. https://doi.org/10.1021/acs.macromol.9b00585.

(38) Sanson, C.; Schatz, C.; Le Meins, J.-F.; Brûlet, A.; Soum, A.; Lecommandoux, S. Biocompatible and Biodegradable Poly(Trimethylene Carbonate)- b -Poly(l -Glutamic Acid) Polymersomes: Size Control and Stability. *Langmuir* **2010**, *26* (4), 2751–2760. https://doi.org/10.1021/la902786t.

(39) Bray, F.; Ferlay, J.; Soerjomataram, I.; Siegel, R. L.; Torre, L. A.; Jemal, A. Global Cancer Statistics 2018: GLOBOCAN Estimates of Incidence and Mortality Worldwide for 36 Cancers in 185 Countries. *CA. Cancer J. Clin.* **2018**, *68* (6), 394–424. https://doi.org/10.3322/caac.21492.

(40) Arroyo-Crespo, J. J.; Armiñán, A.; Charbonnier, D.; Balzano-Nogueira, L.; Huertas-López, F.; Martí, C.; Tarazona, S.; Forteza, J.; Conesa, A.; Vicent, M. J. Tumor Microenvironment-Targeted Poly-L-Glutamic Acid-Based Combination Conjugate for Enhanced Triple Negative Breast Cancer Treatment. *Biomaterials* **2018**, *186*, 8–21. https://doi.org/10.1016/j.biomaterials.2018.09.023.

(41) Chauhan, V. P.; Chen, I. X.; Tong, R.; Ng, M. R.; Martin, J. D.; Naxerova, K.; Wu, M. W.; Huang, P.; Boucher, Y.; Kohane, D. S.; et al. Reprogramming the Microenvironment with Tumor-Selective Angiotensin Blockers Enhances Cancer Immunotherapy. *Proc. Natl. Acad. Sci.* **2019**, *116* (22), 10674–10680. https://doi.org/10.1073/pnas.1819889116.

(42) Binnewies, M.; Roberts, E. W.; Kersten, K.; Chan, V.; Fearon, D. F.; Merad, M.; Coussens, L. M.; Gabrilovich, D. I.; Ostrand-Rosenberg, S.; Hedrick, C. C.; et al. Understanding the Tumor Immune Microenvironment (TIME) for Effective Therapy. *Nat. Med.* **2018**, *24* (5), 541–550. https://doi.org/10.1038/s41591-018-0014-x.

(43) Grund, S.; Bauer, M.; Fischer, D. Polymers in Drug Delivery-State of the Art and Future Trends. *Adv. Eng. Mater.* **2011**, *13* (3), B61–B87. https://doi.org/10.1002/adem.201080088.

(44) Sriraman, S. K.; Aryasomayajula, B.; Torchilin, V. P. Barriers to Drug Delivery in Solid Tumors. *Tissue Barriers* **2014**, *2* (3), e29528. https://doi.org/10.4161/tisb.29528.

(45) Nizzero, S.; Ziemys, A.; Ferrari, M. Transport Barriers and Oncophysics in Cancer Treatment. *Trends in Cancer* **2018**, *4* (4), 277–280. https://doi.org/10.1016/j.trecan.2018.02.008.

(46) Groothuis, D. R. The Blood-Brain and Blood-Tumor Barriers: A Review of Strategies for Increasing Drug Delivery. *Neuro. Oncol.* **2000**, *2* (1), 45–59. https://doi.org/10.1093/neuonc/2.1.45.

(47) Elsabahy, M.; Wooley, K. L. Design of Polymeric Nanoparticles for Biomedical Delivery Applications. *Chem. Soc. Rev.* **2012**, *41* (7), 2545. https://doi.org/10.1039/c2cs15327k.

(48) Fang, J.; Nakamura, H.; Maeda, H. The EPR Effect: Unique Features of Tumor Blood Vessels for Drug Delivery, Factors Involved, and Limitations and Augmentation of the Effect. *Adv. Drug Deliv. Rev.* **2011**, *63* (3), 136–151. https://doi.org/10.1016/j.addr.2010.04.009.

(49) Danhier, F. To Exploit the Tumor Microenvironment: Since the EPR Effect Fails in the Clinic, What Is the Future of Nanomedicine? *J. Control. Release* **2016**, *244*, 108–121. https://doi.org/10.1016/j.jconrel.2016.11.015.

(50) Golombek, S. K.; May, J.-N.; Theek, B.; Appold, L.; Drude, N.; Kiessling, F.; Lammers, T. Tumor Targeting via EPR: Strategies to Enhance Patient Responses. *Adv. Drug Deliv. Rev.* **2018**, *130*, 17–38. https://doi.org/10.1016/j.addr.2018.07.007.

(51) Ali, Y.; Alqudah, A.; Ahmad, S.; Abd Hamid, S.; Farooq, U. Macromolecules as Targeted Drugs Delivery Vehicles: An Overview. *Des. Monomers Polym.* **2019**, *22* (1), 91–97. https://doi.org/10.1080/15685551.2019.1591681.

(52) Ulbrich, K.; Holá, K.; Šubr, V.; Bakandritsos, A.; Tuček, J.; Zbořil, R. Targeted Drug Delivery with Polymers and Magnetic Nanoparticles: Covalent and Noncovalent Approaches, Release Control, and Clinical Studies. *Chem. Rev.* **2016**, *116* (9), 5338–5431. https://doi.org/10.1021/acs.chemrev.5b00589.

(53) Peer, D.; Karp, J. M.; Hong, S.; Farokhzad, O. C.; Margalit, R.; Langer, R. Nanocarriers as an Emerging Platform for Cancer Therapy. *Nat. Nanotechnol.* **2007**, *2* (12), 751–760. https://doi.org/10.1038/nnano.2007.387.

(54) Li, C.; Wallace, S. Polymer-Drug Conjugates: Recent Development in Clinical Oncology. *Adv. Drug Deliv. Rev.* **2008**, *60* (8), 886–898. https://doi.org/10.1016/j.addr.2007.11.009.

(55) Ekladious, I.; Colson, Y. L.; Grinstaff, M. W. Polymer–Drug Conjugate Therapeutics: Advances, Insights and Prospects. *Nat. Rev. Drug Discov.* **2019**, *18* (4), 273–294. https://doi.org/10.1038/s41573-018-0005-0.

(56) Larson, N.; Ghandehari, H. Polymeric Conjugates for Drug Delivery. *Chem. Mater.* **2012**, *24* (5), 840–853. https://doi.org/10.1021/cm2031569.

(57) Seifu, M. F.; Nath, L. K. Polymer-Drug Conjugates: Novel Carriers for Cancer Chemotherapy. *Polym. Technol. Mater.* **2019**, *58* (2), 158–171. https://doi.org/10.1080/03602559.2018.1466172.

(58) Kataoka, K.; Harada, A.; Nagasaki, Y. Block Copolymer Micelles for Drug Delivery: Design, Characterization and Biological Significance. *Adv. Drug Deliv. Rev.* **2012**, *64* (SUPPL.), 37–48. https://doi.org/10.1016/j.addr.2012.09.013.

(59) Lee, J. S.; Feijen, J. Polymersomes for Drug Delivery: Design, Formation and Characterization. *J. Control. Release* **2012**, *161* (2), 473–483. https://doi.org/10.1016/j.jconrel.2011.10.005.

(60) Anajafi, T.; Mallik, S. Polymersome-Based Drug-Delivery Strategies for Cancer Therapeutics. *Ther. Deliv.* **2015**, *6* (4), 521–534. https://doi.org/10.4155/tde.14.125.

(61) Lee, J. S. *Biodegradable Polymersomes for Drug Delivery : Circulation Kinetics and Biodistribution, Modulated Drug Delivery and Cellular Uptake*; 2011.

(62) Huang, J.; Bonduelle, C.; Thévenot, J.; Lecommandoux, S.; Heise, A. Biologically Active Polymersomes from Amphiphilic Glycopeptides. *J. Am. Chem. Soc.* **2012**, *134* (1), 119–122. https://doi.org/10.1021/ja209676p.

(63) Schmutz, M.; Salva, R.; Meins, L.; Sandre, O.; Br, A.; Guenoun, P. Polymersome Shape Transformation at the Nanoscale. *ACS Nano* **2013**, *7* (10), 9298–9311.

(64) Mukalel, A. J.; Riley, R. S.; Zhang, R.; Mitchell, M. J. Nanoparticles for Nucleic Acid Delivery: Applications in Cancer Immunotherapy. *Cancer Lett.* **2019**, *458* (April), 102–112. https://doi.org/10.1016/j.canlet.2019.04.040.

(65) Zhao, H.; Lin, Z. Y.; Yildirimer, L.; Dhinakar, A.; Zhao, X.; Wu, J. Polymer-Based Nanoparticles for Protein Delivery: Design, Strategies and Applications. *J. Mater. Chem. B* **2016**, *4* (23), 4060–4071. https://doi.org/10.1039/c6tb00308g.

(66) Bobo, D.; Robinson, K. J.; Islam, J.; Thurecht, K. J.; Corrie, S. R. Nanoparticle-Based Medicines: A Review of FDA-Approved Materials and Clinical Trials to Date. *Pharm. Res.* **2016**, *33* (10), 2373–2387. https://doi.org/10.1007/s11095-016-1958-5.

(67) Yang, J.; Han, S.; Zheng, H.; Dong, H.; Liu, J. Preparation and Application of Micro/Nanoparticles Based on Natural Polysaccharides. *Carbohydr. Polym.* **2015**, *123*, 53–66. https://doi.org/10.1016/j.carbpol.2015.01.029.

(68) Alavi, M.; Karimi, N.; Safaei, M. Application of Various Types of Liposomes in Drug Delivery Systems. *Adv. Pharm. Bull.* **2017**, *7* (1), 3–9. https://doi.org/10.15171/apb.2017.002.

(69) Sercombe, L.; Veerati, T.; Moheimani, F.; Wu, S. Y.; Sood, A. K.; Hua, S. Advances and Challenges of Liposome Assisted Drug Delivery. *Front. Pharmacol.* **2015**, *6*. https://doi.org/10.3389/fphar.2015.00286.

(70) Palmerston Mendes, L.; Pan, J.; Torchilin, V. Dendrimers as Nanocarriers for Nucleic Acid and Drug Delivery in Cancer Therapy. *Molecules* **2017**, *22* (9), 1401. https://doi.org/10.3390/molecules22091401.

(71) Pandita, D.; Poonia, N.; Kumar, S.; Lather, V.; Madaan, K. Dendrimers in Drug Delivery and Targeting: Drug-Dendrimer Interactions and Toxicity Issues. *J. Pharm. Bioallied Sci.* **2014**, *6* (3), 139. https://doi.org/10.4103/0975-7406.130965.

(72) Alshehri, R.; Ilyas, A. M.; Hasan, A.; Arnaout, A.; Ahmed, F.; Memic, A. Carbon Nanotubes in Biomedical Applications: Factors, Mechanisms, and Remedies of Toxicity. *J. Med. Chem.* **2016**, *59* (18), 8149–8167. https://doi.org/10.1021/acs.jmedchem.5b01770.

(73) Bianco, A.; Kostarelos, K.; Prato, M. Applications of Carbon Nanotubes in Drug Delivery. *Curr. Opin. Chem. Biol.* **2005**, *9* (6), 674–679. https://doi.org/10.1016/j.cbpa.2005.10.005.

(74) Raphey, V. R.; Henna, T. K.; Nivitha, K. P.; Mufeedha, P.; Sabu, C.; Pramod, K. Advanced Biomedical Applications of Carbon Nanotube. *Mater. Sci. Eng. C* **2019**, *100*, 616–630. https://doi.org/10.1016/j.msec.2019.03.043.

(75) Ladj, R.; Bitar, A.; Eissa, M. M.; Fessi, H.; Mugnier, Y.; Le Dantec, R.; Elaissari, A. Polymer Encapsulation of Inorganic Nanoparticles for Biomedical Applications. *Int. J. Pharm.* **2013**, *458* (1), 230–241. https://doi.org/10.1016/j.ijpharm.2013.09.001.

(76) Mohammadpour, R.; Dobrovolskaia, M. A.; Cheney, D. L.; Greish, K. F.; Ghandehari, H. Subchronic and Chronic Toxicity Evaluation of Inorganic Nanoparticles for Delivery Applications. *Adv. Drug Deliv. Rev.* **2019**. https://doi.org/10.1016/j.addr.2019.07.006.

(77) Liu, Q.; Zhan, C.; Kohane, D. S. Phototriggered Drug Delivery Using Inorganic Nanomaterials. *Bioconjug. Chem.* **2017**, *28* (1), 98–104. https://doi.org/10.1021/acs.bioconjchem.6b00448.

(78) Gaspar, R.; Duncan, R. Polymeric Carriers: Preclinical Safety and the Regulatory Implications for Design and Development of Polymer Therapeutics. *Adv. Drug Deliv. Rev.* **2009**, *61* (13), 1220–1231. https://doi.org/10.1016/j.addr.2009.06.003.

(79) Eifler, A. C.; Thaxton, C. S. Nanoparticle Therapeutics: FDA Approval, Clinical Trials, Regulatory Pathways, and Case Study; 2011; pp 325–338. https://doi.org/10.1007/978-1-61779-052-2_21.

(80) Jones, A.-A. D.; Mi, G.; Webster, T. J. A Status Report on FDA Approval of Medical Devices Containing Nanostructured Materials. *Trends Biotechnol.* **2019**, *37* (2), 117–120. https://doi.org/10.1016/j.tibtech.2018.06.003.

(81) Berbel Manaia, E.; Paiva Abuçafy, M.; Chiari-Andréo, B. G.; Lallo Silva, B.; Oshiro-Júnior, J. A.; Chiavacci, L. Physicochemical Characterization of Drug Nanocarriers. *Int. J. Nanomedicine* **2017**, *Volume 12*, 4991–5011. https://doi.org/10.2147/IJN.S133832.

(82) Albanese, A.; Tang, P. S.; Chan, W. C. W. The Effect of Nanoparticle Size, Shape, and Surface Chemistry on Biological Systems. *Annu. Rev. Biomed. Eng.* **2012**, *14* (1), 1–16. https://doi.org/10.1146/annurev-bioeng-071811-150124.

(83) Pelegri-O'Day, E. M.; Lin, E.-W.; Maynard, H. D. Therapeutic Protein–Polymer Conjugates: Advancing Beyond PEGylation. *J. Am. Chem. Soc.* **2014**, *136* (41), 14323–14332. https://doi.org/10.1021/ja504390x.

(84) Singh, V.; Tiwari, M. Structure-Processing-Property Relationship of Poly(Glycolic Acid) for Drug Delivery Systems 1: Synthesis and Catalysis. *Int. J. Polym. Sci.* **2010**, *2010*, 1–23. https://doi.org/10.1155/2010/652719.

(85) Wang, Y.; Wang, P. G. Polysaccharide-Based Systems in Drug and Gene Delivery. *Adv. Drug Deliv. Rev.* **2013**, *65* (9), 1121–1122. https://doi.org/10.1016/j.addr.2013.07.001.

(86) Mizrahy, S.; Peer, D. Polysaccharides as Building Blocks for Nanotherapeutics. *Chem. Soc. Rev.* **2012**, *41* (7), 2623–2640. https://doi.org/10.1039/c1cs15239d.

(87) Schatz, C.; Louguet, S.; Meins, J. F. Le; Lecommandoux, S. Polysaccharide-Block-Polypeptide Copolymer Vesicles: Towards Synthetic Viral Capsids. *Angew. Chemie - Int. Ed.* **2009**, *48* (14), 2572–2575. https://doi.org/10.1002/anie.200805895.

(88) Elchinger, P. H.; Faugeras, P. A.; Boëns, B.; Brouillette, F.; Montplaisir, D.; Zerrouki, R.; Lucas, R. Polysaccharides: The "Click" Chemistry Impact. *Polymers (Basel).* **2011**, *3* (4), 1607–1651. https://doi.org/10.3390/polym3041607.

(89) Swierczewska, M.; Han, H. S. S.; Kim, K.; Park, J. H. H.; Lee, S. Polysaccharide-Based Nanoparticles for Theranostic Nanomedicine. *Adv. Drug Deliv. Rev.* **2016**, *99*, 70–84. https://doi.org/10.1016/j.addr.2015.11.015.

(90) Huh, M. S.; Lee, E. J.; Koo, H.; Yhee, J. Y.; Oh, K. S.; Son, S.; Lee, S.; Kim, S. H.; Kwon, I. C.; Kim, K. Polysaccharide-Based Nanoparticles for Gene Delivery. *Top. Curr. Chem.* **2017**, *375* (2), 1–19. https://doi.org/10.1007/s41061-017-0114-y.

(91) Zheng, Y.; Monty, J.; Linhardt, R. J. Polysaccharide-Based Nanocomposites and Their Applications. *Carbohydr. Res.* **2015**, *405*, 23–32. https://doi.org/10.1016/j.carres.2014.07.016.

(92) Saravanakumar, G.; Jo, D.-G.; H. Park, J. Polysaccharide-Based Nanoparticles: A Versatile Platform for Drug Delivery and Biomedical Imaging. *Curr. Med. Chem.* **2012**, *19* (19), 3212–3229. https://doi.org/10.2174/092986712800784658.

(93) Raemdonck, K.; Martens, T. F.; Braeckmans, K.; Demeester, J.; De Smedt, S. C. Polysaccharide-Based Nucleic Acid Nanoformulations. *Adv. Drug Deliv. Rev.* **2013**, *65* (9), 1123–1147. https://doi.org/10.1016/j.addr.2013.05.002.

(94) Basu, A.; Kunduru, K. R.; Abtew, E.; Domb, A. J. Polysaccharide-Based Conjugates for Biomedical Applications. *Bioconjug. Chem.* **2015**, *26* (8), 1396–1412. https://doi.org/10.1021/acs.bioconjchem.5b00242.

(95) Bonduelle, C.; Makni, F.; Severac, L.; Piedra-Arroni, E.; Serpentini, C. L.; Lecommandoux, S.; Pratviel, G. Smart Metallopoly(l-Glutamic Acid) Polymers: Reversible Helix-to-Coil Transition at Neutral PH. *RSC Adv.* **2016**, *6* (88), 84694–84697. https://doi.org/10.1039/c6ra19753a.

(96) Marguet, M.; Sandre, O.; Lecommandoux, S. Polymersomes in "Gelly" Polymersomes: Toward Structural Cell Mimicry. *Langmuir* **2012**, *28* (4), 2035–2043. https://doi.org/10.1021/la204018w.

(97) Metkar, S.; Sathe, V.; Rahman, I.; Idage, B.; Idage, S. Ring Opening Polymerization of Lactide: Kinetics and Modeling. *Chem. Eng. Commun.* **2019**, *206* (9), 1159–1167. https://doi.org/10.1080/00986445.2018.1550395.

(98) Sanda, F.; Kamatani, J.; Endo, T. Synthesis and Anionic Ring-Opening Polymerization Behavior of Amino Acid-Derived Cyclic Carbonates. *Macromolecules* **2001**, *34* (6), 1564–1569. https://doi.org/10.1021/ma0013307.

(99) Becker, G.; Wurm, F. R. Functional Biodegradable Polymers via Ring-Opening Polymerization of Monomers without Protective Groups. *Chem. Soc. Rev.* **2018**, *47* (20), 7739–7782. https://doi.org/10.1039/C8CS00531A.

(100) Zhong, Y.; Tong, R. Living Ring-Opening Polymerization of O-Carboxyanhydrides: The Search for Catalysts. *Front. Chem.* **2018**, *6*. https://doi.org/10.3389/fchem.2018.00641.

(101) Semsarilar, M.; Perrier, S. "Green" Reversible Addition-Fragmentation Chain-Transfer (RAFT) Polymerization. *Nat. Chem.* **2010**, *2* (10), 811–820. https://doi.org/10.1038/nchem.853.

(102) Moad, G.; Rizzardo, E.; Thang, S. H. Radical Addition–Fragmentation Chemistry in Polymer Synthesis. *Polymer (Guildf).* **2008**, *49* (5), 1079–1131. https://doi.org/10.1016/j.polymer.2007.11.020.

(103) Keddie, D. J. A Guide to the Synthesis of Block Copolymers Using Reversible-Addition Fragmentation Chain Transfer (RAFT) Polymerization. *Chem. Soc. Rev.* **2014**, *43* (2), 496–505. https://doi.org/10.1039/C3CS60290G.

(104) Perrier, S. 50th Anniversary Perspective : RAFT Polymerization—A User Guide. *Macromolecules* **2017**, *50* (19), 7433–7447. https://doi.org/10.1021/acs.macromol.7b00767.

(105) Presolski, S. I.; Hong, V. P.; Finn, M. G. Copper-Catalyzed Azide-Alkyne Click Chemistry for Bioconjugation. In *Current Protocols in Chemical Biology*; John Wiley & Sons, Inc.: Hoboken, NJ, USA, 2011; Vol. 3, pp 153–162. https://doi.org/10.1002/9780470559277.ch110148.

(106) Agut, W.; Taton, D.; Lecommandoux, S. A Versatile Synthetic Approach to Polypeptide Based Rod-Coil Block Copolymers by Click Chemistry. *Macromolecules* **2007**, *40* (16), 5653–5661. https://doi.org/10.1021/ma070579m.

(107) Terzic, I.; Meereboer, N. L.; Loos, K. CuAAC Click Chemistry: A Versatile Approach towards PVDF-Based Block Copolymers. *Polym. Chem.* **2018**, *9* (27), 3714–3720. https://doi.org/10.1039/C8PY00742J.

(108) Quémener, D.; Davis, T. P.; Barner-Kowollik, C.; Stenzel, M. H. RAFT and Click Chemistry: A Versatile Approach to Well-Defined Block Copolymers. *Chem. Commun.* **2006**, No. 48, 5051–5053. https://doi.org/10.1039/B611224B.

(109) Macewan, S. R.; Chilkoti, A. Applications of Elastin-like Polypeptides in Drug Delivery. *J. Control. Release* **2014**, *190*, 314–330. https://doi.org/10.1016/j.jconrel.2014.06.028.

(110) Despanie, J.; Dhandhukia, J. P.; Hamm-Alvarez, S. F.; MacKay, J. A. Elastin-like Polypeptides: Therapeutic Applications for an Emerging Class of Nanomedicines. *J. Control. Release* **2016**, *240*, 93–108. https://doi.org/10.1016/j.jconrel.2015.11.010.

(111) Hassouneh, W.; Zhulina, E. B.; Chilkoti, A.; Rubinstein, M. Elastin-like Polypeptide Diblock Copolymers Self-Assemble into Weak Micelles. *Macromolecules* **2015**, *48* (12), 4183–4195. https://doi.org/10.1021/acs.macromol.5b00431.

(112) Hassouneh, W.; Fischer, K.; MacEwan, S. R.; Branscheid, R.; Fu, C. L.; Liu, R.; Schmidt, M.; Chilkoti, A. Unexpected Multivalent Display of Proteins by Temperature Triggered Self-Assembly of Elastin-like Polypeptide Block Copolymers. *Biomacromolecules* **2012**, *13* (5), 1598–1605. https://doi.org/10.1021/bm300321n.

(113) Jeong, Y. Il; Kim, D. H.; Chung, C. W.; Yoo, J. J.; Choi, K. H.; Kim, C. H.; Ha, S. H.; Kang, D. H. Self-Assembled Nanoparticles of Hyaluronic Acid/Poly(Dl-Lactide-Co-Glycolide) Block Copolymer. *Colloids Surfaces B Biointerfaces* **2012**, *90* (1), 28–35. https://doi.org/10.1016/j.colsurfb.2011.09.043.

(114) Eetezadi, S.; Ekdawi, S. N.; Allen, C. The Challenges Facing Block Copolymer Micelles for Cancer Therapy: In Vivo Barriers and Clinical Translation. *Adv. Drug Deliv. Rev.* **2015**, *91*, 7–22. https://doi.org/10.1016/j.addr.2014.10.001.

(115) Drappier, C.; Oliveira, H.; Sandre, O.; Ibarboure, E.; Combet, S.; Garanger, E.; Lecommandoux, S. Self-Assembled Core-Shell Micelles from Peptide-b-Polymer Molecular Chimeras towards Structure-Activity Relationships. *Faraday Discuss.* **2013**, *166*, 83–100. https://doi.org/10.1039/c3fd00098b.

(116) Kwon, G.; Naito, M.; Yokoyama, M.; Okano, T.; Sakurai, Y.; Kataoka, K. Block Copolymer Micelles for Drug Delivery: Loading and Release of Doxorubicin. *J. Control. Release* **1997**, *48* (2–3), 195–201. https://doi.org/10.1016/S0168-3659(97)00039-4.

(117) Liu, J.; Lee, H.; Allen, C. Formulation of Drugs in Block Copolymer Micelles: Drug Loading and Release. *Curr. Pharm. Des.* **2006**, *12* (36), 4685–4701. https://doi.org/10.2174/138161206779026263.

(118) Rios-Doria, J.; Carie, A.; Costich, T.; Burke, B.; Skaff, H.; Panicucci, R.; Sill, K. A Versatile Polymer Micelle Drug Delivery System for Encapsulation and In Vivo Stabilization of Hydrophobic Anticancer Drugs. *J. Drug Deliv.* **2012**, *2012*, 1–8. https://doi.org/10.1155/2012/951741.

(119) Wang, S. S.-S.; How, S.-C.; Chen, Y.-D.; Tsai, Y.-H.; Jan, J.-S. Bioactive Saccharide-Conjugated Polypeptide Micelles for Acid-Triggered Doxorubicin Delivery. *J. Mater. Chem. B* **2015**, *3* (26), 5220–5231. https://doi.org/10.1039/C5TB00417A.

(120) Blum, A. P.; Kammeyer, J. K.; Rush, A. M.; Callmann, C. E.; Hahn, M. E.; Gianneschi, N. C. Stimuli-Responsive Nanomaterials for Biomedical Applications. *J. Am. Chem. Soc.* **2015**, *137* (6), 2140–2154. https://doi.org/10.1021/ja510147n.

(121) Lu, Y.; Aimetti, A. A.; Langer, R.; Gu, Z. Bioresponsive Materials. *Nat. Rev. Mater.* **2016**, *2* (1). https://doi.org/10.1038/natrevmats.2016.75.

(122) Webb, B. A.; Chimenti, M.; Jacobson, M. P.; Barber, D. L. Dysregulated PH: A Perfect Storm for Cancer Progression. *Nat. Rev. Cancer* **2011**, *11* (9), 671–677. https://doi.org/10.1038/nrc3110.

(123) Vander Heiden, M. G.; Cantley, L. C.; Thompson, C. B. Understanding the Warburg Effect: The Metabolic Requirements of Cell Proliferation. *Science (80-.).* **2009**, *324* (5930), 1029–1033. https://doi.org/10.1126/science.1160809.

(124) Gatenby, R. A.; Gillies, R. J. Why Do Cancers Have High Aerobic Glycolysis? *Nat. Rev. Cancer* **2004**, *4* (11), 891–899. https://doi.org/10.1038/nrc1478.

(125) Brown, J. M.; Wilson, W. R. Exploiting Tumour Hypoxia in Cancer Treatment. *Nat. Rev. Cancer* **2004**, *4* (6), 437–447. https://doi.org/10.1038/nrc1367.

(126) Br ä utigam, L.; Pudelko, L.; Jemth, A.-S.; Gad, H.; Narwal, M.; Gustafsson, R.; Karsten, S.; Carreras Puigvert, J.; Homan, E.; Berndt, C.; et al. Hypoxic Signaling and the Cellular Redox Tumor Environment Determine Sensitivity to MTH1 Inhibition. *Cancer Res.* **2016**, *76* (8), 2366–2375. https://doi.org/10.1158/0008-5472.CAN-15-2380.

(127) de la Rica, R.; Aili, D.; Stevens, M. M. Enzyme-Responsive Nanoparticles for Drug Release and Diagnostics. *Adv. Drug Deliv. Rev.* **2012**, *64* (11), 967–978. https://doi.org/10.1016/j.addr.2012.01.002.

(128) Deryugina, E. I.; Quigley, J. P. Matrix Metalloproteinases and Tumor Metastasis. *Cancer Metastasis Rev.* **2006**, *25* (1), 9–34. https://doi.org/10.1007/s10555-006-7886-9.

(129) Liu, J.; Huang, Y.; Kumar, A.; Tan, A.; Jin, S.; Mozhi, A.; Liang, X.-J. PH-Sensitive Nano-Systems for Drug Delivery in Cancer Therapy. *Biotechnol. Adv.* **2014**, *32* (4), 693–710. https://doi.org/10.1016/j.biotechadv.2013.11.009.

(130) Bolla, P. K.; Rodriguez, V. A.; Kalhapure, R. S.; Kolli, C. S.; Andrews, S.; Renukuntla, J. A Review on PH and Temperature Responsive Gels and Other Less Explored Drug Delivery Systems. *J. Drug Deliv. Sci. Technol.* **2018**, *46*, 416–435. https://doi.org/10.1016/j.jddst.2018.05.037.

(131) Osada, K.; Christie, R. J.; Kataoka, K. Polymeric Micelles from Poly(Ethylene Glycol)–Poly(Amino Acid) Block Copolymer for Drug and Gene Delivery. *J. R. Soc. Interface* **2009**, *6* (suppl_3). https://doi.org/10.1098/rsif.2008.0547.focus.

(132) Aryal, S.; Hu, C.-M. J.; Zhang, L. Polymer−Cisplatin Conjugate Nanoparticles for Acid-Responsive Drug Delivery. *ACS Nano* **2010**, *4* (1), 251–258. https://doi.org/10.1021/nn9014032.

(133) Wang, Y.; Li, P.; Chen, F.; Jia, L.; Xu, Q.; Gai, X.; Yu, Y.; Di, Y.; Zhu, Z.; Liang, Y.; et al. A Novel PH-Sensitive Carrier for the Delivery of Antitumor Drugs: Histidine-Modified Auricularia Auricular Polysaccharide Nano-Micelles. *Sci. Rep.* **2017**, *7* (1), 4751. https://doi.org/10.1038/s41598-017-04428-8.

(134) Rodr ǵuez-Hernández, J.; Lecommandoux, S. Reversible Inside−Out Micellization of PH-Responsive and Water-Soluble Vesicles Based on Polypeptide Diblock Copolymers. *J. Am. Chem. Soc.* **2005**, *127* (7), 2026–2027. https://doi.org/10.1021/ja043920g.

(135) Cai, H.; Wang, X.; Zhang, H.; Sun, L.; Pan, D.; Gong, Q.; Gu, Z.; Luo, K. Enzyme-Sensitive Biodegradable and Multifunctional Polymeric Conjugate as Theranostic Nanomedicine. *Appl. Mater. Today* **2018**, *11*, 207–218. https://doi.org/10.1016/j.apmt.2018.02.003.

(136) ZHONG, Y.-J.; SHAO, L.-H.; LI, Y. Cathepsin B-Cleavable Doxorubicin Prodrugs for Targeted Cancer Therapy. *Int. J. Oncol.* **2013**, *42* (2), 373–383. https://doi.org/10.3892/ijo.2012.1754.

(137) O'hare, K.; Duncan, R.; Strohalm, J.; Ulbrich, K.; Kopeckova, P. Polymeric Drug-Carriers Containing Doxorubicin and Melanocyte-Stimulating Hormone: In Vitro and In Vivo Evaluation Against Murine Melanoma. *J. Drug Target.* **1993**, *1* (3), 217–229. https://doi.org/10.3109/10611869308996079.

(138) Wang, K.; Yin, L.; Miu, T.; Liu, M.; Zhao, Y.; Chen, Y.; Zhou, N.; Zhang, W.; Zhu, X. Design and Synthesis of a Novel Azobenzene-Containing Polymer Both in the Main- and Side-Chain toward Unique

Photocontrolled Isomerization Properties. *Mater. Chem. Front.* **2018**, *2* (6), 1112–1118. https://doi.org/10.1039/C8QM00035B.

(139) Trenor, S. R.; Shultz, A. R.; Love, B. J.; Long, T. E. Coumarins in Polymers: From Light Harvesting to Photo-Cross-Linkable Tissue Scaffolds. *Chem. Rev.* **2004**, *104* (6), 3059–3078. https://doi.org/10.1021/cr030037c.

(140) Chesterman, J. P.; Chen, F.; Brissenden, A. J.; Amsden, B. G. Synthesis of Cinnamoyl and Coumarin Functionalized Aliphatic Polycarbonates. *Polym. Chem.* **2017**, *8* (48), 7515–7528. https://doi.org/10.1039/C7PY01195D.

(141) Li, S.; Ji, S.; Zhou, Z.; Chen, G.; Li, Q. Synthesis and Self-Assembly of o -Nitrobenzyl-Based Amphiphilic Hybrid Polymer with Light and PH Dual Response. *Macromol. Chem. Phys.* **2015**, *216* (11), 1192–1200. https://doi.org/10.1002/macp.201500044.

(142) Zhao, H.; Sterner, E. S.; Coughlin, E. B.; Theato, P. O -Nitrobenzyl Alcohol Derivatives: Opportunities in Polymer and Materials Science. *Macromolecules* **2012**, *45* (4), 1723–1736. https://doi.org/10.1021/ma201924h.

(143) Repasky, E. A.; Evans, S. S.; Dewhirst, M. W. Temperature Matters! And Why It Should Matter to Tumor Immunologists. *Cancer Immunol. Res.* **2013**, *1* (4), 210–216. https://doi.org/10.1158/2326-6066.CIR-13-0118.

(144) Lanzalaco, S.; Armelin, E. Poly(N-Isopropylacrylamide) and Copolymers: A Review on Recent Progresses in Biomedical Applications. *Gels* **2017**, *3* (4), 36. https://doi.org/10.3390/gels3040036.

(145) Watanabe, R.; Takaseki, K.; Katsumata, M.; Matsushita, D.; Ida, D.; Osa, M. Characterization of Poly(N,N-Diethylacrylamide) and Cloud Points in Its Aqueous Solutions. *Polym. J.* **2016**, *48* (5), 621–628. https://doi.org/10.1038/pj.2015.120.

(146) Alexander, A.; Ajazuddin; Khan, J.; Saraf, S.; Saraf, S. Polyethylene Glycol (PEG)–Poly(N-Isopropylacrylamide) (PNIPAAm) Based Thermosensitive Injectable Hydrogels for Biomedical Applications. *Eur. J. Pharm. Biopharm.* **2014**, *88* (3), 575–585. https://doi.org/10.1016/j.ejpb.2014.07.005.

(147) Kovačič, S.; Jeřabek, K.; Krajnc, P. Responsive Poly(Acrylic Acid) and Poly(N-Isopropylacrylamide) Monoliths by High Internal Phase Emulsion (HIPE) Templating. *Macromol. Chem. Phys.* **2011**, *212* (19), 2151–2158. https://doi.org/10.1002/macp.201100229.

(148) Li, Y.; Pan, S.; Zhang, W.; Du, Z. Novel Thermo-Sensitive Core–Shell Nanoparticles for Targeted Paclitaxel Delivery. *Nanotechnology* **2009**, *20* (6), 065104. https://doi.org/10.1088/0957-4484/20/6/065104.

(149) Li, J.; Liu, P. PH/Reduction Dual-Triggered Degradable Poly(Doxorubicin) Prodrug Nanoparticles for Leakage-Free Tumor-Specific Self-Delivery. *Macromol. Rapid Commun.* **2018**, *39* (18), 1800381. https://doi.org/10.1002/marc.201800381.

(150) Hu, X.; Wang, Y.; Zhang, L.; Xu, M.; Zhang, J.; Dong, W. Dual-PH/Magnetic-Field-Controlled Drug Delivery Systems Based on Fe 3 O 4 @SiO 2 -Incorporated Salecan Graft Copolymer Composite Hydrogels. *ChemMedChem* **2017**, *12* (19), 1600–1609. https://doi.org/10.1002/cmdc.201700428.

(151) Tian, Y.; Wang, Y.; Shen, S.; Jiang, X.; Wang, Y.; Yang, W. Temperature and Redox Dual-Responsive Biodegradable Nanogels for Optimizing Antitumor Drug Delivery. *Part. Part. Syst. Charact.* **2015**, *32* (12), 1092–1101. https://doi.org/10.1002/ppsc.201500153.

(152) Qiao, Z.-Y.; Zhang, R.; Du, F.-S.; Liang, D.-H.; Li, Z.-C. Multi-Responsive Nanogels Containing Motifs of Ortho Ester, Oligo(Ethylene Glycol) and Disulfide Linkage as Carriers of Hydrophobic Anti-Cancer Drugs. *J. Control. Release* **2011**, *152* (1), 57–66. https://doi.org/10.1016/j.jconrel.2011.02.029.

(153) Chang, B.; Sha, X.; Guo, J.; Jiao, Y.; Wang, C.; Yang, W. Thermo and PH Dual Responsive, Polymer Shell Coated, Magnetic Mesoporous Silica Nanoparticles for Controlled Drug Release. *J. Mater. Chem.* **2011**, *21* (25), 9239. https://doi.org/10.1039/c1jm10631g.

(154) Bilalis, P.; Chatzipavlidis, A.; Tziveleka, L.-A.; Boukos, N.; Kordas, G. Nanodesigned Magnetic Polymer Containers for Dual Stimuli Actuated Drug Controlled Release and Magnetic Hyperthermia Mediation. *J. Mater. Chem.* **2012**, *22* (27), 13451. https://doi.org/10.1039/c2jm31392h.

(155) Klaikherd, A.; Nagamani, C.; Thayumanavan, S. Multi-Stimuli Sensitive Amphiphilic Block Copolymer Assemblies. *J. Am. Chem. Soc.* **2009**, *131* (13), 4830–4838. https://doi.org/10.1021/ja809475a.

(156) Cheng, R.; Meng, F.; Deng, C.; Klok, H.-A.; Zhong, Z. Dual and Multi-Stimuli Responsive Polymeric Nanoparticles for Programmed Site-Specific Drug Delivery. *Biomaterials* **2013**, *34* (14), 3647–3657. https://doi.org/10.1016/j.biomaterials.2013.01.084.

(157) Mura, S.; Nicolas, J.; Couvreur, P. Stimuli-Responsive Nanocarriers for Drug Delivery. *Nat. Mater.* **2013**, *12* (11), 991–1003. https://doi.org/10.1038/nmat3776.

(158) Chilkoti, A.; Christensen, T.; MacKay, J. A. Stimulus Responsive Elastin Biopolymers: Applications in Medicine and Biotechnology. *Curr. Opin. Chem. Biol.* **2006**, *10* (6), 652–657. https://doi.org/10.1016/j.cbpa.2006.10.010.

(159) McDaniel, J. R.; Callahan, D. J.; Chilkoti, A. Drug Delivery to Solid Tumors by Elastin-like Polypeptides. *Adv. Drug Deliv. Rev.* **2010**, *62* (15), 1456–1467. https://doi.org/10.1016/j.addr.2010.05.004.

(160) Floss, D. M.; Schallau, K.; Rose-John, S.; Conrad, U.; Scheller, J. Elastin-like Polypeptides Revolutionize Recombinant Protein Expression and Their Biomedical Application. *Trends Biotechnol.* **2010**, *28* (1), 37–45. https://doi.org/10.1016/j.tibtech.2009.10.004.

(161) Urry, D. W.; Urry, K. D.; Szaflarski, W.; Nowicki, M. Elastic-Contractile Model Proteins: Physical Chemistry, Protein Function and Drug Design and Delivery. *Adv. Drug Deliv. Rev.* **2010**, *62* (15), 1404–1455. https://doi.org/10.1016/j.addr.2010.07.001.

(162) Urry, D. W. Physical Chemistry of Biological Free Energy Transduction As Demonstrated by Elastic Protein-Based Polymers †. *J. Phys. Chem. B* **1997**, *101* (51), 11007–11028. https://doi.org/10.1021/jp972167t.

(163) Kim, W.; Chaikof, E. L. Recombinant Elastin-Mimetic Biomaterials: Emerging Applications in Medicine. *Adv. Drug Deliv. Rev.* **2010**, *62* (15), 1468–1478. https://doi.org/10.1016/j.addr.2010.04.007.

(164) Rodr ́guez-Cabello, J. C.; Arias, F. J.; Rodrigo, M. A.; Girotti, A. Elastin-like Polypeptides in Drug Delivery. *Adv. Drug Deliv. Rev.* **2016**, *97*, 85–100. https://doi.org/10.1016/j.addr.2015.12.007.

(165) MacEwan, S. R.; Chilkoti, A. Elastin-like Polypeptides: Biomedical Applications of Tunable Biopolymers. *Biopolymers* **2010**, *94* (1), 60–77. https://doi.org/10.1002/bip.21327.

(166) DAAMEN, W.; VEERKAMP, J.; VANHEST, J.; VANKUPPEVELT, T. Elastin as a Biomaterial for Tissue Engineering. *Biomaterials* **2007**, *28* (30), 4378–4398. https://doi.org/10.1016/j.biomaterials.2007.06.025.

(167) Kielty, C. M.; Sherratt, M. J.; Shuttleworth, C. A. Elastic Fibres. *J. Cell Sci.* **2002**, *115* (Pt 14), 2817–2828. https://doi.org/12082143.

(168) Mithieux, S. M.; Weiss, A. S. Elastin. In *Advances in Protein Chemistry*; 2005; Vol. 70, pp 437–461. https://doi.org/10.1016/S0065-3233(05)70013-9.

(169) Wise, S. G.; Yeo, G. C.; Hiob, M. A.; Rnjak-Kovacina, J.; Kaplan, D. L.; Ng, M. K. C.; Weiss, A. S. Tropoelastin: A Versatile, Bioactive Assembly Module. *Acta Biomater.* **2014**, *10* (4), 1532–1541. https://doi.org/10.1016/j.actbio.2013.08.003.

(170) Rnjak, J.; Wise, S. G.; Mithieux, S. M.; Weiss, A. S. Severe Burn Injuries and the Role of Elastin in the Design of Dermal Substitutes. *Tissue Eng. Part B Rev.* **2011**, *17* (2), 81–91. https://doi.org/10.1089/ten.teb.2010.0452.

(171) Urry, D. W.; Long, M. M.; Cox, B. A.; Ohnishi, T.; Mitchell, L. W.; Jacobs, M. The Synthetic Polypentapeptide of Elastin Coacervates and Forms Filamentous Aggregates. *Biochim. Biophys. Acta - Protein Struct.* **1974**, *371* (2), 597–602. https://doi.org/10.1016/0005-2795(74)90057-9.

(172) Urry, D. W. Molecular Machines: How Motion and Other Functions of Living Organisms Can Result from Reversible Chemical Changes. *Angew. Chemie Int. Ed. English* **1993**, *32* (6), 819–841. https://doi.org/10.1002/anie.199308191.

(173) Lee, J.; Macosko, C. W.; Urry, D. W. Elastomeric Polypentapeptides Cross-Linked into Matrixes and Fibers. *Biomacromolecules* **2001**, *2* (1), 170–179. https://doi.org/10.1021/bm0000900.

(174) Rinc ́on, A. C.; Molina-Martinez, I. T.; de las Heras, B.; Alonso, M.; Ba ́ez, C.; Rodr ́guez-Cabello, J. C.; Herrero-Vanrell, R. Biocompatibility of Elastin-like Polymer Poly(VPAVG) Microparticles:In Vitro Andin Vivo Studies. *J. Biomed. Mater. Res. Part A* **2006**, *78A* (2), 343–351. https://doi.org/10.1002/jbm.a.30702.

(175) Yeo, G. C.; Aghaei-Ghareh-Bolagh, B.; Brackenreg, E. P.; Hiob, M. A.; Lee, P.; Weiss, A. S. Fabricated Elastin. *Adv. Healthc. Mater.* **2015**, *4* (16), 2530–2556. https://doi.org/10.1002/adhm.201400781.

(176) Wright, E. R.; Conticello, V. P. Self-Assembly of Block Copolymers Derived from Elastin-Mimetic Polypeptide Sequences. *Adv. Drug Deliv. Rev.* **2002**, *54* (8), 1057–1073.

(177) Tamburro, A. M.; Bochicchio, B.; Pepe, A. Dissection of Human Tropoelastin: Exon-By-Exon Chemical Synthesis and Related Conformational Studies †. *Biochemistry* **2003**, *42* (45), 13347–13362. https://doi.org/10.1021/bi034837t.

(178) Le, D. H. T.; Sugawara-Narutaki, A. Elastin-like Polypeptides as Building Motifs toward Designing Functional Nanobiomaterials. *Mol. Syst. Des. Eng.* **2019**, *4* (3), 545–565. https://doi.org/10.1039/C9ME00002J.

(179) MacEwan, S. R.; Hassouneh, W.; Chilkoti, A. Non-Chromatographic Purification of Recombinant Elastin-like Polypeptides and Their Fusions with Peptides and Proteins from Escherichia Coli. *J. Vis. Exp.* **2014**, No. 88. https://doi.org/10.3791/51583.

(180) Chow, D. C.; Dreher, M. R.; Trabbic-Carlson, K.; Chilkoti, A. Ultra-High Expression of a Thermally Responsive Recombinant Fusion Protein in E. Coli. *Biotechnol. Prog.* **2006**, *22* (3), 638–646. https://doi.org/10.1021/bp0503742.

(181) Christensen, T.; Amiram, M.; Dagher, S.; Trabbic-Carlson, K.; Shamji, M. F.; Setton, L. A.; Chilkoti, A. Fusion Order Controls Expression Level and Activity of Elastin-like Polypeptide Fusion Proteins. *Protein Sci.* **2009**, *18* (7), 1377–1387. https://doi.org/10.1002/pro.157.

(182) Martin, S. L.; Vrhovski, B.; Weiss, A. S. Total Synthesis and Expression in Escherichia Coli of a Gene Encoding Human Tropoelastin. *Gene* **1995**, *154* (2), 159–166. https://doi.org/10.1016/0378-1119(94)00848-M.

(183) Tang, N. C.; Chilkoti, A. Combinatorial Codon Scrambling Enables Scalable Gene Synthesis and Amplification of Repetitive Proteins. *Nat. Mater.* **2016**, *15* (4), 419–424. https://doi.org/10.1038/nmat4521.

(184) Sallach, R. E.; Conticello, V. P.; Chaikof, E. L. Expression of a Recombinant Elastin-like Protein in Pichia Pastoris. *Biotechnol. Prog.* **2009**, NA-NA. https://doi.org/10.1002/btpr.208.

(185) Patel, J.; Zhu, H.; Menassa, R.; Gyenis, L.; Richman, A.; Brandle, J. Elastin-like Polypeptide Fusions Enhance the Accumulation of Recombinant Proteins in Tobacco Leaves. *Transgenic Res.* **2007**, *16* (2), 239–249. https://doi.org/10.1007/s11248-006-9026-2.

(186) Herzog, R. W.; Singh, N. K.; Urry, D. W.; Daniell, H. Expression of a Synthetic Protein-Based Polymer (Elastomer) Gene in Aspergillus Nidulans. *Appl. Microbiol. Biotechnol.* **1997**, *47* (4), 368–372. https://doi.org/10.1007/s002530050942.

(187) Chu, H. S.; Lee, K. H.; Park, J. E.; Kim, D. M.; Kim, B. G.; Won, J. I. Expression Analysis of an Elastin-like Polypeptide (ELP) in a Cell-Free Protein Synthesis System. *Enzyme Microb. Technol.* **2010**, *46* (2), 87–91. https://doi.org/10.1016/j.enzmictec.2009.10.003.

(188) Meyer, D. E.; Chilkoti, A. Purification of Recombinant Proteins by Fusion with Thermally-Responsive Polypeptides. *Nat. Biotechnol.* **1999**, *17* (11), 1112–1115. https://doi.org/10.1038/15100.

(189) McPherson, D. T.; Xu, J.; Urry, D. W. Product Purification by Reversible Phase Transition FollowingEscherichia ColiExpression of Genes Encoding up to 251 Repeats of the Elastomeric Pentapeptide GVGVP. *Protein Expr. Purif.* **1996**, *7* (1), 51–57. https://doi.org/10.1006/prep.1996.0008.

(190) Shamji, M. F.; Betre, H.; Kraus, V. B.; Chen, J.; Chilkoti, A.; Pichika, R.; Masuda, K.; Setton, L. A. Development and Characterization of a Fusion Protein between Thermally Responsive Elastin-like Polypeptide and Interleukin-1 Receptor Antagonist: Sustained Release of a Local Antiinflammatory Therapeutic. *Arthritis Rheum.* **2007**, *56* (11), 3650–3661. https://doi.org/10.1002/art.22952.

(191) Hsueh, Y.-S.; Savitha, S.; Sadhasivam, S.; Lin, F.-H.; Shieh, M.-J. Design and Synthesis of Elastin-like Polypeptides for an Ideal Nerve Conduit in Peripheral Nerve Regeneration. *Mater. Sci. Eng. C* **2014**, *38*, 119–126. https://doi.org/10.1016/j.msec.2014.01.058.

(192) Ro, J.-W.; Choi, H.; Heo, T.-Y.; Choi, S.-H.; Won, J.-I. Characterization of Amphiphilic Elastin-like Polypeptide (ELP) Block Copolymers as Drug Delivery Carriers. *Biotechnol. Bioprocess Eng.* **2018**, *23* (6), 627–633. https://doi.org/10.1007/s12257-018-0365-7.

(193) Ohgo, K.; Kurano, T. L.; Kumashiro, K. K.; Asakura, T. Structure of the Model Peptides of Bombyx m Ori Silk-Elastin Like Protein Studied with Solid State NMR. *Biomacromolecules* **2004**, *5* (3), 744–750. https://doi.org/10.1021/bm034355x.

(194) Schmidt, P.; Dybal, J.; Rodriguez-Cabello, J. C.; Reboto, V. Role of Water in Structural Changes of Poly(AVGVP) and Poly(GVGVP) Studied by FTIR and Raman Spectroscopy and Ab Initio Calculations. *Biomacromolecules* **2005**, *6* (2), 697–706. https://doi.org/10.1021/bm049461t.

(195) Meyer, D. E.; Chilkoti, A. Genetically Encoded Synthesis of Protein-Based Polymers with Precisely Specified Molecular Weight and Sequence by Recursive Directional Ligation: Examples from the Elastin-like Polypeptide System. *Biomacromolecules* **2002**, *3* (2), 357–367.

(196) Luan, C.-H.; Harris, R. D.; Prasad, K. U.; Urry, D. W. Differential Scanning Calorimetry Studies of the Inverse Temperature Transition of the Polypentapeptide of Elastin and Its Analogues. *Biopolymers* **1990**, *29* (14), 1699–1706. https://doi.org/10.1002/bip.360291403.

(197) Fletcher, E. E.; Yan, D.; Kosiba, A. A.; Zhou, Y.; Shi, H. Biotechnological Applications of Elastin-like Polypeptides and the Inverse Transition Cycle in the Pharmaceutical Industry. *Protein Expr. Purif.* **2019**, *153*, 114–120. https://doi.org/10.1016/j.pep.2018.09.006.

(198) Kramer, J. R.; Petitdemange, R.; Bataille, L.; Bathany, K.; Wirotius, A. L.; Garbay, B.; Deming, T. J.; Garanger, E.; Lecommandoux, S. S.; Saint-exupéry, L. A.; et al. Quantitative Side-Chain Modifications of Methionine-Containing Elastin-Like Polypeptides as a Versatile Tool to Tune Their Properties. *ACS Macro Lett.* **2015**, *4* (11), 1283–1286. https://doi.org/10.1021/acsmacrolett.5b00651.

(199) MacEwan, S. R.; Weitzhandler, I.; Hoffmann, I.; Genzer, J.; Gradzielski, M.; Chilkoti, A. Phase Behavior and Self-Assembly of Perfectly Sequence-Defined and Monodisperse Multiblock Copolypeptides. *Biomacromolecules* **2017**, *18* (2), 599–609. https://doi.org/10.1021/acs.biomac.6b01759.

(200) Meyer, D. E.; Chilkoti, A. Quantification of the Effects of Chain Length and Concentration on the Thermal Behavior of Elastin-like Polypeptides. *Biomacromolecules* **2004**, *5* (3), 846–851. https://doi.org/10.1021/bm034215n.

(201) Andrew Mackay, J.; Chilkoti, A. Temperature Sensitive Peptides: Engineering Hyperthermia-Directed Therapeutics. *Int. J. Hyperth.* **2008**, *24* (6), 483–495. https://doi.org/10.1080/02656730802149570.

(202) Shah, M.; Hsueh, P.-Y.; Sun, G.; Chang, H. Y.; Janib, S. M.; MacKay, J. A. Biodegradation of Elastin-like Polypeptide Nanoparticles. *Protein Sci.* **2012**, *21* (6), 743–750. https://doi.org/10.1002/pro.2063.

(203) Nalivaeva, N. N.; Turner, A. J. Post-Translational Modifications of Proteins: Acetylcholinesterase as a Model System. *Proteomics* **2001**, *1* (6), 735–747. https://doi.org/10.1002/1615-9861(200106)1:6<735::AID-PROT735>3.0.CO;2-8.

(204) Wang, Y.-C.; Peterson, S. E.; Loring, J. F. Protein Post-Translational Modifications and Regulation of Pluripotency in Human Stem Cells. *Cell Res.* **2014**, *24* (2), 143–160. https://doi.org/10.1038/cr.2013.151.

(205) Seifried, B. M.; Cao, J.; Olsen, B. D. Multifunctional, High Molecular Weight, Post-Translationally Modified Proteins through Oxidative Cysteine Coupling and Tyrosine Modification. *Bioconjug. Chem.* **2018**, *29* (6), 1876–1884. https://doi.org/10.1021/acs.bioconjchem.7b00834.

(206) Müller, M. M. Post-Translational Modifications of Protein Backbones: Unique Functions, Mechanisms, and Challenges. *Biochemistry* **2018**, *57* (2), 177–185. https://doi.org/10.1021/acs.biochem.7b00861.

(207) Kumar, G. K.; Prabhakar, N. R. Post-Translational Modification of Proteins during Intermittent Hypoxia. *Respir. Physiol. Neurobiol.* **2008**, *164* (1–2), 272–276. https://doi.org/10.1016/j.resp.2008.05.017.

(208) Baslé, E.; Joubert, N.; Pucheault, M. Protein Chemical Modification on Endogenous Amino Acids. *Chem. Biol.* **2010**, *17* (3), 213–227. https://doi.org/10.1016/j.chembiol.2010.02.008.

(209) van Eldijk, M. B.; Smits, F. C. M.; Vermue, N.; Debets, M. F.; Schoffelen, S.; van Hest, J. C. M. Synthesis and Self-Assembly of Well-Defined Elastin-Like Polypeptide–Poly(Ethylene Glycol) Conjugates. *Biomacromolecules* **2014**, *15* (7), 2751–2759. https://doi.org/10.1021/bm5006195.

(210) Zhu, D.; Wang, H.; Trinh, P.; Heilshorn, S. C.; Yang, F. Elastin-like Protein-Hyaluronic Acid (ELP-HA) Hydrogels with Decoupled Mechanical and Biochemical Cues for Cartilage Regeneration. *Biomaterials* **2017**, *127*, 132–140. https://doi.org/10.1016/j.biomaterials.2017.02.010.

(211) Dreher, M. R.; Raucher, D.; Balu, N.; Michael Colvin, O.; Ludeman, S. M.; Chilkoti, A. Evaluation of an Elastin-like Polypeptide-Doxorubicin Conjugate for Cancer Therapy. *J. Control. Release* **2003**, *91* (1–2), 31–43.

(212) Petitdemange, R.; Garanger, E.; Bataille, L.; Dieryck, W.; Bathany, K.; Garbay, B.; Deming, T. J.; Lecommandoux, S.; Dieryck, W.; Petitdemange, R.; et al. Selective Tuning of Elastin-like Polypeptide Properties via Methionine Oxidation. *Biomacromolecules* **2017**, *18* (2), 544–550. https://doi.org/10.1021/acs.biomac.6b01696.

(213) Macewan, S. R.; Chilkoti, A. Controlled Apoptosis by a Thermally Toggled Nanoscale Amplifier of Cellular Uptake. *Nano Lett.* **2014**, *14* (4), 2058–2064. https://doi.org/10.1021/nl5002313.

(214) Kramer, J. R.; Petitdemange, R.; Bataille, L.; Bathany, K.; Wirotius, A. L.; Garbay, B.; Deming, T. J.; Garanger, E.; Lecommandoux, S. Quantitative Side-Chain Modifications of Methionine-Containing Elastin-Like Polypeptides as a Versatile Tool to Tune Their Properties. *ACS Macro Lett.* **2015**, *4* (11), 1283–1286. https://doi.org/10.1021/acsmacrolett.5b00651.

(215) Smits, F. C. M.; Buddingh, B. C.; van Eldijk, M. B.; van Hest, J. C. M. Elastin-Like Polypeptide Based Nanoparticles: Design Rationale Toward Nanomedicine. *Macromol. Biosci.* **2015**, *15* (1), 36–51. https://doi.org/10.1002/mabi.201400419.

(216) Dreher, M. R.; Simnick, A. J.; Fischer, K.; Smith, R. J.; Patel, A.; Schmidt, M.; Chilkoti, A. Temperature Triggered Self-Assembly of Polypeptides into Multivalent Spherical Micelles. *J. Am. Chem. Soc.* **2008**, *130* (2), 687–694. https://doi.org/10.1021/ja0764862.

(217) Simnick, A. J.; Amiram, M.; Liu, W.; Hanna, G.; Dewhirst, M. W.; Kontos, C. D.; Chilkoti, A. In Vivo Tumor Targeting by a NGR-Decorated Micelle of a Recombinant Diblock Copolypeptide. *J. Control. Release* **2011**, *155* (2), 144–151. https://doi.org/10.1016/j.jconrel.2011.06.044.

(218) Garc á-Ar évalo, C.; Bermejo-Mart ń, J. F.; Rico, L.; Iglesias, V.; Mart ń, L.; Rodr guez-Cabello, J. C.; Arias, F. J. Immunomodulatory Nanoparticles from Elastin-Like Recombinamers: Single-Molecules for Tuberculosis Vaccine Development. *Mol. Pharm.* **2013**, *10* (2), 586–597. https://doi.org/10.1021/mp300325v.

(219) Patel, A.; Simnick, A. J.; Chilkoti, A.; Fischer, K.; Schmidt, M.; Dreher, M. R.; Smith, R. J. Temperature Triggered Self-Assembly of Polypeptides into Multivalent Spherical Micelles. *J. Am. Chem. Soc.* **2008**, *130* (2), 687–694. https://doi.org/10.1021/ja0764862.

(220) Shi, P.; Aluri, S.; Lin, Y.-A.; Shah, M.; Edman, M.; Dhandhukia, J.; Cui, H.; MacKay, J. A. Elastin-Based Protein Polymer Nanoparticles Carrying Drug at Both Corona and Core Suppress Tumor Growth in Vivo. *J. Control. Release* **2013**, *171* (3), 330–338. https://doi.org/10.1016/j.jconrel.2013.05.013.

(221) Ribeiro, A.; Arias, F. J.; Reguera, J.; Alonso, M.; Rodr guez-Cabello, J. C. Influence of the Amino-Acid Sequence on the Inverse Temperature Transition of Elastin-Like Polymers. *Biophys. J.* **2009**, *97* (1), 312–320. https://doi.org/10.1016/j.bpj.2009.03.030.

(222) Wright, E. R.; Conticello, V. P. Self-Assembly of Block Copolymers Derived from Elastin-Mimetic Polypeptide Sequences. *Adv. Drug Deliv. Rev.* **2002**, *54* (8), 1057–1073. https://doi.org/10.1016/S0169-409X(02)00059-5.

(223) Sallach, R. E.; Wei, M.; Biswas, N.; Conticello, V. P.; Lecommandoux, S.; Dluhy, R. A.; Chaikof, E. L. Micelle Density Regulated by a Reversible Switch of Protein Secondary Structure. *J. Am. Chem. Soc.* **2006**, *128* (36), 12014–12019. https://doi.org/10.1021/ja0638509.

(224) Huang, W.; Rollett, A.; Kaplan, D. L. Silk-Elastin-like Protein Biomaterials for the Controlled Delivery of Therapeutics. *Expert Opin. Drug Deliv.* **2015**, *12* (5), 779–791. https://doi.org/10.1517/17425247.2015.989830.

(225) Greish, K.; Ghandehari, H.; Cappello, J.; Price, R. A.; Gustafson, J. A. Silk-Elastin-like Hydrogel Improves the Safety of Adenovirus-Mediated Gene-Directed Enzyme−Prodrug Therapy. *Mol. Pharm.* **2010**, *7* (4), 1050–1056. https://doi.org/10.1021/mp100161u.

(226) Weitzhandler, I.; Dzuricky, M.; Hoffmann, I.; Garcia Quiroz, F.; Gradzielski, M.; Chilkoti, A. Micellar Self-Assembly of Recombinant Resilin-/Elastin-Like Block Copolypeptides. *Biomacromolecules* **2017**, *18* (8), 2419–2426. https://doi.org/10.1021/acs.biomac.7b00589.

(227) Qin, G.; Perez, P. M.; Mills, C. E.; Olsen, B. D. Effect of ELP Sequence and Fusion Protein Design on Concentrated Solution Self-Assembly. *Biomacromolecules* **2016**, *17* (3), 928–934. https://doi.org/10.1021/acs.biomac.5b01604.

(228) Le Fer, G.; Portes, D.; Goudounet, G.; Guigner, J.-M.; Garanger, E.; Lecommandoux, S. Design and Self-Assembly of PBLG- b -ELP Hybrid Diblock Copolymers Based on Synthetic and Elastin-like Polypeptides. *Org. Biomol. Chem.* **2017**, *15* (47), 10095–10104. https://doi.org/10.1039/C7OB01945A.

(229) Le Fer, G.; Wirotius, A. L.; Br ûlet, A.; Garanger, E.; Lecommandoux, S. Self-Assembly of Stimuli-Responsive Biohybrid Synthetic- b-Recombinant Block Copolypeptides. *Biomacromolecules* **2019**, *20* (1), 254–272. https://doi.org/10.1021/acs.biomac.8b01390.

(230) Park, S. M.; Cha, J. M.; Nam, J.; Kim, M. S.; Park, S.-J.; Park, E. S.; Lee, H.; Kim, H. R. Formulation Optimization and In Vivo Proof-of-Concept Study of Thermosensitive Liposomes Balanced by Phospholipid, Elastin-Like Polypeptide, and Cholesterol. *PLoS One* **2014**, *9* (7), e103116. https://doi.org/10.1371/journal.pone.0103116.

(231) Mozhdehi, D.; Luginbuhl, K. M.; Simon, J. R.; Dzuricky, M.; Berger, R.; Varol, H. S.; Huang, F. C.; Buehne, K. L.; Mayne, N. R.; Weitzhandler, I.; et al. Genetically Encoded Lipid–Polypeptide Hybrid Biomaterials That Exhibit Temperature-Triggered Hierarchical Self-Assembly. *Nat. Chem.* **2018**, *10* (5), 496–505. https://doi.org/10.1038/s41557-018-0005-z.

(232) Mozhdehi, D.; Luginbuhl, K. M.; Dzuricky, M.; Costa, S. A.; Xiong, S.; Huang, F. C.; Lewis, M. M.; Zelenetz, S. R.; Colby, C. D.; Chilkoti, A. Genetically Encoded Cholesterol-Modified Polypeptides. *J. Am. Chem. Soc.* **2019**, *141* (2), 945–951. https://doi.org/10.1021/jacs.8b10687.

(233) Furgeson, D. Y.; Dreher, M. R.; Chilkoti, A. Structural Optimization of a "Smart" Doxorubicin–Polypeptide Conjugate for Thermally Targeted Delivery to Solid Tumors. *J. Control. Release* **2006**, *110* (2), 362–369. https://doi.org/10.1016/j.jconrel.2005.10.006.

(234) Bidwell, G. L.; Davis, A. N.; Fokt, I.; Priebe, W.; Raucher, D. A Thermally Targeted Elastin-like Polypeptide-Doxorubicin Conjugate Overcomes Drug Resistance. *Invest. New Drugs* **2007**, *25* (4), 313–326. https://doi.org/10.1007/s10637-007-9053-8.

(235) Moktan, S.; Perkins, E.; Kratz, F.; Raucher, D. Thermal Targeting of an Acid-Sensitive Doxorubicin Conjugate of Elastin-like Polypeptide Enhances the Therapeutic Efficacy Compared with the Parent Compound In Vivo. *Mol. Cancer Ther.* **2012**, *11* (7), 1547–1556. https://doi.org/10.1158/1535-7163.MCT-11-0998.

(236) Meyer, D. E.; Kong, G. A.; Dewhirst, M. W.; Zalutsky, M. R.; Chilkoti, A. Targeting a Genetically Engineered Elastin-like Polypeptide to Solid Tumors by Local Hyperthermia. *Cancer Res.* **2001**, *61* (4), 1548–1554.

(237) Xia, X.-X.; Xu, Q.; Hu, X.; Qin, G.; Kaplan, D. L. Tunable Self-Assembly of Genetically Engineered Silk–Elastin-like Protein Polymers. *Biomacromolecules* **2011**, *12* (11), 3844–3850. https://doi.org/10.1021/bm201165h.

(238) Liu, W.; Dreher, M. R.; Furgeson, D. Y.; Peixoto, K. V.; Yuan, H.; Zalutsky, M. R.; Chilkoti, A. Tumor Accumulation, Degradation and Pharmacokinetics of Elastin-like Polypeptides in Nude Mice. *J. Control. Release* **2006**, *116* (2), 170–178. https://doi.org/10.1016/j.jconrel.2006.06.026.

(239) Ryu, J. S.; Raucher, D. Elastin-like Polypeptide for Improved Drug Delivery for Anticancer Therapy: Preclinical Studies and Future Applications. *Expert Opin. Drug Deliv.* **2015**, *12* (4), 653–667. https://doi.org/10.1517/17425247.2015.974546.

(240) Nettles, D. L.; Chilkoti, A.; Setton, L. A. Applications of Elastin-like Polypeptides in Tissue Engineering. *Adv. Drug Deliv. Rev.* **2010**, *62* (15), 1479–1485. https://doi.org/10.1016/j.addr.2010.04.002.

(241) Janorkar, A. V.; Rajagopalan, P.; Yarmush, M. L.; Megeed, Z. The Use of Elastin-like Polypeptide–Polyelectrolyte Complexes to Control Hepatocyte Morphology and Function in Vitro. *Biomaterials* **2008**, *29* (6), 625–632. https://doi.org/10.1016/j.biomaterials.2007.10.022.

(242) Nettles, D. L.; Kitaoka, K.; Hanson, N. A.; Flahiff, C. M.; Mata, B. A.; Hsu, E. W.; Chilkoti, A.; Setton, L. A. In Situ Crosslinking Elastin-Like Polypeptide Gels for Application to Articular Cartilage Repair in a Goat Osteochondral Defect Model. *Tissue Eng. Part A* **2008**, *14* (7), 1133–1140. https://doi.org/10.1089/ten.tea.2007.0245.

(243) McHale, M. K.; Setton, L. A.; Chilkoti, A. Synthesis and in Vitro Evaluation of Enzymatically Cross-Linked Elastin-Like Polypeptide Gels for Cartilaginous Tissue Repair. *Tissue Eng.* **2005**, *11* (11–12), 1768–1779. https://doi.org/10.1089/ten.2005.11.1768.

(244) Martínez-Osorio, H.; Juárez-Campo, M.; Diebold, Y.; Girotti, A.; Alonso, M.; Arias, F. J.; Rodríguez-Cabello, J. C.; García-Vázquez, C.; Calonge, M. Genetically Engineered Elastin-Like Polymer as a Substratum to Culture Cells from the Ocular Surface. *Curr. Eye Res.* **2009**, *34* (1), 48–56. https://doi.org/10.1080/02713680802542053.

(245) Mie, M.; Mizushima, Y.; Kobatake, E. Novel Extracellular Matrix for Cell Sheet Recovery Using Genetically Engineered Elastin-like Protein. *J. Biomed. Mater. Res. Part B Appl. Biomater.* **2008**, *86B* (1), 283–290. https://doi.org/10.1002/jbm.b.31019.

(246) Heilshorn, S. Endothelial Cell Adhesion to the Fibronectin CS5 Domain in Artificial Extracellular Matrix Proteins. *Biomaterials* **2003**, *24* (23), 4245–4252. https://doi.org/10.1016/S0142-9612(03)00294-1.

(247) Caves, J. M.; Kumar, V. A.; Martinez, A. W.; Kim, J.; Ripberger, C. M.; Haller, C. A.; Chaikof, E. L. The Use of Microfiber Composites of Elastin-like Protein Matrix Reinforced with Synthetic Collagen in the Design of Vascular Grafts. *Biomaterials* **2010**, *31* (27), 7175–7182. https://doi.org/10.1016/j.biomaterials.2010.05.014.

(248) Han, X.; Li, Z.; Sun, J.; Luo, C.; Li, L.; Liu, Y.; Du, Y.; Qiu, S.; Ai, X.; Wu, C.; et al. Stealth CD44-Targeted Hyaluronic Acid Supramolecular Nanoassemblies for Doxorubicin Delivery: Probing the Effect of Uncovalent Pegylation Degree on Cellular Uptake and Blood Long Circulation. *J. Control. Release* **2015**, *197*, 29–40. https://doi.org/10.1016/j.jconrel.2014.10.024.

(249) Necas, J.; Bartosikova, L.; Brauner, P.; Kolar, J. Hyaluronic Acid (Hyaluronan): A Review. *Vet. Med. (Praha).* **2008**, *53* (8), 397–411. https://doi.org/10.17221/1930-VETMED.

(250) Wolf, K. J.; Kumar, S. Hyaluronic Acid: Incorporating the Bio into the Material. *ACS Biomater. Sci. Eng.* **2019**, *5* (8), 3753–3765. https://doi.org/10.1021/acsbiomaterials.8b01268.

(251) STERN, R.; ASARI, A.; SUGAHARA, K. Hyaluronan Fragments: An Information-Rich System. *Eur. J. Cell Biol.* **2006**, *85* (8), 699–715. https://doi.org/10.1016/j.ejcb.2006.05.009.

(252) Aruffo, A.; Stamenkovic, I.; Melnick, M.; Underhill, C. B.; Seed, B. CD44 Is the Principal Cell Surface Receptor for Hyaluronate. *Cell* **1990**, *61* (7), 1303–1313. https://doi.org/10.1016/0092-8674(90)90694-A.

(253) Toole, B. P. Hyaluronan in Morphogenesis. *Semin. Cell Dev. Biol.* **2001**, *12* (2), 79–87. https://doi.org/10.1006/scdb.2000.0244.

(254) Spicer, A. P.; Tien, J. Y. L. Hyaluronan and Morphogenesis. *Birth Defects Res. Part C Embryo Today Rev.* **2004**, *72* (1), 89–108. https://doi.org/10.1002/bdrc.20006.

(255) TAKEI, Y.; MARUYAMA, A.; FERDOUS, A.; NISHIMURA, Y.; KAWANO, S.; IKEJIMA, K.; OKUMURA, S.; ASAYAMA, S.; NOGAWA, M.; HASHIMOTO, M.; et al. Targeted Gene Delivery to Sinusoidal Endothelial Cells: DNA Nanoassociate Bearing Hyaluronan-Glycocalyx. *FASEB J.* **2004**, *18* (6), 699–701. https://doi.org/10.1096/fj.03-0494fje.

(256) Asayama, S.; Nogawa, M.; Takei, Y.; Akaike, T.; Maruyama, A. Synthesis of Novel Polyampholyte Comb-Type Copolymers Consisting of a Poly(L-Lysine) Backbone and Hyaluronic Acid Side Chains for a DNA Carrier. *Bioconjug. Chem.* **1998**, *9* (4), 476–481. https://doi.org/10.1021/bc970213m.

(257) Schledzewski, K.; Falkowski, M.; Moldenhauer, G.; Metharom, P.; Kzhyshkowska, J.; Ganss, R.; Demory, A.; Falkowska-Hansen, B.; Kurzen, H.; Ugurel, S.; et al. Lymphatic Endothelium-Specific Hyaluronan Receptor LYVE-1 Is Expressed by Stabilin-1+, F4/80+, CD11b+ Macrophages in Malignant Tumours and Wound Healing Tissuein Vivo and in Bone Marrow Culturesin Vitro: Implications for the Assessment of Lymphangiogenesi. *J. Pathol.* **2006**, *209* (1), 67–77. https://doi.org/10.1002/path.1942.

(258) Choi, K. Y.; Chung, H.; Min, K. H.; Yoon, H. Y.; Kim, K.; Park, J. H.; Kwon, I. C.; Jeong, S. Y. Self-Assembled Hyaluronic Acid Nanoparticles for Active Tumor Targeting. *Biomaterials* **2010**, *31* (1), 106–114. https://doi.org/10.1016/j.biomaterials.2009.09.030.

(259) Dosio, F.; Arpicco, S.; Stella, B.; Fattal, E. Hyaluronic Acid for Anticancer Drug and Nucleic Acid Delivery. *Adv. Drug Deliv. Rev.* **2016**, *97*, 204–236. https://doi.org/10.1016/j.addr.2015.11.011.

(260) Gallo, N.; Nasser, H.; Salvatore, L.; Natali, M. L.; Campa, L.; Mahmoud, M.; Capobianco, L.; Sannino, A.; Madaghiele, M. Hyaluronic Acid for Advanced Therapies: Promises and Challenges. *Eur. Polym. J.* **2019**, *117*, 134–147. https://doi.org/10.1016/j.eurpolymj.2019.05.007.

(261) Huang, G.; Chen, J. Preparation and Applications of Hyaluronic Acid and Its Derivatives. *Int. J. Biol. Macromol.* **2019**, *125*, 478–484. https://doi.org/10.1016/j.ijbiomac.2018.12.074.

(262) Lee, G. Y.; Kim, J. H.; Choi, K. Y.; Yoon, H. Y.; Kim, K.; Kwon, I. C.; Choi, K.; Lee, B. H.; Park, J. H.; Kim, I. S. Hyaluronic Acid Nanoparticles for Active Targeting Atherosclerosis. *Biomaterials* **2015**, *53*, 341–348. https://doi.org/10.1016/j.biomaterials.2015.02.089.

(263) Wickens, J. M.; Alsaab, H. O.; Kesharwani, P.; Bhise, K.; Amin, M. C. I. M.; Tekade, R. K.; Gupta, U.; Iyer, A. K. Recent Advances in Hyaluronic Acid-Decorated Nanocarriers for Targeted Cancer Therapy. *Drug Discov. Today* **2017**, *22* (4), 665–680. https://doi.org/10.1016/j.drudis.2016.12.009.

(264) Huang, G.; Huang, H. Hyaluronic Acid-Based Biopharmaceutical Delivery and Tumor-Targeted Drug Delivery System. *J. Control. Release* **2018**, *278* (February), 122–126. https://doi.org/10.1016/j.jconrel.2018.04.015.

(265) Han, H. S.; Choi, K. Y.; Ko, H.; Jeon, J.; Saravanakumar, G.; Suh, Y. D.; Lee, D. S.; Park, J. H. Bioreducible Core-Crosslinked Hyaluronic Acid Micelle for Targeted Cancer Therapy. *J. Control. Release* **2015**, *200*, 158–166. https://doi.org/10.1016/j.jconrel.2014.12.032.

(266) Cordo Russo, R. I.; García, M. G.; Alaniz, L.; Blanco, G.; Alvarez, E.; Hajos, S. E. Hyaluronan Oligosaccharides Sensitize Lymphoma Resistant Cell Lines to Vincristine by Modulating P-Glycoprotein Activity and PI3K/Akt Pathway. *Int. J. Cancer* **2007**, *122* (5), 1012–1018. https://doi.org/10.1002/ijc.23122.

(267) Schanté, C. E.; Zuber, G.; Herlin, C.; Vandamme, T. F. Chemical Modifications of Hyaluronic Acid for the Synthesis of Derivatives for a Broad Range of Biomedical Applications. *Carbohydr. Polym.* **2011**, *85* (3), 469–489. https://doi.org/10.1016/j.carbpol.2011.03.019.

(268) Tiwari, S.; Bahadur, P. Modified Hyaluronic Acid Based Materials for Biomedical Applications. *Int. J. Biol. Macromol.* **2019**, *121*, 556–571. https://doi.org/10.1016/j.ijbiomac.2018.10.049.

(269) Highley, C. B.; Prestwich, G. D.; Burdick, J. A. Recent Advances in Hyaluronic Acid Hydrogels for Biomedical Applications. *Curr. Opin. Biotechnol.* **2016**, *40*, 35–40. https://doi.org/10.1016/j.copbio.2016.02.008.

(270) Walimbe, T.; Panitch, A.; Sivasankar, P. M. A Review of Hyaluronic Acid and Hyaluronic Acid-Based Hydrogels for Vocal Fold Tissue Engineering. *J. Voice* **2017**, *31* (4), 416–423. https://doi.org/10.1016/j.jvoice.2016.11.014.

(271) Lam, J.; Truong, N. F.; Segura, T. Design of Cell–Matrix Interactions in Hyaluronic Acid Hydrogel Scaffolds. *Acta Biomater.* **2014**, *10* (4), 1571–1580. https://doi.org/10.1016/j.actbio.2013.07.025.

(272) Mehvar, R. Dextrans for Targeted and Sustained Delivery of Therapeutic and Imaging Agents. *J. Control. Release* **2000**, *69* (1), 1–25. https://doi.org/10.1016/S0168-3659(00)00302-3.

(273) Thongchaivetcharat, K.; Jenjob, R.; Seidi, F.; Crespy, D. Programming PH-Responsive Release of Two Payloads from Dextran-Based Nanocapsules. *Carbohydr. Polym.* **2019**, *217* (April), 217–223. https://doi.org/10.1016/j.carbpol.2019.04.023.

(274) Felt, O.; Buri, P.; Gurny, R. Chitosan: A Unique Polysaccharide for Drug Delivery. *Drug Dev. Ind. Pharm.* **1998**, *24* (11), 979–993. https://doi.org/10.3109/03639049809089942.

(275) Shanmuganathan, R.; Edison, T. N. J. I.; LewisOscar, F.; Kumar, P.; Shanmugam, S.; Pugazhendhi, A. Chitosan Nanopolymers: An Overview of Drug Delivery against Cancer. *Int. J. Biol. Macromol.* **2019**, *130*, 727–736. https://doi.org/10.1016/j.ijbiomac.2019.02.060.

(276) Narayanan, D.; Jayakumar, R.; Chennazhi, K. P. Versatile Carboxymethyl Chitin and Chitosan Nanomaterials: A Review. *Wiley Interdiscip. Rev. Nanomedicine Nanobiotechnology* **2014**, *6* (6), 574–598. https://doi.org/10.1002/wnan.1301.

(277) Lee, S. J.; Min, H. S.; Ku, S. H.; Son, S.; Kwon, I. C.; Kim, S. H.; Kim, K. Tumor-Targeting Glycol Chitosan Nanoparticles as a Platform Delivery Carrier in Cancer Diagnosis and Therapy. *Nanomedicine* **2014**, *9* (11), 1697–1713. https://doi.org/10.2217/nnm.14.99.

(278) Lallana, E.; Rios de la Rosa, J. M.; Tirella, A.; Pelliccia, M.; Gennari, A.; Stratford, I. J.; Puri, S.; Ashford, M.; Tirelli, N. Chitosan/Hyaluronic Acid Nanoparticles: Rational Design Revisited for RNA Delivery. *Mol. Pharm.* **2017**, *14* (7), 2422–2436. https://doi.org/10.1021/acs.molpharmaceut.7b00320.

(279) Saranya, N.; Moorthi, A.; Saravanan, S.; Devi, M. P.; Selvamurugan, N. Chitosan and Its Derivatives for Gene Delivery. *Int. J. Biol. Macromol.* **2011**, *48* (2), 234–238. https://doi.org/10.1016/j.ijbiomac.2010.11.013.

(280) Shariatinia, Z. Pharmaceutical Applications of Chitosan. *Adv. Colloid Interface Sci.* **2019**, *263*, 131–194. https://doi.org/10.1016/j.cis.2018.11.008.

(281) Yhee, J. Y.; Son, S.; Kim, S. H.; Park, K.; Choi, K.; Kwon, I. C. Self-Assembled Glycol Chitosan Nanoparticles for Disease-Specific Theranostics. *J. Control. Release* **2014**, *193*, 202–213. https://doi.org/10.1016/j.jconrel.2014.05.009.

(282) Hassani Najafabadi, A.; Abdouss, M.; Faghihi, S. Synthesis and Evaluation of PEG-O-Chitosan Nanoparticles for Delivery of Poor Water Soluble Drugs: Ibuprofen. *Mater. Sci. Eng. C* **2014**, *41*, 91–99. https://doi.org/10.1016/j.msec.2014.04.035.

(283) Yang, Y.; Wang, S.; Wang, Y.; Wang, X.; Wang, Q.; Chen, M. Advances in Self-Assembled Chitosan Nanomaterials for Drug Delivery. *Biotechnol. Adv.* **2014**, *32* (7), 1301–1316. https://doi.org/10.1016/j.biotechadv.2014.07.007.

(284) Xu, Y.; Wu, Y.; Sun, P.; Zhang, F.; Linhardt, R. J.; Zhang, A. Chemically Modified Polysaccharides: Synthesis, Characterization, Structure Activity Relationships of Action. *Int. J. Biol. Macromol.* **2019**, *132*, 970–977. https://doi.org/10.1016/j.ijbiomac.2019.03.213.

(285) Yang, X.; Shi, X.; D'arcy, R.; Tirelli, N.; Zhai, G. Amphiphilic Polysaccharides as Building Blocks for Self-Assembled Nanosystems: Molecular Design and Application in Cancer and Inflammatory Diseases. *J. Control. Release* **2018**, *272*, 114–144. https://doi.org/10.1016/j.jconrel.2017.12.033.

(286) Elschner, T.; Wondraczek, H.; Heinze, T. Syntheses and Detailed Structure Characterization of Dextran Carbonates. *Carbohydr. Polym.* **2013**, *93* (1), 216–223. https://doi.org/10.1016/j.carbpol.2012.01.091.

(287) Li, D.; Xu, W.; Li, P.; Ding, J.; Cheng, Z.; Chen, L.; Yan, L.; Chen, X. Self-Targeted Polysaccharide Prodrug Suppresses Orthotopic Hepatoma. *Mol. Pharm.* **2016**, *13* (12), 4231–4235. https://doi.org/10.1021/acs.molpharmaceut.6b00747.

(288) Hu, Y.; Li, Y.; Xu, F.-J. Versatile Functionalization of Polysaccharides via Polymer Grafts: From Design to Biomedical Applications. *Acc. Chem. Res.* **2017**, *50* (2), 281–292. https://doi.org/10.1021/acs.accounts.6b00477.

(289) Thakur, V. K.; Thakur, M. K. Recent Advances in Graft Copolymerization and Applications of Chitosan: A Review. *ACS Sustain. Chem. Eng.* **2014**, *2* (12), 2637–2652. https://doi.org/10.1021/sc500634p.

(290) Tizzotti, M.; Charlot, A.; Fleury, E.; Stenzel, M.; Bernard, J. Modification of Polysaccharides through Controlled/Living Radical Polymerization Grafting-towards the Generation of High Performance Hybrids. *Macromol. Rapid Commun.* **2010**, *31* (20), 1751–1772. https://doi.org/10.1002/marc.201000072.

(291) Guo, Y.; Wang, X.; Shen, Z.; Shu, X.; Sun, R. Preparation of Cellulose-Graft-Poly(ε-Caprolactone) Nanomicelles by Homogeneous ROP in Ionic Liquid. *Carbohydr. Polym.* **2013**, *92* (1), 77–83. https://doi.org/10.1016/j.carbpol.2012.09.058.

(292) Huang, Y.-C.; Jan, J.-S. Carboxylmethyl Chitosan-Graft-Poly(γ-Benzyl-l-Glutamate) Glycopeptides: Synthesis and Particle Formation as Encapsulants. *Polymer (Guildf).* **2014**, *55* (2), 540–549. https://doi.org/10.1016/j.polymer.2013.12.037.

(293) Chi, P.; Wang, J.; Liu, C. Synthesis and Characterization of Polycationic Chitosan-Graft-Poly (l-Lysine). *Mater. Lett.* **2008**, *62* (1), 147–150. https://doi.org/10.1016/j.matlet.2007.04.117.

(294) Nouvel, C.; Frochot, C.; Sadtler, V.; Dubois, P.; Dellacherie, E.; Six, J.-L. Polylactide-Grafted Dextrans: Synthesis and Properties at Interfaces and in Solution. *Macromolecules* **2004**, *37* (13), 4981–4988. https://doi.org/10.1021/ma049857x.

(295) Nouvel, C.; Dubois, P.; Dellacherie, E.; Six, J.-L. Controlled Synthesis of Amphiphilic Biodegradable Polylactide-Grafted Dextran Copolymers. *J. Polym. Sci. Part A Polym. Chem.* **2004**, *42* (11), 2577–2588. https://doi.org/10.1002/pola.20100.

(296) Wen, Y.; Oh, J. K. Recent Strategies to Develop Polysaccharide-Based Nanomaterials for Biomedical Applications. *Macromol. Rapid Commun.* **2014**, n/a-n/a. https://doi.org/10.1002/marc.201400406.

(297) Ramadan, M. H.; Prata, J. E.; Karácsony, O.; Dunér, G.; Washburn, N. R. Reducing Protein Adsorption with Polymer-Grafted Hyaluronic Acid Coatings. *Langmuir* **2014**, *30* (25), 7485–7495. https://doi.org/10.1021/la500918p.

(298) Huang, W.-C.; Chen, S.-H.; Chiang, W.-H.; Huang, C.-W.; Lo, C.-L.; Chern, C.-S.; Chiu, H.-C. Tumor Microenvironment-Responsive Nanoparticle Delivery of Chemotherapy for Enhanced Selective Cellular Uptake and Transportation within Tumor. *Biomacromolecules* **2016**, *17* (12), 3883–3892. https://doi.org/10.1021/acs.biomac.6b00956.

(299) Lee, H.; Ahn, C.-H.; Park, T. G. Poly[Lactic- Co -(Glycolic Acid)]-Grafted Hyaluronic Acid Copolymer Micelle Nanoparticles for Target-Specific Delivery of Doxorubicin. *Macromol. Biosci.* **2009**, *9* (4), 336–342. https://doi.org/10.1002/mabi.200800229.

(300) Elchinger, P.-H.; Faugeras, P.-A.; Boëns, B.; Brouillette, F.; Montplaisir, D.; Zerrouki, R.; Lucas, R. Polysaccharides: The "Click" Chemistry Impact. *Polymers (Basel).* **2011**, *3* (4), 1607–1651. https://doi.org/10.3390/polym3041607.

(301) Meng, X.; Edgar, K. J. "Click" Reactions in Polysaccharide Modification. *Prog. Polym. Sci.* **2016**, *53*, 52–85. https://doi.org/10.1016/j.progpolymsci.2015.07.006.

(302) Schatz, C.; Lecommandoux, S. Polysaccharide-Containing Block Copolymers: Synthesis, Properties and Applications of an Emerging Family of Glycoconjugates. *Macromol. Rapid Commun.* **2010**, *31* (19), 1664–1684. https://doi.org/10.1002/marc.201000267.

(303) Li, B.-G.; Zhang, L.-M. Synthesis and Characterization of Novel Amphiphilic Block Copolymers Based on Maltoheptaose and Poly(ε-Caprolactone). *Carbohydr. Polym.* **2008**, *74* (3), 390–395. https://doi.org/10.1016/j.carbpol.2008.03.009.

(304) Yagi, S.; Kasuya, N.; Fukuda, K. Synthesis and Characterization of Cellulose-b-Polystyrene. *Polym. J.* **2010**, *42* (4), 342–348. https://doi.org/10.1038/pj.2009.342.

(305) Houga, C.; Meins, J.-F. Le; Borsali, R.; Taton, D.; Gnanou, Y. Synthesis of ATRP-Induced Dextran-b-Polystyrene Diblock Copolymers and Preliminary Investigation of Their Self-Assembly in Water. *Chem. Commun.* **2007**, No. 29, 3063. https://doi.org/10.1039/b706248f.

(306) Kim, S.-H.; Kim, J.-H.; You, D. G.; Saravanakumar, G.; Yoon, H. Y.; Choi, K. Y.; Thambi, T.; Deepagan, V. G.; Jo, D.-G.; Park, J. H. Self-Assembled Dextran Sulphate Nanoparticles for Targeting Rheumatoid Arthritis. *Chem. Commun.* **2013**, *49* (88), 10349. https://doi.org/10.1039/c3cc44260h.

(307) Huang, J.; Zhang, H.; Yu, Y.; Chen, Y.; Wang, D.; Zhang, G.; Zhou, G.; Liu, J.; Sun, Z.; Sun, D.; et al. Biodegradable Self-Assembled Nanoparticles of Poly (d,l-Lactide-Co-Glycolide)/Hyaluronic Acid Block Copolymers for Target Delivery of Docetaxel to Breast Cancer. *Biomaterials* **2014**, *35* (1), 550–566. https://doi.org/10.1016/j.biomaterials.2013.09.089.

(308) Haas, S.; Hain, N.; Raoufi, M.; Handschuh-Wang, S.; Wang, T.; Jiang, X.; Schönherr, H. Enzyme Degradable Polymersomes from Hyaluronic Acid- Block -Poly(ε-Caprolactone) Copolymers for the Detection of Enzymes of Pathogenic Bacteria. *Biomacromolecules* **2015**, *16* (3), 832–841. https://doi.org/10.1021/bm501729h.

(309) Han, H. S.; Thambi, T.; Choi, K. Y.; Son, S.; Ko, H.; Lee, M. C.; Jo, D.-G.; Chae, Y. S.; Kang, Y. M.; Lee, J. Y.; et al. Bioreducible Shell-Cross-Linked Hyaluronic Acid Nanoparticles for Tumor-Targeted Drug Delivery. *Biomacromolecules* **2015**, *16* (2), 447–456. https://doi.org/10.1021/bm5017755.

(310) Zhao, Z.; Yao, X.; Zhang, Z.; Chen, L.; He, C.; Chen, X. Boronic Acid Shell-Crosslinked Dextran- b- PLA Micelles for Acid-Responsive Drug Delivery. *Macromol. Biosci.* **2014**, *14* (11), 1609–1618. https://doi.org/10.1002/mabi.201400251.

(311) Tücking, K.-S.; Grützner, V.; Unger, R. E.; Schönherr, H. Dual Enzyme-Responsive Capsules of Hyaluronic Acid- Block -Poly(Lactic Acid) for Sensing Bacterial Enzymes. *Macromol. Rapid Commun.* **2015**, *36* (13), 1248–1254. https://doi.org/10.1002/marc.201500076.

(312) Bonduelle, C.; Huang, J.; Ibarboure, E.; Heise, A.; Lecommandoux, S. Synthesis and Self-Assembly of "Tree-like" Amphiphilic Glycopolypeptides. *Chem. Commun.* **2012**, *48* (67), 8353. https://doi.org/10.1039/c2cc32970k.

(313) Schatz, C.; Louguet, S.; Le Meins, J.-F.; Lecommandoux, S. Polysaccharide- Block -Polypeptide Copolymer Vesicles: Towards Synthetic Viral Capsids. *Angew. Chemie Int. Ed.* **2009**, *48* (14), 2572–2575. https://doi.org/10.1002/anie.200805895.

(314) Zhang, A.; Zhang, Z.; Shi, F.; Xiao, C.; Ding, J.; Zhuang, X.; He, C.; Chen, L.; Chen, X. Redox-Sensitive Shell-Crosslinked Polypeptide -Block- Polysaccharide Micelles for Efficient Intracellular Anticancer Drug Delivery. *Macromol. Biosci.* **2013**, *13* (9), 1249–1258. https://doi.org/10.1002/mabi.201300175.

(315) Jeong, Y.-I.; Kang, D. H. Doxorubicin-Incorporated Polymeric Micelles Composed of Dextran-b-Poly(DL-Lactide-Co-Glycolide) Copolymer. *Int. J. Nanomedicine* **2011**, 1415. https://doi.org/10.2147/IJN.S19491.

(316) Yang, X.; Shi, X.; D'arcy, R.; Tirelli, N.; Zhai, G. Amphiphilic Polysaccharides as Building Blocks for Self-Assembled Nanosystems: Molecular Design and Application in Cancer and Inflammatory Diseases. *J. Control. Release* **2018**, *272* (October 2017), 114–144. https://doi.org/10.1016/j.jconrel.2017.12.033.

(317) Liu, M.; Du, H.; Zhai, G. Self-Assembled Nanoparticles Based on Chondroitin Sulfate-Deoxycholic Acid Conjugates for Docetaxel Delivery: Effect of Degree of Substitution of Deoxycholic Acid. *Colloids Surfaces B Biointerfaces* **2016**, *146*, 235–244. https://doi.org/10.1016/j.colsurfb.2016.06.019.

(318) Houga, C.; Giermanska, J.; Lecommandoux, S.; Borsali, R.; Taton, D.; Gnanou, Y.; Le Meins, J.-F. Micelles and Polymersomes Obtained by Self-Assembly of Dextran and Polystyrene Based Block Copolymers. *Biomacromolecules* **2009**, *10* (1), 32–40. https://doi.org/10.1021/bm800778n.

(319) Guan, Q.; Sun, D.; Zhang, G.; Sun, C.; Wang, M.; Ji, D.; Yang, W. Docetaxel-Loaded Self-Assembly Stearic Acid-Modified Bletilla Striata Polysaccharide Micelles and Their Anticancer Effect: Preparation, Characterization, Cellular Uptake and In Vitro Evaluation. *Molecules* **2016**, *21* (12), 1641. https://doi.org/10.3390/molecules21121641.

(320) Saldías, C.; Velásquez, L.; Quezada, C.; Leiva, A. Physicochemical Assessment of Dextran-g-Poly (ε-Caprolactone) Micellar Nanoaggregates as Drug Nanocarriers. *Carbohydr. Polym.* **2015**, *117*, 458–467. https://doi.org/10.1016/j.carbpol.2014.09.035.

(321) Hu, K.; Zhou, H.; Liu, Y.; Liu, Z.; Liu, J.; Tang, J.; Li, J.; Zhang, J.; Sheng, W.; Zhao, Y.; et al. Hyaluronic Acid Functional Amphipathic and Redox-Responsive Polymer Particles for the Co-Delivery of Doxorubicin and Cyclopamine to Eradicate Breast Cancer Cells and Cancer Stem Cells. *Nanoscale* **2015**, *7* (18), 8607–8618. https://doi.org/10.1039/C5NR01084E.

(322) Vafaei, S. Y.; Esmaeili, M.; Amini, M.; Atyabi, F.; Ostad, S. N.; Dinarvand, R. Self Assembled Hyaluronic Acid Nanoparticles as a Potential Carrier for Targeting the Inflamed Intestinal Mucosa. *Carbohydr. Polym.* **2016**, *144*, 371–381. https://doi.org/10.1016/j.carbpol.2016.01.026.

(323) Upadhyay, K. K.; Meins, J.-F. Le; Misra, A.; Voisin, P.; Bouchaud, V.; Ibarboure, E.; Schatz, C.; Lecommandoux, S. Biomimetic Doxorubicin Loaded Polymersomes from Hyaluronan- Block -Poly(γ-Benzyl Glutamate) Copolymers. *Biomacromolecules* **2009**, *10* (10), 2802–2808. https://doi.org/10.1021/bm9006419.

(324) Upadhyay, K. K.; Bhatt, A. N.; Mishra, A. K.; Dwarakanath, B. S.; Jain, S.; Schatz, C.; Le Meins, J.-F.; Farooque, A.; Chandraiah, G.; Jain, A. K.; et al. The Intracellular Drug Delivery and Anti Tumor Activity of Doxorubicin Loaded Poly(γ-Benzyl l-Glutamate)-b-Hyaluronan Polymersomes. *Biomaterials* **2010**, *31* (10), 2882–2892. https://doi.org/10.1016/j.biomaterials.2009.12.043.

(325) Li, F.; Bae, B.; Na, K. Acetylated Hyaluronic Acid/Photosensitizer Conjugate for the Preparation of Nanogels with Controllable Phototoxicity: Synthesis, Characterization, Autophotoquenching Properties, and in Vitro Phototoxicity against HeLa Cells. *Bioconjug. Chem.* **2010**, *21* (7), 1312–1320. https://doi.org/10.1021/bc100116v.

(326) Zhang, L.; Yao, J.; Zhou, J.; Wang, T.; Zhang, Q. Glycyrrhetinic Acid-Graft-Hyaluronic Acid Conjugate as a Carrier for Synergistic Targeted Delivery of Antitumor Drugs. *Int. J. Pharm.* **2013**, *441* (1–2), 654–664. https://doi.org/10.1016/j.ijpharm.2012.10.030.

(327) Chiesa, E.; Dorati, R.; Pisani, S.; Conti, B.; Bergamini, G.; Modena, T.; Genta, I. The Microfluidic Technique and the Manufacturing of Polysaccharide Nanoparticles. *Pharmaceutics* **2018**, *10* (4), 267. https://doi.org/10.3390/pharmaceutics10040267.

(328) Geijtenbeek, T. B. H.; Gringhuis, S. I. Signalling through C-Type Lectin Receptors: Shaping Immune Responses. *Nat. Rev. Immunol.* **2009**, *9* (7), 465–479. https://doi.org/10.1038/nri2569.

(329) Mantuano, N. R.; Oliveira-Nunes, M. C.; Alisson-Silva, F.; Dias, W. B.; Todeschini, A. R. Emerging Role of Glycosylation in the Polarization of Tumor-Associated Macrophages. *Pharmacol. Res.* **2019**, *146*, 104285. https://doi.org/10.1016/j.phrs.2019.104285.

(330) Chen, F.; Huang, G. Application of Glycosylation in Targeted Drug Delivery. *Eur. J. Med. Chem.* **2019**, *182*, 111612. https://doi.org/10.1016/j.ejmech.2019.111612.

(331) Mereiter, S.; Balmaña, M.; Campos, D.; Gomes, J.; Reis, C. A. Glycosylation in the Era of Cancer-Targeted Therapy: Where Are We Heading? *Cancer Cell* **2019**, *36* (1), 6–16. https://doi.org/10.1016/j.ccell.2019.06.006.

(332) David, A.; Kopecková, P.; Kopeček, J.; Rubinstein, A. The Role of Galactose, Lactose, and Galactose Valency in the Biorecognition of N-(2-Hydroxypropyl)Methacrylamide Copolymers by Human Colon Adenocarcinoma Cells. *Pharm. Res.* **2002**, *19* (8), 1114–1122. https://doi.org/10.1023/A:1019885807067.

(333) Kammona, O.; Kiparissides, C. Recent Advances in Nanocarrier-Based Mucosal Delivery of Biomolecules. *J. Control. Release* **2012**, *161* (3), 781–794. https://doi.org/10.1016/j.jconrel.2012.05.040.

(334) Cao, J.; Zhang, Y.; Wu, Y.; Wu, J.; Wang, W.; Wu, Q.; Yuan, Z. The Effects of Ligand Valency and Density on the Targeting Ability of Multivalent Nanoparticles Based on Negatively Charged Chitosan Nanoparticles. *Colloids Surfaces B Biointerfaces* **2018**, *161*, 508–518. https://doi.org/10.1016/j.colsurfb.2017.11.015.

(335) Fievez, V.; Plapied, L.; des Rieux, A.; Pourcelle, V.; Freichels, H.; Wascotte, V.; Vanderhaeghen, M.-L.; Jerôme, C.; Vanderplasschen, A.; Marchand-Brynaert, J.; et al. Targeting Nanoparticles to M Cells with Non-Peptidic Ligands for Oral Vaccination. *Eur. J. Pharm. Biopharm.* **2009**, *73* (1), 16–24. https://doi.org/10.1016/j.ejpb.2009.04.009.

(336) Lai, S. K.; Wang, Y.-Y.; Hanes, J. Mucus-Penetrating Nanoparticles for Drug and Gene Delivery to Mucosal Tissues. *Adv. Drug Deliv. Rev.* **2009**, *61* (2), 158–171. https://doi.org/10.1016/j.addr.2008.11.002.

(337) Sosnik, A.; Menaker Raskin, M. Polymeric Micelles in Mucosal Drug Delivery: Challenges towards Clinical Translation. *Biotechnol. Adv.* **2015**, *33* (6), 1380–1392. https://doi.org/10.1016/j.biotechadv.2015.01.003.

(338) Ohba, S.; Fujii, H.; Ito, S.; Fujimaki, M.; Matsumoto, F.; Furukawa, M.; Yokoyama, J.; Kusunoki, T.; Ikeda, K.; Hino, O. Overexpression of GLUT-1 in the Invasion Front Is Associated with Depth of Oral Squamous Cell Carcinoma and Prognosis. *J. Oral Pathol. Med.* **2010**, *39* (1), 74–78. https://doi.org/10.1111/j.1600-0714.2009.00814.x.

(339) Amann, T.; Maegdefrau, U.; Hartmann, A.; Agaimy, A.; Marienhagen, J.; Weiss, T. S.; Stoeltzing, O.; Warnecke, C.; Schölmerich, J.; Oefner, P. J.; et al. GLUT1 Expression Is Increased in Hepatocellular Carcinoma and Promotes Tumorigenesis. *Am. J. Pathol.* **2009**, *174* (4), 1544–1552. https://doi.org/10.2353/ajpath.2009.080596.

(340) Calvaresi, E. C.; Hergenrother, P. J. Glucose Conjugation for the Specific Targeting and Treatment of Cancer. *Chem. Sci.* **2013**, *4* (6), 2319. https://doi.org/10.1039/c3sc22205e.

(341) Aft, R. L.; Zhang, F. W.; Gius, D. Evaluation of 2-Deoxy-D-Glucose as a Chemotherapeutic Agent: Mechanism of Cell Death. *Br. J. Cancer* **2002**, *87* (7), 805–812. https://doi.org/10.1038/sj.bjc.6600547.

(342) Lin, Y.-S.; Tungpradit, R.; Sinchaikul, S.; An, F.-M.; Liu, D.-Z.; Phutrakul, S.; Chen, S.-T. Targeting the Delivery of Glycan-Based Paclitaxel Prodrugs to Cancer Cells via Glucose Transporters. *J. Med. Chem.* **2008**, *51* (23), 7428–7441. https://doi.org/10.1021/jm8006257.

(343) Zhang, Y.; Chan, J. W.; Moretti, A.; Uhrich, K. E. Designing Polymers with Sugar-Based Advantages for Bioactive Delivery Applications. *J. Control. Release* **2015**, *219*, 355–368. https://doi.org/10.1016/j.jconrel.2015.09.053.

(344) Biomimetic Doxorubicin Loaded Polymersomes from Hyaluronan-Block- Poly(γ-Benzyl Glutamate) Copolymers. *Biomacromolecules* **2009**, *10* (10), 2802–2808. https://doi.org/10.1021/bm9006419.

(345) Upadhyay, K. K.; Mishra, A. K.; Chuttani, K.; Kaul, A.; Schatz, C.; Le Meins, J.-F.; Misra, A.; Lecommandoux, S. The in Vivo Behavior and Antitumor Activity of Doxorubicin-Loaded Poly(γ-Benzyl l-Glutamate)-Block-Hyaluronan Polymersomes in Ehrlich Ascites Tumor-Bearing BalB/c Mice. *Nanomedicine Nanotechnology, Biol. Med.* **2012**, *8* (1), 71–80. https://doi.org/10.1016/j.nano.2011.05.008.

(346) Upadhyay, K. K.; Bhatt, A. N.; Castro, E.; Mishra, A. K.; Chuttani, K.; Dwarakanath, B. S.; Schatz, C.; Le Meins, J.-F.; Misra, A.; Lecommandoux, S. In Vitro and In Vivo Evaluation of Docetaxel Loaded Biodegradable Polymersomes. *Macromol. Biosci.* **2010**, n/a-n/a. https://doi.org/10.1002/mabi.200900415.

(347) Li, Q.; Liu, W.; Dai, J.; Zhang, C. Synthesis of Polysaccharide-Block-Polypeptide Copolymer for Potential Co-Delivery of Drug and Plasmid DNA. *Macromol. Biosci.* **2015**, *15* (6), 756–764. https://doi.org/10.1002/mabi.201400454.

CHAPTER 2

POLYSACCHARIDE-*b*-POLYPEPTIDE BIOCONJUGATES: TOWARDS BIOACTIVE THERMO-SENSITIVE SELF-ASSEMBLIES

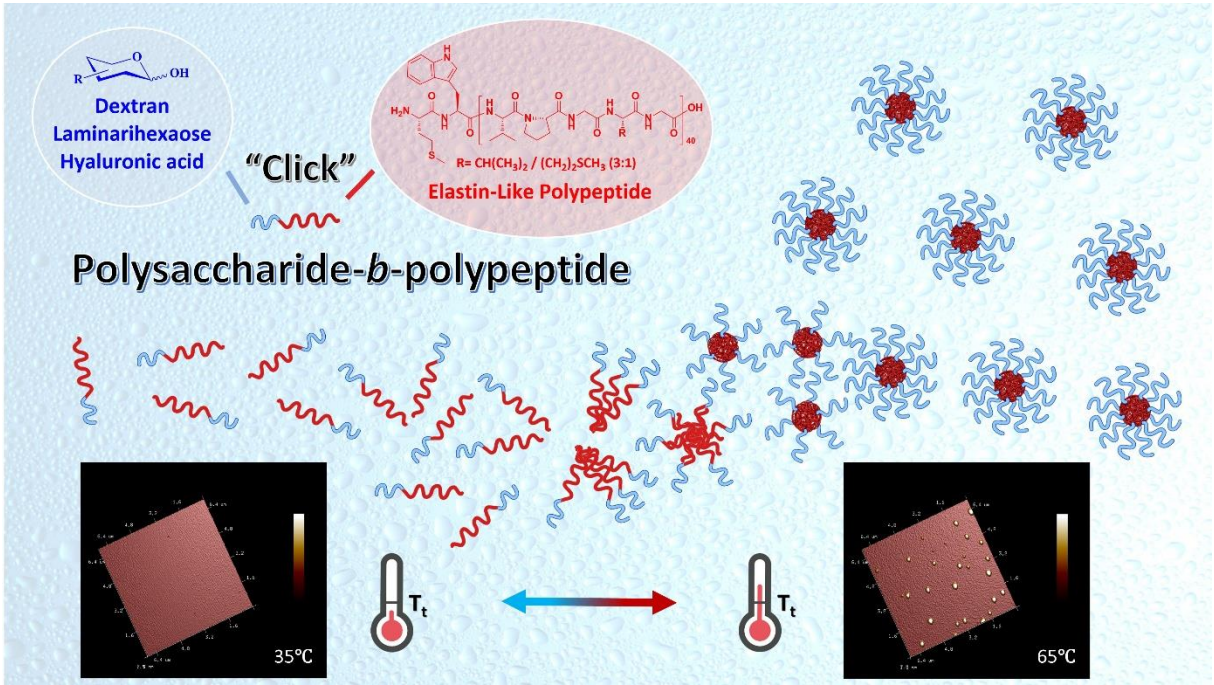

ABSTRACT

The advantageous biological properties of polysaccharides and precise stimuli-responsiveness of elastin-like polypeptides (ELPs) are of great interest for the design of polysaccharide and polypeptide-based amphiphilic block copolymers for biomedical applications. Herein, we report the synthesis and characterization of a series of polysaccharide-*block*-ELP copolymers, containing two biocompatible and biodegradable blocks coupled *via* copper(I)-catalyzed azide-alkyne cycloaddition (CuAAC). The resulting bioconjugates are capable of self-assembling into well-defined nanoparticles in aqueous solution upon raising the solution temperature above a specific transition temperature (T_t) – a characteristic of the ELP moiety. To the best of our knowledge, this is the first study where bioactive polysaccharides were combined with a stimuli-responsive ELP for the preparation of bioactive thermo-sensitive self-assemblies, providing insight into novel pathways for designing bioinspired stimuli-responsive self-assemblies for biomedical applications.

1. INTRODUCTION

Nanostructured carriers resulting from the self-assembly of amphiphilic block copolymers have been developed for a broad range of applications, ranging from biomimetics[1-3] to nanomedicines.[4,5] Numerous synthetic polymers have been selected as building blocks due to their biocompatibility and low cytotoxicity, such as poly(ethylene glycol),[6,7] poly(L-glutamic acid),[8,9] poly(γ-benzyl-L-glutamate),[10-12] poly(2-hydroxyethyl methacrylate),[13,14] polylactide,[15,16] polycaprolactone,[17] and poly(trimethylene carbonate),[9,18] and have been approved for biomedical applications by regulatory agencies. Additionally, biologically derived or inspired polymers, like polysaccharides[19-21] and polypeptides[22], show considerable promise as block copolymer constructs since they are naturally biodegradable, biocompatible and are potentially biofunctional. Regarding the biomedical application of block copolymers as carriers, a key challenge is to enhance accumulation of the active components at the biological target.[23] A typical method to achieve this goal is to introduce bioactive targeting moieties on the surface of nano-objects.[24-26] Such surface decorated strategies have led to the design of original bioactive block copolymers that favor the use of natural targeting functionalities.[27-29] In this respect, bioactive polysaccharides-based (*e.g.*, chitosan,[30,31] galactan,[32] fucoidan,[33] hyaluronan[11,34]) block copolymers able to recognize and bind to specific receptors demonstrate particularly promising interest for potential biomedical applications.[35]

Recently, stimuli-responsive polymer nanosystems[36-41] have been extensively explored due to their ability of supramolecular assembly or disassembly in response to "internal stimuli", such as pH,[42,43] reductive-oxidative environment[44,45] and enzymes,[46] or "external stimuli", such as temperature,[47,48] light[49,50] and magnetic field[51]. Among them, recombinant elastin-like polypeptides (ELPs) have gained significant attention as stimuli-responsive protein-like polymers.[52-54] In aqueous solution, ELPs display a lower critical solution temperature (LCST), similar to synthetic thermo-responsive polymers such as poly(*N*-isopropyl acrylamide) PNIPAM,[55] also referred to as inverse transition temperature (T_t) that actually corresponds to the cloud point temperature. Below the T_t, ELPs are water soluble, while upon heating the solution temperature above the T_t, ELPs aggregate into insoluble coacervates, this phase transition being fully reversible. T_t can be highly tunable either by playing with molecular parameters such as varying amino acid residues composition and protein molecular weight, or by controlling environmental parameters such as concentration, pH or cosolutes.[56-58] Post-translational chemical modification of ELPs, for example, chemoselective modifications of ELPs at the *C*- or *N*-terminal end,[59] or at specific residues such as methionine,[60-62] cysteine,[63,64] tyrosine,[65] or lysine,[66,67] has also been exploited for tuning the T_t of specific ELPs, as well as for facilitating subsequent conjugation of ELPs with polymers,[59,66] dyes,[64] or drugs[67,68]. ELP diblock copolymers could be obtained by fusing ELP blocks with different T_t, which self-assembled into micelles by triggering the phase transition of the ELP block with the lowest T_t.[69-72] The stimuli-responsive property of ELPs has also been exploited to obtain well-defined ELP-based nanomedicines, such as ELP-proteins,[73] ELP-drug conjugates,[67] and ELP-nucleic acid complexes.[74] Moreover, as a building block of copolymers, combinations of ELPs with other types of polymer-based blocks, such as poly(γ-benzyl-L-glutamate),[75] poly(L-glutamic acid),[8] poly(aspartic acid),[76] and poly(ethylene glycol),[59,77] has demonstrated to be a fascinating strategy to obtain functional block copolymers which could self-assemble in aqueous conditions above a specific and tunable T_t.

Although polysaccharides and polypeptides-based block copolymers were reported for decades, benefits from conjugates of polysaccharides with ELPs have not yet been investigated, since a highly efficient and proper conjugation method is required. We previously synthesized polysaccharide-*b*-polypeptide block copolymers *via* copper(I)-catalyzed azide-alkyne cycloaddition (CuAAC) for the preparation of glycoprotein biomimetic vesicles,[11,12] and demonstrated the interest of such design as drug-delivery nanocarriers.[78,79] To be able to use CuAAC "click" chemistry for conjugation, polysaccharides and ELPs need to be functionalized

with either an azide or an alkyne group.[80] Polysaccharides can be readily modified at the reducing end with azide-containing linkers using reductive amination,[11,12] or by using bifunctional oxyamine, oxime or *N*-methoxyamine linkers[81,82]. Regarding the introduction of an alkyne group at the ELP chain end, an alkyne functionalized *N*-hydroxysuccinimide ester (NHS-ester) can be easily prepared and coupled with the *N*-terminal primary amine group, granting the ELP with a functional moiety to conjugate with the polysaccharide.[83]

The aim of this study is to combine bioactive polysaccharides and precise stimuli-responsive ELPs into block copolymers capable of self-assembling into nanoparticles in aqueous solution upon heating above a specific T_t. Three different polysaccharides namely dextran,[10,12] laminarihexaose[84,85] and hyaluronic acid,[11,25,34] were functionalized with an azide moiety at their reducing end, while the ELP was modified with an alkyne moiety at the *N*-terminus by NHS-coupling chemistry. Three polysaccharide-*b*-ELP bioconjugates were thus prepared through click chemistry, isolated and subsequently fully characterized. Their transition temperature behaviors were studied through turbidity measurements by ultraviolet–visible (UV-Vis) spectroscopy and their self-assembly properties were subsequently investigated by temperature-varying dynamic light scattering (DLS) and temperature-controlled liquid atomic force microscopy (Liquid AFM). To our knowledge, the synthesis and temperature-triggered self-assembly behavior study of polysaccharide-*b*-ELPs block copolymers were demonstrated for the first time, providing insight into original pathways for designing bioactive thermo-sensitive self-assemblies for biomedical applications.

2. EXPERIMENTAL SECTION

2.1 Materials

Acrolein (95%), sodium azide (NaN_3, 99.5%), acetic acid (AcOH, 99.8%), methoxylamine hydrochloride (98%), sodium cyanoborohydride ($NaBH_3CN$, 95%), hydrochloric acid (HCl, 37%), 4-pentynoic acid (97%), *N*,*N'*-dicyclohexylcarbodiimide (DCC, 99%), *N*-hydroxysuccinimide (NHS, 98%), trimethylamine (TEA, 99%), copper(II) sulfate pentahydrate ($CuSO_4$, 99%), dichloromethane (DCM, 99.9%), *N*,*N*-dimethylformamide (DMF, 99.8%), dimethyl sulfoxide (DMSO, 99.7%), methanol (MeOH, 99.8%), diethyl ether (99.9%) and anhydrous magnesium sulfate ($MgSO_4$, 99.5%) were purchased from Sigma-Aldrich. *N*,*N*-Diisopropylethylamine (DIPEA, 99%), sodium acetate (AcONa, 99%) and sodium ascorbate (NaAsc, 99%) were obtained from Alfa Aesar. Tris(benzyltriazolylmethyl)amine (TBTA, 97%)

were purchased from TCI. Cuprisorb® was purchased from Seachem. Dextran (Dex, T10) was purchased from pharmacosmos. Laminarihexaose (Lam) was purchased from Megazyme. Sodium hyaluronate (HA) was purchased from Lifecore Biomedical. Water was purified using an ELGA PURELAB Classic system. Solvent was purified using PureSolv MD-5 solvent purification system from Innovative Technology. Dialysis was conducted using a Spectra/Por®6 dialysis membrane.

2.2 Synthetic Procedure

Synthesis of N-(3-azidopropyl)-O-methylhydroxylamine (Azide-linker, 1). Acrolein (1.84 mL, 27.4 mmol) was added to acetic acid (4 mL) at -20 ℃, followed by dropwise addition of a solution of sodium azide (2.38 g, 41.2 mmol) in H_2O (10.4 mL). The reaction mixture was let to stir at -20 ℃ for 1.5 hour. It was then quenched with a saturated solution of $NaHCO_3$ (80 mL) and the resulting mixture was extracted with DCM (2 × 100 mL). The combined organic extracts were washed with sat. aq. $NaHCO_3$ (150 mL), dried over $MgSO_4$, filtered and concentrated *in vacuo* to 100 mL. To the solution in DCM, methoxylamine hydrochloride (2.68 g, 31.68 mmol) and sodium acetate (4.42 g, 54 mmol) were added and the mixture was stirred overnight at r.t. Sat. aq. $NaHCO_3$ (150 mL) was added to quench the reaction and the resulting mixture was then extracted with DCM (2 × 100 mL). The combined organic extracts were washed with Sat. aq. $NaHCO_3$ (150 mL), dried over $MgSO_4$, filtered and concentrated *in vacuo* to 100 mL. To the solution in DCM, $NaBH_3CN$ (2 g, 32 mmol) was added, followed by dropwise addition of 1M ethanolic HCl (32 mL, freshly prepared by adding acetyl chloride to ethanol). The reaction mixture was stirred at r.t for 1.5 hour, concentrated and the resulting white solid suspended in sat. aq. $NaHCO_3$ (150 mL) and extracted with DCM (2 × 100 mL). The combined organic extracts were washed with sat. aq. $NaHCO_3$ (150 mL), dried over $MgSO_4$, filtered and concentrated *in vacuo* to afford the crude *N*-(3-azidopropyl)-*O*-methylhydroxylamine as a yellow oil. Purification of the crude product by silica gel column chromatography (1-3% MeOH in DCM) yielded *N*-(3-azidopropyl)-*O*-methylhydroxylamine as a colorless oil (Azide-linker, 2.2 g, 62% over 3 steps). ^{1}H NMR (400 MHz, $CDCl_3$): δ 3.55 (s, 3H, C*H*$_3$O), 3.41 (t, 2H, C*H*$_2$N$_3$), 3.00 (t, 2H, NHC*H*$_2$), 1.83 (p, 2H, CH$_2$C*H*$_2$CH$_2$). ^{13}C NMR (101 MHz, $CDCl_3$): δ 62.01 (*C*H$_3$O), 49.44 (*C*H$_2$N$_3$), 48.94 (NH*C*H$_2$), 26.87 (CH$_2$*C*H$_2$CH$_2$). In agreement with the literature data.[81]

Synthesis of Dextran-Azide (Dex-N_3, 2). The azide-linker (380 mg, 2.9 mmol) was added to a solution of dextran (MW=8,000 Da, 1 g, 125 μmol) in acetate buffer (AcOH / AcONa, 2 M, pH

4.6, 4.2 mL), and the reaction mixture was incubated at 40 ℃ with shaking, for 9 days. The product was purified by dialysis (dialysis bag MWCO 1 kDa) against pure water for 24 hour (changing water 3 times per day), followed by lyophilization to obtain the product as a white powder (805 mg, 79% yield). ^{1}H NMR (400 MHz, D_2O): δ 4.98 (d, H-1), 4.18 (d, C*H*N(OCH_3)CH_2), 4.04-3.97 (m, H-6), 3.95–3.89 (m, H-5), 3.69–3.80 (br m, H-6', H-3), 3.61–3.37 (br m, H-2, H-4, CH_2N_3), 3.20–3.13 (dt, CHN(OCH_3)CH_2), 3.01–2.93 (dt, CHN(OCH_3)C$H_{2'}$), 1.92–1.88 (m, $CH_2CH_2CH_2$). FT-IR (ATR): 3368, 2906, 2106 (υ_{azide}), 1351, 1148, 1164, 1007, 915, 846, 763, 545, 429 cm^{-1}.

Synthesis of Laminarihexaose-Azide (Lam-N_3, 3). The azide-linker (900 mg, 6.9 mmol) was added to a solution of laminarihexaose (500 mg, 0.5 mmol) in acetate buffer (AcOH / AcONa, 2 M, pH 4.6, 5 mL), and the reaction mixture incubated at 40 ℃ with shaking, for 8 days (vortexing 3 times per day). Then the mixture was lyophilized and re-dissolved in water 5 mL, purified by dialysis (dialysis bag MWCO 100 Da) against pure water for 3 days (changing water 3 times per day and transferring excess dialysis solution to new dialysis bag every 12 hour), followed by lyophilization to obtain the product as a white powder (302 mg, 54% yield). ^{1}H NMR (400 MHz, D_2O): δ 4.81 (d, H-1), 4.23 (m, C*H*N(OCH_3)CH_2), 3.97–3.88 (m, H-6), 3.86–3.68 (br m, H-6',H-3), 3.67–3.33 (br m, H-2,H-4,H-5, CH_2N_3), 3.22–3.13 (m, CHN(OCH_3)C$H_{2'}$), 3.03–2.95 (m, CHN(OCH_3)CH_2), 1.91 (m, $CH_2CH_2CH_2$). FT-IR (ATR): 3434, 3151, 2890, 2100 (υ_{azide}), 1568, 1403, 1308, 1159, 1072, 1022, 896, 557 cm^{-1}.

Synthesis of Hyaluronan-Azide (HA-N_3, 4). The azide-linker (520 mg, 4 mmol) and sodium cyanoborohydride (65 mg, 1 mmol) were added to a solution of sodium hyaluronate (MW= 7,000 Da, 1 g, 0.14 mmol) in acetate buffer (AcOH / AcONa, 2 M, pH 5.5, 5 mL), and the reaction mixture was incubated at 50 ℃ with shaking, for 5 days. The product was purified by dialysis (dialysis bag MWCO 1 kDa) against pure water for 24 hour (changing water 3 times per day), followed by lyophilization to obtain the product as a white powder. (610 mg, 60% yield). ^{1}H NMR (400 MHz, D_2O): δ 4.56 (d, GlcNAc H-1), 4.48 (d, GlcUA H-1), 3.99–3.67 (br m, GlcNAc H-6, H-2, H-3, H-5, GlcUA H-4), 3.66–3.41 (br m, GlcNAc H-4, GlcUA H-3, H-5, CH_2N_3), 3.35 (t, GlcUA H-2), 2.94–2.86 (m, $CH_2N(OCH_3)CH_2$), 2.03 (s, GlcNAc $COCH_3$), 1.87 (m, $CH_2CH_2CH_2$). FT-IR (ATR): 3323, 2892, 2107 (υ_{azide}), 1729, 1642, 1555, 1376, 1315, 1152, 1042, 610 cm^{-1}.

Synthesis of 4-Pentynoic Acid Succinimidyl Ester (Pentynoic NHS-ester, 5). *N, N*'-dicyclohexylcarbodiimide (480 mg, 2.3 mmol) was added to a solution of pentynoic acid (210

mg, 2.14 mmol) in DCM (8mL) and the mixture was stirred at r.t for 5 min and then N-hydroxysuccinimide (260 mg, 2.3 mmol) was added. The reaction was continuously stirred at r.t for 3 hours more. Afterwards, the precipitated dicyclohexylurea was filtered over Celite and washed with cold DCM (2×10mL). The filtrate was collected and DCM was removed *in vacuo*. The crude product was re-dissolved in EtOAc (10 mL) and cooled in a refrigerator at 0 ℃ for 20 min. The precipitate was filtered over Celite, and the filtrate was washed with saturated $NaHCO_3$ (2×50 mL) and brine (2×50 mL), dried over $MgSO_4$, filtered and concentrated *in vacuo* to give the crude product as a colorless oil. Purification of the oil by silica gel column chromatography (petroleum ether/EtOAc = 2:1) yielded pentynoic NHS-ester as a white solid (300 mg, 72% yield). ^{1}H NMR (400 MHz, $CDCl_3$): δ 2.90–2.82 (m, 6H, COCH_2CH_2CO, OCOCH_2CH_2), 2.62 (ddd, 2H, CH_2C≡CH), 2.05 (t, 1H, C≡C*H*). ^{13}C NMR (101 MHz, $CDCl_3$): δ 168.89 (*C*OCH_2CH_2CO), 167.02 (O*C*OCH_2), 80.84 (CH_2*C*≡CH), 70.04 (CH_2C≡*C*H), 30.31 (OCO*C*H2), 25.57 (CO*C*H_2*C*H_2CO), 14.09 (*C*H_2C≡CH).

Synthesis of ELP-Alkyne (ELP-Alk, 6). Pentynoic NHS-ester (92 mg, 0.47 mmol) and *N*,*N*-diisopropylethylamine (1.7 mg, 13.2 μmol) were added to a solution of ELP (MW= 17,035 Da, 225 mg, 13.2 μmol) in anhydrous DMSO (18 mL) and the mixture was stirred at r.t for 72h. It was then diluted with pure water (20 mL). The product was purified by dialysis (dialysis bag MWCO 15 kDa) against pure water for 48 h (changing water 3 times per day), followed by lyophilization to obtain the ELP-Alk as a white powder (210 mg, 93% yield). ^{1}H NMR (400 MHz, D_2O): *δ* 7.63–7.09 (br, indole *H* Trp), 4.57 (m, CH_α Met), 4.45 (m, CH_α Val, Pro), 4.19 (d, CH_α Val_{Xaa}), 4.06–3.89 (br m, C$H_{2\alpha}$ Gly, C$H_{2\delta}$ Pro), 3.75 (m, C$H_{2',\delta}$ Pro), 2.69–2.46 (br m, C$H_{2\gamma}$ Met, CH_2CH_2C≡CH), 2.33 (m, C$H_{2\beta}$ Pro), 2.18–1.91 (m, C$H_{2\beta}$ Met, C$H_{2',\beta}$ Pro, C$H_{2\gamma}$ Pro, CH_β Val, C$H_{3\varepsilon}$ Met, CH$_2$C≡C*H*), 1.05–0.91 (m, C$H_{3\gamma}$ Val). MALDI-TOF: Calculated Mass = 17,115 Da, Experimental Mass $[M+H]^+$ = 17,120.5 Da.

Synthesis of Dextran-b-ELP (Dex-b-ELP, 7). Copper sulfate (6 mg, 22.8 μmol), sodium ascorbate (10 mg, 45.6 μmol) and TBTA (12 mg, 22.8 μmol) were added to a solution of ELP-Alk (65 mg, 3.8 μmol) and Dex-N_3 (46 mg, 5.7 μmol) in anhydrous DMSO (8 mL) under argon atmosphere and the reaction mixture was stirred at r.t for 3 days. It was then diluted with cold water (20 mL) and cooled in a refrigerator at 4 ℃ for 20 min. TBTA was precipitated and removed by centrifugation. Cuprisorb (120 mg) was added to the resulting solution and it was then incubated at r.t with shaking, for 18 h to remove the copper. The solution containing cuprisorb was centrifuged and the supernatant was purified by dialysis (dialysis bag 15 kDa)

against pure water for 5 days (changing water 3 times per day), followed by lyophilization to obtain the product as a white powder (92 mg, 90 % yield). ^{1}H NMR (400 MHz, D_2O): δ 7.75 (s, triazole H), 7.63–7.09 (br, indole *H* Trp), 4.99 (d, Dex H-1), 4.55 (m, CH_α Met), 4.44 (m, CH_α Val, Pro), 4.17 (d, CH_α Val_{Xaa}), 4.06–3.87 (br m, C$H_{2\alpha}$ Gly, C$H_{2\delta}$ Pro, Dex H-6,H-5), 3.82-3.67 (m, C$H_{2',\delta}$ Pro, Dex H-6',H-3), 3.62–3.49 (Dex H-2,H-4), 2.69–2.48 (br m, C$H_{2\gamma}$ Met), 2.31 (m, C$H_{2\beta}$ Pro), 2.18–1.89 (m, C$H_{2\beta}$ Met, C$H_{2',\beta}$ Pro, C$H_{2\gamma}$ Pro, CH_β Val, C$H_{3\varepsilon}$ Met), 1.03–0.88 (m, C$H_{3\gamma}$ Val). FT-IR (ATR): 3332, 2929, 1653, 1527, 1443, 1342, 1152, 1106, 1017, 917, 547 cm^{-1}.

Synthesis of Laminarihexaose-b-ELP (Lam-b-ELP, 8). Copper sulfate (5.5 mg, 22 μmol), sodium ascorbate (9 mg, 45.4 μmol) were added to a solution of ELP-Alk (62 mg, 3.6 μmol) and Lam-N_3 (20 mg, 18.1 μmol) in anhydrous DMSO (8mL) under argon atmosphere and the reaction mixture was stirred at r.t for 3 days. It was then diluted with cold water (20 mL), after which Cuprisorb (110 mg) was added and the resulted solution was incubated at r.t with shaking, for overnight to remove the copper. The solution containing cuprisorb was centrifuged and the supernatant was purified by dialysis (dialysis bag MWCO 15 kDa) against pure water for 5 days (changing water 3 times per day), followed by lyophilization to obtain the product as a white powder (60 mg, 93% yield). ^{1}H NMR (400 MHz, D_2O): δ 7.74 (s, triazole H), 7.60–7.09 (br, indole *H* Trp), 4.80 (m, Lam H-1), 4.55 (m, CH_α Met), 4.43 (m, CH_α Val, Pro), 4.17 (d, CH_α Val_{Xaa}), 4.05–3.85 (br m, C$H_{2\alpha}$ Gly, C$H_{2\delta}$ Pro, Lam H-6), 3.82-3.66 (m, C$H_{2',\delta}$ Pro, Lam H-6',H-3), 3.62–3.34 (Lam H-2,H-4, H-5), 2.69–2.48 (br m, C$H_{2\gamma}$ Met), 2.41–2.24 (m, C$H_{2\beta}$ Pro), 2.19–1.88 (m, C$H_{2\beta}$ Met, C$H_{2',\beta}$ Pro, C$H_{2\gamma}$ Pro, CH_β Val, C$H_{3\varepsilon}$ Met), 1.05–0.85 (m, C$H_{3\gamma}$ Val). FT-IR (ATR): 3322, 2917, 1654, 1522, 1440, 1221, 1105, 1063, 1027, 562 cm^{-1}.

Synthesis of Hyaluronan-b-ELP (HA-b-ELP, 9). HA-N_3 was first acidified by adding aq. HCl, so as to be totally soluble in DMSO. HA-N_3 (18mg, 3.5 μmol), copper sulfate (9 mg, 36 μmol), sodium ascorbate (18 mg, 90 μmol) and TBTA (22 mg, 41 μmol) were added to a solution of ELP-Alk (60 mg, 3.5 μmol) in anhydrous DMSO (6 mL) under argon atmosphere. The mixture was stirred at 40 ℃ for 4 days, after which the reaction was diluted with cold water (20 mL) and cooled in a refrigerator at 4 ℃ for 20 min. TBTA was precipitated and removed by centrifugation. Cuprisorb (180 mg) was added to the resulted solution and it was then incubated at r.t with shaking, for overnight to remove the copper. The solution containing cuprisorb was centrifuged and the supernatant was purified by dialysis (dialysis bag MWCO 15 kDa) against pure water for 5 days (changing water 3 times per day), followed by lyophilization to obtain the

crude product (53 mg). The crude product was redissolved in deionized water (5.3 mL) and the solution was then heated to 40 ℃ and kept for 1 h. The insoluble unreacted ELPs were centrifuged at 13,000 g for 20 min at 40 ℃. The supernatant was lyophilized to give the final product as a white powder (42 mg, 54 % yield). ^{1}H NMR (400 MHz, D_2O): δ 7.75 (s, triazole H), 7.60–7.09 (br, indole *H* Trp), 4.62–4.37 (br, CH_{α} Met, Val, Pro, GlcUA H-1, GlcNAc H-1), 4.17 (d, CH_{α} Val_{Xaa}), 4.04–3.66 (br, C$H_{2\alpha}$ Gly, C$H_{2\delta}$ Pro, C$H_{2',\delta}$ Pro, GlcUA H-4, GlcNAc H-2, H-3, H-5, H-6), 3.65–3.42 (GlcUA H-3, H-5), 3.41–3.30 (t, GlcUA H-2), 2.69–2.48 (br m, C$H_{2\gamma}$ Met), 2.41–2.25 (m, C$H_{2\beta}$ Pro), 2.20–1.89 (m, C$H_{2\beta}$ Met, C$H_{2',\beta}$ Pro C$H_{2\gamma}$ Pro, CH_{β} Val, C$H_{3\varepsilon}$ Met, CH_3 GlcNAc), 1.06–0.88 (m, C$H_{3\gamma}$ Val). FT-IR (ATR): 3298, 2964, 1631, 1528, 1440, 1232, 1153, 1044, 541 cm^{-1}.

2.3 Characterization Methods

Nuclear Magnetic Resonance Spectrometry Analysis (NMR)

NMR spectra were acquired in D_2O or $CDCl_3$ at 298 K on a Bruker Avance I NMR spectrometer operating at 400.2 MHz and equipped with a Bruker multinuclear z-gradient direct probe head capable of producing gradients in the z direction with 53.5 $G.cm^{-1}$ strength. The relaxation time was fixed to 3 seconds for homonuclear correlation spectroscopy (COSY) measurements.

Mass Spectrometry Analysis (MS)

Mass spectrometry analyses were performed on a MALDI TOF/TOF (Ultraflex III, Bruker Daltonics, Bremen, Germany) equipped with a SmartBeam laser (Nd:YAG, 355 nm). Solutions of ELPs were prepared as follows: lyophilized ELPs were resuspended in water/acetonitrile (1/1, v/v) to obtain a final concentration lower than 100 μM. Samples were then mixed with the matrix solution of sinapinic acid prepared at the concentration of 10 mg/mL in water/acetonitrile (1/1, v/v). All MALDI-MS measurements were acquired in the linear positive mode and a mixture of standard proteins was used for external calibration in the suitable mass range (10−20 kDa).

Size Exclusion Chromatography (SEC)

SEC analysis was performed on a SEC-MALS system with refractive index and laser scattering detectors (WYATT Technology Optilab rEX and HELEOS-II) using an aqueous buffer (0.1 M $NaNO_3$, 0.01 M Na_2HPO_4, 0.02 M NaN_3) with a flow rate of 0.6 mL/min at 22 ℃. The specific

refractive index increment (dn/dc) of polysaccharide-*b*-ELP bioconjugates were measured by means of a differential refractometer (Wyatt Optilab rEX) operating at a wavelength of 658 nm at 26 ℃. A single concentration of each bioconjugate was used to determine the dn/dc coefficient through the calculation module implemented in the Astra 7.1 software. The measured dn/dc values of polysaccharide-*b*-ELP bioconjugates were applied for the calculation of weight average molecular weight (M_w).

Fourier Transform Infrared Spectroscopy (FT-IR)

FT-IR spectra were recorded using a Bruker Vertex 70 spectrometer with a GladiATR diamond. Spectra were recorded directly on a powder samples at 400-4000 cm^{-1} (resolution of 4 wavenumber) range by using attenuated total reflection mode.

Transition Temperature Measurements (T_t)

Cloud points measurements were performed at 350 nm between 10 and 80 ℃ at a 1 ℃ / min^{-1} scan rate for different concentrations of ELP and ELP bioconjugates in DI water. Data were collected on a Cary 100 UV−Vis spectrophotometer equipped with a multicell thermoelectric temperature controller from Agilent Technologies (Les Ulis, FR). The T_t, corresponding to the cloud point at a specific concentration, is defined as the temperature of the inflection point (maximum of first derivative) of the absorbance versus temperature plot.

Dynamic Light Scattering Measurements (DLS)

Dynamic light scattering measurements were performed on NanoZS instrument (Malvern, U.K.) at a 90 ° angle at a constant position in the cuvette (constant scattering volume). The derived count rate (DCR) was defined as the mean scattered intensity normalized by the attenuation factor. The DCR was plotted against temperature and the T_t is defined as the temperature corresponding to the point where the DCR starts increasing on this plot.

Temperature-controlled Liquid Atomic Force Microscopy (Liquid AFM)

Temperature-controlled liquid atomic force microscopy measurements were performed using a Dimension FastScan Bruker AFM system. The topography images of the bioconjugates were obtained in Peak Force tapping mode, using a Silicon cantilever (ScanAsyst-Fluid+, Bruker) with a typical tip radius of 5 nm. The cantilever resonance was 150 kHz and the spring constant

was 0.7 N/m. Substrates were purchased from Agar Scientific. Samples were prepared by drop-casting a bioconjugates water solution of 50 µM (150 µM for HA-*b*-ELP) onto a freshly cleaved mica or HOPG surface, which was directly applied for imaging. AFM imaging process was conducted in liquid environment at specific temperature. An external heating stage (Bruker) was used to achieve the target temperature at the substrate surface.

3. RESULTS AND DISCUSSION

3.1 Synthesis of polysaccharide-*b*-ELP block copolymers

The synthetic strategy was based on a coupling reaction between the polysaccharide and ELP blocks *via* copper(I)-catalyzed azide-alkyne cycloaddition (CuAAC) which has previously been applied for biomacromolecular conjugation with high selectivity and coupling efficiency.[86] For this purpose, the three selected polysaccharides and the ELP needed to be functionalized with either an azide or an alkyne group. In most cases, polysaccharides can be straightforwardly modified at their reducing end by azide-containing amines in acidic conditions with excellent functionalization degrees. Regarding the introduction of an alkyne group at the ELP chain end, an activated alkyne-functionalized NHS-ester can be exploited and subsequently substituted by the *N*-terminal primary amine of the ELP.[83] Herein the different polysaccharides were modified at their reducing end with an azide group using a bifunctional *N*-methoxyoxyamine linker and the ELP was modified at the *N*-terminal end with an alkyne moiety (Scheme 1), allowing the subsequent coupling of the two blocks by CuAAC as illustrated on Scheme 1C.

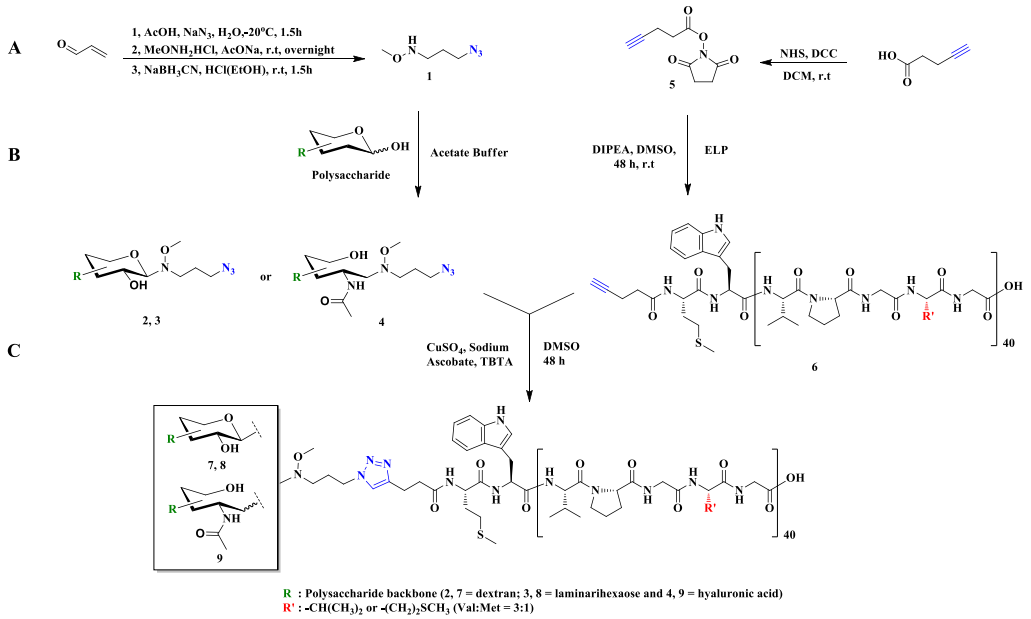

***Scheme 1**. Synthetic strategy of polysaccharide-b-elastin-like polypeptide block copolymers. (A) Synthesis of the bifunctional linker **1** and of the NHS-alkyne ester **5**. (B) Reducing-end functionalization of polysaccharides and modification of ELP at the N-terminus. (C) Huisgen's cycloaddition between the azide-functionalized polysaccharides and the alkyne-functionalized ELP.*

3.1.1 Reducing-end functionalization of polysaccharides

Primary amines have been extensively used for the functionalization of polysaccharides by reductive amination to form an open-chain monosaccharide at its reducing end.[11,12] Recently the use of functional oxyamine linkers for conjugation to glycans has been demonstrated with highly efficient coupling.[81,82] In comparison to the conventional reductive amination of glycans with primary amines, the use of oxyamine linkers in acetate buffer without any reducing agent was able to produce the native closed conformation of the reducing sugar, which is essential for the recognition of some saccharides to the relevant receptors. In order to explore more on this methodology for the functionalization of polysaccharides, we first prepared the azide-functionalized oxyamine linker **1** *via* a three-step one-pot strategy (Scheme 1A) and characterized it by 1D and 2D NMR (Figure S1).[81] This azide-linker contains an *N*-methoxyamine functional group for conjugation to the reducing end of the polysaccharides and a chain end azide group for subsequent conjugation to the ELP.[81,82] The modification reactions of Dex and Lam by the oxyamine linker were carried out in acetate buffer at 40 ℃ at pH 4.6 (Scheme 1B). The ^{1}H, HSQC and COSY NMR spectra in D_2O of modified polysaccharides were recorded and all peaks were assigned (see Figures S2, S3). Full conversion of Dex and Lam were confirmed by comparing the integral of the peak at 1.84 ppm corresponding to the resonance of the β-methylene of oxyamine linker with the integral of the peak at 4.1 ppm for Dex and 4.2 ppm for Lam (anomeric proton of the reducing sugar). The two protons of α-methylene in oxyamine linker have different resonance frequencies (2.89 ppm and 3.08 ppm) illustrating a stereochemical non-equivalence of the two protons, which indicated that the reducing sugar retained its closed conformation with a β-anomeric configuration due to the stereochemical effect of the methoxy group[81], and the proton coupling constant of a β-linked sugar (J = 8.9 Hz).

Applying the same strategy on the modification of HA by the oxyamine linker, either at pH 4.6 or 5.5 of acetate buffer gave a conversion below 50 %. This may due to the high negative charge density of HA. Thus conventional reductive amination was applied to couple the reducing end of HA with the oxyamine linker, using sodium cyanoborohydride ($NaBH_3CN$) as a reducing

agent (Figure S4). As a result of the reduction, the protons of the α-methylene in the oxyamine linker have stereochemical equivalence (2.88 ppm), revealing an open chain reducing end of HA (Figure S5). Successful azide-functionalization of the three polysaccharides was also assessed by tracking the appearance of azide vibration signal at 2100 cm^{-1} in FTIR spectra (Figure S6, S7, S8).

3.1.2 Alkyne functionalization at the N-terminal end of ELP

The ELP used in this work was prepared by recombinant DNA and protein engineering techniques in *Escherichia coli* as described previously.[60] This ELP contains in total 40 pentapeptide repeats with the protein sequence $MW[(VPGVG)(VPGMG)(VPGVG)_2]_{10}$, corresponding to a molecular weight of 17,035 Da. The MS and NMR spectra characterization of this "starting" ELP are provided in Figure S9 and S10. In order to introduce an alkyne group on the ELP, the activated NHS-alkyne ester **5** was synthesized by a coupling reaction between *N*-hydroxysuccinimide and 4-pentynoic acid (Scheme 1A). The reaction of the primary amine of ELP with the NHS-alkyne ester **5** was thereafter verified by ^1H NMR and MALDI-Tof mass spectrometry (Figure S9, S12). Even though the terminal alkyne moiety was not detected by ^1H NMR spectroscopy of the purified chain end-functionalized ELP, the appearance of peaks for two methylene groups of the alkyne linker at 2.3 ppm was an indication of successful modification (Figure S12). Full alkyne functionalization of ELP was also confirmed by the MS shift to 17,119 Da after NHS-coupling chemistry (Figure S9).

3.1.3 Synthesis of polysaccharide-b-ELP copolymers

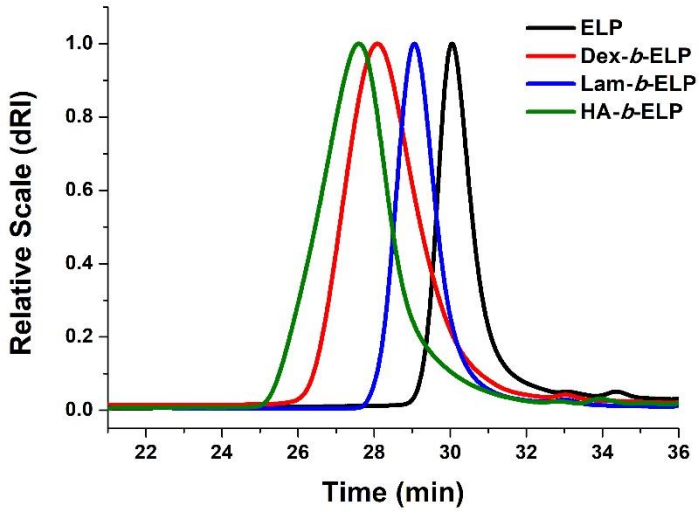

Figure 1. *SEC traces of ELP and polysaccharide-b-ELP bioconjugates in aqueous buffer (0.1 M $NaNO_3$, 0.01 M Na_2HPO_4, 0.02 M NaN_3) using a RI detector.*

The emergence of "click chemistry" has revolutionized bioconjugate chemistry by affording excellent selectivity and using soft reaction conditions amenable to both synthetic polymers and fragile biomacromolecules, such as proteins or DNAs.[87] A widely used "click reaction" is the Cu(I)-catalyzed azide-alkyne cycloaddition or Huisgen's cycloaddition.[86] Herein, conjugations of ELP and polysaccharides were carried out *via* Huisgen's cycloaddition in DMSO as common solvent for the ELP and polysaccharides (Scheme 1C). TBTA, a powerful stabilizing ligand for copper(I), was used in the conjugation of Dex and HA as they have a much higher molecular weight than Lam. The success of the click reaction was subsequently monitored by SEC, as well as by ^{1}H, HSQC and COSY NMR and FTIR spectroscopy.

The conjugation of polysaccharides to the ELP coincided with a clear increase in the molecular weight of the different block copolymers as observed in Figure 1. SEC also highlights the low dispersity of the resulting block copolymers (Table 1). All the peaks in ^{1}H NMR spectra were assigned with the help of corresponding HSQC and COSY NMR, indicating both polysaccharide block and ELP block (see Figure S13, S14, and S15). All NMR spectra displayed the characteristic anomeric peaks of polysaccharides at around 5.0 ppm and the triazole proton peak was found at 7.8 ppm (Figure 2) confirming the desired structures of the block copolymers. FTIR spectra of the bioconjugates, after the click reaction, were also compared with the ones of alkyne-functionalized ELP and corresponding azide-functionalized polysaccharides (Figure S6, S7 and S8). The complete disappearance of the azide band at 2100 cm^{-1} in the bioconjugates proved the success of the "click reaction" bioconjugation.

Bioconjugates	M_w[a] (kDa)	Polysaccharide mass fraction	PDI[a]	T_t in water[b] (125 µM)
Dex-*b*-ELP	24.9	32 %	1.01	39 ℃
Lam-*b*-ELP	18.2	5 %	1.03	36 ℃
HA-*b*-ELP	24.3	30 %	1.02	48 ℃

Table 1. *Characteristics of the polysaccharide-b-ELP bioconjugates synthesized. [a]Weight average molecular weight (M_w) and polydispersity index (PDI) were determined by SEC in aqueous buffer. [b]T_t was measured by turbidity on UV-Vis.*

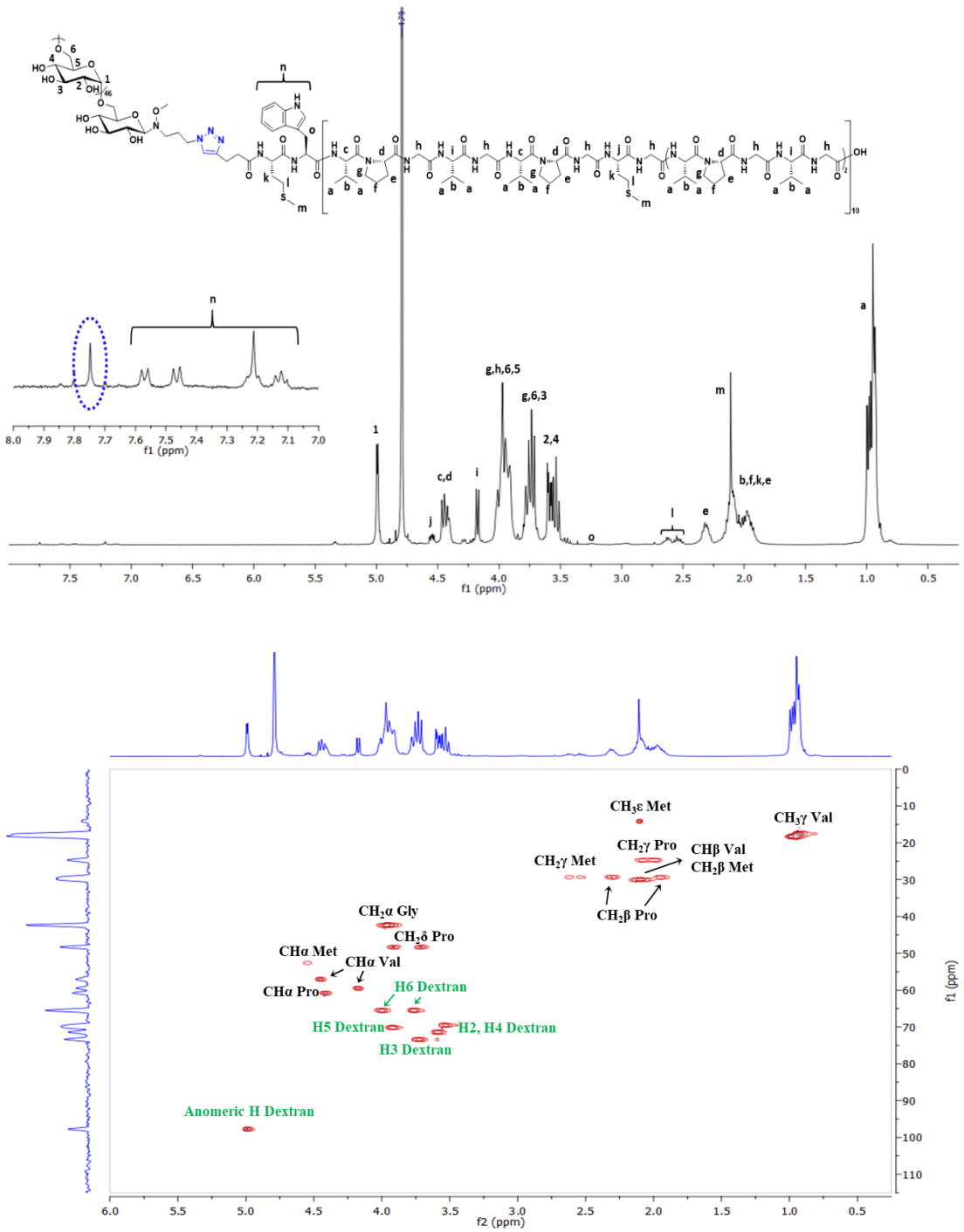

Figure 2. *^{1}H and HSQC NMR Spectra of Dex-b-ELP in D_2O at 25 ℃.*

3.2 Temperature-triggered self-assembly of polysaccharide-*b*-ELP copolymers

3.2.1 Thermo-responsive properties

The thermo-responsive properties of the different polysaccharide-*b*-ELP block copolymers were first studied by measuring the T_t values by turbidity measurement at 350 nm. In contrast with T_t of ELP (32 ℃) at same concentration (Figure 3A), T_t of the bioconjugates shifted to higher temperature depending on the hydrophilicity of polysaccharides (36 ℃, 39 ℃ and 48 ℃ for Lam-*b*-ELP, Dex-*b*-ELP and HA-*b*-ELP, respectively). Consistently, the higher the hydrophilicity of the polysaccharide, the larger the T_t. One can note that the slight decrease in absorption of HA-*b*-ELP at high temperature was most likely due to the formation of large aggregates, which may sediment (Figure S22). The T_t values of ELP and ELP bioconjugates were then plotted as functions of concentration (Figure 3B) and the data were fitted using the empirical law proposed by Chilkoti and coworkers.[56] This equation gave satisfactory fits of T_t, concentration and temperature, enabling accurate prediction of the T_t of ELP and its bioconjugates at specific concentrations. As the hydrophilicity of the ELP bioconjugates decreased, the slope of the fit became flatter. This result is consistent with the observations reported by Chilkoti and coworkers.[56]

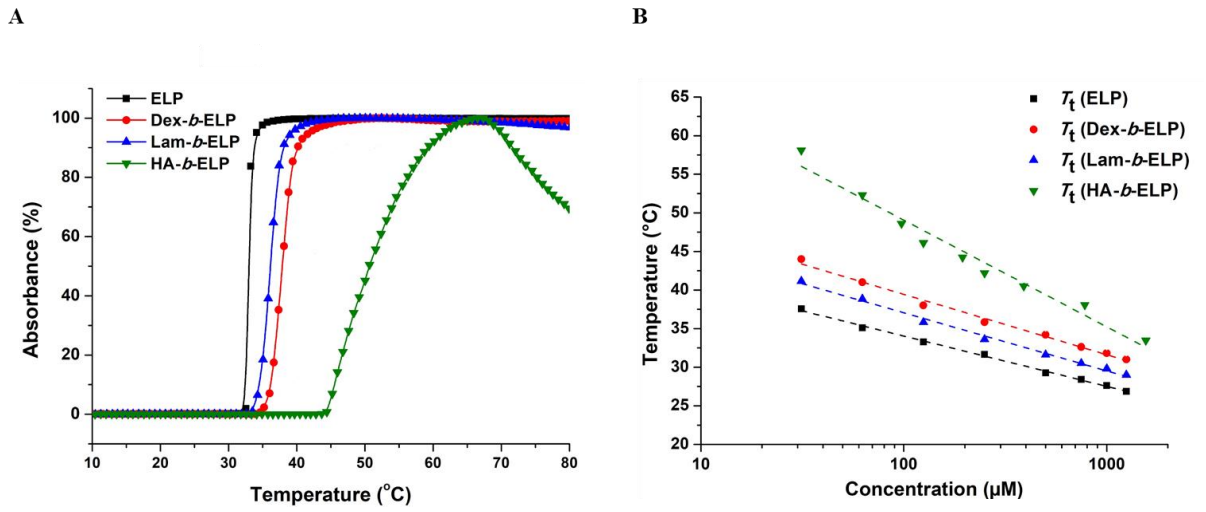

Figure 3. *Turbidity study of ELP and polysaccharide-b-ELP bioconjugates. (A) Absorbance measured at 125 μM in water as function of temperature. (B) T_t values plotted as function of concentration in water.*

3.2.2 Self-assembly of polysaccharide-b-ELP block copolymers

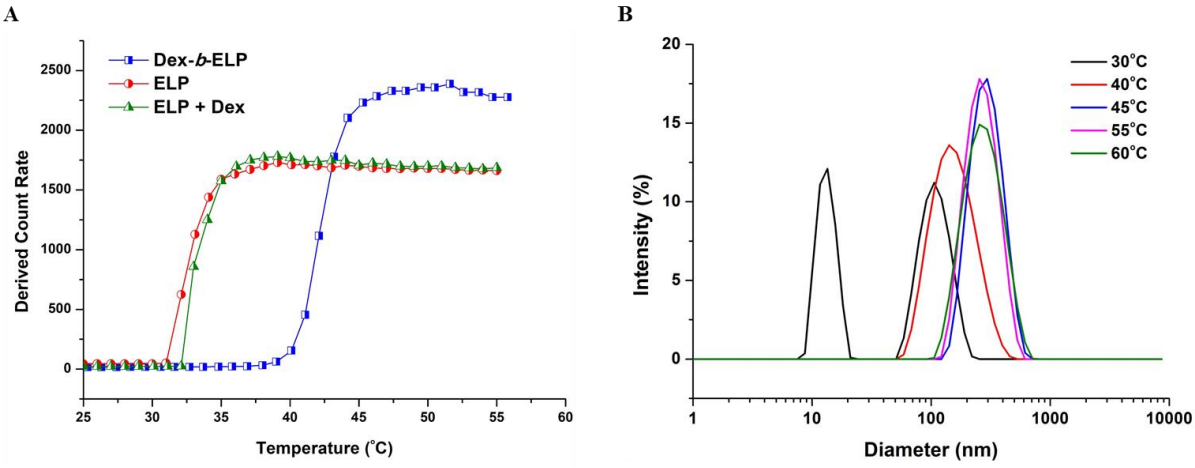

Figure 4. *Dynamic light scattering analysis of the self-assembly of ELP, Dex-b-ELP and physical mixture of ELP and Dex at 125 μM in water. (A) Scattered intensity as a function of temperature upon heating. (B) Size distribution in intensity of Dex-b-ELP at selected temperatures.*

In a next step, we were interested in studying the self-assembly properties of polysaccharide-*b*-ELP copolymers and their ability to form well-defined micellar structures. The behavior of Dex-*b*-ELP (125 μM in water) was first analyzed by DLS. Measuring the total scattering intensity with temperature allowed the determination of T_t that was found to be around 40 ℃. Consistently with turbidity measurements, this value was comparable and larger than the T_t of single ELP determined at the same concentration (Figure 4A) due to the conjugation of a hydrophilic polysaccharide segment. Interestingly, the physical mixture of ELP and Dex did not influence the T_t of ELP (Figure 4A, S16). As observed in Figure 4A, at low temperature (30 ℃) below T_t of Dex-*b*-ELP, the scattering intensity is very low, due to the presence of free copolymer chains in solution and a few aggregates. The scattering intensity sharply increased at the transition temperature (around 40 ℃) and triggered the self-assembly to form structures with hydrodynamic diameter (D_h) around 165 nm. Once Dex-*b*-ELP was heated above 45 ℃, the nanoparticles showed little changes in diameter with a D_h of approximately 290 nm (Figure 4B), being stable until 60 ℃. Repeated heating and cooling on Dex-*b*-ELP showed similar D_h and PDI values, illustrating that this temperature-responsive behavior is fully reversible, which offers a simple method for controlling the transition of ELPs (Figure S17). Atomic force microscopy in a liquid cell was conducted to investigate the morphology of the nanostructures formed by Dex-*b*-ELP below/above T_t. Consistent with the DLS results, very small objects were observed below T_t at 35 ℃ (Figure 5A), and spherical-shaped particles were observed with an average diameter of approximately 280-300 nm above T_t at 65 ℃ (Figure 5B).

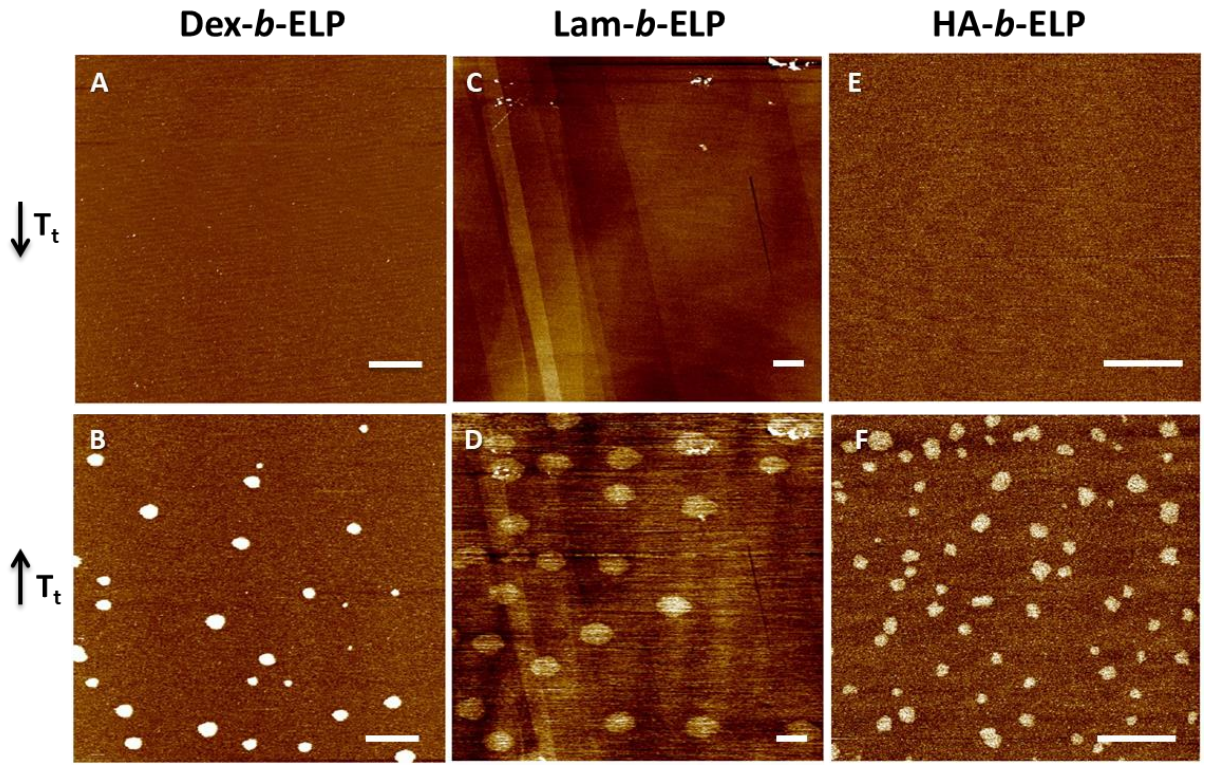

Figure 5. *Liquid AFM images of Dex-b-ELP (50 μM in water) on mica substrate at: (A) 35 ℃ and (B) 65 ℃. Lam-b-ELP (50 μM in water) on HOPG substrate at: (C) 30 ℃ and (D) 55 ℃. HA-b-ELP (150 μM in water) on mica substrate at: (E) 25 ℃ and (F) 52 ℃. The scale bar indicates 1 μm.*

Due to the small hydrophilic fraction of Lam-*b*-ELP, the T_t of Lam-*b*-ELP was found around 33 ℃, which is slightly higher when compared to the T_t of ELP (Figure S18). At low temperature (30 ℃), below T_t of Lam-*b*-ELP, small objects and a few aggregates were observed with very low scattering intensity. The scattering intensity sharply increased at transition temperature (around 33 ℃) and triggered the self-assembly to form structures with D_h around 210 nm. Unlike Dex-*b*-ELP, a peak located at 36-38 ℃ was most likely due to the formation of unstable big particles, which precipitated thus decreasing the concentration in the detected area. Repeated heating and cooling of Lam-*b*-ELP from 25 ℃ to 36 ℃ on DLS also illustrated this unstable behavior (Figure S19). Nevertheless the temperature-responsive behavior of Lam-*b*-ELP is fully reversible. When temperature was heated above 45 ℃, the nanoparticles showed little changes in scattering intensity and displayed diameter with a D_h of approximately 400-500 nm (Figure S18). Liquid AFM even recorded larger diameters (500-900) for the aggregates of Lam-*b*-ELP above the T_t (Figure 5D).

Similar to the UV-vis measurements, the T_t of HA-*b*-ELP on DLS heating ramp was found around 45 ℃. At low temperature (35 ℃) below T_t of HA-*b*-ELP, small objects were observed with very low scattering intensity. The scattering intensity sharply increased at transition temperature and triggered the self-assembly to form structures with D_h around 300 nm at 48-50 ℃ (Figure S20). Once HA-*b*-ELP was heated above 55 ℃, the diameter of nanoparticles became unstable and separated into two size distributions, which was also confirmed by liquid AFM (Figure S22). Nanoparticles with an average diameter of approximately 220-280 nm were observed by liquid AFM at 50 ℃ (Figure 5F) at the same concentration. The stability of the HA-*b*-ELP assemblies at 48 ℃ was investigated by repeated heating and cooling on DLS. This temperature-responsive system was again found fully reversible and HA-*b*-ELP nanoparticles proved relatively stable at 48 ℃ for 20 minutes with an average diameter around 280 nm on every single heating time (Figure S21).

Bioconjugates	**Conc.(μM)**	T_t **DLS**	**DLS**		**Conc.(μM)**	**AFM**	
			T(℃)	Size(nm)		T(℃)	Size(nm)
Dex-*b*-ELP	125	39 ℃	45	300	50	35	/
						65	190-340
Lam-*b*-ELP	125	33 ℃	33	210	50	30	/
			45	520		55	500-900
HA-*b*-ELP	150	46 ℃	48	300	150	25	/
						52	200-300

Table 2. Self-assembly characteristics of polysaccharide-*b*-ELP block copolymers.

To summarize, polysaccharide-*b*-ELP bioconjugates were able to self-assemble into nano-objects of different sizes (characteristics summarized in Table 2). Stable objects with a size of a few hundreds nanometers have been evidenced, especially when the hydrophilic polysaccharide segment was large enough. In addition, the self-assembly process was fully reversible by controlling the temperature, which provides a prospect of polysaccharide-*b*-ELP bioconjugates for applications in biomaterial, drug delivery and receptor recognition.

4. CONCLUSION

We herein presented a modular approach to combine inert (Dex) and bioactive (Lam and HA) polysaccharides with a stimuli-responsive elastin-like polypeptide (ELP) into well-defined block copolymers. Polysaccharides were successfully functionalized with an azide moiety at the reducing end using a bifunctional *N*-methoxyoxyamine linker for further conjugation to the ELP. NHS-ester coupling chemistry was utilized to modify the *N*-terminal primary amine of ELP with an alkyne group. Thereafter, smart polysaccharide-*b*-ELP block copolymers were produced by CuAAC, and their thermal responsiveness was studied by turbidity measurements. Increasing temperature above the phase transition of ELP bioconjugates resulted in the formation of amphiphiles, which self-assembled into well-defined and stable nano-objects. This is the first study that proposes the conjugation of bioactive polysaccharides with stimuli-responsive ELPs for the preparation of thermo-sensitive bioactive self-assemblies, providing insight into novel pathways for designing "smart" and biologically-active nanocarriers for biomedical applications.

REFERENCES

(1) Peyret, A.; Zhao, H.; Lecommandoux, S. Preparation and Properties of Asymmetric Synthetic Membranes Based on Lipid and Polymer Self-Assembly. *Langmuir* **2018**, *34* (11), 3376–3385.

(2) Trantidou, T.; Friddin, M.; Elani, Y.; Brooks, NJ.; Law, RV.; Seddon, JM.; Ces, O. Engineering Compartmentalized Biomimetic Micro- and Nanocontainers. *ACS Nano.* **2017**, *11* (7), 6549–6565.

(3) Huang, G.; Li, F.; Zhao, Xin.; Ma, Y.; Y Li.; Lin, M.; Jin, G.; Lu, TJ.; Genin, GM.; Xu, F. Functional and Biomimetic Materials for Engineering of the Three-Dimensional Cell Microenvironment. *Chem. Rev.* **2017**, *117* (20), 12764–12850.

(4) Kataoka, K.; Harada, A.; Nagasaki, Y. Block Copolymer Micelles for Drug Delivery: Design, Characterization and Biological Significance. *Adv. Drug Delivery Rev.* **2001**, *47*(1), 113–131.

(5) Eetezadi, S.; Ekdawi, SN.; Allen, C. The Challenges Facing Block Copolymer Micelles for Cancer Therapy: In Vivo Barriers and Clinical Translation. *Adv. Drug Delivery Rev.* **2015**, *91*, 7–22.

(6) Kutikov, AB.; Song, J. Biodegradable PEG-Based Amphiphilic Block Copolymers for Tissue Engineering Applications. *ACS Biomater. Sci. Eng.* **2015**, *1* (7), 463–480.

(7) Hou, Y.; Lu, H. Protein PEPylation: A New Paradigm of Protein-Polymer Conjugation. *Bioconjug. Chem.* **2019**, *30* (6), 1604–1616.

(8) Le Fer, G.; Wirotius, AL.; Brûlet, A.; Garanger, E.; Lecommandoux, S. Self-Assembly of Stimuli-Responsive Biohybrid Synthetic-*b*-Recombinant Block Copolypeptides. *Biomacromolecules* **2019**, *20* (1), 254–272.

(9) Sanson, C.; Schatz, C.; Le Meins, JF.; Brûlet, A.; Soum, A.; Lecommandoux, S. Biocompatible and Biodegradable Poly(trimethylene carbonate)-*b*-Poly(l-glutamic acid) Polymersomes: Size Control and Stability. *Langmuir* **2010**, *26* (4), 2751–2760.

(10) Zhang, A.; Zhang, Z.; Shi, F.; Xiao, C.; Ding, J.; Zhuang, X.; He, C.; Chen, L.; Chen, X. Redox-Sensitive Shell-Crosslinked Polypeptide-block-Polysaccharide Micelles for Efficient Intracellular Anticancer Drug Delivery. *Macromol. Biosci.* **2013**, *13* (9), 1249–1258.

(11) UpadHAy, KK.; Le Meins, JF.; Misra, A.; Voisin, P.; Bouchaud, V.; Ibarboure, E.; Schatz, C.; Lecommandoux, S. Biomimetic Doxorubicin Loaded Polymersomes from Hyaluronan-block-Poly(γ-benzyl glutamate) Copolymers. *Biomacromolecules* **2009**, *10* (10), 2802–2808.

(12) Schatz, C.; Louguet, S.; Le Meins, JF.; Lecommandoux. S. Polysaccharide-block-Polypeptide Copolymer Vesicles: Towards Synthetic Viral Capsids. *Angew. Chem., Int. Ed.* **2009**, *48* (14), 2572–2575.

(13) Guo, J.; Hong, H.; Chen, G.; Shi, S.; Nayak, TR.; Theuer, CP.; Barnhart, TE.; Cai, W.; Gong, S. Theranostic Unimolecular Micelles Based on Brush-Shaped Amphiphilic Block Copolymers for Tumor-Targeted Drug Delivery and Positron Emission Tomography Imaging. *ACS Appl. Mater. Interfaces.* **2014**, *6* (24), 21769–21779.

(14) Schöttner, S.; Schaffrath, HJ.; Gallei, M. Poly(2-hydroxyethyl methacrylate)-Based Amphiphilic Block Copolymers for High Water Flux Membranes and Ceramic Templates. *Macromolecules* **2016**, *49* (19), 7286–7295.

(15) Stimulus-Responsive Degradable Polylactide-Based Block Copolymer Nanoassemblies for Controlled/Enhanced Drug Delivery. *Mol. Pharm.* **2017**, *14* (8), 2460–2474.

(16) Tyler, B.; Gullotti, D.; Mangraviti, A.; Utsuki, T.; Brem, H. Polylactic acid (PLA) Controlled Delivery Carriers for Biomedical Applications. *Adv. Drug Deliv. Rev.* **2016**, *107*, 163–175.

(17) Dash, TK.; Konkimalla. VB. Polymeric Modification and Its Implication in Drug Delivery: Poly-ε-caprolactone (PCL) as a Model Polymer. *Mol. Pharm.* **2012**, *9* (9), 2365–2379.

(18) Bacinello, D.; Garanger, E.; Taton, D.; Tam, KC.; Lecommandoux, S. Enzyme-Degradable Self-Assembled Nanostructures from Polymer-Peptide Hybrids. *Biomacromolecules* **2014**, *15* (5), 1882−1888.

(19) Swierczewska, M.; Han, HS.; Kim, K.; Park, JH.; Lee, S. Polysaccharide-Based Nanoparticles for Theranostic Nanomedicine. *Adv. Drug Delivery Rev.* **2016**, *99* (Pt A), 70–84.

(20) Liu, Z.; Jiao, Y.; Wang, Y.; Zhou, C.; Zhang, Z. Polysaccharides-Based Nanoparticles as Drug Delivery Systems. *Adv. Drug Delivery Rev.* **2008**, *60* (15), 1650–1662.

(21) Rosselgong, J.; Chemin, M.; Cabral Almada, C.; Hemery, G.; Guigner, J.-M.; Chollet, Gu; Labat, G.; da Silva Perez, D.; Ham-Pichavant, F.; Grau, E.; Grelier, S.; Lecommandoux, S; Cramail, H. Synthesis and Self-Assembly of Xylan-Based Amphiphiles: From Bio-Based Vesicles to Antifungal Properties. *Biomacromolecules* **2019**, *20* (1), 118–129.

(22)Rabotyagova, OS.; Cebe, P.; Kaplan, DL. Protein-Based Block Copolymers. *Biomacromolecules* **2011**, *12* (2), 269–289.
(23)Seidi, K.; Neubauer, HA.; Moriggl, R.; Jahanban-Esfahlan, R.; Javaheri, T. Tumor Target Amplification: Implications for Nano Drug Delivery Systems. *J. Controlled Release* **2018**, *275*, 142–161.
(24)Cai, L.; Gu, Z.; Zhong, J.; Wen, D.; Chen, G.; He, L.; Wu, J.; Gu, Z. Advances in Glycosylation-Mediated Cancer-Targeted Drug Delivery. *Drug Discov. Today* **2018**, *23* (5), 1126–1138.
(25)Huang, GL.; Huang, HL. Hyaluronic Acid-based Biopharmaceutical Delivery and Tumor-Targeted Drug Delivery System. *J. Controlled Release* **2018**, *278*, 122–126.
(26)Wang, SS.-S.; How, S-C.; Chen, Y-D.; Tsaic, Y-H.; Jan J-S. Bioactive Saccharide-Conjugated Polypeptide Micelles for Acid-Triggered Doxorubicin Delivery. *J. Mater. Chem. B*, **2015**, *3*, 5220–5231.
(27)Huang, J.; Bonduelle, C.; Thévenot, J.; Lecommandoux, S.; Heise, A. Biologically Active Polymersomes from Amphiphilic Glycopeptides. *J. Am. Chem. Soc.* **2012**, *134* (1), 119−122.
(28)Garanger, E.; Lecommandoux, S. Towards Bioactive Nanovehicles Based on Protein Polymers. *Angew. Chem., Int. Ed.* **2012**, *51* (13), 3060–3062.
(29)Bonduelle, C.; Lecommandoux, S. Synthetic Glycopolypeptides as Biomimetic Analogues of Natural Glycoproteins. *Biomacromolecules* **2013**, *14* (9), 2973–2983.
(30)Ahsan, SM.; Thomas, M.; Reddy, KK.; Sooraparaju, SG.; Asthana, A.; Bhatnagar, I. Chitosan as biomaterial in drug delivery and tissue engineering. *Int. J. Biol. Macromol.* **2018**, *110*, 97–109.
(31)VK Thakur.; MK Thakur. Recent Advances in Graft Copolymerization and Applications of Chitosan: A Review. *ACS Sustainable Chem. Eng.* **2014**, *212*, 2637–2652.
(32)Gu, D.; Huang, L.; Chen, X.; Wu, Q.; Ding, K. Structural Characterization of a Galactan From Ophiopogon Japonicus and Anti-Pancreatic Cancer Activity of Its Acetylated Derivative. *Int. J. Biol. Macromol.* **2018**, *113*, 907–915.
(33)Chiang, CS.; Lin, YJ.; Lee, R.; Lai, YH.; Cheng, HW.; Hsieh, CH.; Shyu, WC.; Chen, SY. Combination of Fucoidan-Based Magnetic Nanoparticles and Immunomodulators Enhances Tumour-Localized Immunotherapy. *Nat. Nanotechnol.* **2018**, *13* (8), 746–754.
(34)Duan, H.; Donovan, M.; Foucher, A.; Schultze, X.; Lecommandoux, S. Multivalent and Multifunctional Polysaccharide-Based Particles for Controlled Receptor Recognition. *Sci. Rep.* **2018**, *8* (1), 14730.
(35)Schatz, C.; Lecommandoux, S. Polysaccharide-Containing Block Copolymers: Synthesis, Properties and Applications of an Emerging Family of Glycoconjugates. *Macromol. Rapid Commun.* **2010**, *31*(19), 1664–1684.
(36)Hu, X.; Zhang, Y.; Xie, Z.; Jing, X.; Bellotti, A.; Gu, Z. Stimuli-Responsive Polymersomes for Biomedical Applications. *Biomacromolecules* **2017**, *18* (3), 649–673.
(37)Cobo, I.; Li, M.; Sumerlin, BS.; Perrier, S. Smart Hybrid Materials by Conjugation of Responsive Polymers to Biomacromolecules. *Nat. Mater.* **2015**, *14* (2), 143–159.
(38)Stuart, M. A. C.; Huck, W. T.; Genzer, J.; Müller, M.; Ober, C.; Stamm, M.; Sukhorukov, G. B.; Szleifer, I.; Tsukruk, V. V.; Urban, M. Emerging Applications of Stimuli-Responsive Polymer Materials. *Nat. Mater.* **2010**, *9* (2), 101–113.
(39)Hoffman, AS. Stimuli-Responsive Polymers: Biomedical Applications and Challenges for Clinical Translation. *Adv. Drug Deliv. Rev.* **2013**, *65* (1), 10–16.
(40)Bajpai, A.K.; Shukla, SK.; Bhanu, S.; Kankane, S. Responsive Polymers in Controlled Drug Delivery. *Prog. Polym. Sci*. **2008**, *33* (11), 1088–1118.
(41)Roy, D.; Cambre, JN.; Sumerlin, BS. Future Perspectives and Recent Advances in Stimuli-Responsive Materials. *Prog. Polym. Sci*. **2010**, *35* (1-2), 278–301.
(42)Pang, X.; Jiang, Y.; Xiao, Q.; Leung, AW.; Hua, H.; Xu, C. pH-responsive polymer-drug conjugates: Design and progress. *J. Controlled Release.* **2016**, *222*, 116–129.
(43)Peeler, DJ.; Sellers, DL.; Pun, SH. pH-Sensitive Polymers as Dynamic Mediators of Barriers to Nucleic Acid Delivery. *Bioconjugate Chem.* **2019**, *30* (2), 350–365.
(44)Sun, H.; Zhang, Y.; Zhong, Z. Reduction-Sensitive Polymeric Nanomedicines: An Emerging Multifunctional Platform for Targeted Cancer Therapy. *Adv. Drug Deliv. Rev.* **2018**, *132*, 16–32.
(45)An, X.; Zhu, A.; Luo, H.; Ke, H.; Chen, H.; Zhao, Y. Rational Design of Multi-Stimuli-Responsive Nanoparticles for Precise Cancer Therapy. *ACS Nano.* **2016**, *10* (6), 5947–5958.
(46)Anderson, C. F.; Cui, H. Protease-Sensitive Nanomaterials for Cancer Therapeutics and Imaging. *Ind Eng Chem Res*. **2017**, *56* (20), 5761–5777.
(47)Kim, W.; Thévenot, J.; Ibarboure, E.; Lecommandoux, S.; Chaikof, E. L. Self-Assembly of Thermally Responsive Amphiphilic Diblock Copolypeptides into Spherical Micellar Nanoparticles. *Angew. Chem., Int. Ed.* **2010**, *122* (25), 4353– 4356.

(48)Strandman, S.; Zhu, X.X. Thermo-Responsive block Copolymers with Multiple Phase Transition Temperatures in Aqueous Solutions. *Prog. Polym. Sci.* **2015**, *42*, 154–176.
(49)Beauté, L.; McClenaghan, N.; Lecommandoux, S. Photo-Triggered Polymer Nanomedicines: From Molecular Mechanisms to Therapeutic Applications. *Adv. Drug Deliv. Rev.* **2019**, *138*, 148–166.
(50)Zhao, Y. Light-Responsive Block Copolymer Micelles. *Macromolecules* **2012**, *45* (9), 3647–3657.
(51)Reddy, LH.; Arias, JL.; Nicolas, J.; Couvreur, P. Targeted Drug Delivery with Polymers and Magnetic Nanoparticles: Covalent and Noncovalent Approaches, Release Control, and Clinical Studies. *Chem. Rev.* **2012**, *112* (11), 5818–5878.
(52)MacEwan, S. R.; Chilkoti, A. Applications of Elastin-like Polypeptides in Drug Delivery. *J. Controlled Release* **2014**, *190*, 314–330.
(53)McDaniel, J. R.; Callahan, D. J.; Chilkoti, A. Drug Delivery to Solid Tumors by Elastin-Like Polypeptides. *Adv. Drug Delivery Rev.* **2010**, *62* (15), 1456–1467.
(54)Despanie, J.; Dhandhukia, JP.; Hamm-Alvarez, SF.; MacKay, JA. Elastin-Like Polypeptides: Therapeutic Applications for an Emerging Class of Nanomedicines. *J. Controlled Release* **2016**, *240*, 93–108.
(55)Halperin, A.; Kröger, M.; Winnik, FM. Poly(N-isopropylacrylamide) Phase Diagrams: Fifty Years of Research. *Angew. Chem., Int. Ed*. **2015**, *54* (51), 15342–15367.
(56)Meyer, D. E.; Chilkoti, A. Quantification of the Effects of Chain Length and Concentration on the Thermal Behavior of Elastin-like Polypeptides. *Biomacromolecules* **2004**, *5* (3), 846−851.
(57)Li, N. K.; Roberts, S.; Quiroz, F. G.; Chilkoti, A.; Yingling, Y. G. Sequence Directionality Dramatically Affects LCST Behavior of Elastin-Like Polypeptides. *Biomacromolecules* **2018**, *19* (7), 2496–2505.
(58)MacEwan, S. R.; Weitzhandler, I.; Hoffmann, I.; Genzer, J.; Gradzielski, M.; Chilkoti, A. Phase Behavior and Self-Assembly of Perfectly Sequence-Defined and Monodisperse Multiblock Copolypeptides. *Biomacromolecules* **2017**, *18* (2), 599–609.
(59)van Eldijk, MB.; Smits, FC.; Vermue, N.; Debets, MF.; Schoffelen, S.; van Hest, JC. Synthesis and Self-Assembly of Well-Defined Elastin-Like Polypeptide-Poly (ethylene glycol) Conjugates. *Biomacromolecules* **2014**, *15* (7), 2751–2759.
(60)Petitdemange, R.; Garanger, E.; Bataille, L.; Dieryck, W.; Bathany, K.; Garbay, B.; Deming, TJ.; Lecommandoux, S. Selective Tuning of Elastin-like Polypeptide Properties via Methionine Oxidation. *Biomacromolecules* **2017**, *18* (2), 544–550.
(61)Petitdemange, R.; Garanger, E.; Bataille, L.; Bathany, K.; Garbay, B.; Deming, TJ.; Lecommandoux, S. Tuning Thermoresponsive Properties of Cationic Elastin-like Polypeptides by Varying Counterions and Side-Chains. *Bioconjugate Chem.* 2**017**, *28* (5), 1403–1412.
(62)Kramer, J. R.; Petitdemange, R.; Bataille, L.; Bathany, K.; Wirotius, A.-L.; Garbay, B.; Deming, T. J.; Garanger, E.; Lecommandoux, S. Quantitative Side-Chain Modifications of Methionine-Containing Elastin-Like Polypeptides as a Versatile Tool to Tune Their Properties. *ACS Macro. Lett.* **2015**, *4* (11), 1283–1286.
(63)Malho, JM.; Brand, J.; Pecastaings, G.; Ruokolainen, J.; Gröschel, A.; Sèbe, G.; Garanger, E.; Lecommandoux, S. Multifunctional Stimuli-Responsive Cellulose Nanocrystals via Dual Surface Modification with Genetically Engineered Elastin-Like Polypeptides and Poly(acrylic acid). *ACS Macro. Lett.* **2018**, *7* (6), 646–650.
(64)Ott, W.; Nicolaus, T.; Gaub, HE.; Nash, MA. Sequence-Independent Cloning and Post-Translational Modification of Repetitive Protein Polymers through Sortase and Sfp-Mediated Enzymatic Ligation. *Biomacromolecules* **2016**, *17* (4), 1330–1338.
(65)Seifried, BM.; Cao, J.; Olsen, BD. Multifunctional, High Molecular Weight, Post-Translationally Modified Proteins through Oxidative Cysteine Coupling and Tyrosine Modification. *Bioconjugate Chem.* **2018**, *29* (6), 1876-1884.
(66)Zhu, D.; Wang, H.; Trinh, P.; Heilshorn, SC. Yang F. Elastin-like Protein-Hyaluronic Acid (ELP-HA) Hydrogels with Decoupled Mechanical and Biochemical Cues for Cartilage Regeneration. *Biomaterials* **2017**, *127*, 132–140.
(67)Dreher, M. R.; Raucher, D.; Balu, N.; Colvin, O. M.; Ludeman, S. M.; Chilkoti, A. Evaluation of an Elastin-Like Polypeptide–Doxorubicin Conjugate for Cancer Therapy. *J. Controlled Release* **2003**, *91* (1-2), 31–43.
(68)Wang, Z.; He, Q.; Zhao, W.; Luo, J.; Gao, W. Tumor-homing, pH- and Ultrasound-Responsive Polypeptide-Doxorubicin Nanoconjugates Overcome Doxorubicin Resistance in Cancer Therapy. *J. Controlled Release* **2017**, *264*, 66–75.

(69)Dreher, M. R.; Simnick, A. J.; Fischer, K.; Smith, R. J.; Patel, A.; Schmidt, M.; Chilkoti, A. Temperature Triggered Self-Assembly of Polypeptides into Multivalent Spherical Micelles. *J. Am. Chem. Soc.* **2008**, *130* (2), 687–694.
(70)Hassouneh, W.; Zhulina, E. B.; Chilkoti, A.; Rubinstein, M. Elastin-Like Polypeptide Diblock Copolymers Self-Assemble into Weak Micelles. *Macromolecules* **2015**, *48* (12), 4183–4195.
(71)Garanger, E.; MacEwan, S. R.; Sandre, O.; Br ûlet, A.; Bataille, L.; Chilkoti, A.; Lecommandoux, S. Structural Evolution of a Stimulus-Responsive Diblock Polypeptide Micelle by Temperature Tunable Compaction of its Core. *Macromolecules* **2015**, *48* (18), 6617–6627.
(72)Hassouneh W1, Fischer K, MacEwan SR, Branscheid R, Fu CL, Liu R, Schmidt M, Chilkoti A. Unexpected Multivalent Display of Proteins by Temperature Triggered Self-Assembly of Elastin-like Polypeptide Block Copolymers. *Biomacromolecules* **2012**, *13* (5), 1598-1605.
(73)Pille, J.; van Lith, SA.; van Hest, JC.; Leenders, WP. Self-Assembling VHH-Elastin-Like Peptides for Photodynamic Nanomedicine. *Biomacromolecules* **2017**, *18* (4), 1302–1310.
(74)Chen, TH.; Bae, Y.; Furgeson, DY. Intelligent Biosynthetic Nanobiomaterials (IBNs) for Hyperthermic Gene Delivery. *Pharm. Res.* **2008**, *25* (3), 683–691.
(75)Le Fer, G.; Portes, D.; Goudounet, G.; Guigner, J.-M.; Garanger, E.; Lecommandoux, S. Design and Self-Assembly of PBLG-b-ELP Hybrid Diblock Copolymers Based on Synthetic and Elastin-Like Polypeptides. *Org. Biomol. Chem.* **2017**, *15* (47), 10095–10104.
(76)Fujita, Y.; Mie, M.; Kobatake, E. Construction of Nanoscale Protein Particle Using Temperature-Sensitive Elastin-like Peptide and Polyaspartic Acid Chain. *Biomaterials* **2009**, *30* (20), 3450–3457.
(77)Ara újo, A.; Olsen, BD.; Machado, AV. Engineering Elastin-Like Polypeptide-Poly (ethylene glycol) Multiblock Physical Networks. *Biomacromolecules* **2018**, *19* (2), 329–339.
(78)Jeannot, V.; Gauche, C.; Mazzaferro, S.; Couvet, M.; Vanwonterghem, L.; Henry, M.; Didier, C.; Vollaire, J.; Josserand, V.; Coll, JL.; Schatz, C.; Lecommandoux, S.; Hurbin, A. Anti-Tumor Efficacy of Hyaluronan-based Nanoparticles for the Co-Delivery of Drugs in Lung Cancer. *J. Controlled Release* **2018**, *275*, 117–128.
(79)Jeannot, V.; Mazzaferro, S.; Lavaud, J.; Vanwonterghem, L.; Henry, M.; Arbol éas, M.; Vollaire, J.; Josserand, V.; Coll, JL.; Lecommandoux, S.; Schatz, C.; Hurbin, A. Targeting CD44 Receptor-Positive Lung Tumors Using Polysaccharide-Based Nanocarriers: Influence of Nanoparticle Size and Administration Route. *Nanomedicine* **2016**, *12* (4), 921–932.
(80)Pickens, CJ.; Johnson, SN.; Pressnall, MM.; Leon, MA.; Berkland, CJ. Practical Considerations, Challenges, and Limitations of Bioconjugation via Azide-Alkyne Cycloaddition. *Bioconjugate Chem.* **2018**, *29* (3), 686−701.
(81)Munneke, S.; Prevost, JR.; Painter, GF.; Stocker, BL.; Timmer, MS. The Rapid and Facile Synthesis of Oxyamine Linkers for the Preparation of Hydrolytically Stable Glycoconjugates. *Org. Lett.* **2015**, *17* (3), 624–627.
(82)Munneke, S.; Hill, JC.; Timmer, MS.; Stocker, BL.; Synthesis and Hydrolytic Stability of N- and O-Methyloxyamine Linkers for the Synthesis of Glycoconjugates. *Eur. J. Org. Chem.* **2017**, *25*, 3722–3728.
(83)Ward, CC. ; Kleinman, JI. ; Nomura, DK. NHS-Esters as Versatile Reactivity-Based Probes for Mapping Proteome-Wide Ligandable Hotspots. *ACS Chem. Biol.* **2017**, *12* (6), 1478–1483.
(84)Tanaka, H,; Kawai, T.; Adachi, Y.; Ohno, N.; Takahashi, T. β(1,3) Branched Heptadeca-and Linear Hexadeca-Saccharides Possessing an Aminoalkyl Group as a Strong Ligand to Dectin-1. *Chem. Commun.* **2010**, *46* (43), 8249–8251.
(85)Palma, AS.; Feizi, T.; Zhang, Y.; Stoll, MS.; Lawson, AM.; D áz-Rodr íguez, E.; Campanero-Rhodes, MA.; Costa, J.; Gordon, S.; Brown, GD.; Chai, W. Ligands for the β-Glucan Receptor, Dectin-1, Assigned Using "Designer" Microarrays of Oligosaccharide Probes (Neoglycolipids) Generated from Glucan Polysaccharides. *J. Biol. Chem.* **2006**, *281* (9), 5771–5779.
(86)Tiwari, VK.; Mishra, BB1.; Mishra, KB.; Mishra, N.; Singh, AS.; Chen, X. Cu-Catalyzed Click Reaction in Carbohydrate Chemistry. *Chem. Rev.* **2016**, *116* (5), 3086–3240.
(87)Thirumurugan, P.; Matosiuk, D.; Jozwiak, K. Click Chemistry for Drug Development and Diverse Chemical–Biology Applications. *Chem. Rev.* **2013**, *113* (7), 4905–4979.

SUPPORTING INFORMATION

^{1}H NMR spectrum of **Azide-linker** in $CDCl_3$

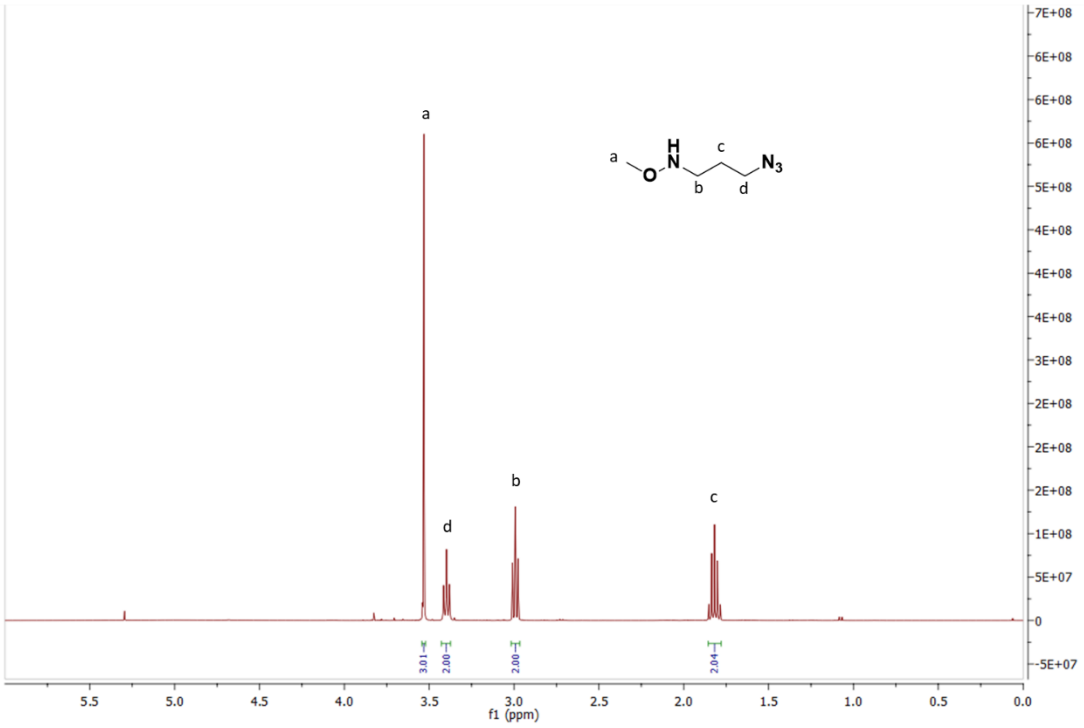

C^{13} NMR spectrum of **Azide-linker** in $CDCl_3$

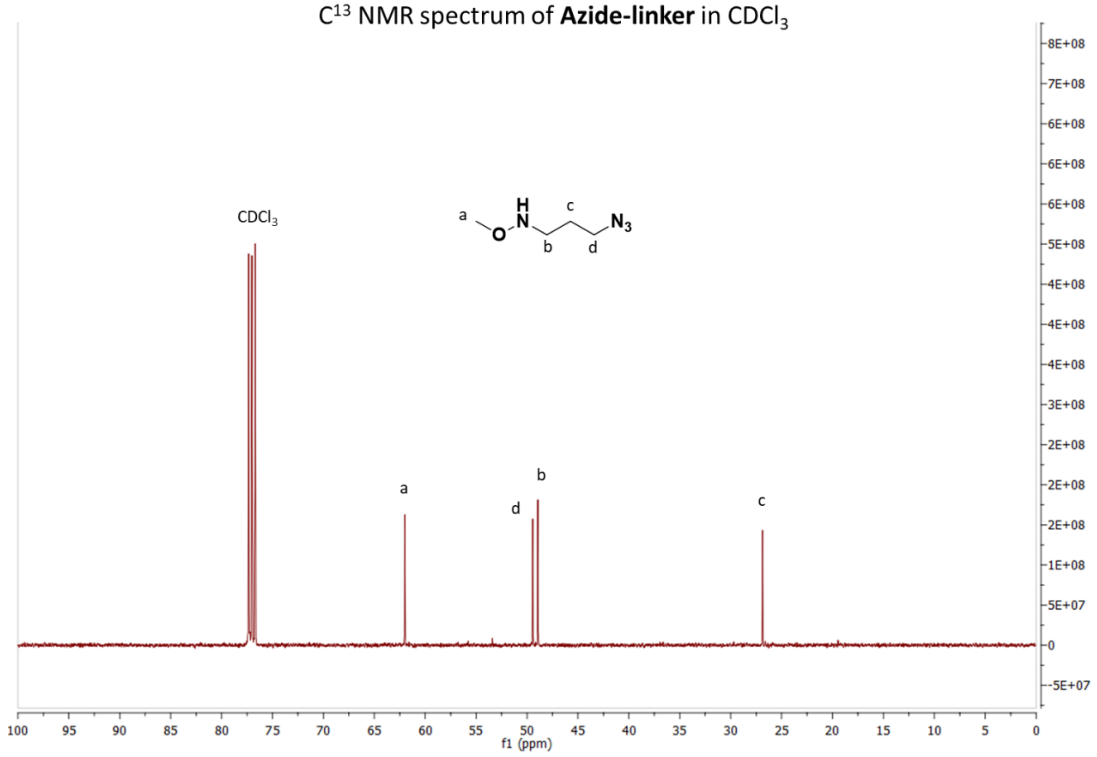

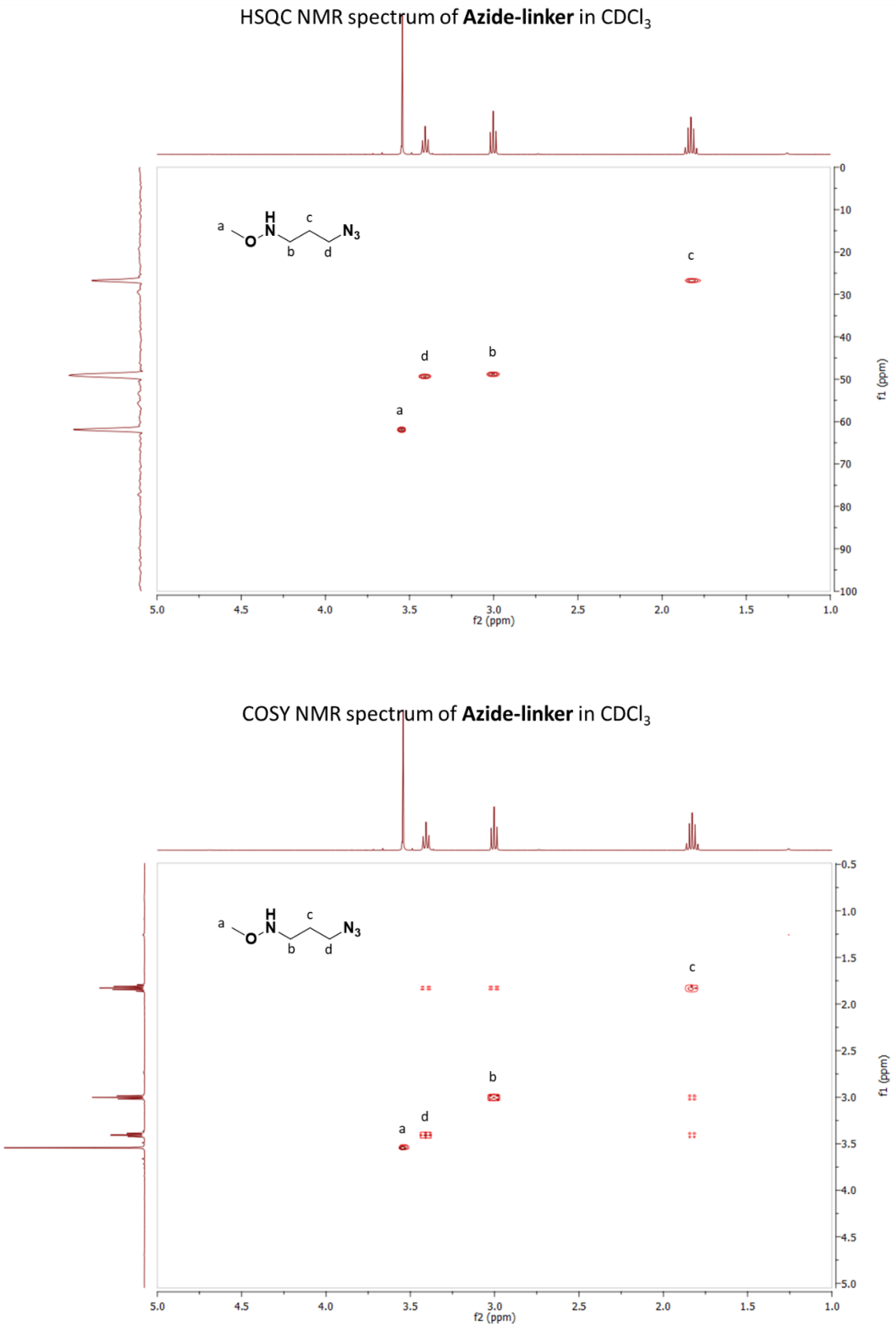

Figure S1. ^{1}H, ^{13}C, HSQC and COSY NMR spectra of Azide-linker.

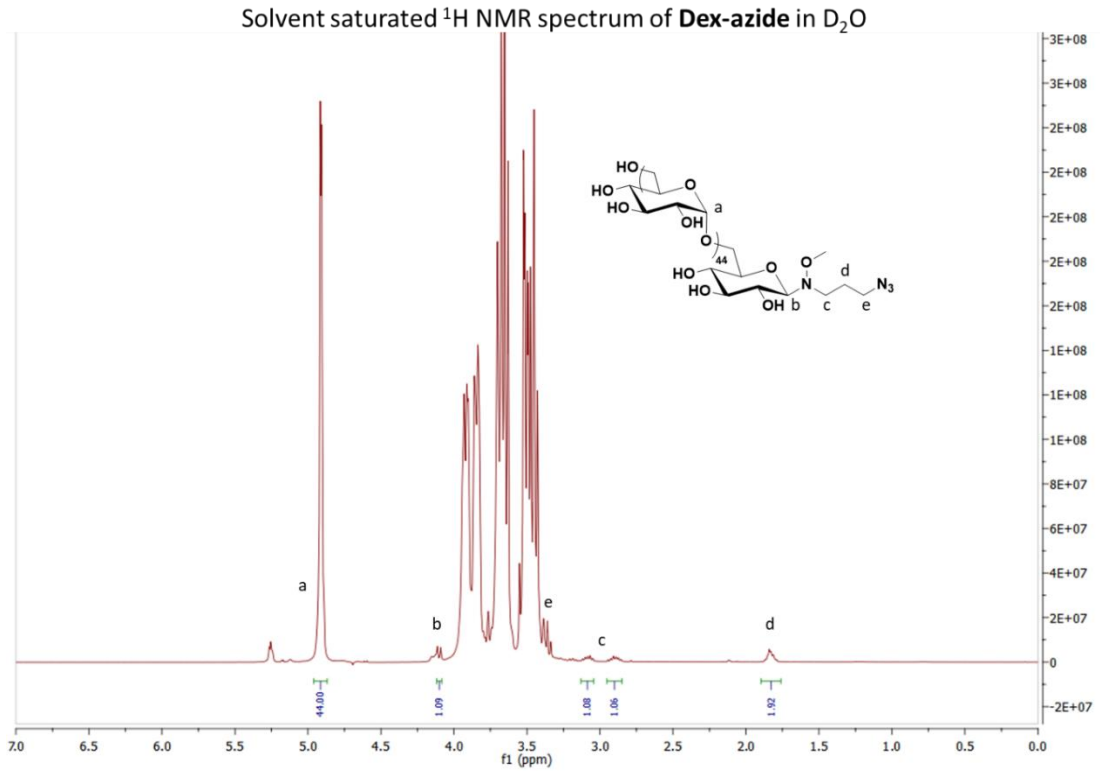
Solvent saturated ^{1}H NMR spectrum of **Dex-azide** in D_2O
a
b
c
d
e
44.00
1.09
1.08
1.06
1.92
f1 (ppm)

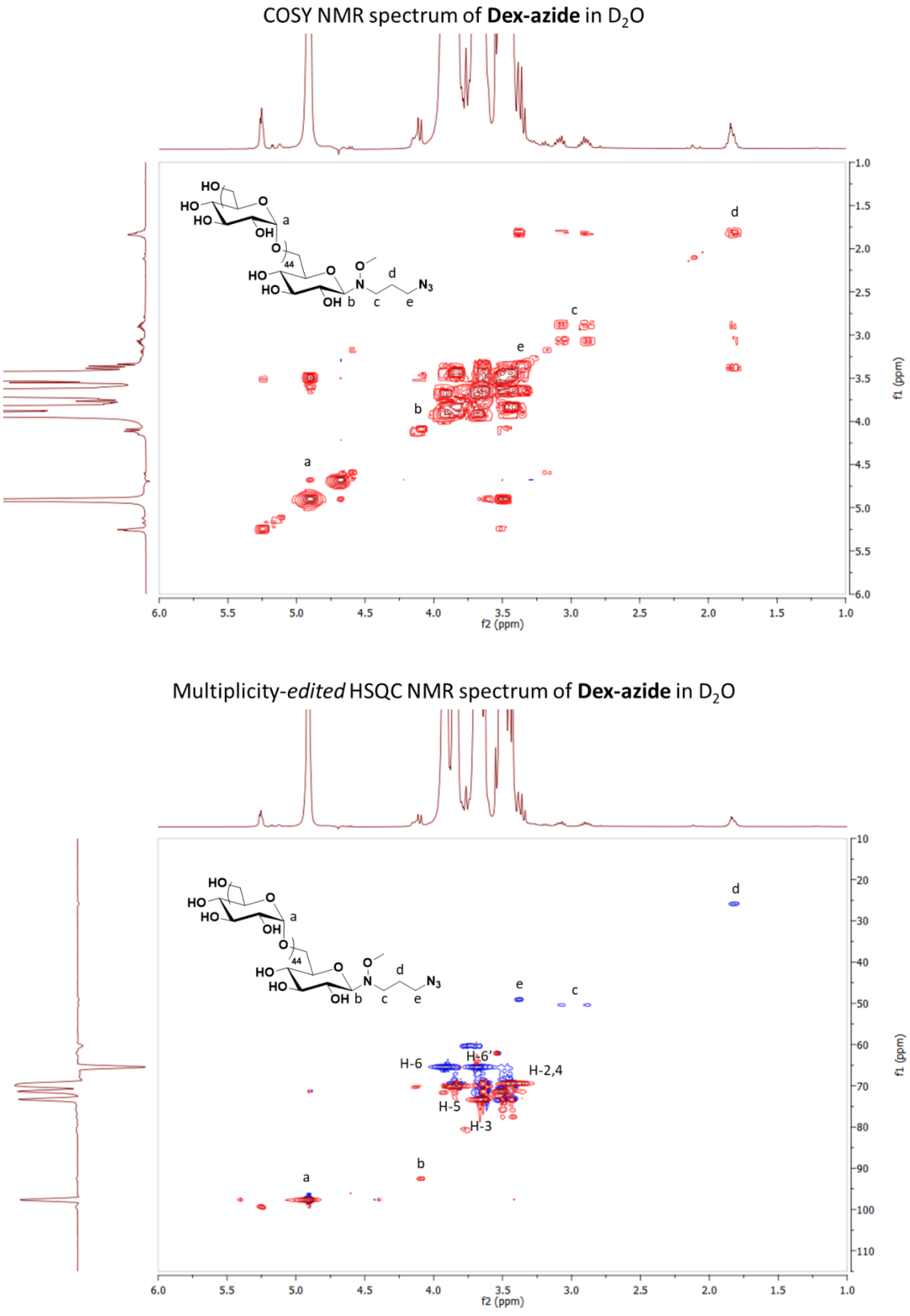

Figure S2. ^{1}H, COSY and HSQC NMR spectra of Dex-N_3.

^{1}H NMR spectrum of **Lam-azide** in D_2O

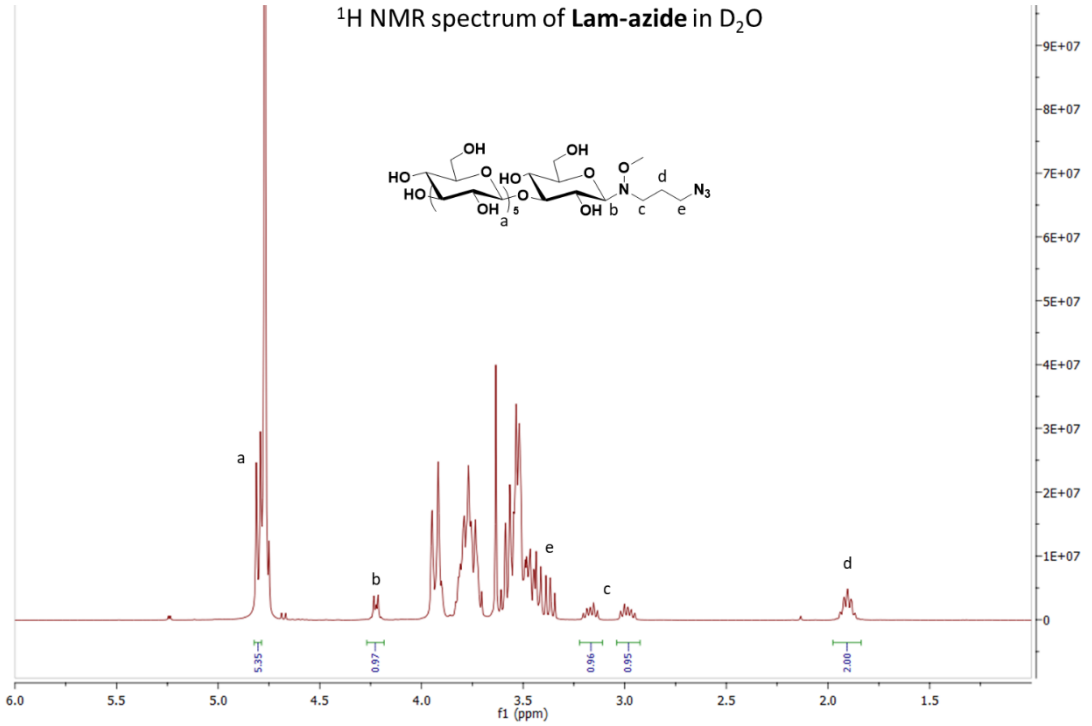

HSQC NMR spectrum of **Lam-azide** in D_2O

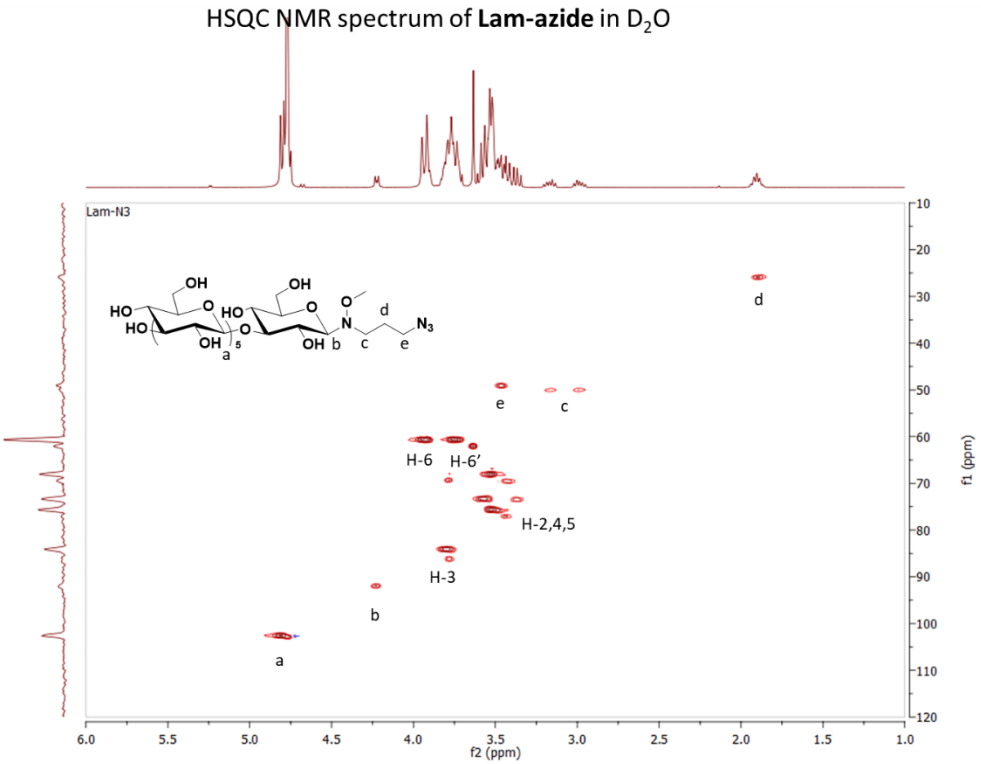

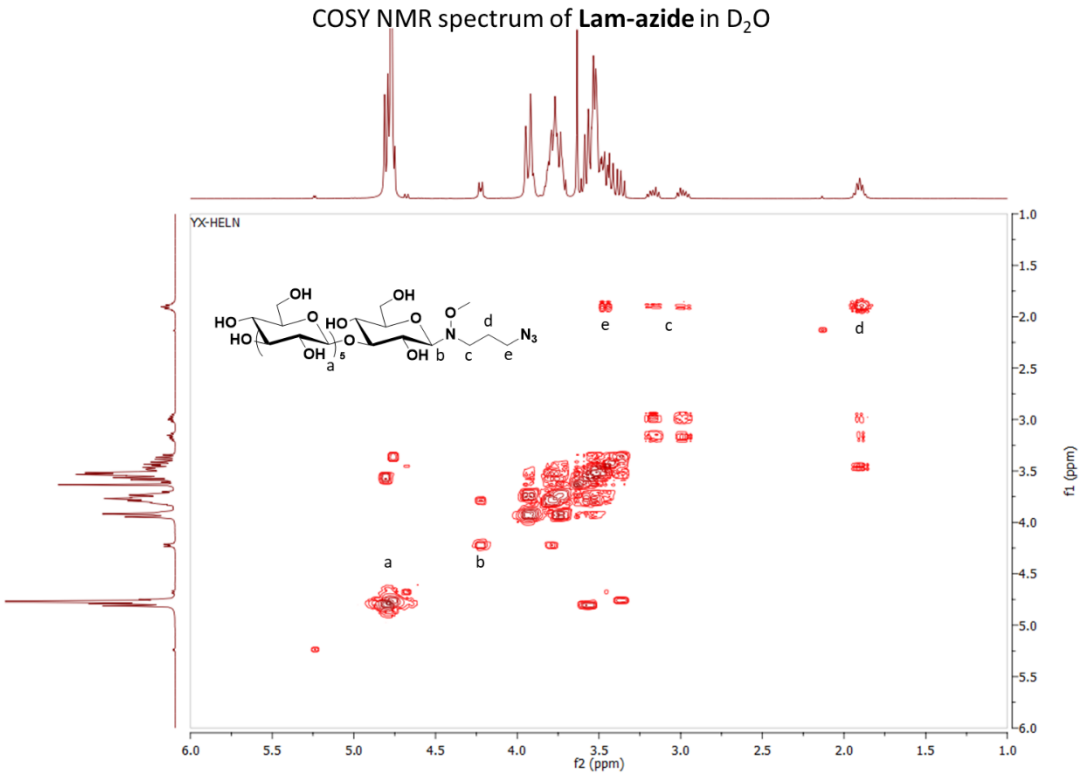

Figure S3. ^{1}H, HSQC, and COSY NMR spectra of Lam-N_3.

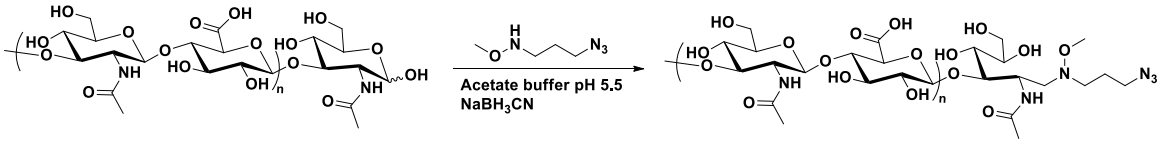

Figure S4. Synthesis of HA-N_3 by reductive amination.

^{1}H NMR spectrum of **HA-azide** in D_2O

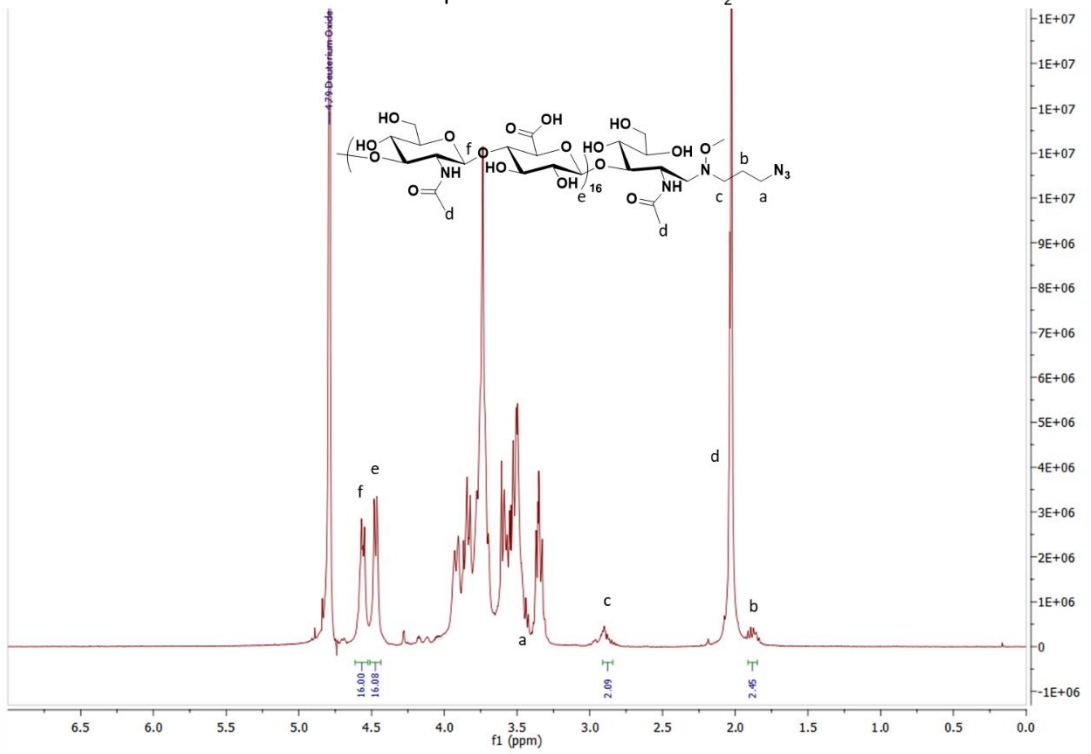

Multiplicity-*edited* HSQC NMR spectrum of **HA-azide** in D_2O

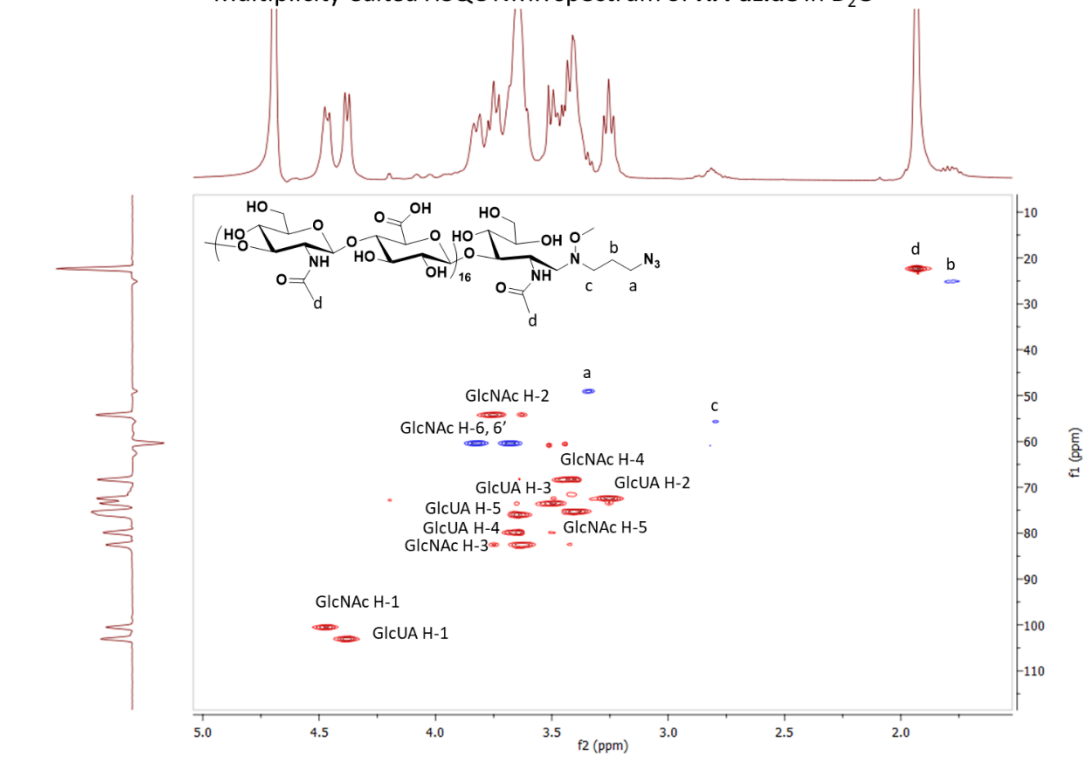

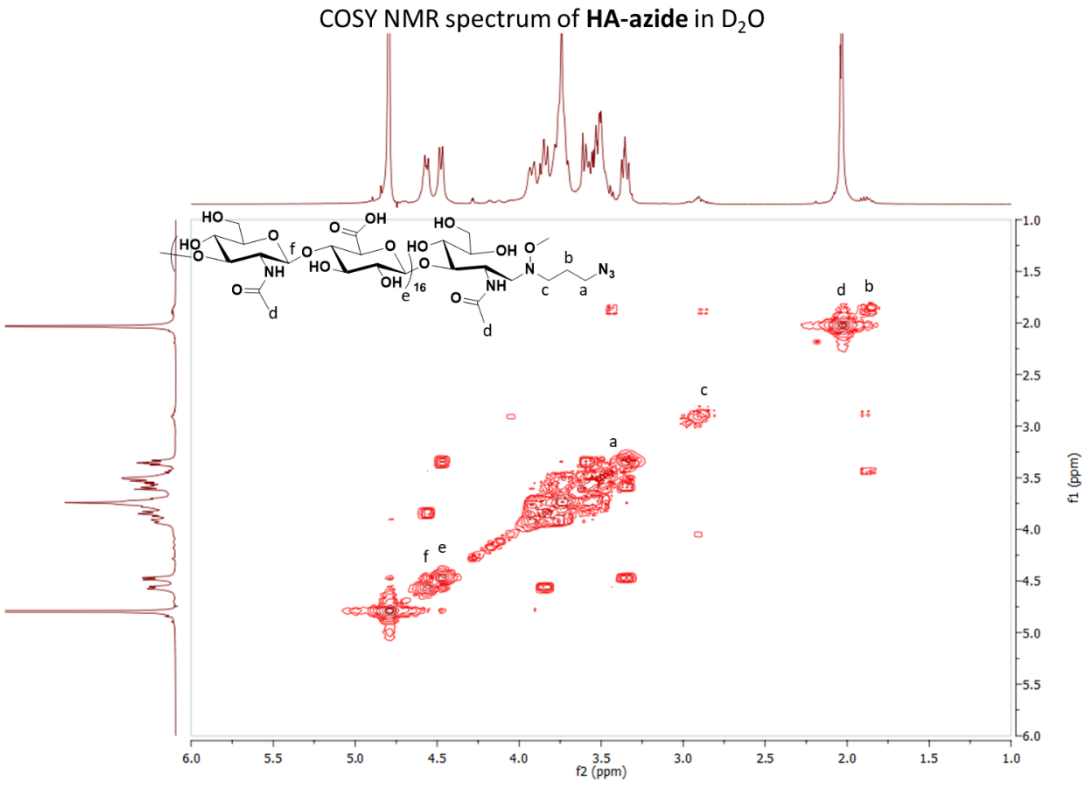

Figure S5. ^{1}H, HSQC and COSY NMR spectra of HA-N_3.

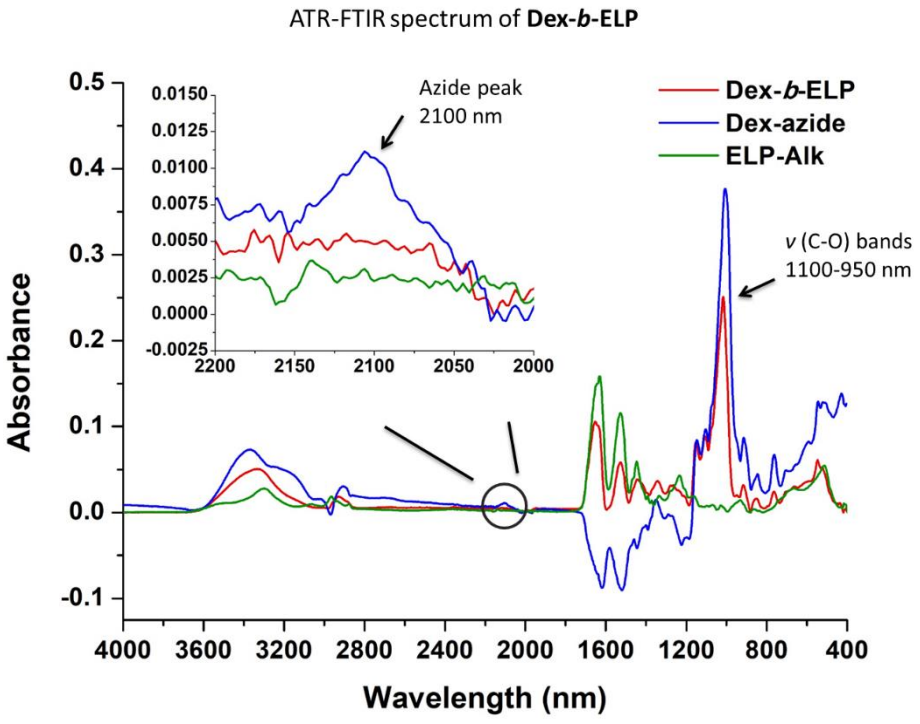

Figure S6. FTIR spectroscopy of ELP-Alk, Dex-N_3, Dex-*b*-ELP.

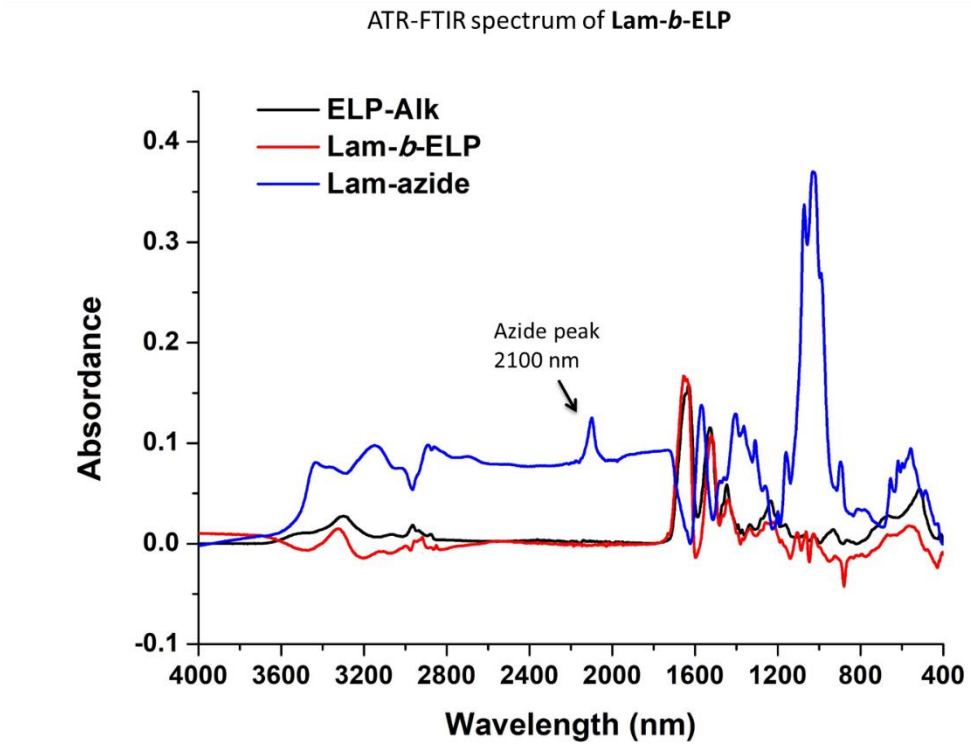

Figure S7. FTIR spectroscopy of ELP-Alk, Lam-N_3, Lam-*b*-ELP.

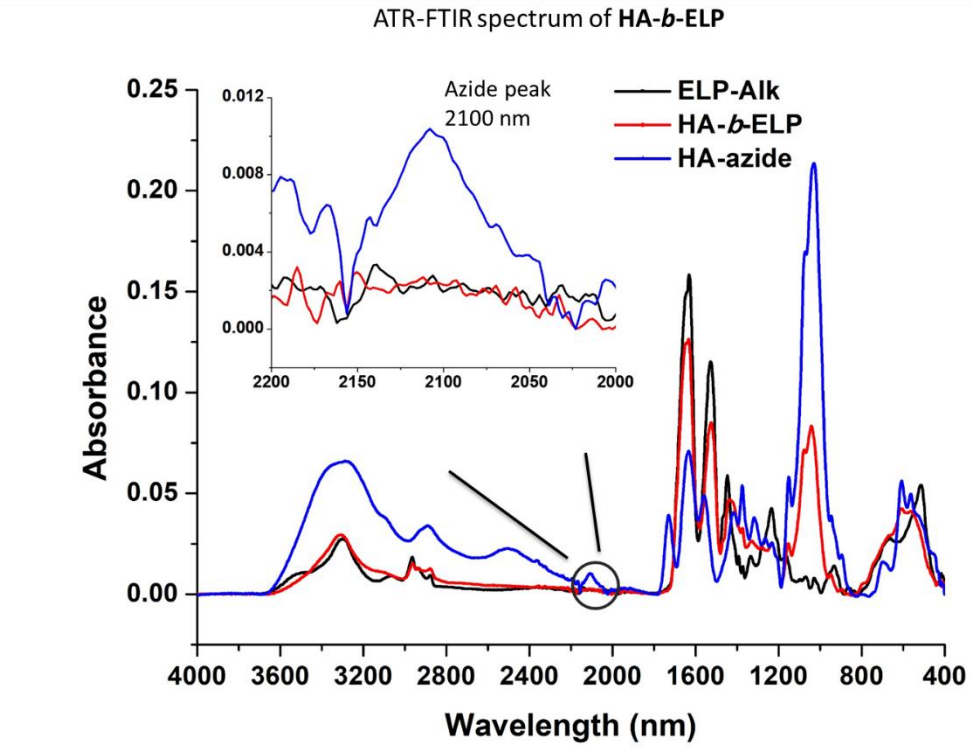

Figure S8. FTIR spectroscopy of ELP-Alk, HA-N_3, HA-*b*-ELP.

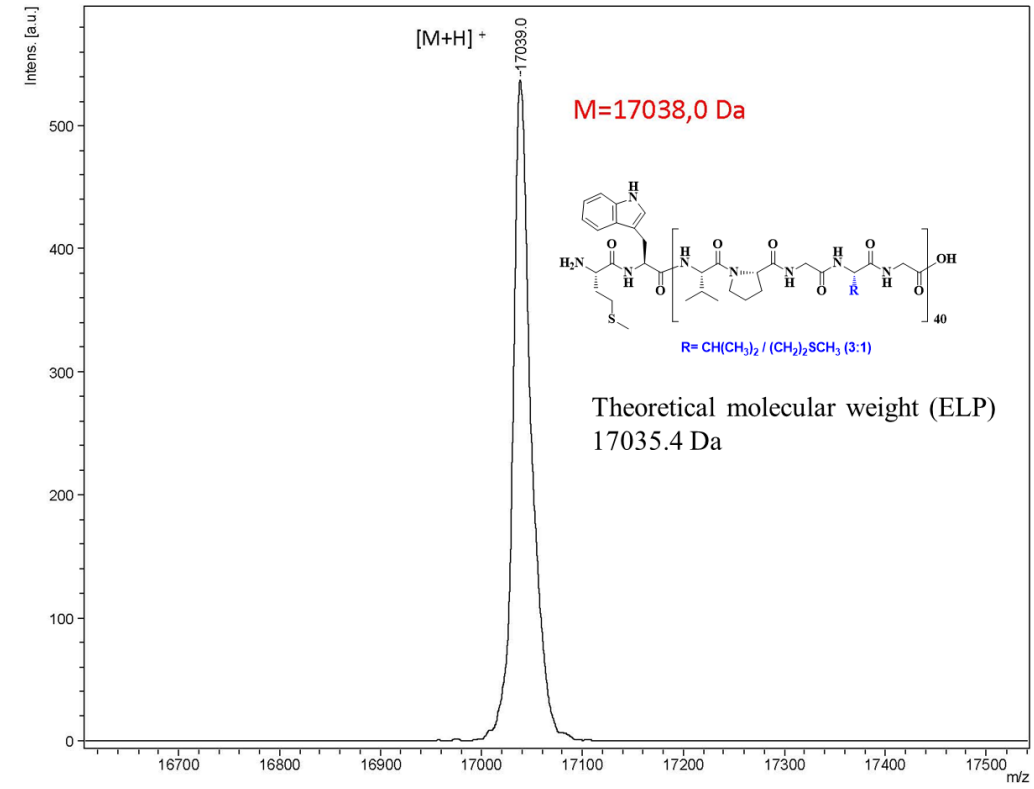

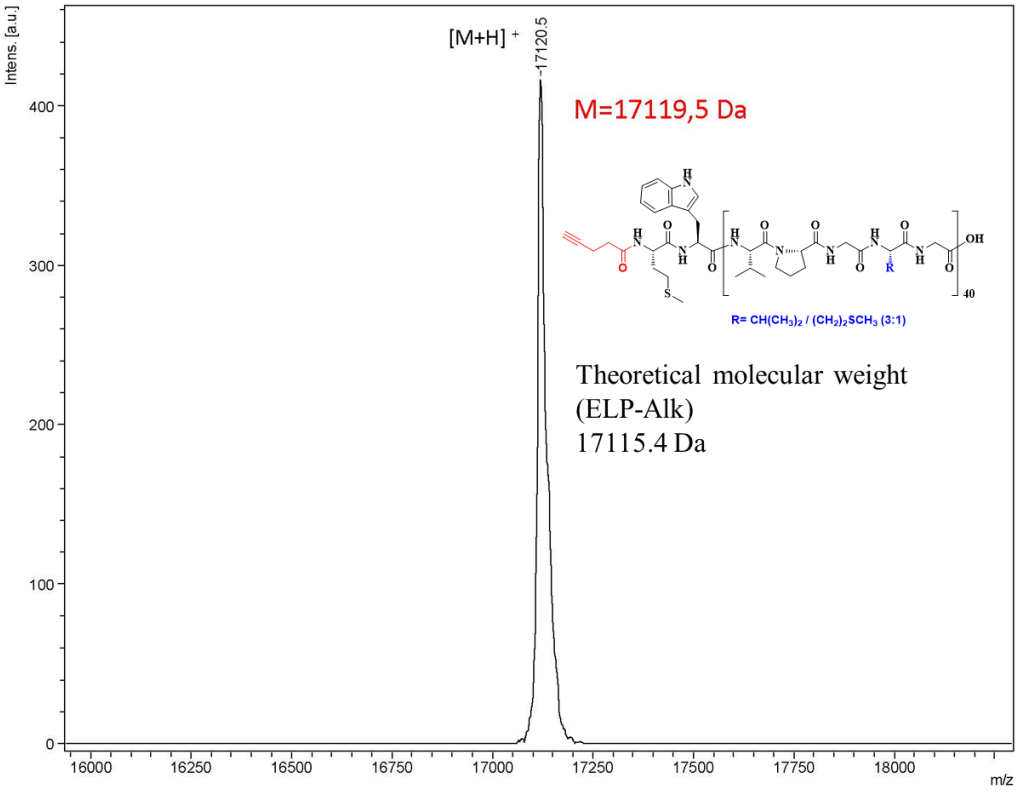

Figure S9. MALDI spectra of ELP and ELP-Alk.

^{1}H NMR spectrum of **ELP** in D_2O

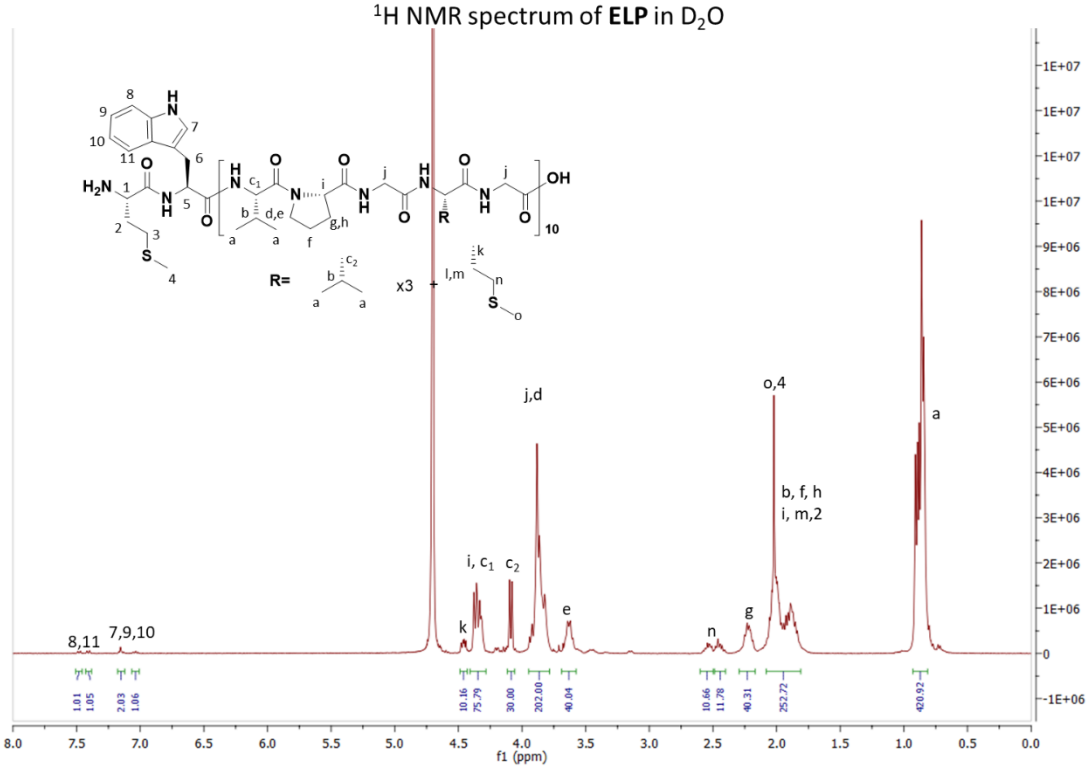

HSQC NMR spectrum of **ELP** in D_2O

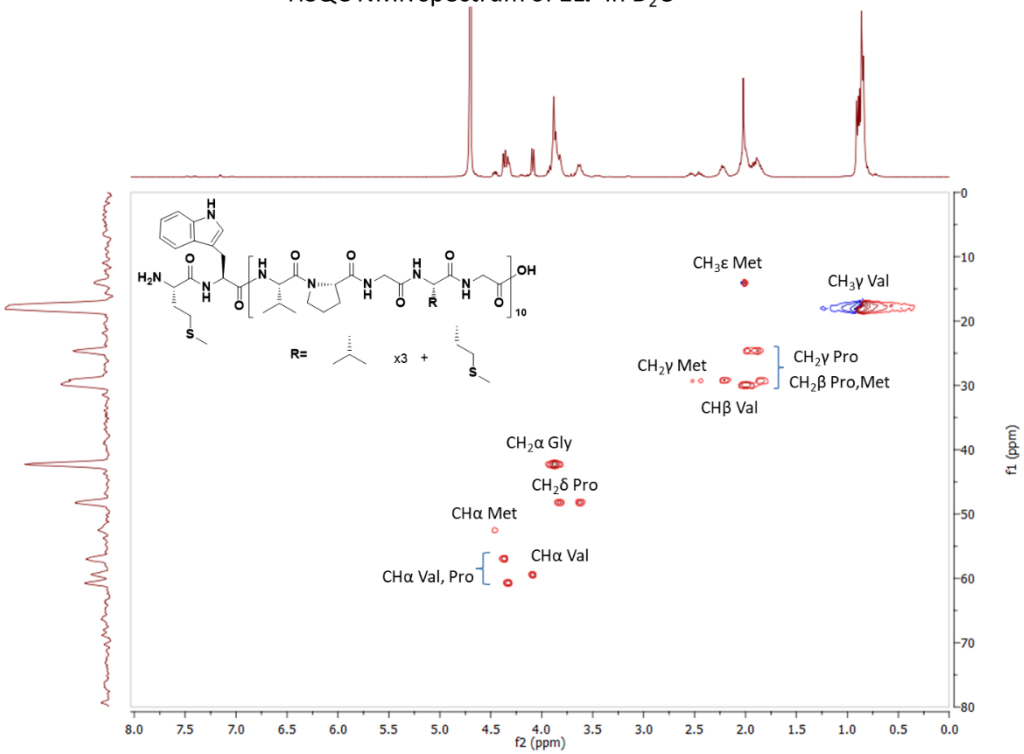

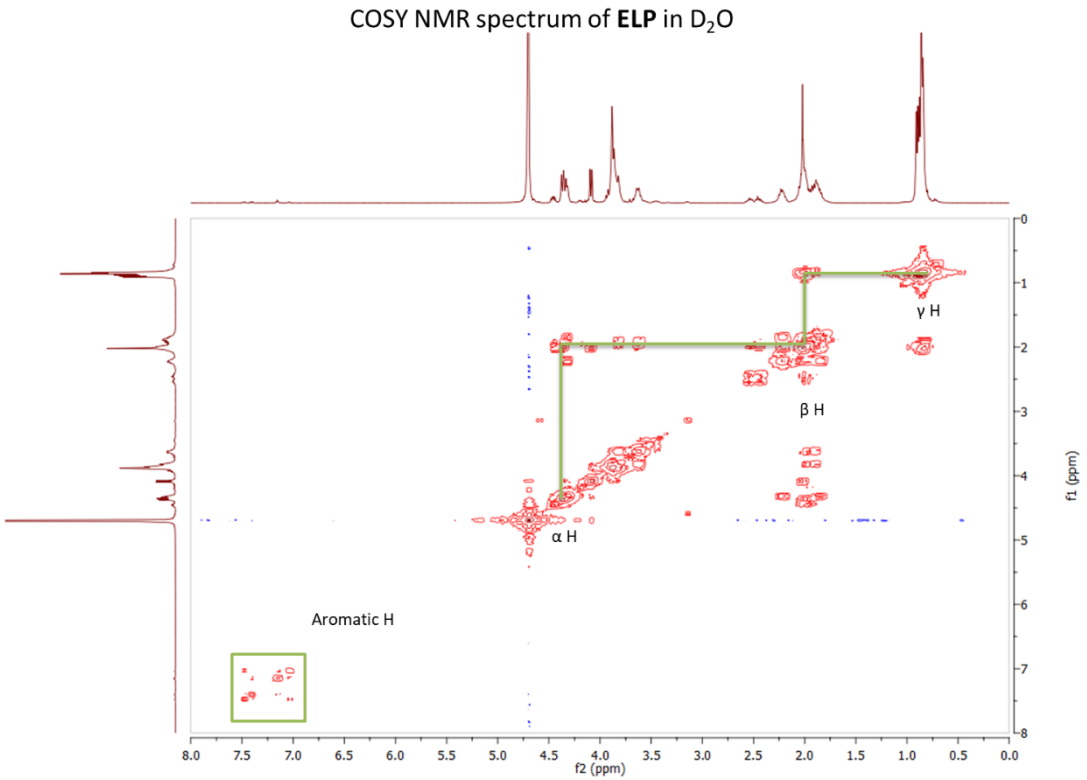

Figure S10. ^{1}H, HSQC and COSY NMR spectra of ELP.

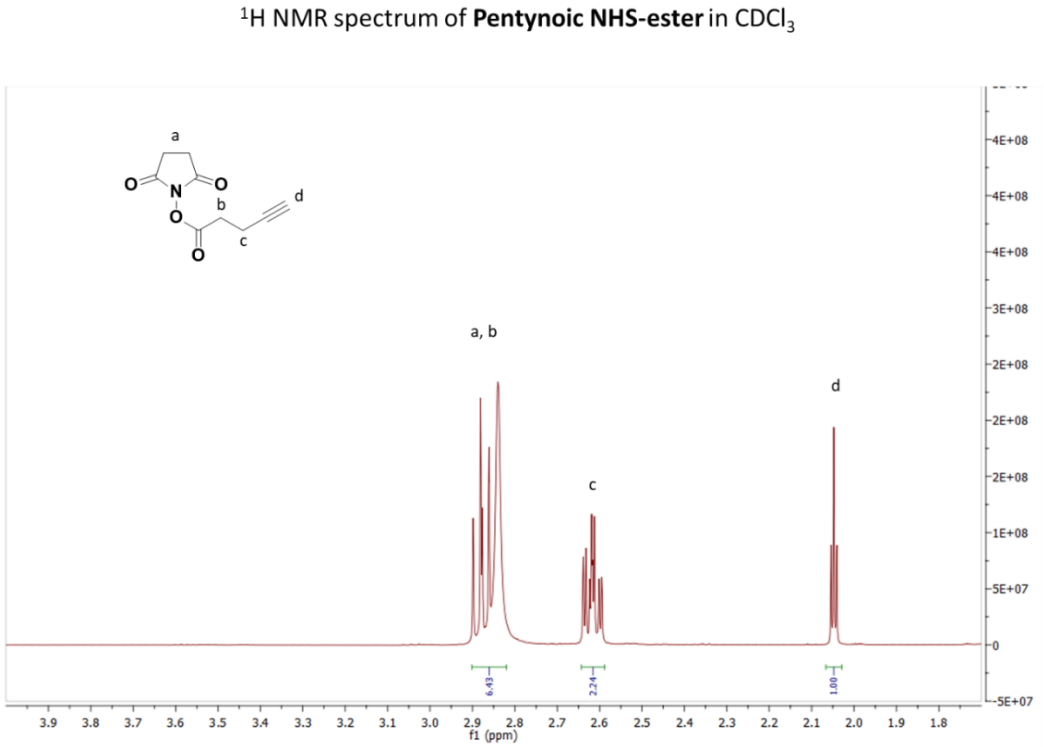

C^{13} NMR spectrum of **Pentynoic NHS-ester** in $CDCl_3$

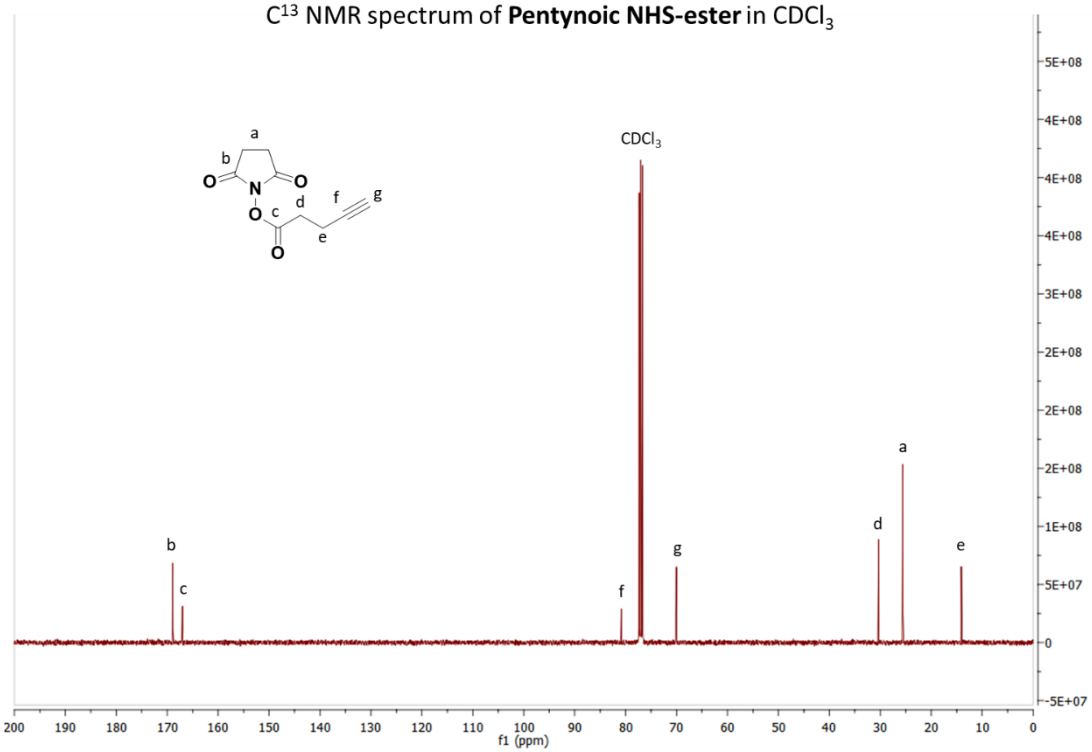

HSQC NMR spectrum of **Pentynoic NHS-ester** in $CDCl_3$

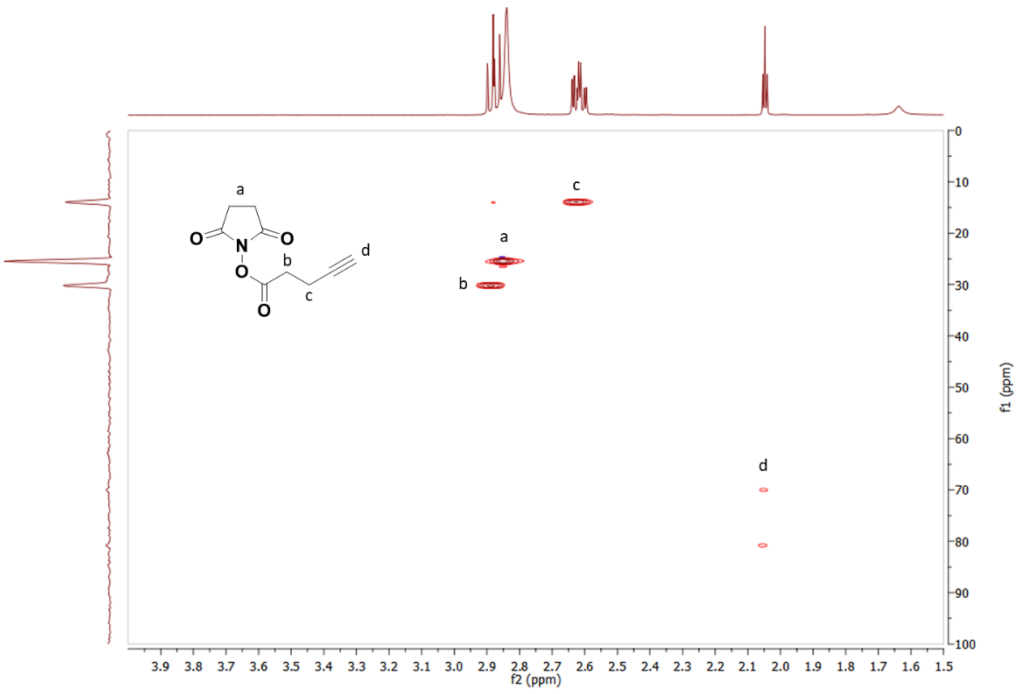

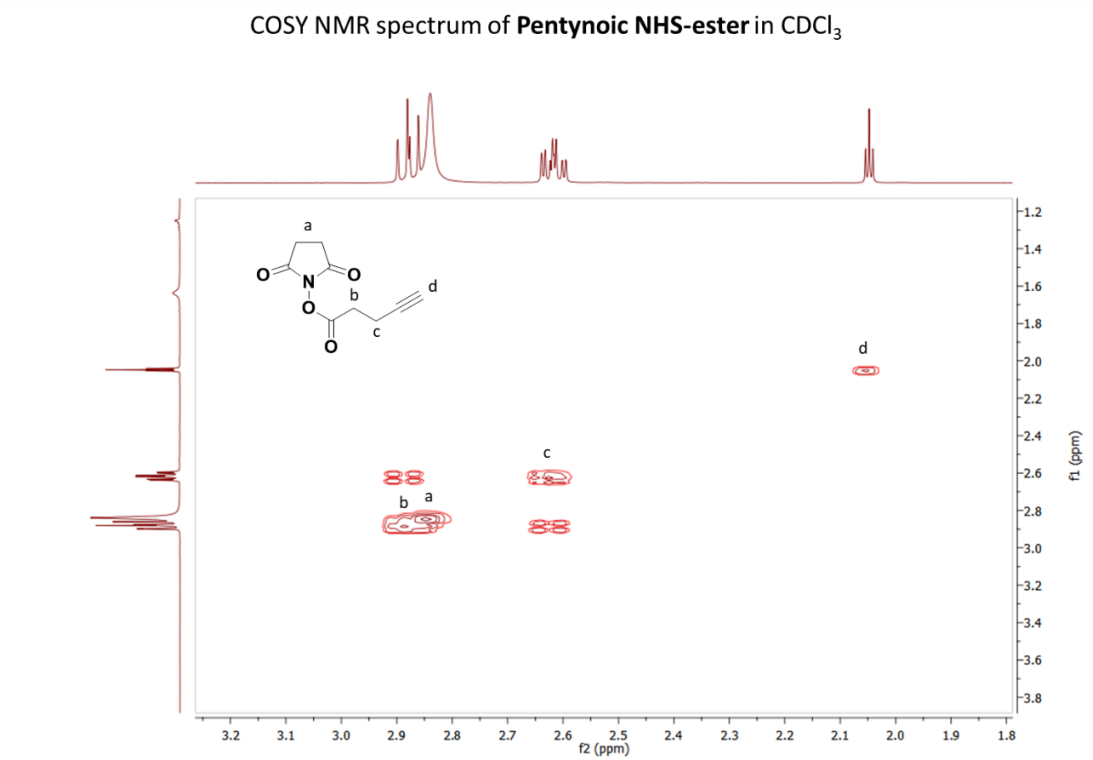

Figure S11. ^{1}H, ^{13}C, HSQC and COSY NMR spectra of Pentynoic NHS-ester.

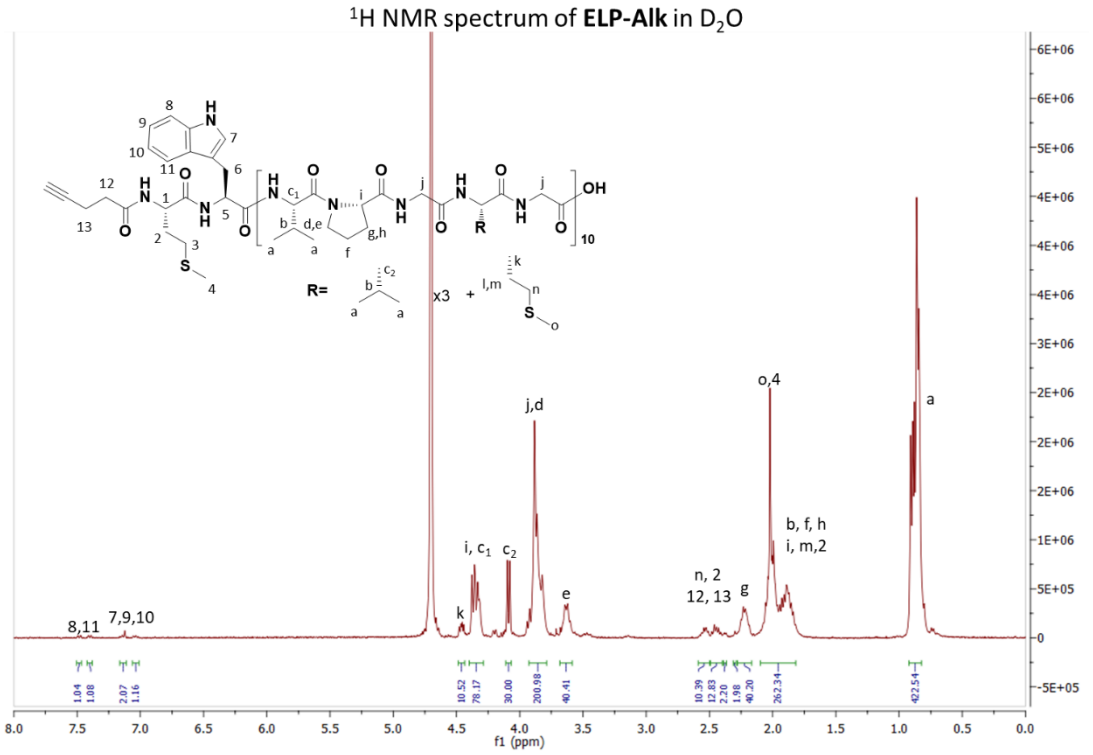

Figure S12. ^{1}H NMR spectrum of ELP-Alk.

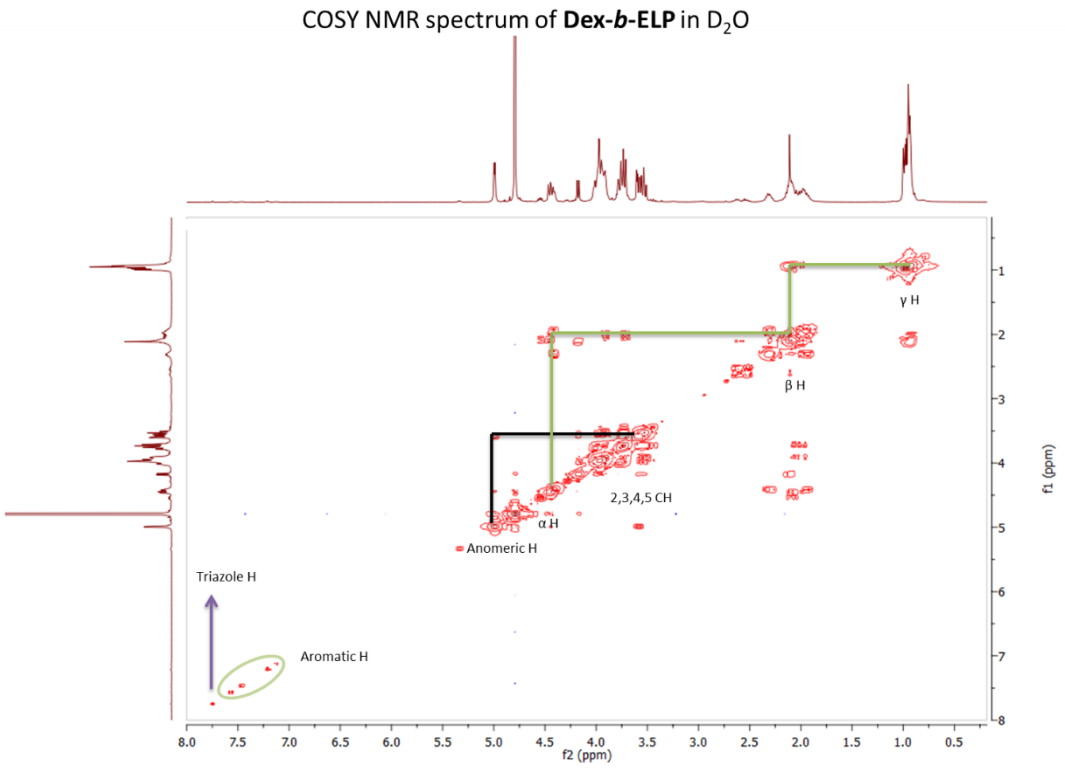

Figure S13. COSY NMR spectrum of Dex-*b*-ELP.

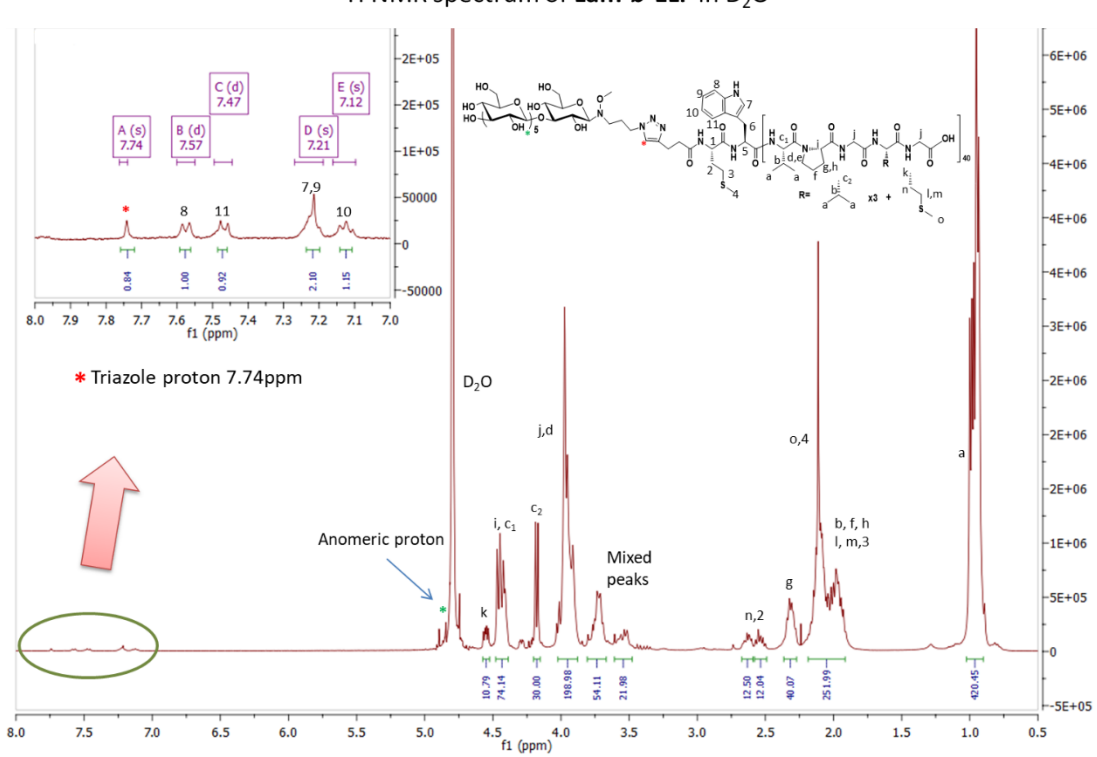

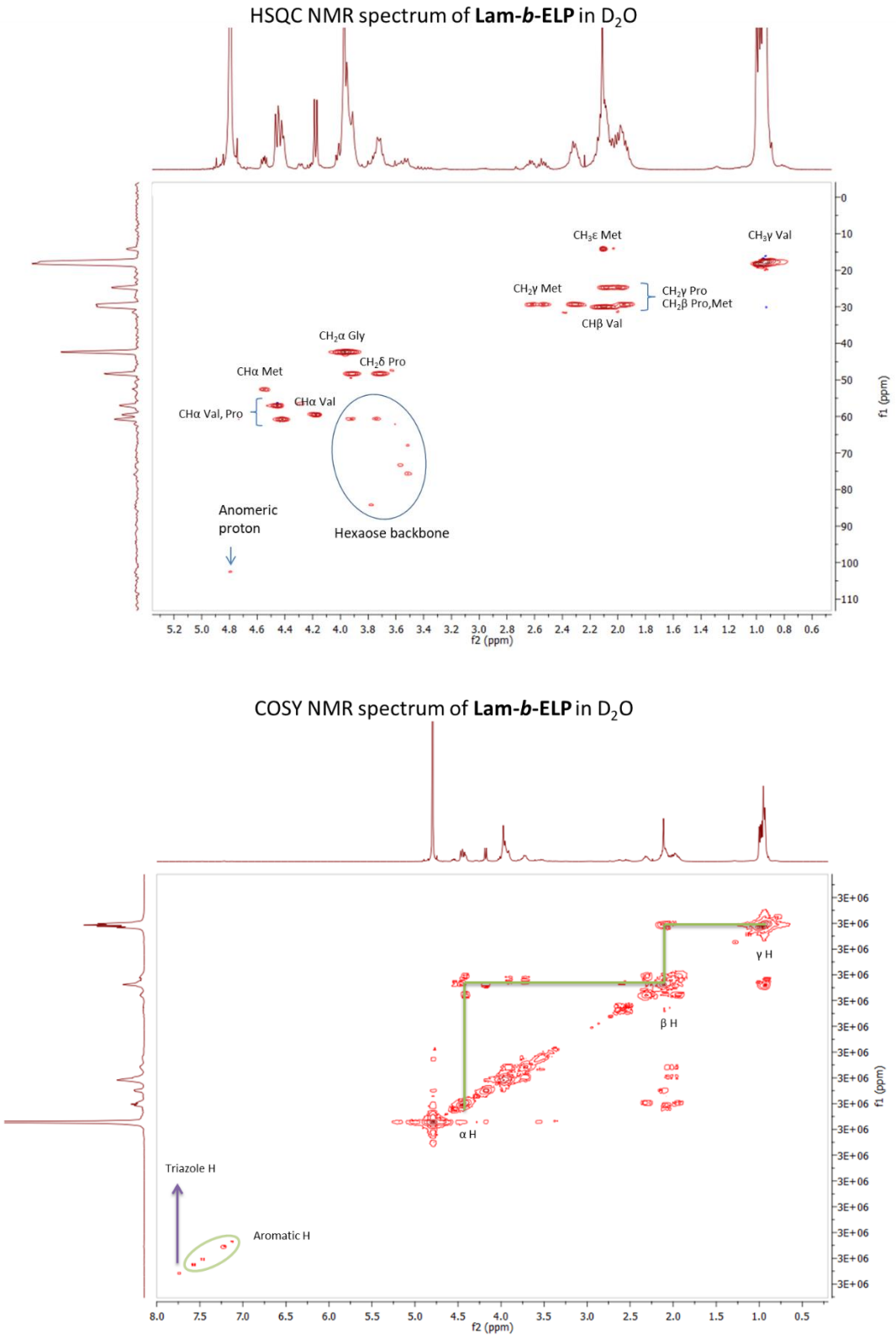

Figure S14. ^{1}H, HSQC and COSY NMR spectra of Lam-*b*-ELP.

^{1}H NMR spectrum of **HA-*b*-ELP** in D_2O

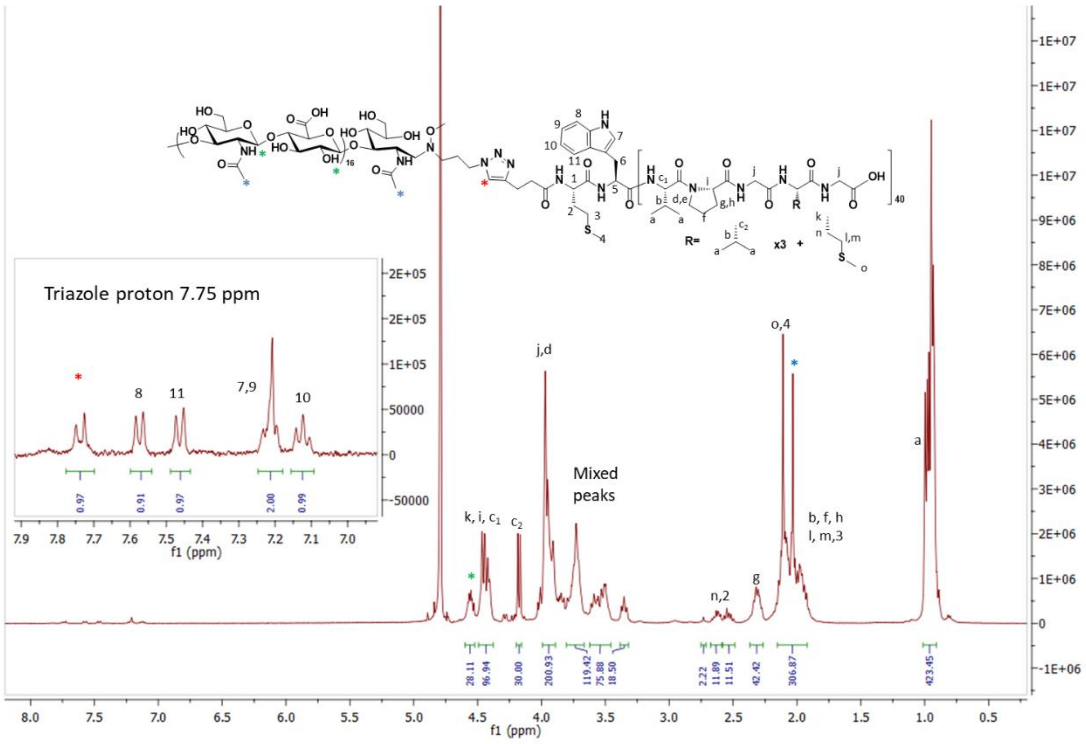

HSQC NMR spectrum of **HA-*b*-ELP** in D_2O

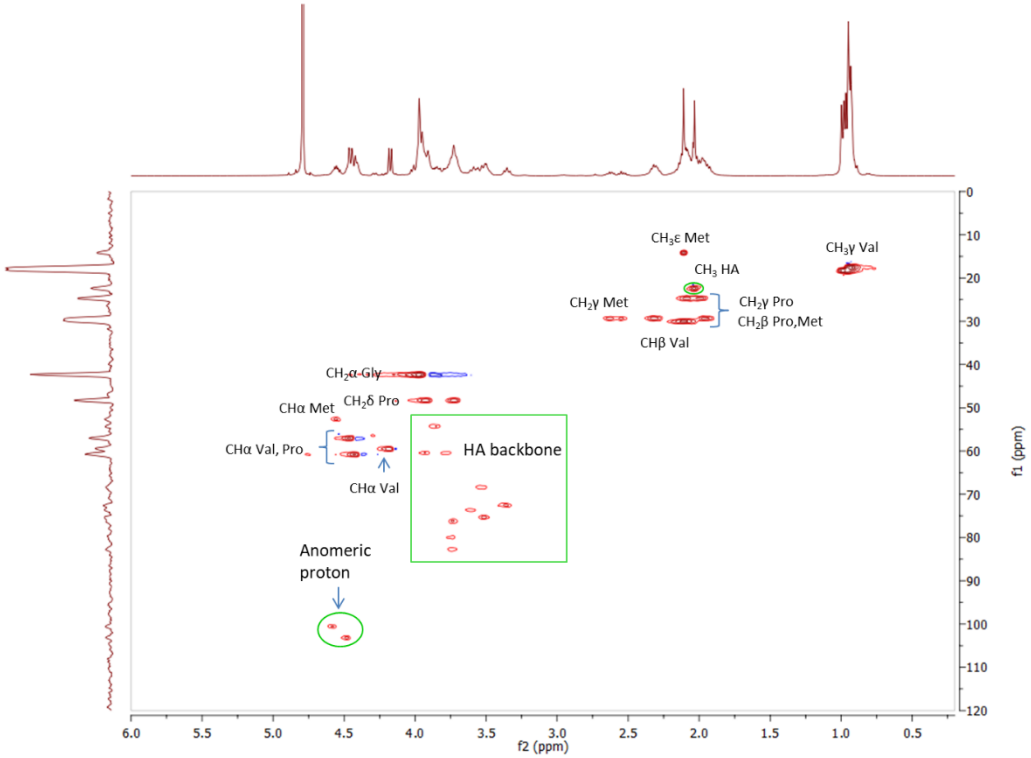

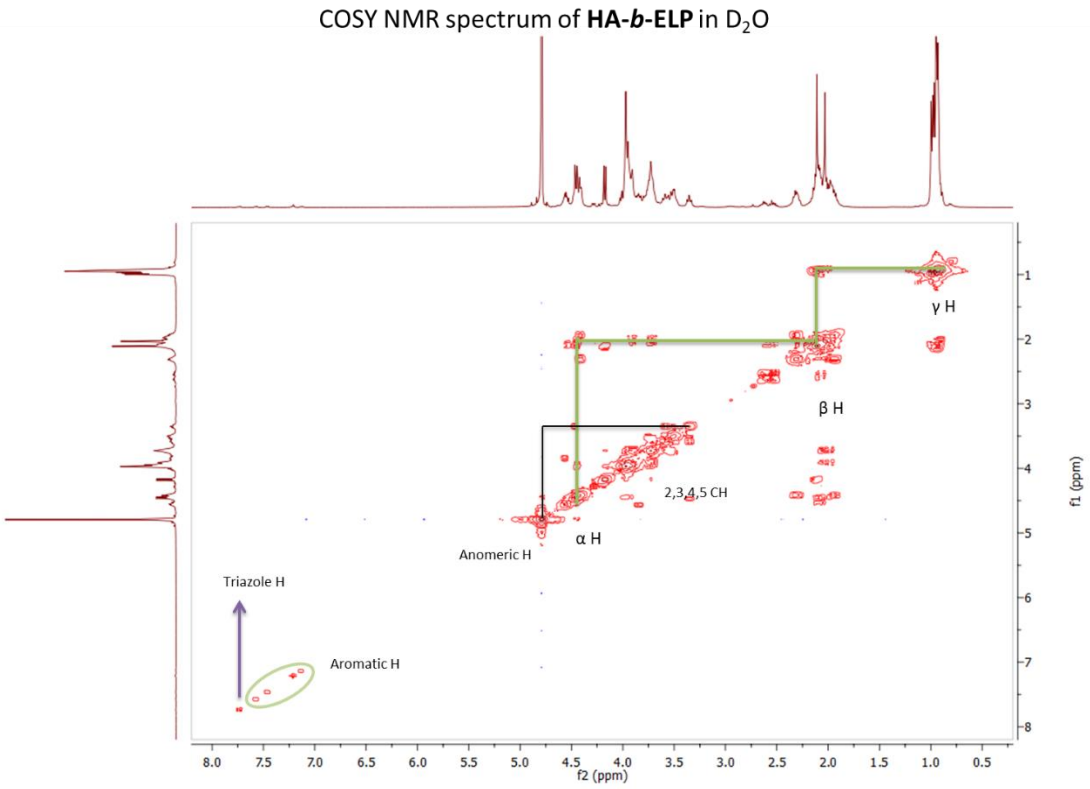

Figure S15. ^{1}H, HSQC and COSY NMR spectra of HA-*b*-ELP.

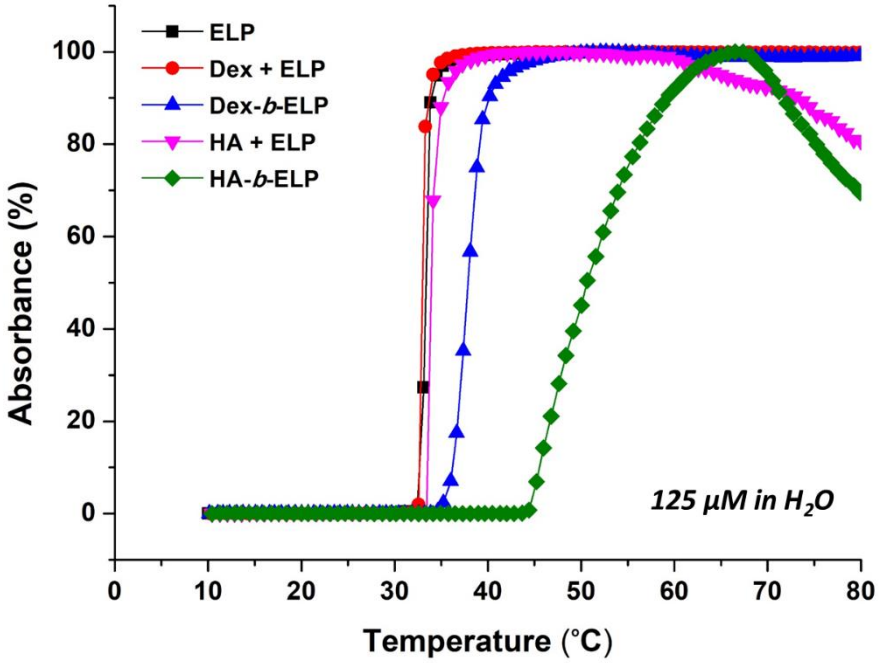

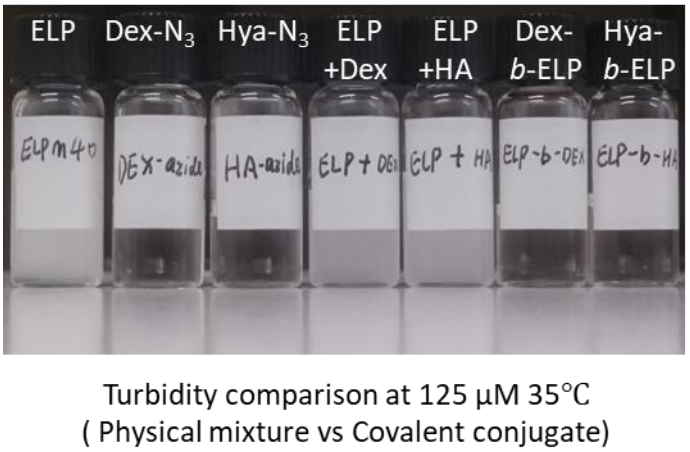

Figure S16. Turbidity study of physical mixture of polysaccharide with ELP.

Turbidity of ELP, Dex-N_3, HA-N_3, physical mixture (ELP+Dex) and (ELP+HA), chemical covalent (Dex-*b*-ELP) and (HA-*b*-ELP) 125 µM in water at 35 ℃. Apparently, ELP and physical mixture were turbid while polysaccharide and polysaccharide conjugated ELP were transparent.

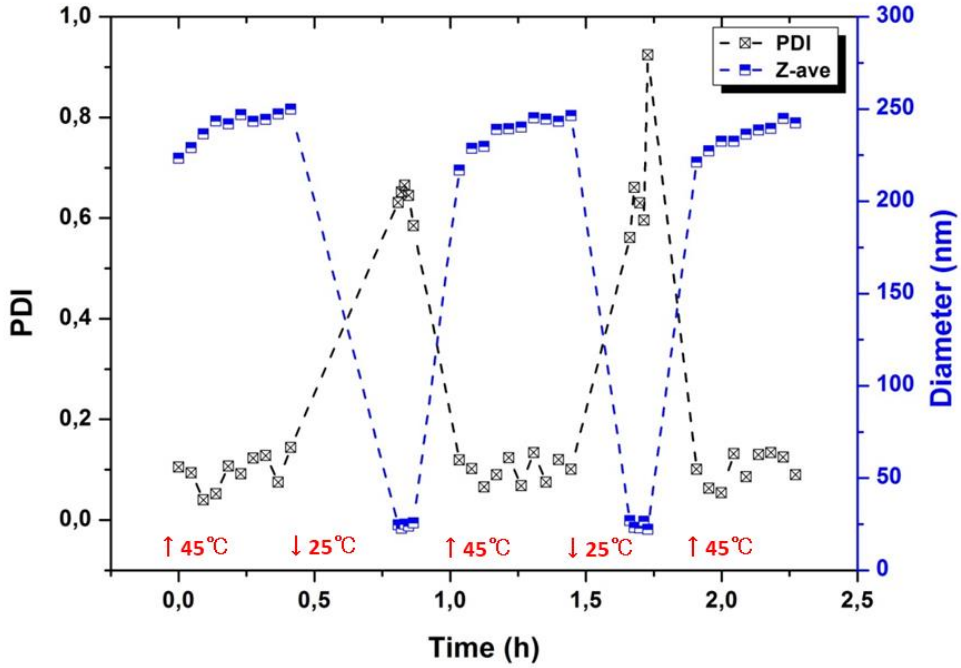

Figure S17. Z-average size and polydispersity as a function of time upon repeated heating (45 ℃) and cooling (25 ℃) of Dex-*b*-ELP.

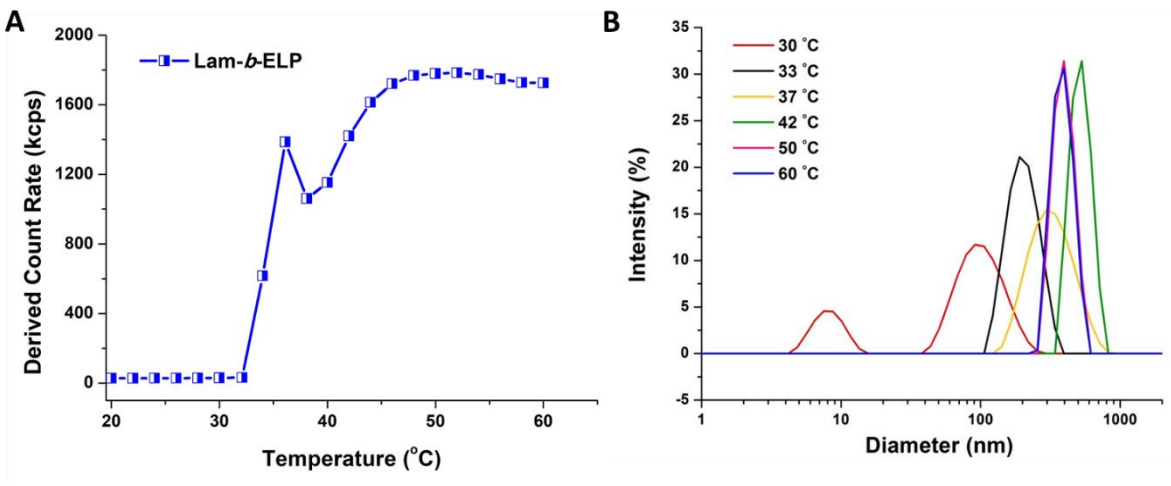

Figure S18. Dynamic light scattering analysis of the assembly of Lam-*b*-ELP (125 μM) in water. (A) Scattering intensity as a function of temperature upon fast heating. (B) Size distribution in intensity at select temperature.

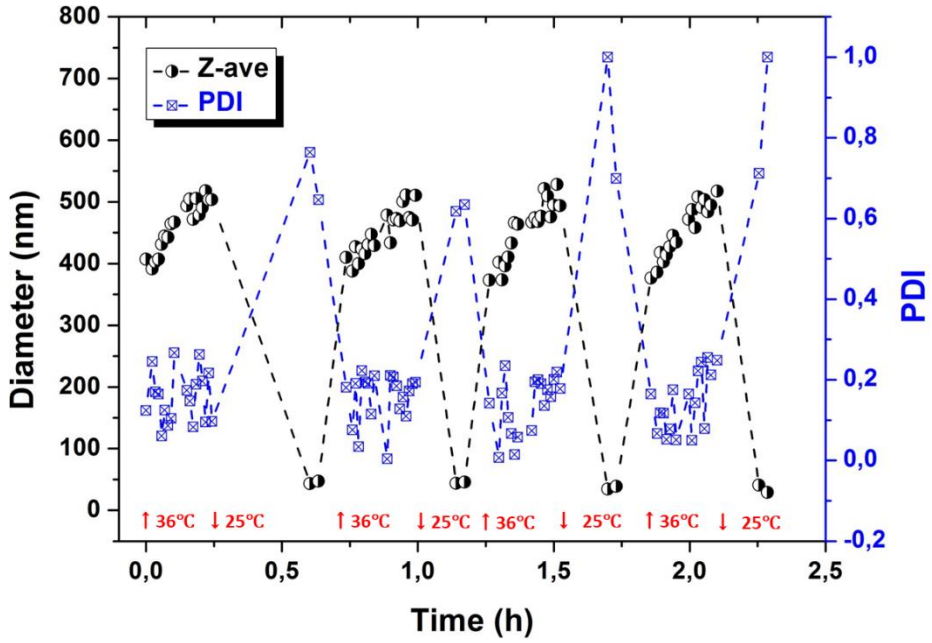

Figure S19. Z-average size and polydispersity as a function of time upon repeated fast heating (36 ℃) and cooling (25 ℃) of Lam-*b*-ELP.

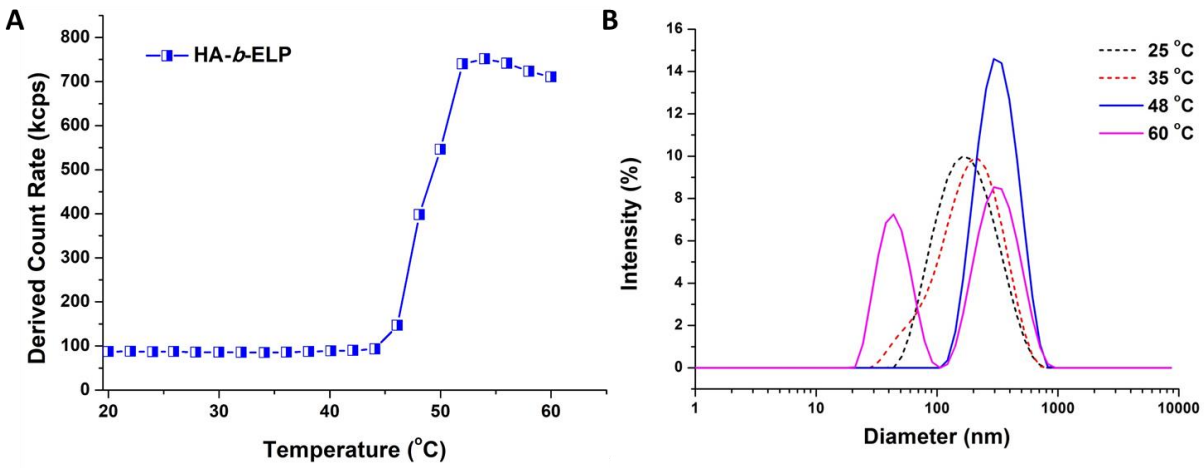

Figure S20. Dynamic light scattering analysis of the assembly of HA-*b*-ELP (150 µM) in water. (A) Scattering intensity as a function of temperature upon fast heating. (B) Size distribution in intensity at select temperature.

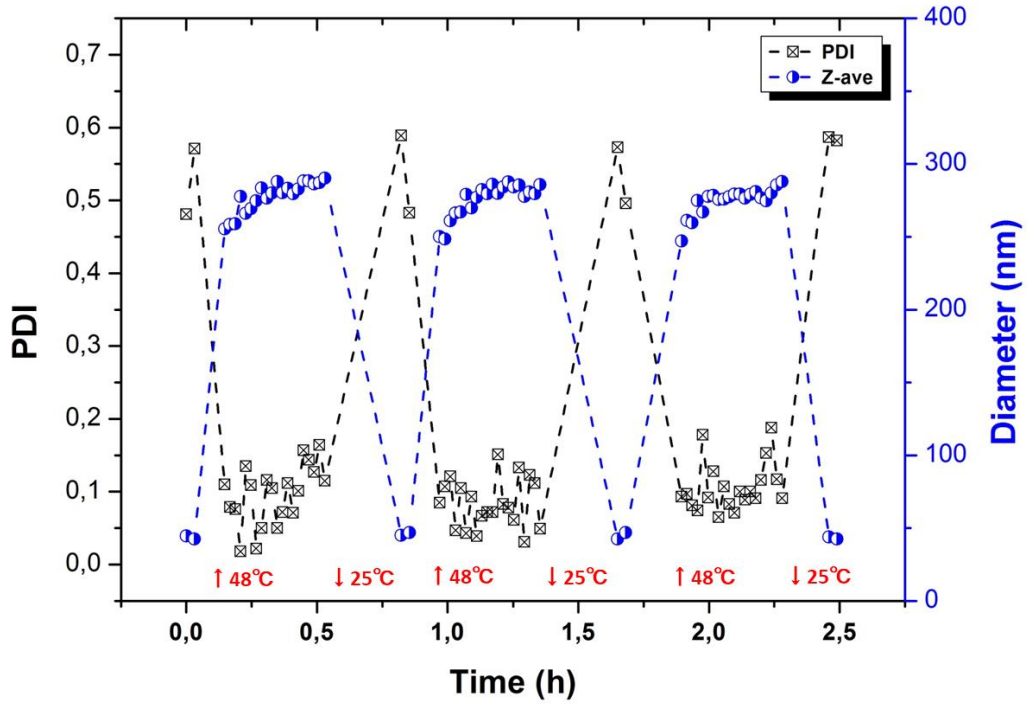

Figure S21. Z-average size and polydispersity as a function of time upon repeated fast heating (48 ℃) and cooling (25 ℃) of HA-*b*-ELP.

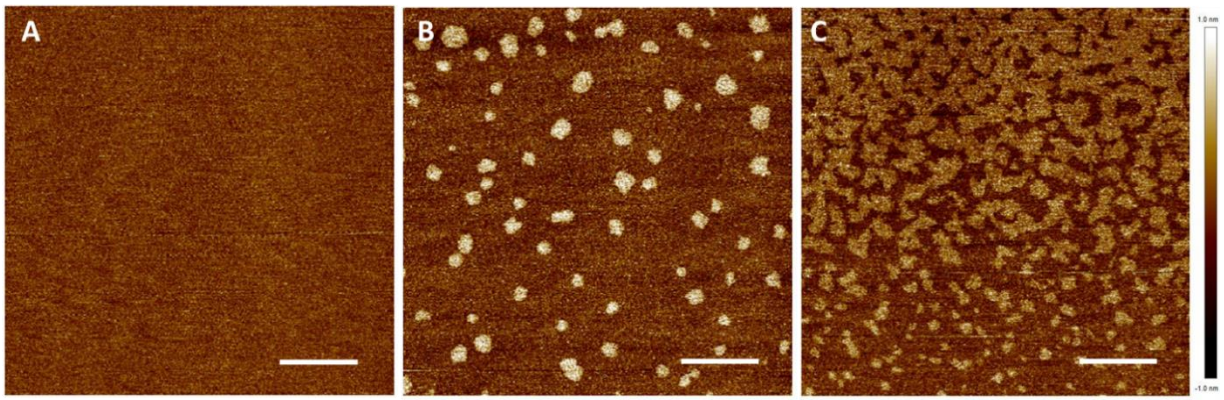

Figure S22. Liquid AFM images of HA-*b*-ELP (150 μM in water) on mica substrate at (A) 25 ℃, (B) 52 ℃, and (C) 55 ℃. Scale bar indicates 1 μM.

CHAPTER 3

STRUCTURAL EVOLUTION OF THERMO-RESPONSIVE POLYSACCHARIDE-*b*-ELP BIOCONJUGATES: FROM UNIMER TO SELF-ASSEMBLED NANOSTRUCTURE

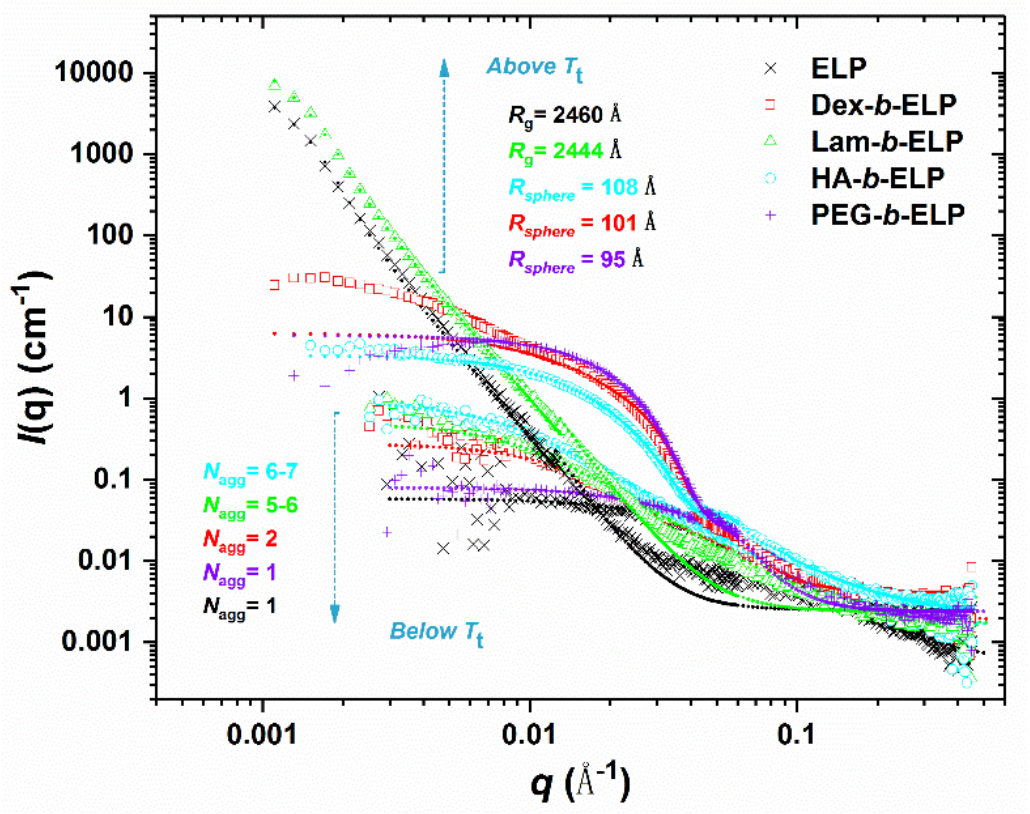

ABSTRACT

With well-defined architecture and stimuli-responsive property of elastin-like polypeptides (ELPs), self-assembly of ELP-based block copolymer presents an elegant strategy for controlling nanostructure formation using temperature as a trigger. Recent work has shown that ELP-diblock copolymers, ELP-protein fusions and ELP-polymer bioconjugates can self-assemble into spherical micelles, wormlike micelles or vesicles. In the context of studying ELP-polymer bioconjugates self-assembly, the flexibility and versatility of synthetic modifications on ELP backbone allows tuning its properties while maintaining its thermo-responsive character. In the present work, the impact of polysaccharide as hydrophilic block on the self-assembly of polysaccharide-*b*-ELP block copolymers are explored and discussed, using PEG as a control. By using click chemistry, we synthesized three polysaccharide-*b*-ELP and PEG-*b*-ELP bioconjugates. Dynamic light scattering study of these bioconjugates demonstrated fully reversible self-assembly/disassembly process by controlling the temperature above/below the ELP transition temperature (T_t). Their thermally triggered structural evolution from unimers to self-assembled nanostructures were further investigated by multi-angle dynamic and static light scattering, and small angle neutron scattering (SANS). Below the T_t, polysaccharide-*b*-ELP chains behave as unimer with little aggregation. Above the T_t, ELP chains of polysaccharide-*b*-ELP bioconjugates collapse, leading to structural evolution of polysaccharide-*b*-ELP from unimer to self-assembled nanostructure. The influence of concentration, hydrophilicity of polysaccharide, and interactions of physical mixtures in temperature-triggered self-assembly process were also discussed and compared, providing insight into the thermally-induced self-assembly study of ELP-polymer biomaterials.

1. INTRODUCTION

Stimuli-responsive block polymers are promising candidates for biomedical applications, such as controlled drug delivery.[1–6] Recently, elastin-like polypeptides (ELPs) have attracted increasing attention as stimuli-responsive protein-like polymers and serve as an attractive alternative to synthetic polypeptides obtained by conventional polymerization methods.[7–11] ELPs are a class of biopolymers derived from a repeat sequence (VPGXG) from human tropoelastin (the guest residue X can be any amino acid except proline).[12] Genetically encoded and recombinantly synthesized, ELPs allows for precise and well-defined polymers with accurate control over the sequence and molecular weight, which is unmatched with conventional synthetic polymers. ELPs exhibit a fast and reversible phase transition behavior

at a specific temperature referred to as the lower critical solution temperature (LCST), commonly described as the inverse transition temperature (T_t) when determined at a certain concentration. Below the T_t, ELP chains assume a close-to-random coil conformation and highly soluble in aqueous solution. When rising the solution temperature above the T_t, ELP chains hydrophobically collapse into insoluble aggregates to form a coacervate. This transition is entirely reversible, such that the aggregated ELPs become totally soluble when the temperature is lowered below the T_t. Conformational changes and aggregation of ELP above the T_t was recently studied with small angle neutron scattering (SANS).[13] T_t can be highly tunable either by playing with molecular parameters such as varying amino acid residues composition and protein molecular weight, or by controlling environmental parameters such as concentration, pH or cosolutes.[14,15] In addition, Chilkoti and coworkers established an empirical model that correlates T_t values to the ELP composition, concentration and chain length in a single equation, enabling accurate prediction of the T_t of well-defined ELP at specific concentration.[16]

Progress in genetic engineering allow *de novo* design and synthesis of tailor-made ELP block copolymers that covalently associate two or more ELP segments with different T_t value.[17,18] Below a critical temperature, both blocks are soluble. As the temperature is raised, the more hydrophobic block is selectively dehydrated while the hydrophilic block remains solvated. When reaching a critical temperature, that is, defined as the critical micelle temperature (CMT), the diblock ELP gains sufficient amphiphilicity to trigger its self-assembly into micelles with a core composed of hydrophobic ELP block and a corona composed of hydrophilic ELP block. Upon heating the solution further, the more hydrophilic block starts to dehydrate, and at another critical temperature, defined as aggregation temperature, triggered the aggregation of micelles into macroaggregates. The structural evolution of a series of ELP diblocks in water solution was systematically studied by Garanger et al. using multi-angle light scattering and neutron scattering techniques, providing a comprehensive structural analysis of the self-assembly process of ELP diblock copolymers.[19] Additionally, self-assembly studies of an ELP diblock forming vesicles was also reported.[20]

To take advantage of this thermally triggered self-assembly properties, various ELP-based hybrid systems were thereby developed and investigated. ELP-protein fusions, for example, ELP-antibody fusions,[21] ELP-mCherry fusions[22], resilin-elastin-like block copolypeptides,[23] and silk-elastin-like protein,[24] were reported capable of self-assembly into spherical micelles,

wormlike micelles, and vesicles. ELP-polymer bioconjugates, in which ELP as a building block was combined with other synthetic polymer, were also recently reported. These conjugation of polymers include poly(ethylene glycol),[12,25] poly(γ-benzyl-L-glutamate),[26] poly(L-glutamic acid)[27] and poly(aspartic acid).[28]

In the context, the impact of polysaccharide as hydrophilic block on the self-assembly properties of polysaccharide-*b*-ELP block copolymers was explored and discussed. Since attractive interactions have been shown between polysaccharide and proteins,[29,30] this chapter also involved mixture of polysaccharide and ELP, and mixture of different polysaccharide-*b*-ELP. By using click chemistry,[31–33] we prepared three typical polysaccharide-*b*-ELP, as well as PEG-*b*-ELP. Temperature triggered self-assembly behavior of the synthesized ELP bioconjugates were first studied by extensive dynamic light scattering and multi-angle dynamic and static light scattering. These bioconjugates demonstrated fully reversible assembly and disassembly process. Thereafter, their thermally triggered structural evolution from unimers to self-assembled nanostructures was further investigated by SANS. The influence of concentration, hydrophilicity of polysaccharide, and interactions of physical mixtures were also discussed and compared.

2. EXPERIEMNTAL SECTION

2.1 Materials

Sodium azide (NaN_3, 99.5%), hydrochloric acid (HCl, 37%), trimethylamine (TEA, 99%), copper(II) sulfate pentahydrate ($CuSO_4$, 99%), dichloromethane (DCM, 99.9%), N,N-dimethylformamide (DMF, 99.8%), dimethyl sulfoxide (DMSO, 99.7%), diethyl ether (99.9%) and anhydrous magnesium sulfate ($MgSO_4$, 99.5%) were purchased from Sigma-Aldrich. Sodium ascorbate (NaAsc, 99%) were obtained from Alfa Aesar. Methoxypolyethylene glycol ($mPEG_{2000}$) and 4-toluenesulfonyl chloride (TsCl, 99%) were purchased from TCI. Cuprisorb® was purchased from Seachem. Water was purified using an ELGA PURELAB Classic system. Solvent was purified using PureSolv MD-5 solvent purification system from Innovative Technology. Dialysis was conducted using a Spectra/Por®6 dialysis membrane. The ELP used in this work was prepared by recombinant DNA and protein engineering techniques in Escherichia coli as described previously. The functionalization of *N*-terminal end of ELP with an alkyne moiety and its "click" approach to the azide-functionalized polysaccharides were demonstrated in details on last chapter.

2.2 Synthesis and characterization of poly(ethylene glycol)-*b*-ELP bioconjugate

Synthesis of α-Methoxy ω-Azido Poly (ethylene glycol) (PEG-N_3). Trimethylamine (1.2 ml, 8.6 mmol) and p-toluenesulfonyl chloride (600 mg, 3 mmol) was added to a solution of methoxypolyethylene glycol (mPEG) (MW 2000) (2 g, 1 mmol) in DCM (10 mL) and the reaction was stirred at r.t for 48h. Afterwards, the reaction mixture was diluted with pure water (50 mL). The resulted solution was extracted with DCM (2 ×100 mL). The combined organic extracts were washed with 2M aq.HCl (2 ×40 mL), water (2 ×60 mL) and brine (60 mL), dried over $MgSO_4$, filtered and concentrated *in vacuo* to give the crude product as an off-yellow oil. Purification of the crude product by precipitation in ice-cooled diethyl ether afforded α-methoxy ω-(4-toluenesulfonyl) Poly (ethylene glycol) (mPEG-OTs) as a white powder (1.6 g, 74 % yield). Sodium azide (252 mg, 3.8 mmol) was added to a solution of mPEG-OTs (1.6 g, 0.7 mmol) in DMF (20 mL) and the reaction mixture was stirred at r.t for overnight. Pure water (50 mL) was added and the resulted solution was extracted with DCM (2 × 100 mL). The combined organic extracts were washed with 2M aq.HCl (2 ×40 mL), water (2 ×60 mL) and brine (60 mL), dried over $MgSO_4$, filtered and concentrated *in vacuo* to give the crude product as an off-yellow oil. Purification of the crude product by precipitation in ice-cooled diethyl ether yielded PEG-N_3 as a white solid (1.1 g, 73 % yield). ^{1}H NMR (400 MHz, $CDCl_3$): δ 3.63–3.54 (m, $CH_3OCH_2CH_2O$), 3.50–3.46 (m, CH_2N_3), 3.31 (s, $CH_3OCH_2CH_2O$). FT-IR (ATR): 2881, 2101 (υ_{azide}), 1466, 1341, 1279, 1240, 1146, 1097, 1059, 946, 841, 529 cm^{-1}.

Synthesis of α-Methoxy ω-Azido Poly (ethylene glycol)-b-ELP (PEG-b-ELP). mPEG2000-N_3 (12.3 mg, 5.8 μmol), copper sulfate (4.4 mg, 17.6 μmol) and sodium ascorbate (7 mg, 35.2 μmol) were added to a solution of alkyne-functionalized ELP (50 mg, 2.9 μmol) in anhydrous DMSO (5 mL) under argon atmosphere. The reaction was stirred at r.t for 3 days, after which the mixture was diluted with cold water (12 mL). Cuprisorb (90 mg) was added to the resulted solution and it was then incubated at r.t with shaking, for overnight to remove the copper. Cuprisorb was removed by centrifuge and the supernatant was purified by dialysis (dialysis bag MWCO 15kDa) against pure water for 5 days (changing water 3 times per day), followed by lyophilization to obtain the final product as a white powder (53 mg, 91% yield). ^{1}H NMR (400 MHz, D_2O): δ 7.78 (s, triazole H), 7.60–7.09 (br, indole *H* Trp), 4.55 (m, CH_α Met), 4.44 (m, CH_α Val, Pro), 4.17 (d, CH_α Val_{Xaa}), 4.04–3.86 (br m, $CH_{2\alpha}$ Gly, $CH_{2\delta}$ Pro), 3.77-3.60 (m, $CH_{2'\delta}$ Pro, mPEG OCH_2CH_2O), 3.39 (mPEG OCH_3), 2.68–2.48 (br m, $CH_{2\gamma}$ Met), 2.40–2.25 (m,

C$H_{2\beta}$ Pro), 2.20–1.87 (m, C$H_{2\beta}$ Met, C$H_{2',\beta}$ Pro C$H_{2\gamma}$ Pro, CH_{β} Val, C$H_{3\varepsilon}$ Met), 1.04–0.86 (m, C$H_{3\gamma}$ Val). FT-IR (ATR): 3299, 2962, 2874, 1628, 1521, 1443, 1230, 1098, 932, 542 cm^{-1}.

Nuclear Magnetic Resonance Spectrometry Analysis (NMR). NMR spectra were acquired in D_2O or $CDCl_3$ at 298 K on a Bruker Avance I NMR spectrometer operating at 400.2 MHz and equipped with a Bruker multinuclear z-gradient direct probe head capable of producing gradients in the z direction with 53.5 $G.cm^{-1}$ strength. The relaxation time was fixed to 3 seconds for homonuclear correlation spectroscopy (COSY) measurements.

Mass Spectrometry Analysis (MS). Mass spectrometry analyses were performed on a MALDI TOF/TOF (Ultraflex III, Bruker Daltonics, Bremen, Germany) equipped with a SmartBeam laser (Nd:YAG, 355 nm). Solutions of ELPs and bioconjugates were prepared as follows: lyophilized ELPs were resuspended in water/acetonitrile (1/1, v/v) to obtain a final concentration lower than 100 μM. Samples were then mixed with the matrix solution of sinapinic acid prepared at the concentration of 10 mg/mL in water/acetonitrile (1/1, v/v). All MALDI-MS measurements were acquired in the linear positive mode and a mixture of standard proteins was used for external calibration in the suitable mass range (10−20 kDa).

2.3 Transition temperature measurements (T_t)

T_t were determined by measuring the turbidity at 350 nm between 10 and 80 ℃ at a 1 ℃ / min^{-1} scan rate at different concentrations in DI water. Data were collected on a Cary 100 UV−Vis spectrophotometer equipped with a multicell thermoelectric temperature controller from Agilent Technologies (Les Ulis, FR). The T_t is defined as the temperature corresponding to the point where the maximum standard deviation on the absorbance versus temperature plots.

2.4 Dynamic light scattering measurements

Dynamic light scattering measurements were performed on NanoZS instrument (Malvern, U.K.) at a 90° angle at a constant position in the cuvette (constant scattering volume). The derived count rate (DCR) was defined as the mean scattered intensity normalized by the attenuation factor. The DCR was plotted against temperature and the T_t is defined as the temperature corresponding to the point where the DCR starts increasing on this plot.

2.5 Multiangle dynamic and static light scattering (DLS, SLS)

Multiangle dynamic and static light scattering measurements were performed using an ALV/CG6-8F goniometer, with a full digital correlator in combination with a spectra physics laser (emitting vertically polarized light at λ= 632.8 nm) and a thermo-regulated bath controller (ranging from 20 to 50 °C). The data were acquired with the ALV correlator software, the counting time was typically 15 seconds at each different scattering angles ranging from 30º to 150º, in 10 increments.

Hydrodynamic radius (R_h) was determined from the apparent diffusion coefficient and the Stokes-Einstein equation.[34]

$$D = \frac{k_B T}{6\pi\eta_S R_H} \quad (1)$$

where D is calculated from the slope of the curve $1/\tau$ as a function of q^2. The main correlation time (τ) is determined by the second order cumulant analysis of the autocorrelogram. k_B is the Boltzmann constant and T is the temperature in Kelvin. q is the scattering vector defined as $q = (4\pi/\lambda)\ sin(\theta/2)$ with λ the wavelength and θ the scattering angle. η_S is the viscosity of the solvent at the corresponding temperature.

The radius of gyration (R_g) was determined from a Guinier plot of the scattered intensity $In\ I\ (q)$ as a function of q^2.

$$In\ I(q) = In\ I\ (0) - \frac{q^2 R_g^2}{3} \quad (2)$$

where $R_g^2 / 3$ corresponds to the slope of the curve.

2.6 Small angle neutron scattering (SANS)

SANS measurements were performed on D11 at the Institut Laue-Langevin (ILL) in Grenoble, France. The samples of ELP and ELP bioconjugates were prepared in fresh D_2O at 125 μM or 250 μM (for the study influence of concentration). Mixture samples were prepared by mixing ELP with polysaccharide / PEG, Dex-*b*-ELP with HA-*b*-ELP, Dex-*b*-ELP with PEG-*b*-ELP, HA-*b*-ELP with PEG-*b*-ELP, at a mole ration 1:1 and with concentration of 125 μM in total. Mixtures of ELP bioconjugates were adjusted to 125 μM with a mole ratio 1:1. Three different configurations were used with a wavelength of λ = 0.6 nm, sample-to-detector distances (SD) of 1.4, 8, and 39 m and collimation lengths of 8, 8, and 40.5 m, respectively, covering a q-range

of 0.02-4 nm^{-1}. A temperature-controlling holder on the cuvette was used to precisely control a temperature range of 17-60 °C.

2.7 Modeling of individual chains (unimers) below the T_t

The aim of analyzing scattering intensity is to obtain the characteristic sizes, the shape and the interactions, which are represented by the form factor *P(q)* and the structure factor *S(q)*. The form factor *P(q)* describes the structure of individual particles while the structure factor *S(q)* describes the interaction between particles. Classical equation of the scattering intensity per unit volume of spherically symmetric particles writes as follows:

$$I(q) = n\Delta\rho^2 {V_{part}}^2 P(q)S(q) \quad (3)$$

where n is the number density of particles, $\Delta\rho$ is the difference in the neutron scattering length density between the particles and the solvent, and V_{part} is the unit volume of the particles. In the absence of interactions (meaning *S(q) equals to 1*) and by introducing the volume fraction of particles ($\Phi = nV_{part}$), eq 3 becomes:

$$I(q) = \Phi\Delta\rho^2 V_{part} P(q) \quad (4)$$

In order to investigate the behavior of polysaccharide-*b*-ELP bioconjugates at low temperature (below the T_t), we focused on polymer chain models. For individual unimer chains, the volume V_{part} is defined by the weight-average molecular weight Mw of one mole of chains, the molar mass m and the volume v of one unimer as $V_{chain} = Mw \cdot v/m$. Thus, for a solution of polymer of weight concentration c, occupying a volume fraction $\Phi = N_A \cdot v \cdot c/m$, where N_A is the Avogadro constant, eq 3 becomes

$$I(q) = v^2\Delta\rho^2 \frac{c}{m^2} N_A M_w P(q) \quad (5)$$

Generally, the radius of gyration R_g of polymers can be deduced from the fit to this equation using Debye function[34] as form factor:

$$P_{Debye}(q, R_g) = \frac{2}{(q^2 {R_g}^2)^2}(exp(-q^2 {R_g}^2) + q^2 {R_g}^2 - 1) \quad (6)$$

By introducing the mass density of the polymer $d = m/(N_A \cdot v)$, aggregates number of polymer chains N_{agg}, we obtain:

$$I(q) = N_{agg}(\rho_{D_2O} - \rho_{ELP})^2 \frac{c}{1.35^2 \times 6022} M_w \frac{2}{(q^2 {R_g}^2)^2} \left(exp\left(-q^2 {R_g}^2\right) + q^2 {R_g}^2 - 1\right) \quad (7)$$

With known concentration (c), molecular weight (M_w) and scattering length densities (ρ_{ELP}) of polysaccharide-*b*-ELP bioconjugates, R_g and N_{agg} can be deduced from the fit to equation 7.

2.8 Modeling of self-assembled nanostructures above T_t

To fit the SANS scattering curves above the T_t of the ELP and ELP bioconjugates, the self-assembled structures were represented typically by two classes of particles: macroaggregates and nanosized particles. Guinier-Porod function model was used to fit macroaggregates.[35] Guinier-Porod function is a classical model that can be used to determine the size and dimensionality of scattering objects, including asymmetric ones. In terms of self-assembled nanosized particles, three sphere models with slight difference were applied depending on different form factors: (i) Core-shell sphere model provides the form factor *P(q)* for a monodisperse spherical particle with a core-shell structure; (ii) Polymer micelle model provides the form factor *P(q)* for a micelle with a spherical core and Gaussian polymer chains attached to the surface, thus suitable for block copolymer micelles; (iii) Simple sphere model fits spheres with uniform scattering length density (see supporting info). All the fits were achieved with the SasView program (http://www.sasview.org/). Size distribution (∑) with appropriate weighting were taken into account in all the fitting procedures.[35]

3. RESULTS AND DISCUSSION

3.1 Synthesis and characterization of polysaccharide-*b*-ELP bioconjugates

As we presented in previous chapter, inert (dextran) and bioactive (laminarihexose and hyaluronic acid) polysaccharides were combined with a stimuli-responsive elastin-like polypeptide (ELP) into well-defined block copolymers. Briefly, polysaccharides were successfully functionalized with an azide moiety at the reducing end using a biofunctional *N*-methoxyoxamine linker for further conjugation to the ELP. NHS-ester coupling chemistry was utilized to modify the *N*-terminal primary amine of ELP with an alkyne group. Thereafter, three polysaccharide-*b*-ELP bioconjugates were produced by click CuAAC reaction allowing to combine the ELPS and polysaccharide segments in a efficient manner.

In order to investigate the structural effect of polysaccharides on polysaccharide-*b*-ELP bioconjugates assemblies, poly(ethylene glycol) as a non-carbohydrate polymer, was

functionalized and conjugated with ELP. Van Hest's group reported a copper-free strain-promoted alkyne-azide cycloaddition approach to prepare a series of poly(ethylene glycol)-*b*-ELP block copolymers.[25] Herein, to be consistent with previous synthetic strategy of polysaccharide-*b*-ELP, PEG was functionalized with an azide moiety by two successive steps and subsequently combined with ELP *via* CuAAC (Scheme S1). The success of the conjugation reaction was confirmed by ^{1}H, HSQC and COSY NMR, as well as MALDI-TOF, SEC and FTIR spectroscopy. The detail characterization information was provided in supporting information. SEC and T_t of all ELP bioconjugates are shown in Figure S5. The main characteristics of the ELP bioconjugates are summarized in Table 1.

ELP/ Bioconjugates	M_w[a] (kDa)	Hydrophilicity mass fraction	PDI[a]	T_t in water[b] (125 μM)
Dex-*b*-ELP	24.9	32 %	1.01	39 ℃
Lam-*b*-ELP	18.2	5 %	1.03	36 ℃
HA-*b*-ELP	24.3	30 %	1.02	48 ℃
PEG-*b*-ELP	19.2	10 %	1.04	42 ℃

Table 1. *Characteristics of the ELP and ELP bioconjugates synthesized. [a]Weight average molecular weight (M_w) and polydispersity index (PDI) were determined by SEC in aqueous buffer. [b]T_t was measured by turbidity on UV-Vis.*

3.2 Self-assembly study of polysaccharide-*b*-ELP bioconjugates by dynamic light scattering and multiangle dynamic and static light scattering

In the previous chapter, we studied the self-assembly properties of polysaccharide-*b*-ELP copolymers by DLS and temperature-controlled liquid AFM and revealed their ability to form well-defined micellar structures. Increasing the temperature above the phase transition temperature of ELP bioconjugates resulted in the formation of amphiphiles, which self-assembled into well-defined and stable nano-objects. To further investigate the influence of different parameters during the temperature-induced process of self-assembly, extensive DLS as well as multiangle dynamic and static light scattering measurements of ELP and ELP bioconjugates were carried out.

3.2.1 Initial self-assembly study of polysaccharide-b-ELP bioconjugates

As observed in DLS heating ramp study previously, at low temperature below T_t of polysaccharide-*b*-ELP bioconjugates, the scattering intensity is very low due to the presence of free unimer chains in solution and a few aggregates. The scattering intensity sharply increased at T_t (39, 36, 48, 42 ℃ for Dex-*b*-ELP, Lam-*b*-ELP, HA-*b*-ELP, PEG-*b*-ELP, respectively) and triggered the self-assembly to form nanostructures. At high temperature above T_t, the scattering intensity showed little changes indicating a relatively stable stage had reached. DLS cooling ramp on polysaccharide-*b*-ELP and PEG-*b*-ELP bioconjugates showed a delayed decrease of scattering intensity, indicating a relatively slow disassemble behavior of nanostructure to unimers (Figure S6B, S7B, S9B and S11B).

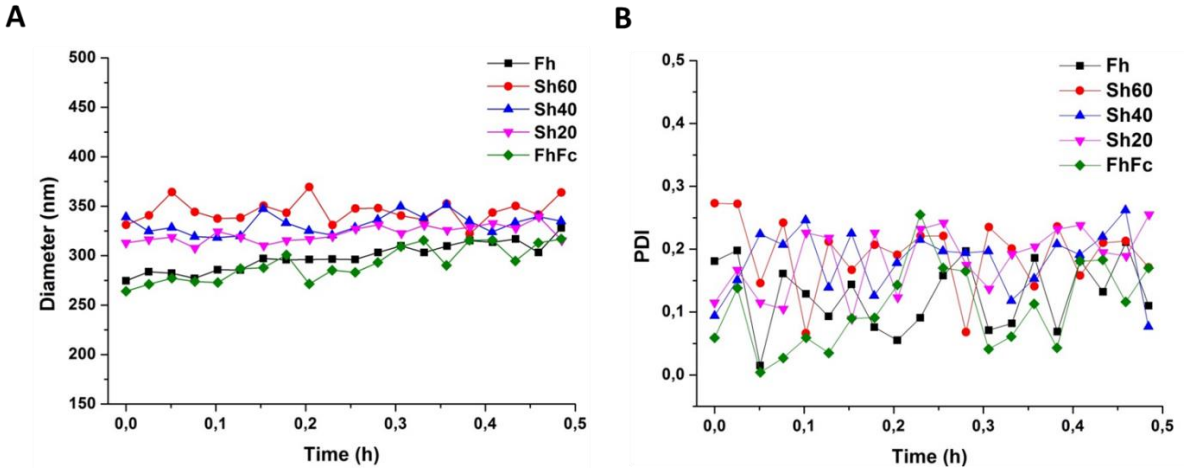

Figure 1. *Different heating methods to induce self-assembly as followed by DLS, recording (A) diameter (B) polydispersity during 30 mins. Fast heat: 2min to 45°C (Fh); Slow heat : 60 min to 45°C (Sh60); Slow heat : 40 min to 45°C (Sh40); Slow heat : 20 min to 45°C (Sh20); Fast heat to 70 °C then fast cooling to 45°C (FhFc). Once temperature reached 45 °C, equilibrated for 5 min, thereafter DLS recorded diameter and PDI in 30 min.*

As an example, the thermodynamics properties and stability of the Dex-*b*-ELP assemblies above T_t were investigated by conducting various heating methods from 25 ℃ to 45 ℃. As shown in Figure 1, the heating speed of a Dex-*b*-ELP solution was follow by DLS analysis and demonstrated that the obtained average diameter D_h only slightly varied during 30 min, reaching around 300-350 nm. In the meantime, PDI was measured and did not show significant difference, with low values in the rage 0.1-0.2 (Figure 1B). Fast heating process (Fh and FhFc) demonstrated slight smaller D_h in contrast to other slow heating ones. Consequently, a fast heating process was applied to all the following experiments.

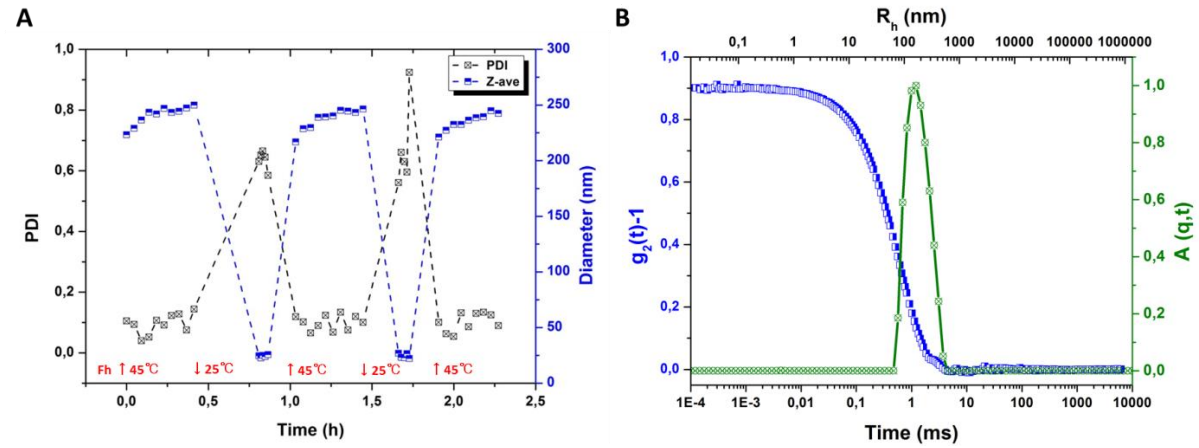

Figure 2. *(A) Z-average size and polydispersity as a function of time upon repeated fast heating (45 °C) and cooling (25 °C) of Dex-b-ELP (125 μM) in water on DLS. (B) DLS autocorrelation function (g2(t)-1) and relaxation-time distribution (A(q,t)) for Dex-bELP (125 μM) in water at 45 °C, 90°.*

Repeated heating and cooling DLS measurements were also performed to evaluate the reversibility of these polysaccharide-*b*-ELP systems (Figure 2A, S7A, S9A, S11A). As shown in Figure 2A, Dex-*b*-ELP self-assembled in a fast process to obtain nanostructured particles above 45 ℃, the size and dispersity of these nanoparticles being stabled after 5 min, with an average diameter around 250 nm. Afterwards Dex-*b*-ELP nanoparticles were cooled down to 25 ℃ and kept for 10-15 min in order to fully disassemble (Figure S6). Small objects with an average diameter 25 nm and high PDI were observed after cooling, which indicated a disassembly process of Dex-*b*-ELP from nanostructure to unimer, with a quite large dispersity due to the presence of few aggregates. The process is fully reversible several times, giving similar sizes and dispersities. HA-*b*-ELP and PEG-*b*-ELP presented similar reversible self-assembly behavior as Dex-*b*-ELP (Figure S9A, S11A). Unlike other bioconjugates, D_h of Lam-*b*-ELP assemblies was found to significantly increase with time, which may due to insufficient hydrophilic fraction of Lam-*b*-ELP. Nevertheless, the self-assembly of Lam-*b*-ELP from unimer to aggregates was still fully reversible (Figure S7A), illustrating that the temperature-induced self-assembly/disassembly of polysaccharide-*b*-ELP is reversible and controllable by varying temperature above/ below the T_t.

3.2.2 Self-assembly study by multiangle dynamic and static light scattering

Subsequently, nano-objects formed from self-assembly of polysaccharide-*b*-ELP and PEG-*b*-ELP bioconjugates above T_t were analyzed by multiangle dynamic and static light scattering

(Figure 2B and 3). The detailed angular analyses in dynamic (diffusion coefficient determination) and static mode (Guinier plots) are provided in (Figure S6E-F, S8, S10 and S12).

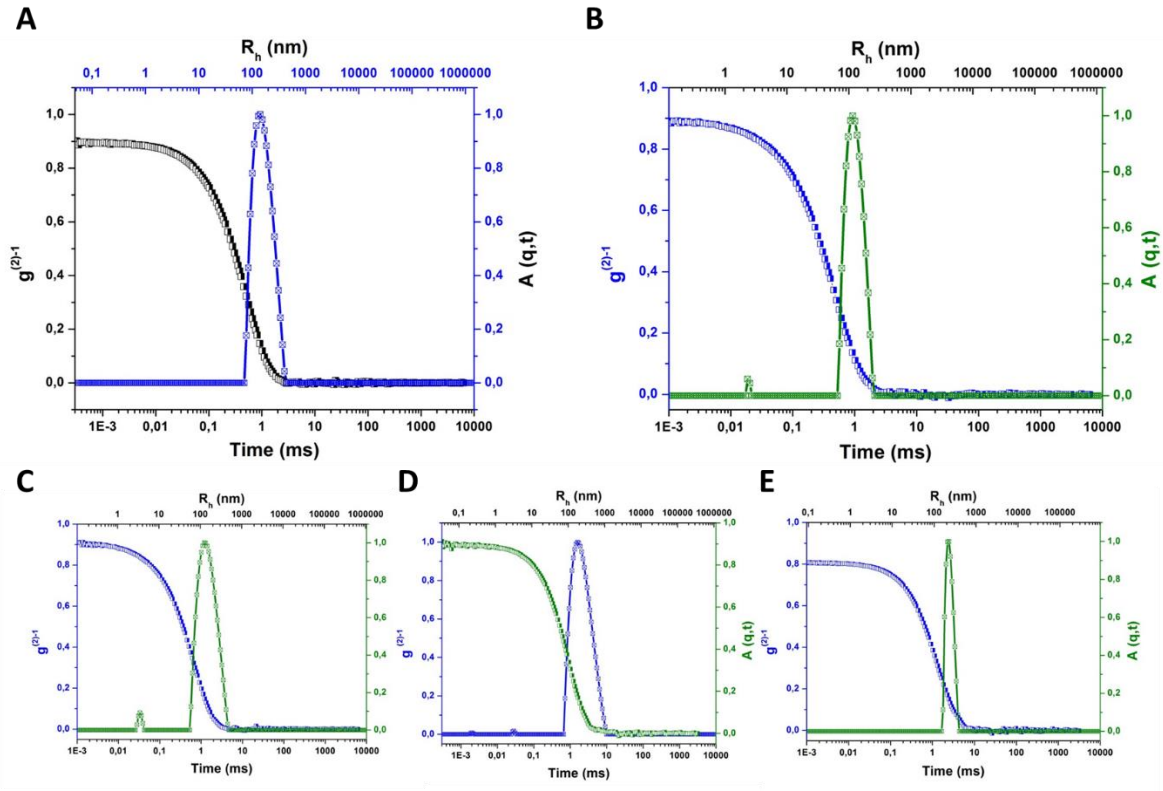

Figure 3. *DLS autocorrelation function (g2(t)-1) and relaxation-time distribution (A(q,t)) at 90° for (A) HA-b-ELP 150 µM in water at 50 °C; (B) PEG-b-ELP 125 µM at 40 °C. Lam-b-ELP 125 µM at (C) 33 °C, (D) 37 °C, (E) 45 °C.*

Structural characteristics of polysaccharide-*b*-ELP nano-objects, namely Z-average size (D_h), radius of gyration (R_g), hydrodynamic radius (R_h) and R_g/R_h ratio were summarized in Table 2. Similar average D_h of ~300 nm were obtained for Dex-*b*-ELP and HA-*b*-ELP while PEG-*b*-ELP was smaller, around 220 nm. In terms of R_g/R_h ratio of the nano-objects was found to be close to 0.75 for Dex-*b*-ELP and HA-*b*-ELP assemblies and close to 0.9 for PEG-*b*-ELP, indicating possible spherical particle morphology of these three bioconjugates. In contrast to DLS results, slightly larger R_h of Dex-*b*-ELP and PEG-*b*-ELP were found on SLS, which may due to the growing trend of diameter upon longer heating time on SLS. Similarly to repeating heating-cooling measurements, Lam-*b*-ELP showed a growing trend of D_h upon heating and formed stable aggregates ~500 nm at high temperature.

To shed light on morphologies of these self-assembled nano-objects, we next investigated the ELP and entire ELP bioconjugates by small angle neutron scattering (SANS) as a function of

temperature. However, one has to note that it is difficult to directly compare values of D_h, R_g, R_h and N_{agg} obtained by these two techniques as the contrast providing the scattering signal is different for neutron and light scattering techniques (the atomic neutron scattering cross-section in SANS and the refractive index increment in SLS, respectively).

Bioconjugates	***Conc.(μM)***	***DLS***		***SLS***			
		T(℃)	***D_h(nm)***	***T(℃)***	***R_g(nm)***	***R_h(nm)***	***R_g/R_h***
Dex-*b*-ELP	125	45	330	45	132	183	0.72
		33	210	33	100	130	0.77
Lam-*b*-ELP	125	37	318	37	140	259	0.54
		45	520	45	128	252	0.51
HA-*b*-ELP	150	48	300	50	120	152	0.79
PEG-*b*-ELP	125	40	221	40	111	124	0.89

Table 2. *Structural characteristics of polysaccharide-b-ELP nano-objects determined by multiangle dynamic and static light scattering.*

3.3 SANS study

The entire set of ELP and ELP bioconjugates, as well as physical mixture of ELP and polysaccharide, mixture of different ELP bioconjugates, were studied from minimum 17 °C to maximum 60 °C, a temperature range that fully covered the transition temperature of ELP. SANS curves of ELP (Figure S13) showed two clear regime, which represented unimers and coacervates. Similarly, self-assembly of unimers into nanostructures with gradual increase in temperature were also observed in all ELP bioconjugates (Figure 4).

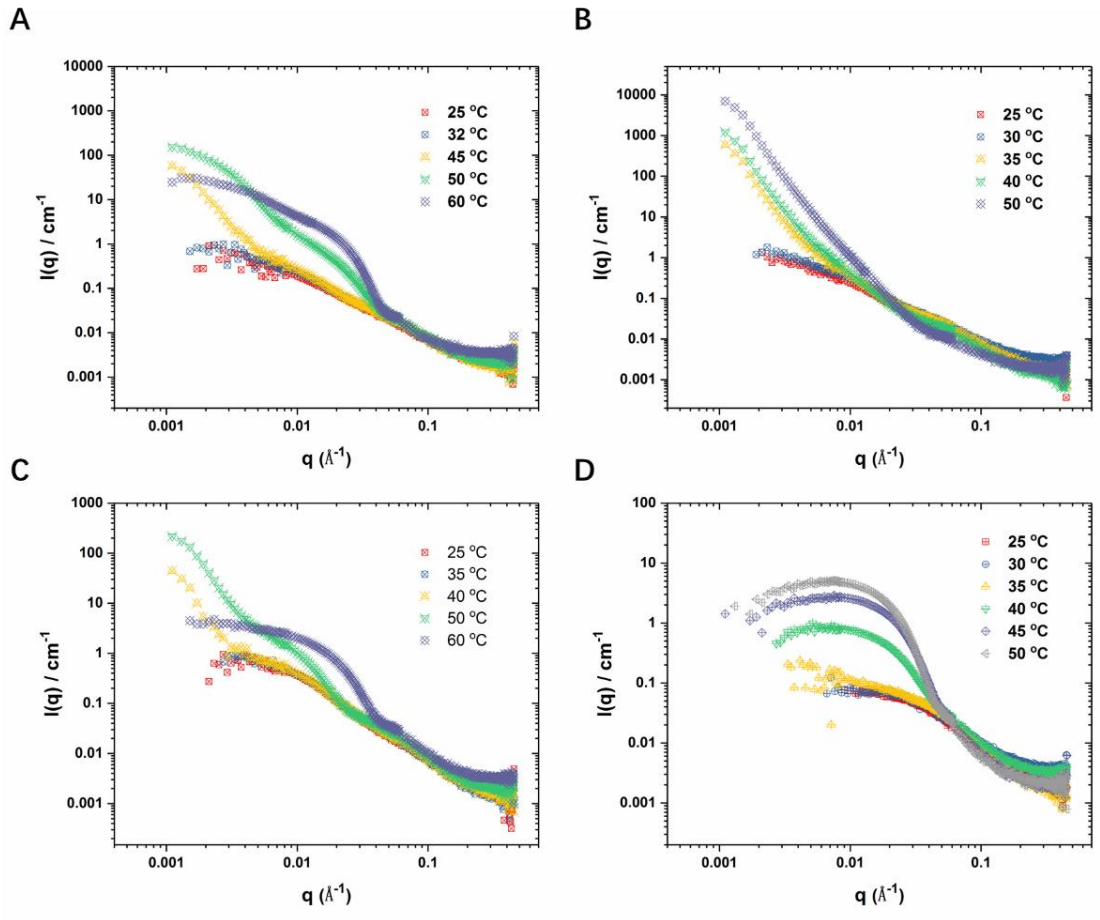

Figure 4. *SANS curves of bioconjugates at 125 µM in D_2O at different temperature: (A) Dex-b-ELP, (B) Lam-b-ELP, (C) HA-b-ELP, (D) PEG-b-ELP.*

3.3.1 Studies of individual chains (unimers) below T_t

A significant dispersed upturn of the scattering intensity at low *q* was observed for all polysaccharide-*b*-ELP, Dex-*b*-ELP, Lam-*b*-ELP and HA-*b*-ELP (Figure 5, S14), which may be due to the attractive interactions between individual chains. The signal of aggregation was verified by introducing aggregates number in the Debye function (eq 7). Nevertheless, all curves were well-fitted using the Debye function eq 7, indicating that ELP bioconjugates chains behave like unimer chains.

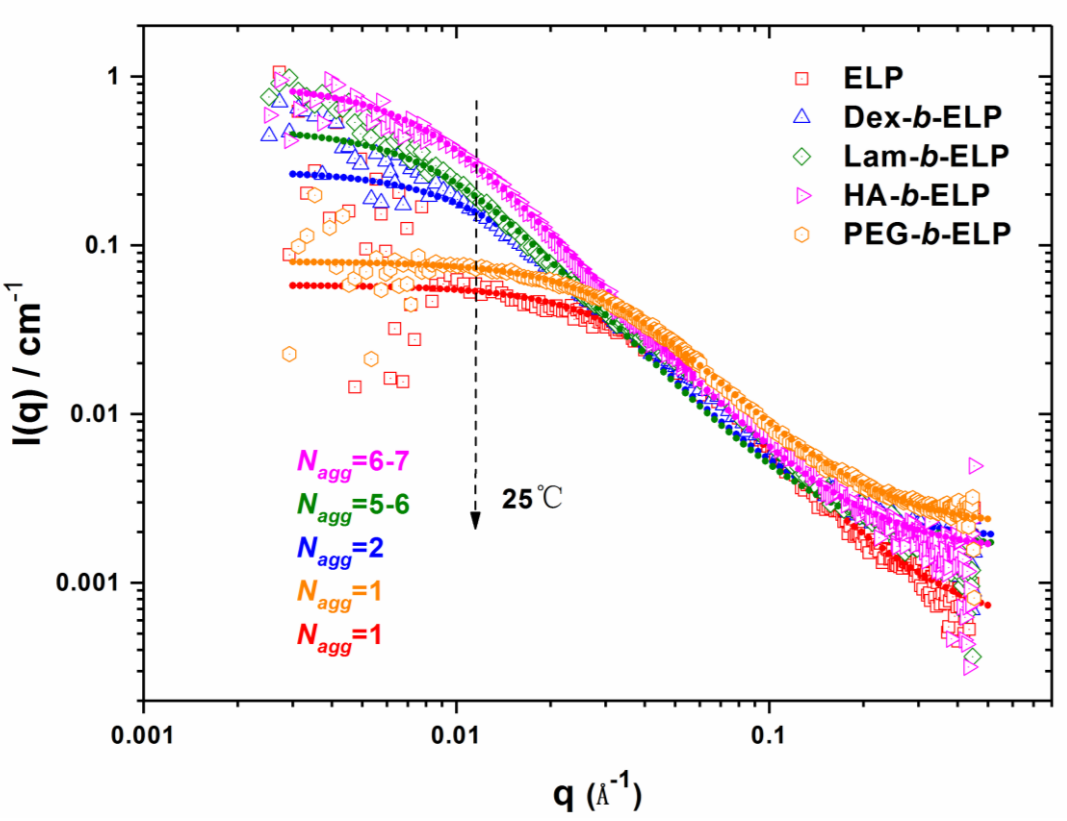

Figure 5. *SANS curves of ELP and bioconjugates at 125 μM in D_2O at 25°C. Dotted lines are the best fits to the Debye function (best fit parameters are summarized in Table 3).*

Given the known molecular weights of ELP bioconjugates, assuming a density d = 1.35 g·cm^{-3} as reported for proteins in the crystalline state[36] and theoretical scattering length densities (ρ_{ELP}) calculated from the corresponding bioconjugate molecular formulas and the scattering lengths of respective atoms, best fits of to eq 7 gave the R_g and aggregates number (N_{agg}) of the ELP and bioconjugates (Table 3). From these set of data, one can confirmed that concentration of ELP samples did not have a clear effect on N_{agg} and SANS curves of double concentration can be nearly perfectly recovered by normalizing the signal with concentration (see Figure S14). Unexpectedly, PEG-*b*-ELP were the only bioconjugates showing perfect unimer chains with no aggregation while unimer aggregation number of Dex-*b*-ELP, Lam-*b*-ELP and HA-*b*-ELP were found to be 2, 5-6 and 6-7, respectively. In order to investigate possible interactions between ELP and polysaccharides, physical mixture of ELP and polysaccharide and mixture of different polysaccharide-*b*-ELP was thereafter investigated by SANS.

ELPs	Conc.(μM)	$T_{t\ D2O}$(℃)	T_{below} (℃)	R_g (Å)	N_{agg}
ELP	125	31	25	44.2	0.9
	250	30	17	46.4	0.9
Dex-*b*-ELP	125	37	25	123.4	1.9
	250	35	20	122.6	1.8
Lam-*b*-ELP	125	32	25	168.2	6.2
	250	31	17	141.8	4.6
HA-*b*-ELP	125	45	25	190.6	6.9
	250	38	20	185.4	5.8
PEG-*b*-ELP	125	40	25	44.9	0.9
	250	38	20	46.8	0.9

Table 3. *Characteristics of ELP, polysaccharide-b-ELP and PEG-b-ELP in D_2O measured by SANS at T_{below} (temperature below T_t, T_t values were measured in D_2O by DLS heating ramp).*

3.3.2 Studies of unimer mixtures below T_t

As shown in Figure S16-17, SANS curve of ELP/Dex mixture and ELP/ PEG mixture showed little changes in comparison with ELP alone, demonstrated unattractive interaction between ELP and Dex, ELP and PEG. It was also proved by mixture of Dex-*b*-ELP with PEG-*b*-ELP (abbreviated to Dex/PEG-*b*-ELP), which gave a N_{agg} of 1.2 (Table 4). Moreover, ELP/HA mixture presented a significant aggregation between ELP and HA with N_{agg} of 27, which was possibly due to the hydrogen bonding interaction between carboxylic acid group on HA and amide group on ELP. However, HA-*b*-ELP bioconjugate may reduce this interaction due to the macromolecular steric hindrance effect, which indeed leaded to a smaller N_{agg} of 6-7. Unlike the mixture of ELP with polysaccharide, SANS curve of mixture of two ELP bioconjugates were found very close to the theoretical one and fit parameters were also close to the average of that two bioconjugates alone, revealing an independent unimers nature of bioconjugate at temperature below T_t (Figure S18). The theoretical curves describe a simulate plot corresponding to the addition of the individual form factors of individual bioconjugates form factors normalized by their concentration.

ELPs	*Conc.(μM)*	T_{below} (℃)	R_g (Å)	N_{agg}
ELP + Dex	125	17	44.4	0.9
ELP + HA	125	17	573.2	27
ELP + PEG	125	17	46.3	1
Dex/HA-*b*-ELP	125	17	213.8	5.8
Dex/PEG-*b*-ELP	125	17	82.7	1.2
HA/PEG-*b*-ELP	125	17	114.4	2.7

Table 4. *Characteristics of mixture of ELP and polysaccharide, and mixture of different ELP bioconjugates in D_2O measured by SANS at 17 °C below T_t.*

3.3.3 Self-assembled nanostructures above T_t

Upon rising the temperature above the T_t, a significantly increase of more than 1 order of magnitude of the scattering intensities was observed (Figure 6). For the Dex-*b*-ELP, HA-*b*-ELP and PEG-*b*-ELP bioconjugates, a clear oscillation was seen in the range 0.04-0.06 $Å^{-1}$, characteristic of form factor of spherical nanostructures. Except for Lam-*b*-ELP, the scattering curves at low *q* did not reach a plateau as the hydrophilic mass fraction was not sufficient to provide enough amphiphilicity for self-assembly, resulting in macromolecular aggregation similarly to what was observed on ELP alone.

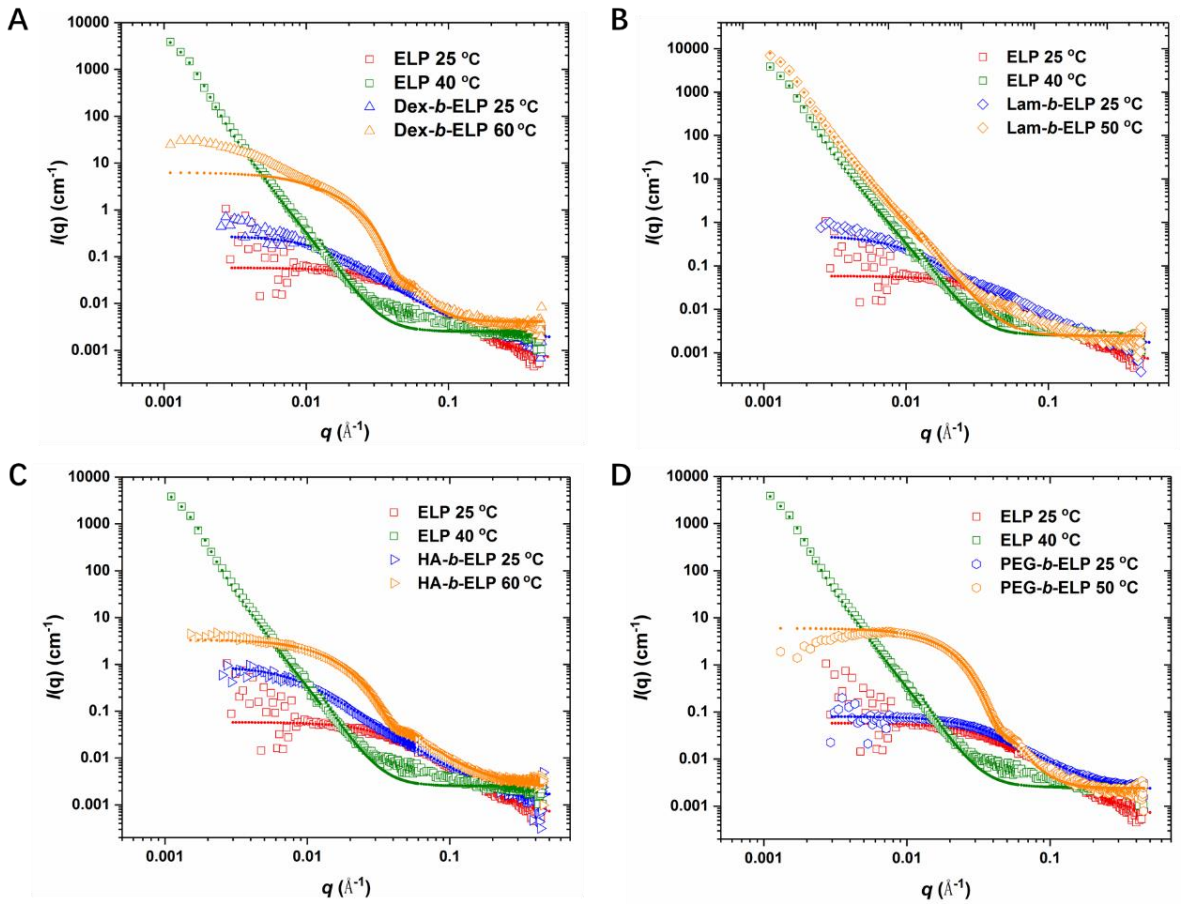

Figure 6. *SANS curves of ELP bionconjugates at 125 μM in D_2O at temperature below and above T_t. (A) Dex-b-ELP, (B) Lam-b-ELP, (C) HA-b-ELP, (D) PEG-b-ELP. Dotted red and blue lines are the best fits to the Debye function. Dotted green and orange lines are the best fit to the (A) core-shell sphere model, (B) guinier-porod function,(C) polymer micelle model, (D) sphere model, respectively. (best fit parameters are listed in Table 3 and 5).*

As compared to Figure 7A, scattering curves characteristics of two classes of nanostructures were clearly observed. Above T_t, ELP and Lam-*b*-ELP formed macroaggregates while Dex-*b*-ELP, HA-*b*-ELP and PEG-*b*-ELP were able to self-assemble into sphere nanoparticles. The aggregation of ELP and Lam-*b*-ELP were fitted with a Guinier-Porod sphere function to determine the size of the resulting macroaggregates. The size of Lam-*b*-ELP bioconjugates was found 244 nm, which was consistent with previous DLS measurements. Three spherical models were applied to best fit the scattering curves of spherical nanostructures above T_t. Scattering curve of PEG-*b*-ELP showing a clear oscillation at large q was well-fitted with the simple sphere model by providing SLD of the bioconjugate and solvent. This fitting method leaded to spherical particle PEG-*b*-ELP with radius of 95 Å. Core-shell sphere model was used to fit scattering curves of Dex-*b*-ELP by introducing SLD of solvent, hydrophobic ELP core and hydrophilic dextran shell. The fitted radius value of self-assembled nanostructure of Dex-*b*-

ELP was 101 Å. Scattering curve of HA-*b*-ELP was also well fitted with a sphere polymer micelle model, indicating a radius of 108 Å of the self-assembled spherical nanostructure. All fitting characteristics were summarized in Table 5.

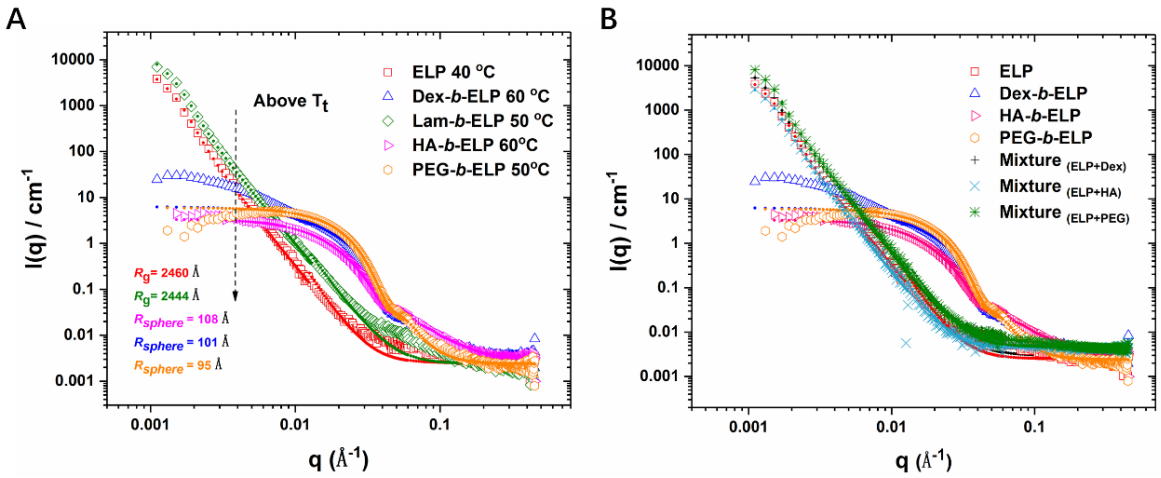

Figure 7. *(A) SANS curves of ELP and ELP bioconjugates in D_2O at temperature above T_t. Dotted lines are the best fits to the corresponding models (best fit parameters are summarized in Table 5). (B) SANS curves of ELP, polysaccharide-b-ELP bioconjugates and physical mixture of polysaccharide and ELP in D_2O at the temperature above T_t.*

ELPs	***Conc.(μM)***	***T_{above} (℃)***	***Model***	***R_g (Å)***	***R_s (Å)***	***Σ***
ELP	125	40	Guinier-Porod Sphere Function	2460	-	-
Dex-*b*-ELP	125	60	Core-Shell Sphere	-	101	0.17
Lam-*b*-ELP	125	50	Guinier-Porod Sphere Function	2444	-	-
HA-*b*-ELP	125	60	Polymer Micelle	64	108	-
PEG-*b*-ELP	125	50	Sphere	-	95	0.18

Table 5. *Characteristics of ELP, polysaccharide-b-ELP and PEG-b-ELP in D_2O as determined by fitting SANS data as measured at temperature above T_t.*

3.3.4 Studies of nano-objects mixtures above T_t

The scattering curves of polysaccharide-*b*-ELP bioconjugates were also compared with mixture of polysaccharide and ELP, and with mixture of different bioconjugates. Not surprisingly, all

mixtures of polysaccharide and ELP were aggregated at the temperature above T_t (Figure 7B). This feature revealed that interactions between ELP and polysaccharide were not able to provide any impact on colloidal stability, and that ELPs are just forming coacervates of large size (Table 6).

ELPs	*Conc.(μM)*	T_{above} (℃)	*Model*	R_g (Å)	R_s(Å)	Σ
ELP +Dex	125	45	Guinier-Porod Sphere Function	2737	-	-
ELP + HA	125	45	Guinier-Porod Sphere Function	2390	-	-
ELP + PEG	125	55	Guinier-Porod Sphere Function	2654	-	-
Dex/HA-b-ELP	125	55	Polymer Micelle	105	122	-
Dex/PEG-*b*-ELP	125	55	Sphere	-	107	0.16
HA/PEG-*b*-ELP	125	55	Polymer Micelle	49	96	-
			Sphere	-	224	0.2
			Guinier-Porod Sphere Function	1125	-	-

Table 6. *Characteristics of mixture of ELP and polysaccharide, and mixture of different ELP bioconjugates in D_2O measured by SANS at temperature above T_t.*

As mentioned above, ELP bioconjugates demonstrated independent nature when mixed two ELP bioconjugates together at low temperature. However, mixing two ELP bioconjugates at temperature above T_t may induce spatially either co-assemble or separated-assemble behavior of mixture, interesting for some applications.

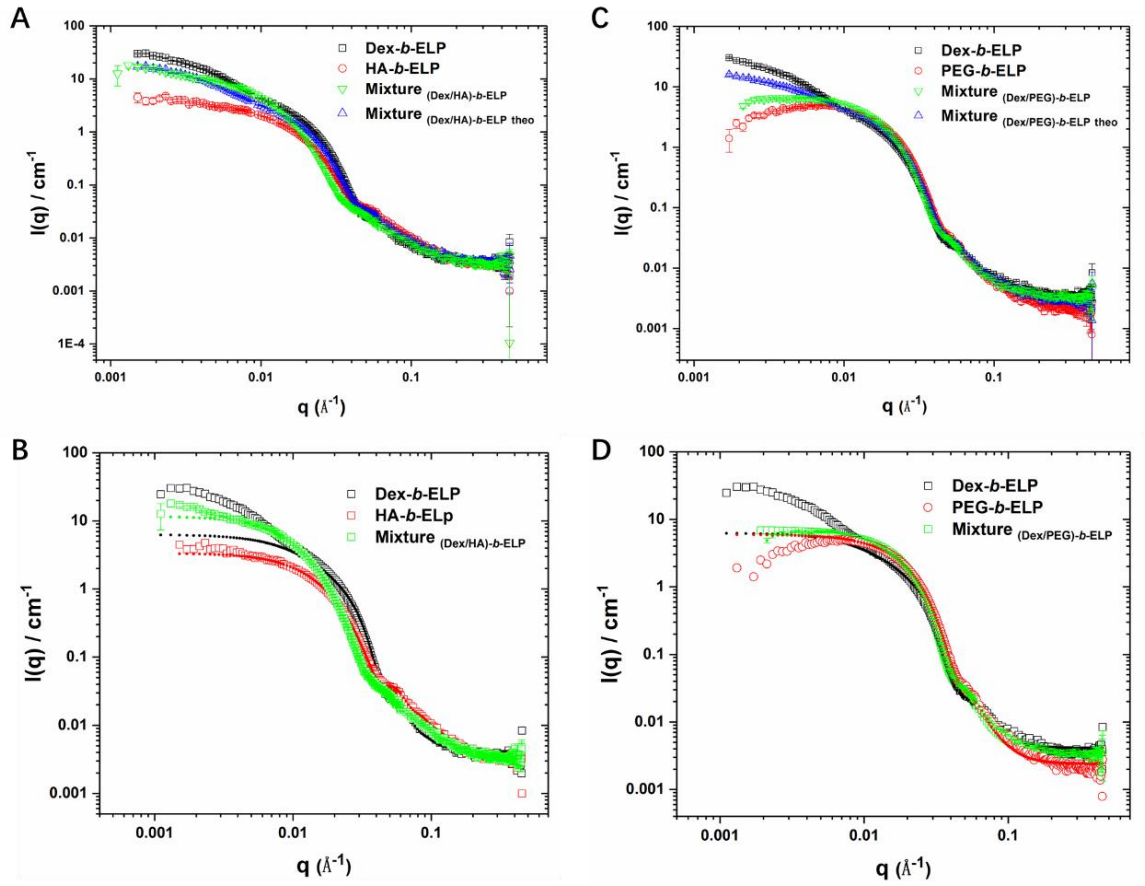

Figure 8. *SANS curves of physical mixture of different ELP bionconjugates and their theoretical mixture curves in D_2O at temperature above T_t. (A, B) Mixture of Dex/HA-b-ELP; (C, D) Mixture of Dex/PEG-b-ELP. Theoretical mixture curves were normalized with concentration. Dotted lines on the bottom side indicate the best fits to the corresponding model (best fit parameters are listed in Table 6).*

As compared in Figure 8, mixing Dex-*b*-ELP with HA-*b*-ELP or PEG-*b*-ELP also showed similarly structural evolution from unimer to self-assembled spherical particles. Scattering curves of Dex/PEG-*b*-ELP mixture and Dex/HA-*b*-ELP mixture presented similar behavior compared to the corresponding theoretical curves and exhibited a simple form factor that can be further fitted with sphere models. We mean by theoretical curve, a simulate plot corresponding to the addition of the individual form factors of individual bioconjugates form factors normalized by their concentration. The fact the experimental and theoretical curves are very similar could be related to the formation of separated micelles. However, as the size of individual micelles and the *Tt* of bioconjugates are very close, we cannot discard the formation of mixed micelles. The use of fluorescently labeled bioconjugates and FRET experiments may help understanding deeper this phenomenon. In contrast to individual bioconjugates, spherical radius of mixture was found to negligible increase in both Dex/PEG-*b*-ELP mixutre and

Dex/HA-*b*-ELP mixture.

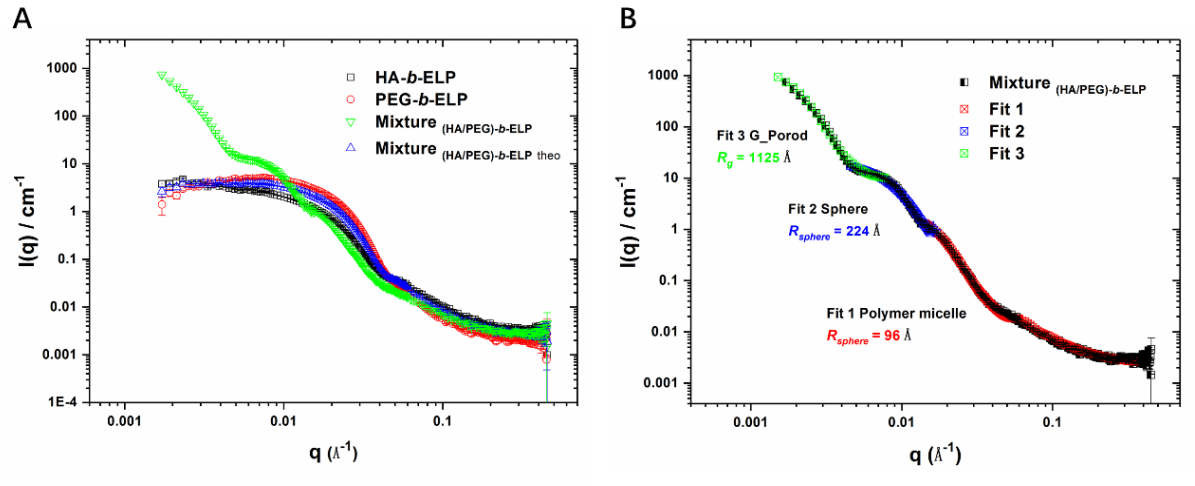

Figure 9. *(A) SANS curves of physical mixture of HA-b-ELP and PEG-b-ELP in D_2O at temperature above T_t. Theoretical mixture curves were normalized with concentration. ELP bionconjugates and their theoretical mixture curves in D_2O at 25°C. (B) Three best fits to the mixture (best fit parameters are listed in Table 6).*

On the contrary, HA/PEG-*b*-ELP mixture showed a significantly different behavior (Figure 9). Three oscillations were found in the range of 0.004-0.0006 $Å^{-1}$, 0.03-0.05 $Å^{-1}$ and 0.01-0.02 $Å^{-1}$. The self-assembly behavior in that case was obviously complex, leading to a morphology that cannot be fitted with a simple model. Nevertheless, in an attempt to extract some information, were able to fit with Guinier-Porod sphere function, simple sphere model and polymer micelle model, respectively in different scattering regions. Characteristics of the fitting parameters from these mixtures were summarized in Table 6. The formation of such complex nano-objects might be due to the structural interaction effect of these two bioconjugates, giving rise to a kind an aggregation/coacervation of micelles. Additional experiments, especially using cryo-TEM or cryo-SEM may be performed, even challenging, as we would have to capture and freeze structures obtained at rather high temperature.

4. CONCLUSION

We herein presented a comprehensive structural analysis of a series of polysaccharide-*b*-ELP bioconjugates that provided insight and understanding into the thermally-triggered self-assembly process of polysaccharide-*b*-ELP bioconjugates. Light scattering studies demonstrated a fully reversible self-assembly/disassembly process by controlling the temperature above/below the T_t. Below the T_t, polysaccharide-*b*-ELP chains behave as unimer with little aggregation. Although HA showed an attractive interaction with ELP, mixing HA-*b*-ELP with Dex-*b*-ELP or PEG-*b*-ELP presented independent nature. Above the T_t, ELP chains of polysaccharide-*b*-ELP bioconjugates hydrophobically collapsed, leading to structural evolution of polysaccharide-*b*-ELP from unimer to self-assembled nanostructure. Insufficient hydrophilicity of Lam-*b*-ELP led to aggregation. Mixing Dex-*b*-ELP with HA-*b*-ELP or PEG-*b*-ELP also showed similarly structural evolution from unimer to self-assembled spherical particles. Additional FRET experiments would be necessary to differentiate between the formation of individual micelles or mixed micelles. However, mixture of HA/PEG-*b*-ELP indicated a more complex behavior, with a three regimes of particle distribution, which might due to the structural interaction of these two bioconjugates. Again, additional experiments, using fluorescently labeled bioconjugates or electron microscopy experiments may provide a better understanding.

REFERENCES

(1) Mura, S.; Nicolas, J.; Couvreur, P. Stimuli-Responsive Nanocarriers for Drug Delivery. *Nat. Mater.* **2013**, *12* (11), 991–1003. https://doi.org/10.1038/nmat3776.

(2) Cabane, E.; Zhang, X.; Langowska, K.; Palivan, C. G.; Meier, W. Stimuli-Responsive Polymers and Their Applications in Nanomedicine. *Biointerphases* **2012**, *7* (1), 9. https://doi.org/10.1007/s13758-011-0009-3.

(3) Fleige, E.; Quadir, M. A.; Haag, R. Stimuli-Responsive Polymeric Nanocarriers for the Controlled Transport of Active Compounds: Concepts and Applications. *Adv. Drug Deliv. Rev.* **2012**, *64* (9), 866–884. https://doi.org/10.1016/j.addr.2012.01.020.

(4) Cheng, R.; Meng, F.; Deng, C.; Klok, H.-A.; Zhong, Z. Dual and Multi-Stimuli Responsive Polymeric Nanoparticles for Programmed Site-Specific Drug Delivery. *Biomaterials* **2013**, *34* (14), 3647–3657. https://doi.org/10.1016/j.biomaterials.2013.01.084.

(5) Montero de Espinosa, L.; Meesorn, W.; Moatsou, D.; Weder, C. Bioinspired Polymer Systems with Stimuli-Responsive Mechanical Properties. *Chem. Rev.* **2017**, *117* (20), 12851–12892. https://doi.org/10.1021/acs.chemrev.7b00168.

(6) Blum, A. P.; Kammeyer, J. K.; Rush, A. M.; Callmann, C. E.; Hahn, M. E.; Gianneschi, N. C. Stimuli-Responsive Nanomaterials for Biomedical Applications. *J. Am. Chem. Soc.* **2015**, *137* (6), 2140–2154. https://doi.org/10.1021/ja510147n.

(7) Monfort, D. A.; Koria, P. Recombinant Elastin-Based Nanoparticles for Targeted Gene Therapy. *Gene Ther.* **2017**, *24* (10), 610–620. https://doi.org/10.1038/gt.2017.54.

(8) Kim, W.; Chaikof, E. L. Recombinant Elastin-Mimetic Biomaterials: Emerging Applications in Medicine. *Adv. Drug Deliv. Rev.* **2010**, *62* (15), 1468–1478. https://doi.org/10.1016/j.addr.2010.04.007.

(9) MacEwan, S. R.; Chilkoti, A. Elastin-like Polypeptides: Biomedical Applications of Tunable Biopolymers. *Biopolymers* **2010**, *94* (1), 60–77. https://doi.org/10.1002/bip.21327.

(10) Le, D. H. T.; Sugawara-Narutaki, A. Elastin-like Polypeptides as Building Motifs toward Designing Functional Nanobiomaterials. *Mol. Syst. Des. Eng.* **2019**, *4* (3), 545–565. https://doi.org/10.1039/C9ME00002J.

(11) Despanie, J.; Dhandhukia, J. P.; Hamm-Alvarez, S. F.; MacKay, J. A. Elastin-like Polypeptides: Therapeutic Applications for an Emerging Class of Nanomedicines. *J. Control. Release* **2016**, *240*, 93–108. https://doi.org/10.1016/j.jconrel.2015.11.010.

(12) Araújo, A.; Olsen, B. D.; Machado, A. V. Engineering Elastin-Like Polypeptide-Poly(Ethylene Glycol) Multiblock Physical Networks. *Biomacromolecules* **2018**, *19* (2), 329–339. https://doi.org/10.1021/acs.biomac.7b01424.

(13) Matt, A.; Kuttich, B.; Grillo, I.; Weißheit, S.; Thiele, C. M.; Stühn, B. Temperature Induced Conformational Changes in the Elastin-like Peptide GVG(VPGVG)3. *Soft Matter* **2019**, *15* (20), 4192–4199. https://doi.org/10.1039/c9sm00583h.

(14) MacEwan, S. R.; Weitzhandler, I.; Hoffmann, I.; Genzer, J.; Gradzielski, M.; Chilkoti, A. Phase Behavior and Self-Assembly of Perfectly Sequence-Defined and Monodisperse Multiblock Copolypeptides. *Biomacromolecules* **2017**, *18* (2), 599–609. https://doi.org/10.1021/acs.biomac.6b01759.

(15) Li, N. K.; Roberts, S.; Quiroz, F. G.; Chilkoti, A.; Yingling, Y. G. Sequence Directionality Dramatically Affects LCST Behavior of Elastin-Like Polypeptides. *Biomacromolecules* **2018**, *19* (7), 2496–2505. https://doi.org/10.1021/acs.biomac.8b00099.

(16) Meyer, D. E.; Chilkoti, A. Quantification of the Effects of Chain Length and Concentration on the Thermal Behavior of Elastin-like Polypeptides. *Biomacromolecules* **2004**, *5* (3), 846–851. https://doi.org/10.1021/bm034215n.

(17) Hassouneh, W.; Fischer, K.; MacEwan, S. R.; Branscheid, R.; Fu, C. L.; Liu, R.; Schmidt, M.; Chilkoti, A. Unexpected Multivalent Display of Proteins by Temperature Triggered Self-Assembly of Elastin-like Polypeptide Block Copolymers. *Biomacromolecules* **2012**, *13* (5), 1598–1605. https://doi.org/10.1021/bm300321n.

(18) Hassouneh, W.; Zhulina, E. B.; Chilkoti, A.; Rubinstein, M. Elastin-like Polypeptide Diblock Copolymers Self-Assemble into Weak Micelles. *Macromolecules* **2015**, *48* (12), 4183–4195. https://doi.org/10.1021/acs.macromol.5b00431.

(19) Garanger, E.; MacEwan, S. R.; Sandre, O.; Brûlet, A.; Bataille, L.; Chilkoti, A.; Lecommandoux, S. Structural Evolution of a Stimulus-Responsive Diblock Polypeptide Micelle by Temperature Tunable

Compaction of Its Core. *Macromolecules* **2015**, *48* (18), 6617–6627. https://doi.org/10.1021/acs.macromol.5b01371.

(20) Martín, L.; Castro, E.; Ribeiro, A.; Alonso, M.; Rodríguez-Cabello, J. C. Temperature-Triggered Self-Assembly of Elastin-Like Block Co-Recombinamers:The Controlled Formation of Micelles and Vesicles in an Aqueous Medium. *Biomacromolecules* **2012**, *13* (2), 293–298. https://doi.org/10.1021/bm201436y.

(21) Aluri, S. R.; Shi, P.; Gustafson, J. A.; Wang, W.; Lin, Y.-A.; Cui, H.; Liu, S.; Conti, P. S.; Li, Z.; Hu, P.; et al. A Hybrid Protein–Polymer Nanoworm Potentiates Apoptosis Better than a Monoclonal Antibody. *ACS Nano* **2014**, *8* (3), 2064–2076. https://doi.org/10.1021/nn403973g.

(22) Mills, C. E.; Michaud, Z.; Olsen, B. D. Elastin-like Polypeptide (ELP) Charge Influences Self-Assembly of ELP–MCherry Fusion Proteins. *Biomacromolecules* **2018**, *19* (7), 2517–2525. https://doi.org/10.1021/acs.biomac.8b00147.

(23) Weitzhandler, I.; Dzuricky, M.; Hoffmann, I.; Garcia Quiroz, F.; Gradzielski, M.; Chilkoti, A. Micellar Self-Assembly of Recombinant Resilin-/Elastin-Like Block Copolypeptides. *Biomacromolecules* **2017**, *18* (8), 2419–2426. https://doi.org/10.1021/acs.biomac.7b00589.

(24) Huang, W.; Rollett, A.; Kaplan, D. L. Silk-Elastin-like Protein Biomaterials for the Controlled Delivery of Therapeutics. *Expert Opin. Drug Deliv.* **2015**, *12* (5), 779–791. https://doi.org/10.1517/17425247.2015.989830.

(25) van Eldijk, M. B.; Smits, F. C. M.; Vermue, N.; Debets, M. F.; Schoffelen, S.; van Hest, J. C. M. Synthesis and Self-Assembly of Well-Defined Elastin-Like Polypeptide–Poly(Ethylene Glycol) Conjugates. *Biomacromolecules* **2014**, *15* (7), 2751–2759. https://doi.org/10.1021/bm5006195.

(26) Le Fer, G.; Portes, D.; Goudounet, G.; Guigner, J.-M.; Garanger, E.; Lecommandoux, S. Design and Self-Assembly of PBLG- b -ELP Hybrid Diblock Copolymers Based on Synthetic and Elastin-like Polypeptides. *Org. Biomol. Chem.* **2017**, *15* (47), 10095–10104. https://doi.org/10.1039/C7OB01945A.

(27) Le Fer, G.; Wirotius, A. L.; Brûlet, A.; Garanger, E.; Lecommandoux, S. Self-Assembly of Stimuli-Responsive Biohybrid Synthetic- b-Recombinant Block Copolypeptides. *Biomacromolecules* **2019**, *20* (1), 254–272. https://doi.org/10.1021/acs.biomac.8b01390.

(28) Fujita, Y.; Mie, M.; Kobatake, E. Construction of Nanoscale Protein Particle Using Temperature-Sensitive Elastin-like Peptide and Polyaspartic Acid Chain. *Biomaterials* **2009**, *30* (20), 3450–3457. https://doi.org/10.1016/j.biomaterials.2009.03.012.

(29) Otteson, E. W.; Welch, W. H.; Kozel, T. R. Protein-Polysaccharide Interactions. A Monoclonal Antibody Specific for the Capsular Polysaccharide of Cryptococcus Neoformans. *J. Biol. Chem.* **1994**, *269* (3), 1858–1864.

(30) Comert, F.; Malanowski, A. J.; Azarikia, F.; Dubin, P. L. Coacervation and Precipitation in Polysaccharide–Protein Systems. *Soft Matter* **2016**, *12* (18), 4154–4161. https://doi.org/10.1039/C6SM00044D.

(31) Presolski, S. I.; Hong, V. P.; Finn, M. G. Copper-Catalyzed Azide-Alkyne Click Chemistry for Bioconjugation. In *Current Protocols in Chemical Biology*; John Wiley & Sons, Inc.: Hoboken, NJ, USA, 2011; Vol. 3, pp 153–162. https://doi.org/10.1002/9780470559277.ch110148.

(32) Elchinger, P. H.; Faugeras, P. A.; Boëns, B.; Brouillette, F.; Montplaisir, D.; Zerrouki, R.; Lucas, R. Polysaccharides: The "Click" Chemistry Impact. *Polymers (Basel).* **2011**, *3* (4), 1607–1651. https://doi.org/10.3390/polym3041607.

(33) Palomo, J. M. Click Reactions in Protein Chemistry: From the Preparation of Semisynthetic Enzymes to New Click Enzymes. *Org. Biomol. Chem.* **2012**, *10* (47), 9309–9318. https://doi.org/10.1039/c2ob26409a.

(34) Miller, C. C. The Stokes-Einstein Law for Diffusion in Solution. *Proc. R. Soc. A Math. Phys. Eng. Sci.* **1924**, *106* (740), 724–749. https://doi.org/10.1098/rspa.1924.0100.

(35) Pedersen, J. S. Analysis of Small-Angle Scattering Data from Colloids and Polymer Solutions: Modeling and Least-Squares Fitting. *Adv. Colloid Interface Sci.* **1997**, *70*, 171–210. https://doi.org/10.1016/S0001-8686(97)00312-6.

(36) Andersson, K. M.; Hovmöller, S. The Average Atomic Volume and Density of Proteins. *Zeitschrift für Krist. - Cryst. Mater.* **1998**, *213* (7–8). https://doi.org/10.1524/zkri.1998.213.7-8.369.

SUPPORTING INFORMATION

Models of Self-Assembled Nanostructures Above the Transition Temperature

Guinier-Porod function model was employed to fit macroaggregates. It is an empirical model that can be used to determine the size and dimensionality of scattering objects, including asymmetric objects. Functional form is used as following:

$$I(q) = \begin{cases} \frac{G}{Q^s} exp\left[\frac{-Q^2 R_g^2}{3-s}\right] Q \leq Q1 \\ \frac{D}{Q^m} \qquad\qquad Q \geq Q1 \end{cases} \quad (8)$$

This is based on the generalized Guinier law for such elongated objects. For ELP macroaggregates, we hypothesized a 3D globular objects, thus s = 0 was applied in Guinier-Porod function.

Core-shell sphere model provides the form factor *P(q)*, for a monodisperse spherical particle with a core-shell structure. The form factor is normalized by the particle volume.

$$\mathrm{P(q)} = \frac{scale}{V} F^2(q) + background \ (9)$$

where

$$\mathrm{F(q)} = \frac{3}{V_s}[V_c(\rho_{c-}\rho_s)\frac{\sin(qr_c)-qr_c\cos(qr_c)}{(qr_c)^3} + V_s(\rho_s - \rho_{solv})\frac{\sin(qr_s)-qr_s\cos(qr_s)}{(qr_c)^3} \ (10)$$

where V_s is the volume of the whole particle, V_c is the volume of the core, r_s = radius + thickness is the radius of the particle, r_c is the radius of the core, ρ_c is the scattering length density of the core, ρ_s is the scattering length density of the shell, ρ_{solv}, is the scattering length density of the solvent.

Polymer micelle model provides the form factor *P(q)*, for a micelle with a spherical core and Gaussian polymer chains attached to the surface, thus suitable for block copolymer micelles.

$$\mathrm{P(q)} = \mathrm{N}^2\beta_s^2\Phi(q\mathrm{r})^2 + N\beta_c^2 P_c(q) + 2\mathrm{N}^2\beta_s\beta_c S_{sc}(q) + N(N-1)\beta_c^2 S_{cc}(q) \ (11)$$

$$\beta_s = V_{core}(\rho_{core} - \rho_{solvent}) \quad (12)$$

$$\beta_c = V_{corona}(\rho_{corona} - \rho_{solvent}) \ (13)$$

Simple sphere model fits spheres with uniform scattering length density

$$I(q) = \frac{scale}{V}\left[3V(\Delta\rho)\frac{\sin(qr)-qr\cos(qr)}{(qr)^3}\right] + background \quad (14)$$

where *scale* is a volume fraction, *V* is the volume of the scatterer, *r* is the radius of the sphere and *background* is the background level. *sld* and *sld_solvent* are the scattering length densities (SLDs) of the scatterer and the solvent respectively, whose difference is $\Delta\rho$.

Synthesis of PEG-b-ELP

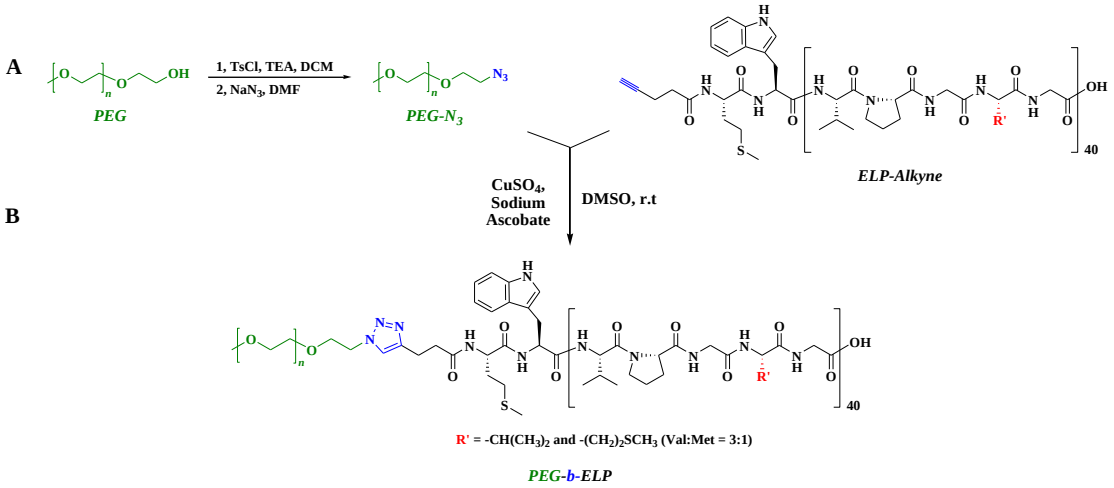

Scheme S1. Synthetic strategy of poly(ethylene glycol)-*b*-elastin-like polypeptide block copolymer. (A) Functionlization of PEG with an azide group. (B) Copper-catalyzed azide-alkyne cycloaddition between the azide-functionalized PEG and the alkyne functionalized ELP.

As shown in NMR spectra (Figure S2), characteristic peak (-OCH_2CH_2O-) of PEG was at around 3.6 ppm and the trizole proton peak was found at 7.78 ppm confirming the desired structure of block copolymer. FTIR spectra of PEG-*b*-ELP was compared with the ones of PEG-N_3 and alkyne-functionalized ELP (Figure S4). The complete disappearance of azide band at 2100 cm^{-1} in the bioconjugates also proved the success of conjugation. MALDI-TOF mass spectra recorded an average mass 19406.3 Da of PEG-*b*-ELP (Figure S3).

Characterization of PEG-b-ELP

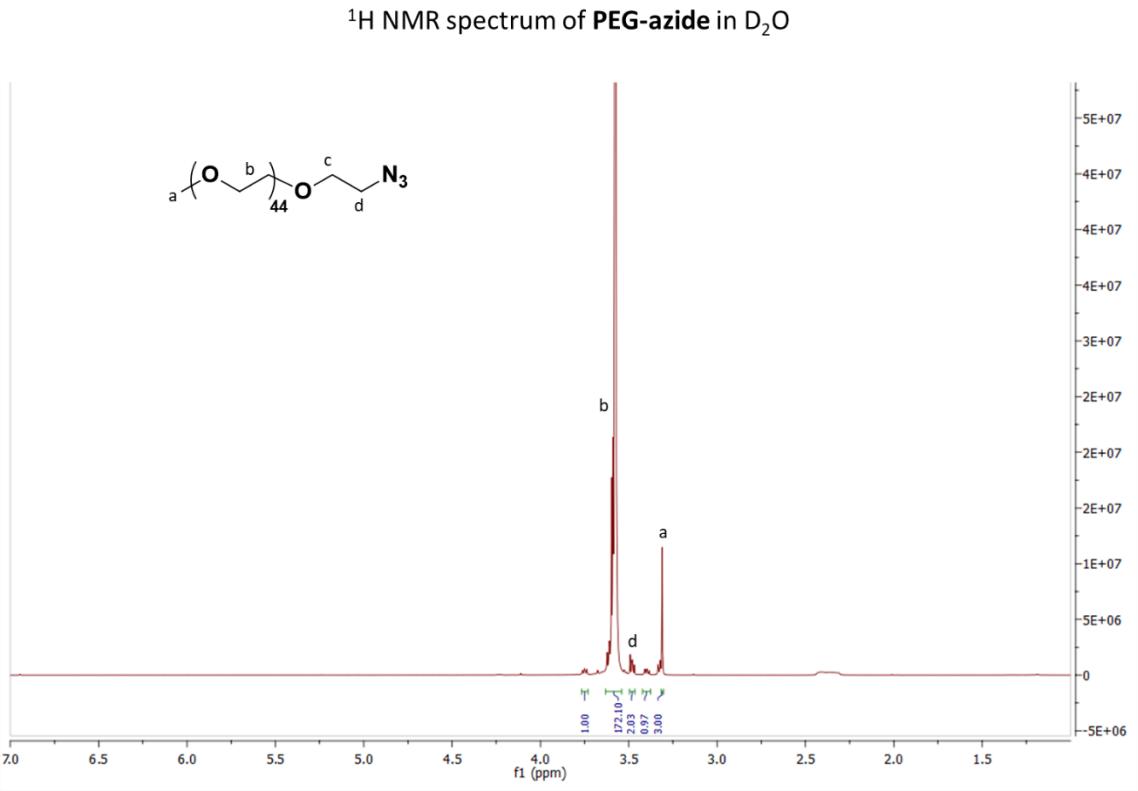

Figure S1. ^{1}H NMR spectrum of PEG-azide in D_2O at 25 °C.

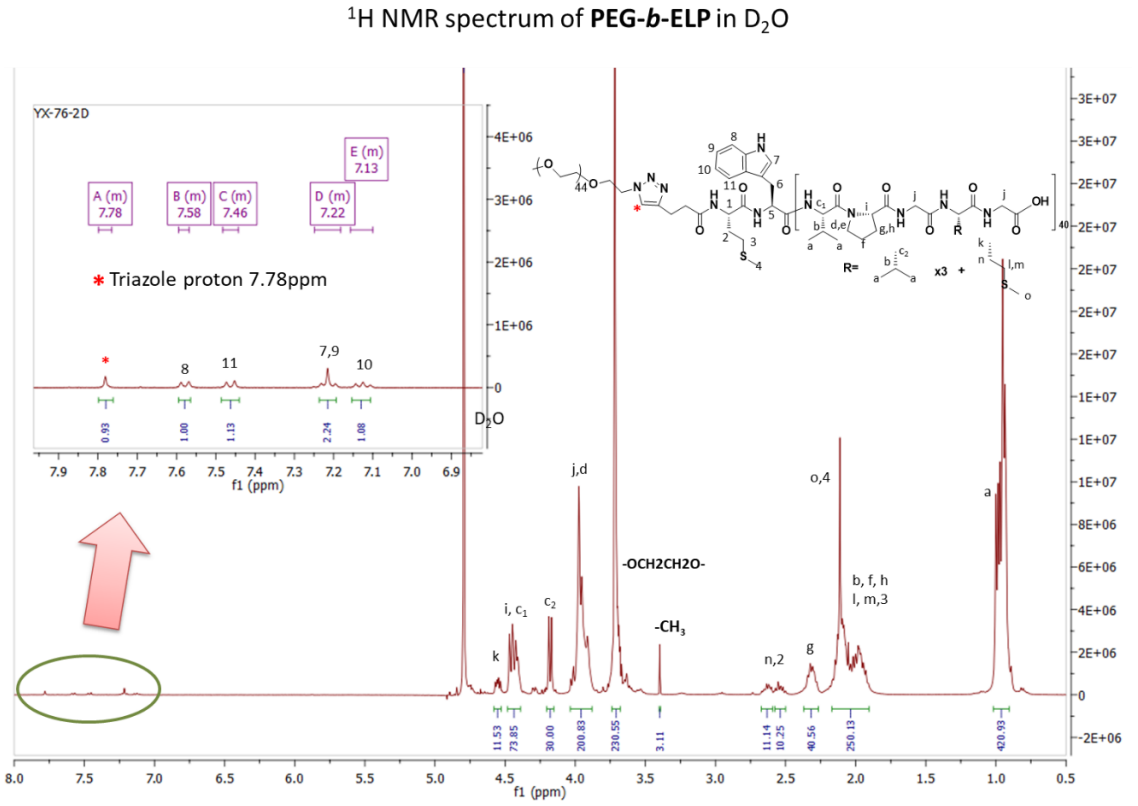

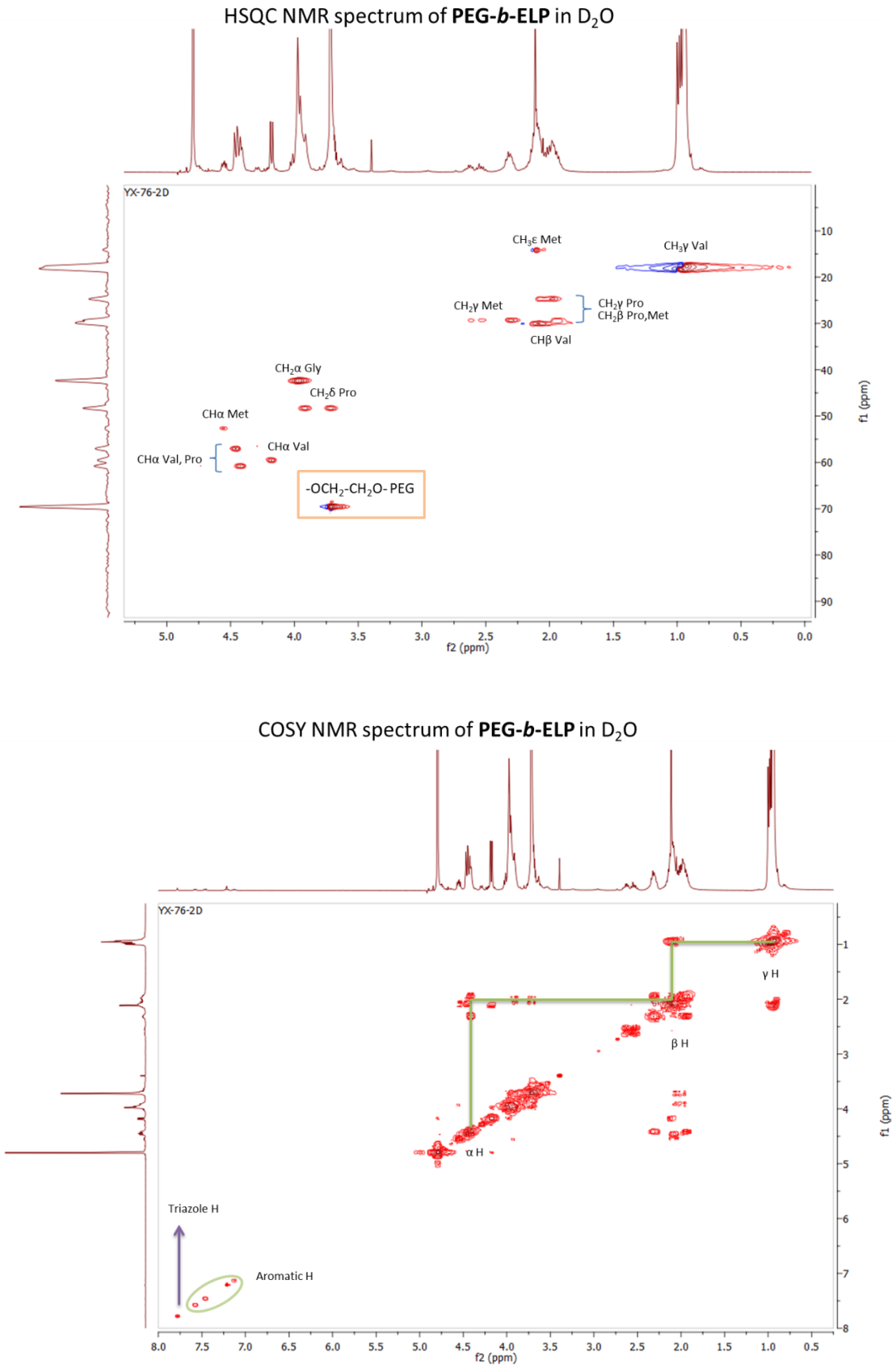

Figure S2. ^{1}H, HSQC, and COSY NMR spectra of PEG-*b*-ELP in D_2O at 25 °C.

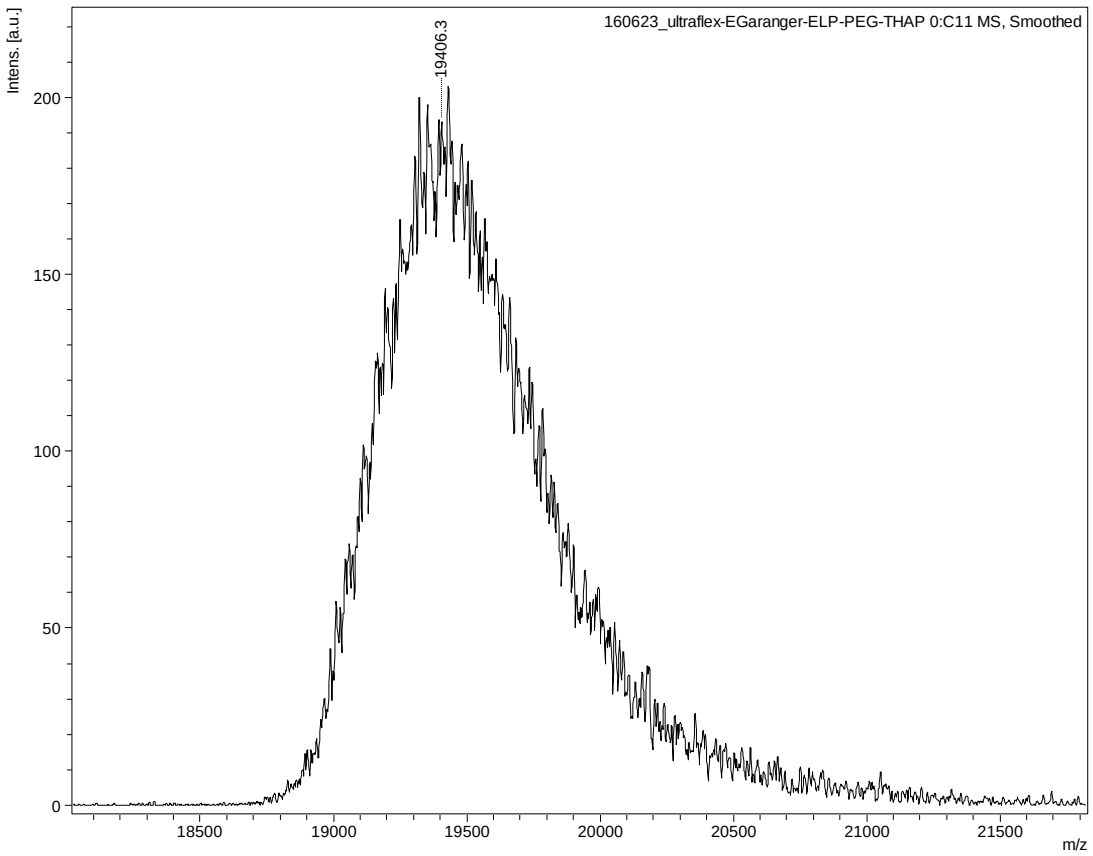

Figure S3. MALDI-TOF spectra of PEG-*b*-ELP.

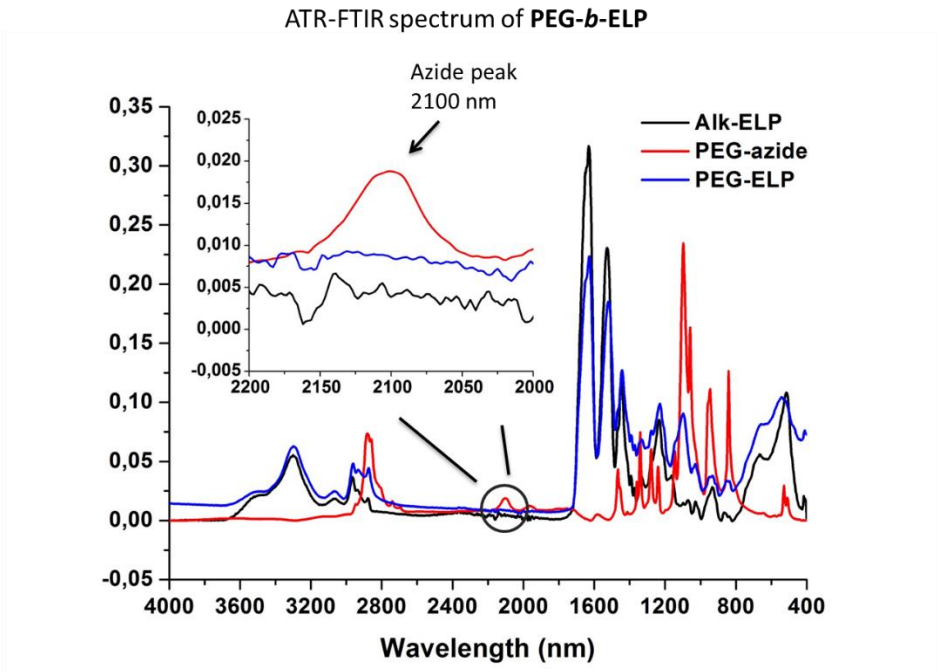

Figure S4. ATR-FTIR spectrum of PEG-*b*-ELP

SEC trace and T_t values of ELP and ELP bioconjugates

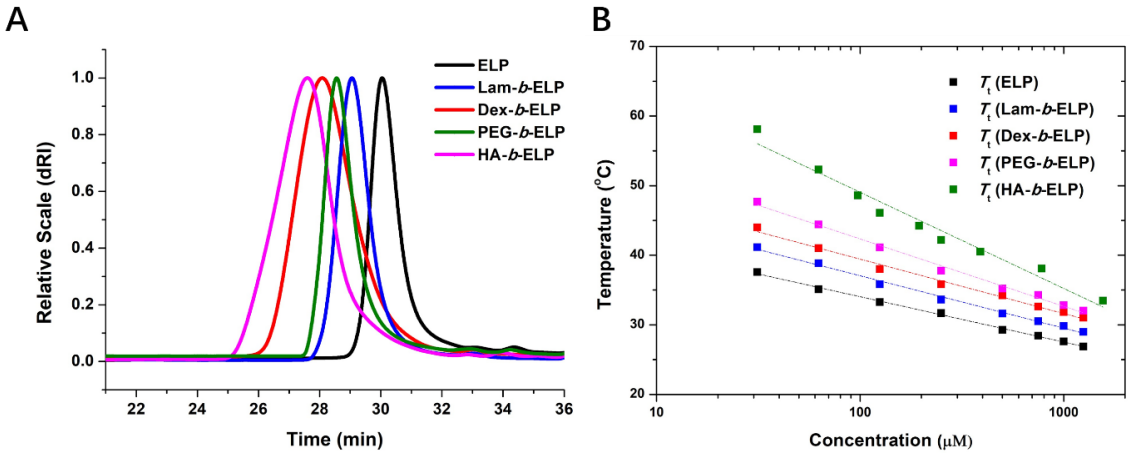

Figure S5. (A) SEC trace of ELP and ELP bioconjugates in aqueous buffer (0.1 M $NaNO_3$, 0.01 M Na_2HPO_4, 0.02 M NaN_3) using a RI detector. (B) T_t values of ELP and ELP bioconjugates plotted as function of concentration in water.

DLS/ SLS study of Dex-b-ELP

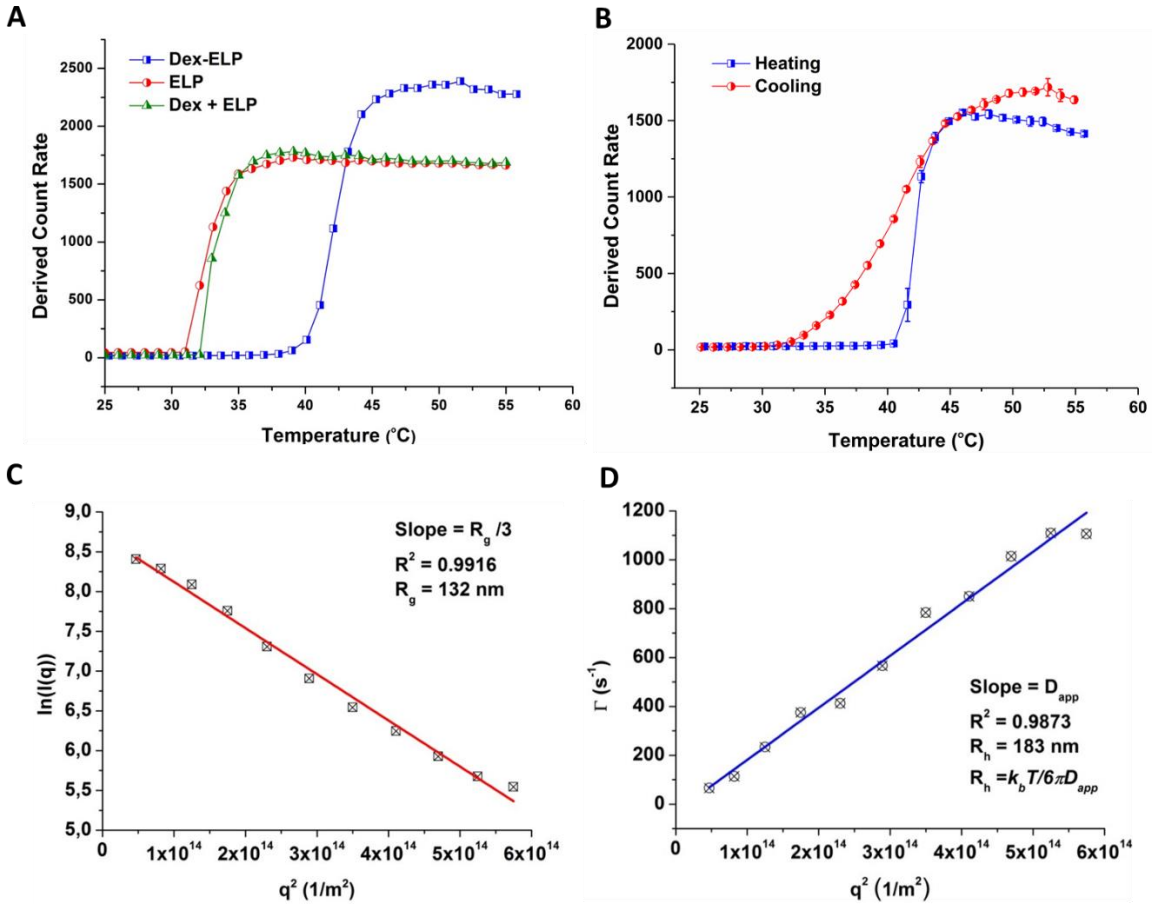

Figure S6. (A) Scattering intensity of ELP, Dex-*b*-ELP and physical mixture (125 µM in water) as a function of temperature upon heating. (B) Scattering intensity of Dex-*b*-ELP as a function of temperature upon heating(from 25 °C to 45 °C). Multi-angle scattering analysis of Dex-*b*-ELP obtained at 45 °C. Guinier plot and R_g determination (C). Variation of decay rate versus squared vector and R_h determination (D).

DLS/ SLS study of Lam-b-ELP

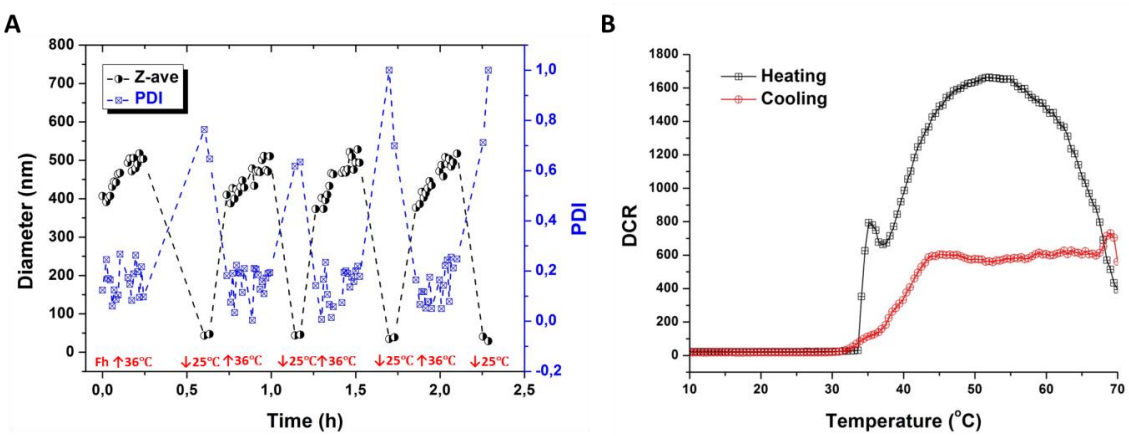

Figure S7. (A) Z-average size and polydispersity as a function of time upon repeated fast heating (45 °C) and cooling (25 °C) of Lam-*b*-ELP (125 μM) in water on DLS. (B) Scattering intensity of Lam-*b*-ELP as a function of temperature upon slow heating and cooling.

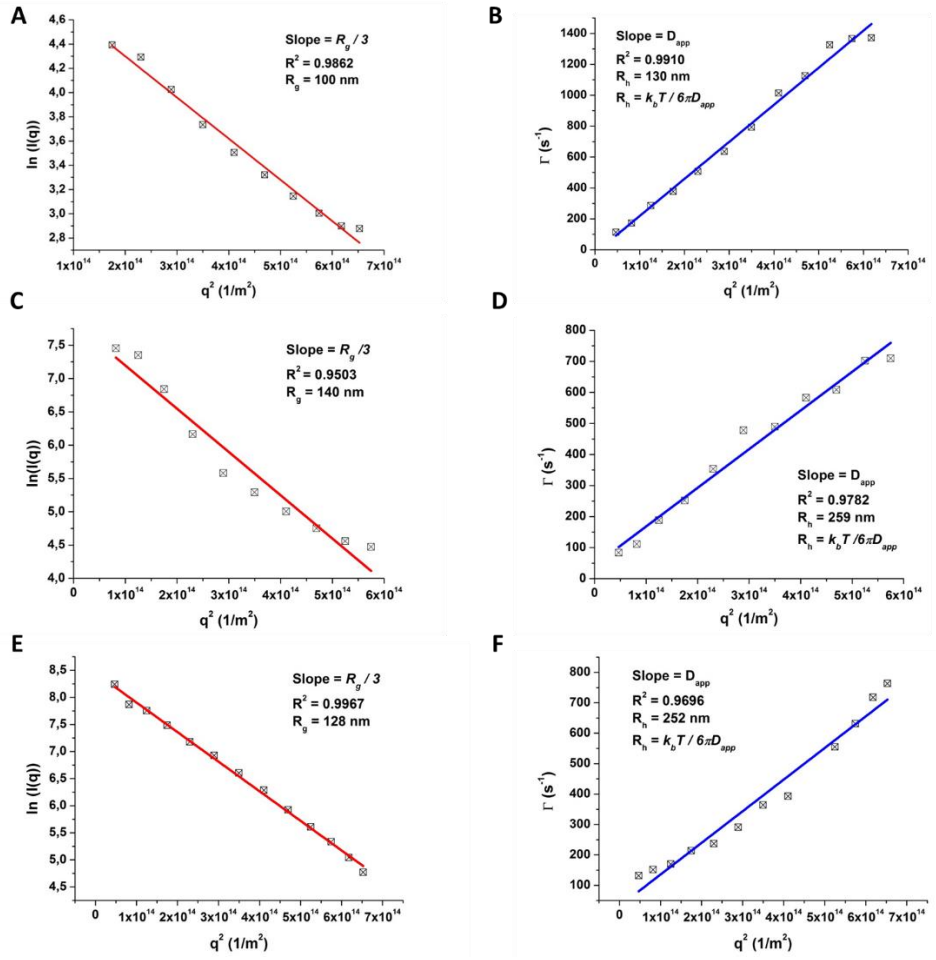

Figure S8. Guinier plot and diffusion coefficient determination of Lam-*b*-ELP at (A, B) 33 °C; (D, E) 37 °C; (H, G) 45 °C. DLS autocorrelation function (g_2(t)-1) and relaxation-time distribution (A(q,t)) for Lam-*b*-ELP at 90°, (C) 33 °C; (F) 37 °C; (I) 45 °C.

DLS/ SLS study of HA-b-ELP

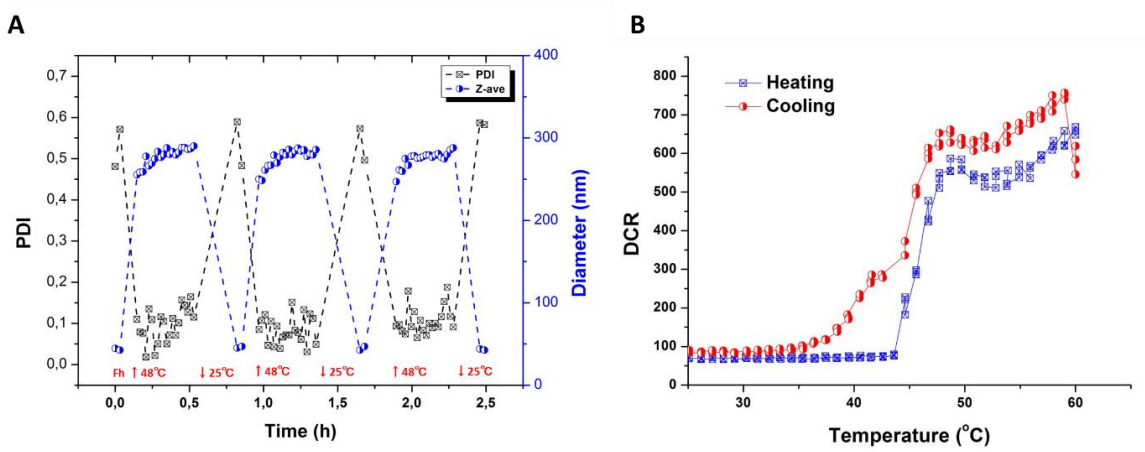

Figure S9. (A) Z-average size and polydispersity as a function of time upon repeated fast heating (48 °C) and cooling (25 °C) of HA-*b*-ELP (150 μM) in water on DLS. (B) Scattering intensity of HA-*b*-ELP as a function of temperature upon slow heating and cooling.

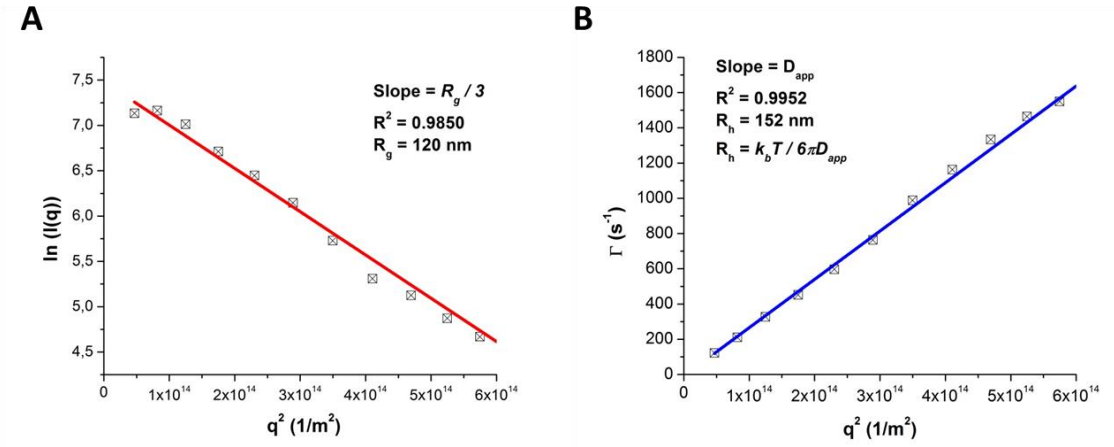

Figure S10. (A) Guinier plot and (B) diffusion coefficient determination of HA-*b*-ELP at 50 °C.

DLS/ SLS study of PEG-b-ELP

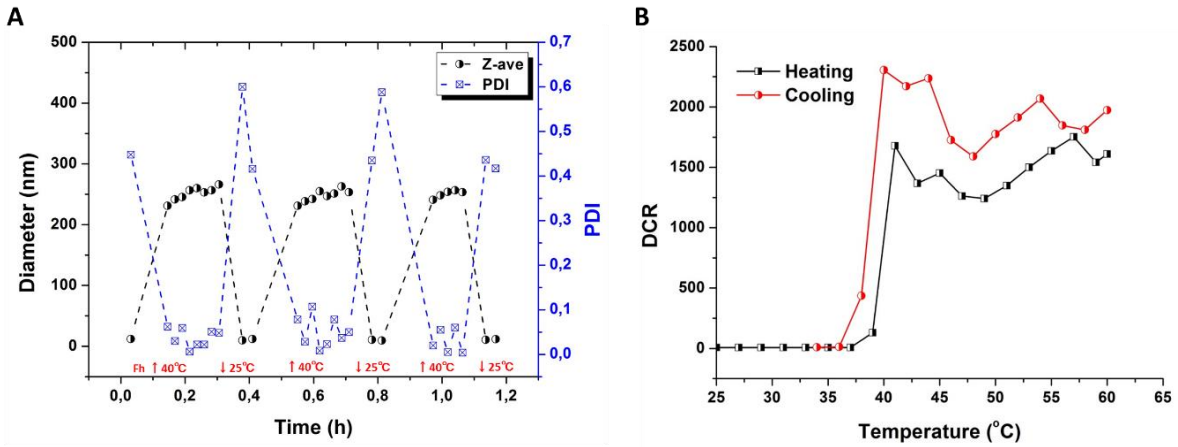

Figure S11. (A) Z-average size and polydispersity as a function of time upon repeated fast heating (40 °C) and cooling (25 °C) of PEG-*b*-ELP (125 μM) in water on DLS. (B) Scattering intensity of PEG-*b*-ELP as a function of temperature upon slow heating and cooling.

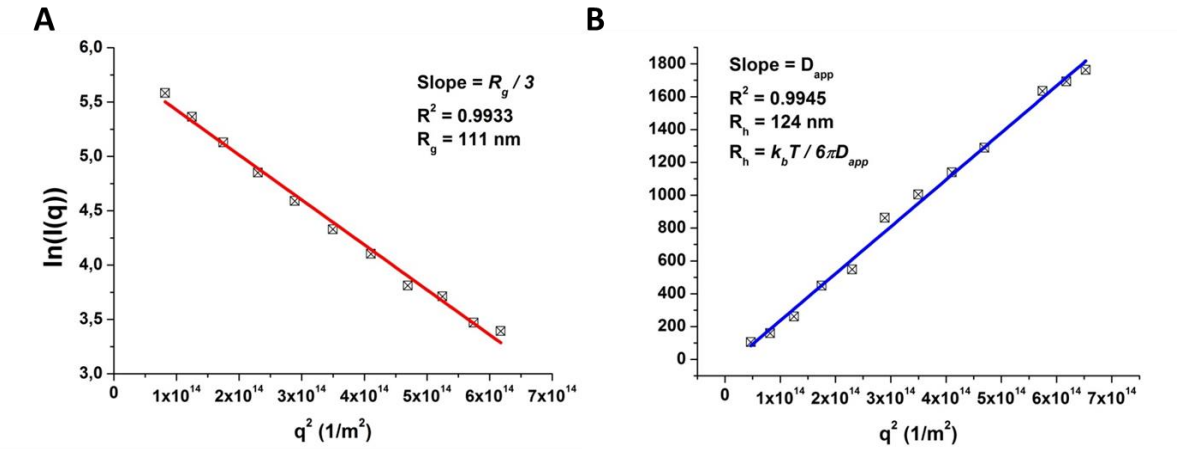

Figure S12. (A) Guinier plot and (B) diffusion coefficient determination of PEG-*b*-ELP at 40 °C.

SANS curves of ELP and ELP-bioconjugates mixtures upon heating

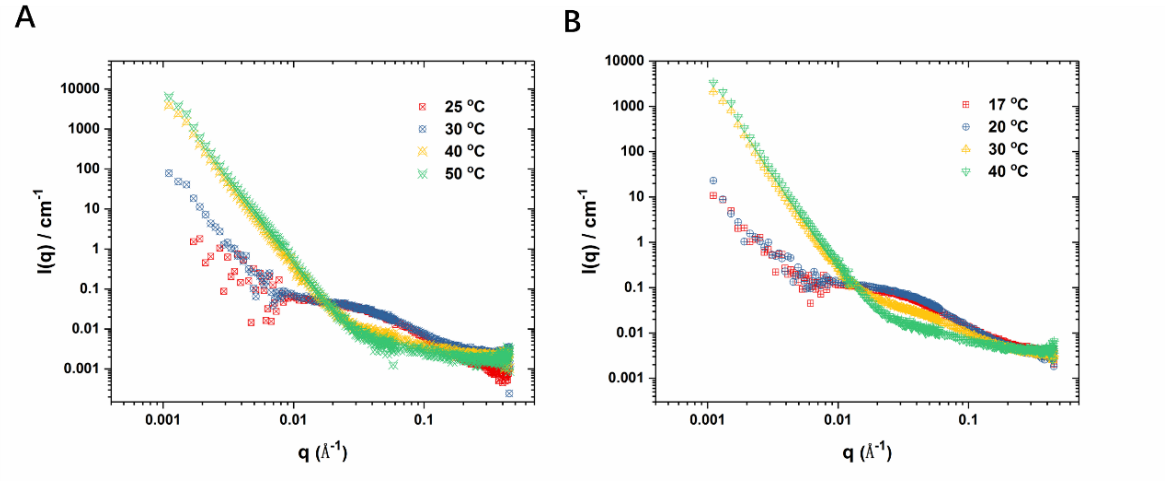

Figure S13. SANS curves of ELP (A) 125 µM, (B) 250 µM in D_2O at different temperature.

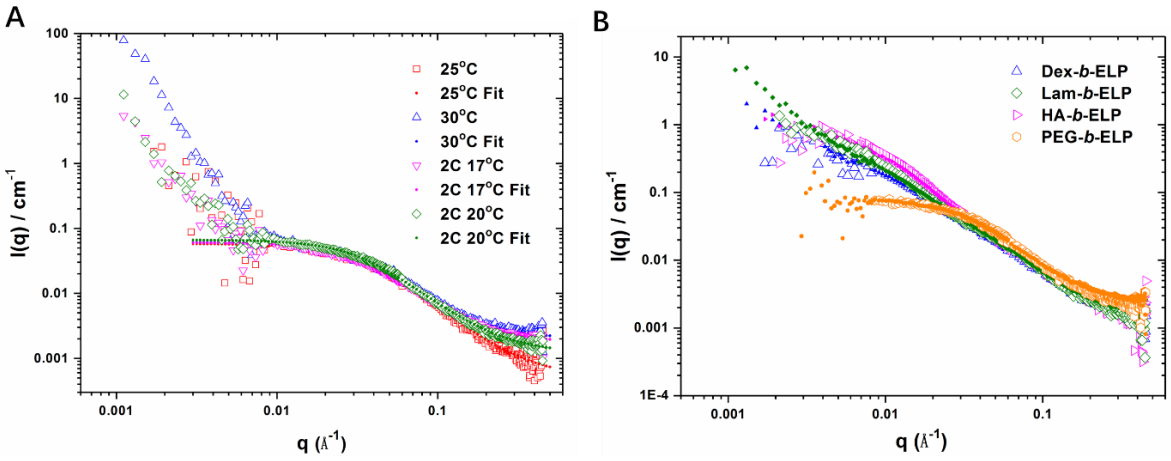

Figure S14. (A) SANS curves of ELP at 125 µM and 2C (250 µM, normalized with concentration) in D_2O at the temperature below T_t. Dotted lines are the best fits to the Debye function (best fit parameters are summarized in Table 3). (B) SANS curves of ELP bioconjugates at 125 µM (Hollow) and 250 µM (dotted lines normalized with concentration)

SANS curves of ELP bioconjugates mixtures

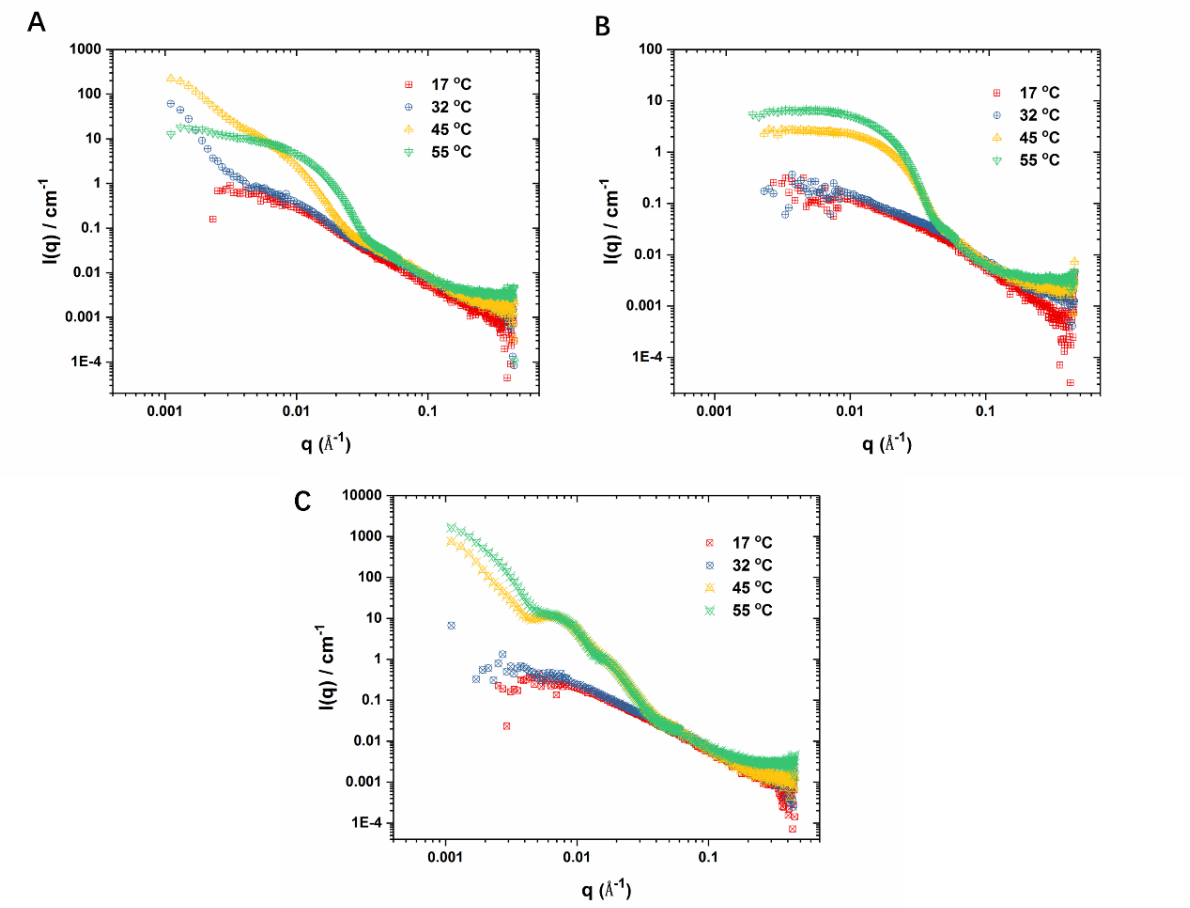

Figure S15. SANS curves of different bioconjugates mixture (mole ratio 1: 1) in D_2O at different temperature: (A) (Dex/HA)-*b*-ELP; (B) (Dex/PEG)-*b*-ELP; (C) (HA/PEG)-*b*-ELP.

SANS curves of the mixing ELP and polysaccharide below T_t

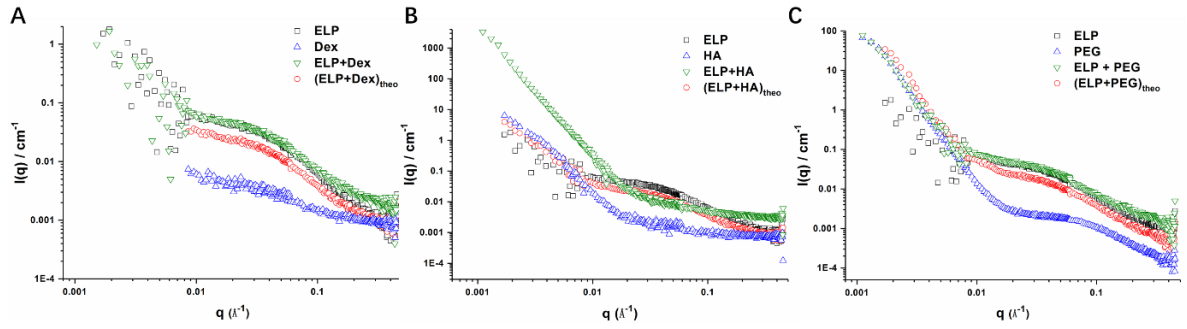

Figure S16. SANS curves of ELP, polysaccharide, their physical mixture and theoretical mixture curves in D_2O at the temperature below T_t. (A) Dex-*b*-ELP, (B) HA-*b*-ELP, (C) PEG-*b*-ELP. Theoretical mixture curves were normalized with concentration.

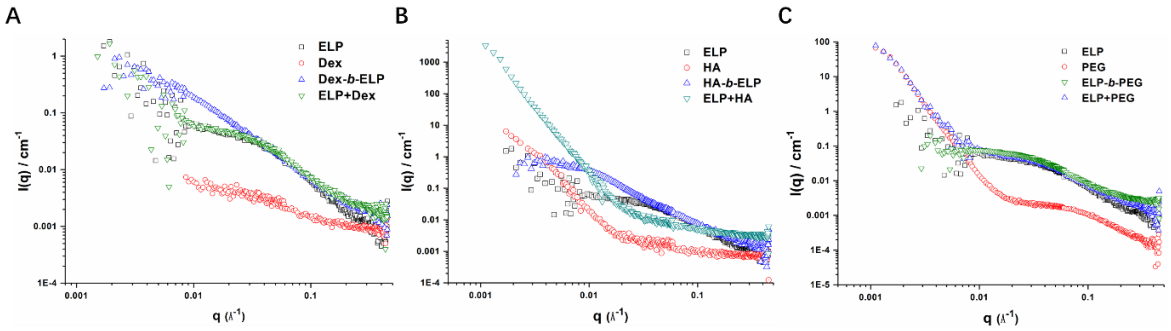

Figure S17. SANS curves of ELP, polysaccharide, their physical mixture and bioconjugate in D_2O at the temperature below T_t. (A) Dex-*b*-ELP, (B) HA-*b*-ELP, (C) PEG-*b*-ELP.

SANS curves of the mixture of Dex/HA-b-ELP, mixture of Dex/PEG-b-ELP, and mixture of HA/PEG-b-ELP below T_t

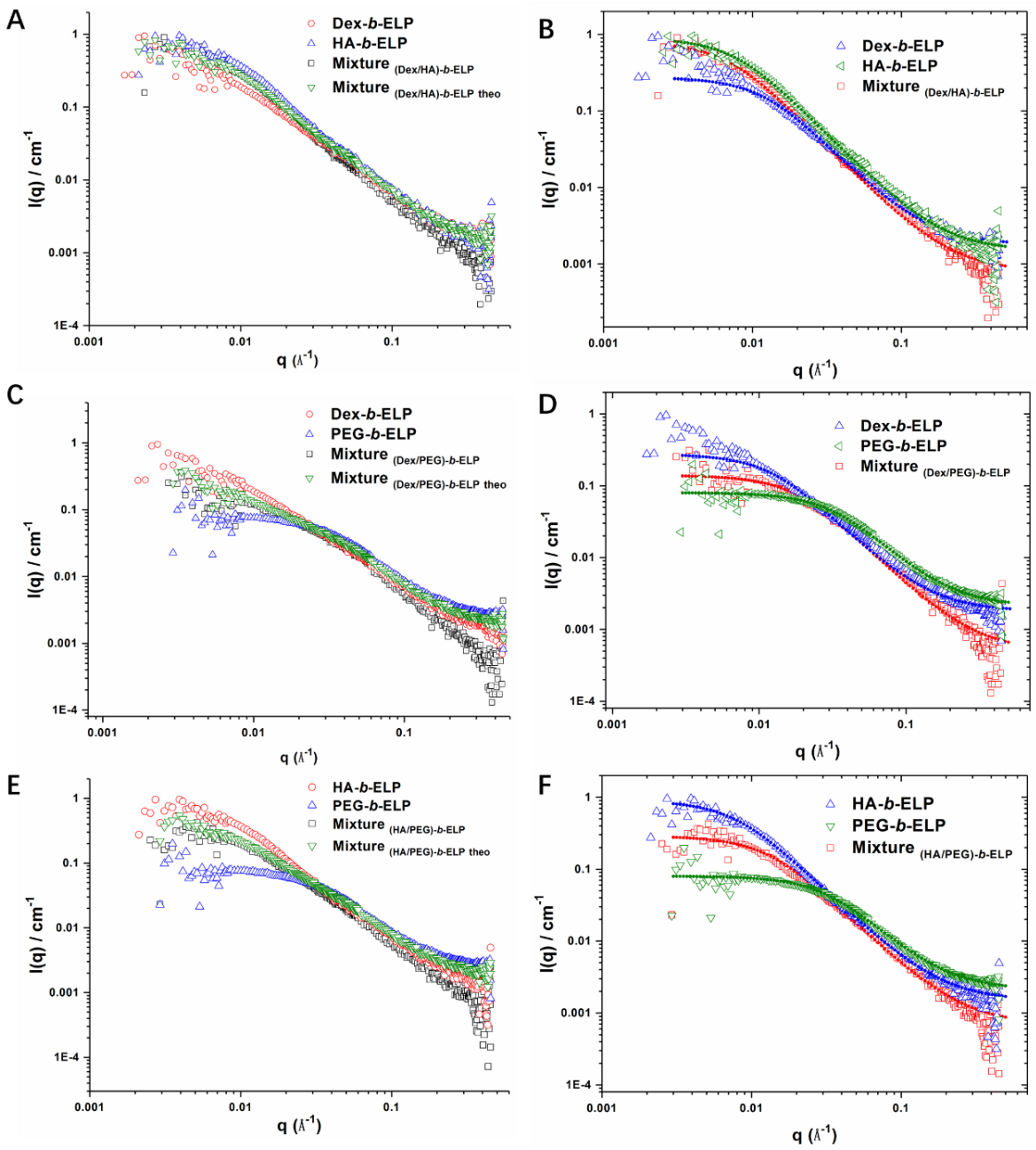

Figure S18. SANS curves of physical mixture of different ELP bionconjugates and their theoretical mixture curves in D_2O at 25°C. (A, B) Mixture of Dex/HA-*b*-ELP; (C, D) Mixture of Dex/PEG-*b*-ELP; (E, F) Mixture of HA/PEG-*b*-ELP. Theoretical mixture curves were normalized with concentration. Dotted lines on the right side indicate the best fits to the Debye function (best fit parameters are listed in Table 4).

CHAPTER 4

EXPANDING THE TOOLBOX OF CHEMOSELECTIVE MODIFICATIONS OF ELASTIN-LIKE POLYPEPTIDES AT METHIONINE RESIDUES

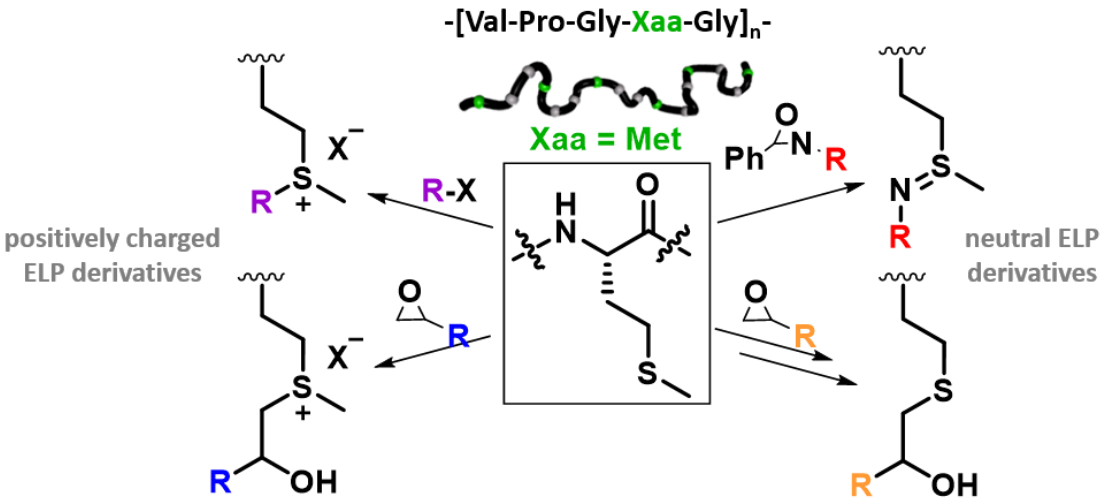

Abstract

Selective modifications at methionine residues in proteins have attracted particular attention in recent years. Previously described methods to chemoselectively modify the methionine side chain in elastin-like polypeptides (ELPs) involved nucleophilic addition using alkyl halides or epoxides yielding a sulfonium group with a positive charge strongly affecting ELPs' physico-chemical properties, in particular their thermal responsiveness. We herein explored the recently reported ReACT method based on the use of oxaziridine reagents, a redox-based reaction yielding an uncharged sulfimide derivative as an alternative route for chemoselective modification of methionine-containing ELPs in aqueous medium. The different synthetic strategies are herein compared in order to provide a furnished toolbox for further biorthogonal post-modifications.

1. INTRODUCTION

Protein-based materials are attractive sources for the design of promising high performance biologically-inspired materials for a variety of applications such as biomaterials, therapeutic drug delivery and targeting.[1–4] Precise structure-function relationships have been elucidated for certain proteins allowing the design of artificial protein materials with superior properties.[1] Elastin is one example of a well-known naturally occurring structural protein that imparts elasticity to a variety of tissues.[5,6] Understanding of the sequence and properties of elastin has inspired the design of elastin-like polypeptides (ELPs),[7] which are artificial elastin mimics composed of repeating peptide sequences from the hydrophobic domain presenting similar thermal and mechanical properties.[5,8] Bioproduction of ELPs using recombinant DNA and protein-engineering techniques allows an exquisite level of control of their primary sequence with exact amino acid composition, chain length, and molecular weight.[2] ELPs constitute attractive biocompatible, biodegradable and inert thermo-responsive protein polymers.[9,10] Constituted of repetitive -[Val-Pro-Gly-Xaa-Gly]- pentapeptide units, where Xaa corresponds to any amino acid except proline,[7] ELPs present a reversible temperature-triggered soluble-to-insoluble phase transition behavior in aqueous medium. The thermal responsiveness of a specific ELP can be quantified by its transition temperature (T_t) defined as the characteristic temperature at which soluble ELP chains self-associate and aggregate into an insoluble ELP-rich phase. Interestingly, this unique feature is highly tunable playing with molecular parameters (*e.g.*, guest residue composition, molecular mass) as well as with environmental parameters (*e.g.*, salts and cosolutes, ionic strength, pH). An alternative to the design of

recombinant ELPs with different sequences by genetic techniques to access ELPs with different T_ts rely on the chemical modification of a unique ELP backbone applying orthogonal chemoselective bioconjugation reactions as an easy means to access a variety of ELP derivatives with different thermal responsiveness.

Post-translational modifications of proteins, involving chemical changes after proteins translation play a fundamental role in the regulation of proteins' structures and functions.[11] This has strongly motivated the development of different bioconjugation strategies to mimic nature's ability to chemoselectively modify proteins in order to modify or enhance their properties.[12,13] One alternative rely on the use of functional non-natural amino acids. However, despite significant technological advancements, incorporation of non-canonical residues into recombinant proteins remains non trivial, sometimes complex, expensive, and time-consuming.[14–17] A second method therefore rely on synthetic strategies to selectively modify natural amino acid residues presenting functional side chains or employing proteins' terminal ends. Biorthogonal reactions have been and are still extensively developed, and various chemical methods are currently available to selectively modify cysteine, lysine, tyrosine or tryptophan residues by carefully balancing reactivity and selectivity.[18–21]

Because of its relatively low nucleophilicity at physiological conditions, post-modification at methionine remains less explored in proteins and peptides as compared to lysine and cysteine, the most commonly modified amino acids. However, the unique reactivity of the thioether group under acidic conditions allows specific biorthogonal alkylation of methionine's side chain at low pH without the need for any protecting group for other residues, as pioneered by Toennies using alkyl halides.[22,23] Similar modifications were further applied on synthetic poly(methionine) polymers, copolymers and block copolymers,[24–26] before the development by Deming and co-workers of a more versatile method based on the use of epoxides that significantly enlarged the scope of methionine modifications.[27] Recently, Lin and co-workers reported a potent strategy to chemoselectively functionalize proteins at methionine residues using oxaziridine-based reagents.[28] Based on a redox-activated chemical tagging (ReACT) method, this strategy rely on the electrophilic amination of the sulfur-containing methionine with well-designed oxaziridine derivatives leading to the formation of an isoelectronic sulfimide conjugate. It's worth noting that due to the extremely high reactivity of oxaziridine derivatives, particular attention should be paid to the *N*-substituent on the nitrogen of the oxaziridine in order to favor the amination process (nitrogen-transfer product, NTP) instead of

the competitive oxidation (oxygen-transfer product, OTP) of the sulfur moiety.[29] The chemoselective coupling of oxaziridine and methionine partner occurs under mild biocompatible conditions (aqueous conditions at neutral pH), with a very highly selectivity to methionine's modification over other amino acids with an extremely fast reaction time.

A few years ago, our group started to explore chemoselective modifications of ELPs at methionine residues as an easy means to modulate their thermo-responsive properties and introduce various functionalities.[30–32] In particular, applying nucleophilic addition reactions using alkyl halides and epoxides, methionine-containing ELPs were functionalized with different pendant groups yielding polycationic derivatives. Herein, we aimed at expanding the scope of chemoselective modifications of ELPs at methionine exploring the ReACT strategy giving access to uncharged sulfimide ELPs derivatives. We were particularly interested in performing a comparative study between the three main synthetic methods to achieve quantitative chemoselective modifications of ELPs at methionine residues and evidence their advantages and drawbacks, especially for subsequent functionalization with bioactive motifs.

2. EXPERIMENTAL SECTION

2.1 Materials

All of the reagents and solvents are commercially available from standard suppliers, except for oxaziridine derivatives (Ox-ethyl, Ox-alkyne, Ox-N_3) that have been prepared following the published procedure.[28] Methyl iodine, propylene oxide, allyl glycidyl ether, glycidyl propargyl ether, formic acid, glacial acetic acid, Trizma®, hexafluoroisopropanol (HFIP), *N,N,N′,N″,N″*-pentamethyldiethylenetriamine (PMDETA) were obtained from Sigma-Aldrich (FR). Deionized water (18 MΩ-cm) was obtained by using a Millipore Milli-Q Biocel A10 purification unit. Cuprisorb was purchased from Seachem. Ethanol (96.0%, EtOH), methanol (98.5%, MeOH), tetrahydrofuran (99%), DMF (99%), DCM (99.5%), acetonitrile (99.9%, ACN) and $CuSO_4.5H_2O$ were obtained from VWR international. NaCl (99%) was purchased from Alfa Aesar (FR). β-D-galactopyranosyl azide (Gal-N_3) was obtained from Carbosynth (UK). Ammonium Acetate and Ammonium pyrrolidinedithiocarbamate, APDC and sodium ascorbate were purchased from Fisher Scientific (FR) were obtained from Fisher Scientific (FR). Amicon® ultra-15 centrifugal filter tube 3 000 MWCO was obtained from Merck millipore. Tris buffer was prepared with 0.05 M of Trisma-HCland 0.15 M of NaCl in Milli-Q water, the pH of the solution was then adjusted to 7.6 with NaOH 0.1M.

Alkylation of ELP[V_3M_1-*40*] (procedure A). ELP[V_3M_1-*40*] was dissolved in 0.2 M aqueous formic acid (20 mg/mL). Alkyl halide (40 equiv. per Met residue) was added as a solution in THF (50 mg/mL). The reaction was stirred for 5 days at room temperature under Argon atmosphere. The excess of alkyl halide was removed by extraction with diethyl ether, the organic layer was pipetted off and discarded. The aqueous phase was then transferred to a 3,000 MWCO ultra-centrifugal filter tube and washed with 40 mL of Milli-Q water at 20 ℃. The product was lyophilized to dryness to give a white powder.

Alkylation of ELP[V_3M_1-*40*] (procedure B). ELP[V_3M_1-*40*] was dissolved an AcOH/HFIP mixture (9/1, v/v) at 20 mg/mL. The solution was degassed with Ar. and the epoxide was added to the mixture (10 equiv. per methionine residue). After 24h of stirring, a second portion of epoxide (10 equiv. per methionine residue) was added and the reaction was stirred 48h in total, at room temperature and under Ar. atmosphere. The obtained mixture was transferred into a 3 000 MWCO Amicon® ultra-15 centrifugal filter tube, washed with 40 mL of Milli-Q water and freeze-dried.

2.2 Synthetic procedure

2.2.1 Alkylation of ELP[V_3M_1-*40*] with alkyl halide.

Compound 1A. Alkylation with methyl iodine, procedure A. ^{1}H NMR (400 MHz, D_2O, 25 ℃): (main peaks) δ 4.67−4.61 (m, 11 H, CHα Met), δ 4.47−4.40 (m, 80 H, CHα Val and Pro, VPGXG), 4.18-4.16 (d, 30 H, CHα Val, VPGVG), 3.41-3.37 (t, 22H, CH_2S Met), 2.95−2.94 (d, 66 H, SCH_3 Met), 1.00−0.93 (br m, 420 H, CH_3 Val). Yield= 61 %.

2.2.2 Alkylation of ELP[V_3M_1-*40*] with epoxide.

Compound 1B. Alkylation with propylene oxide, procedure B. ^{1}H NMR (400 MHz, D_2O, 25 ℃): (main peaks) δ 4.66−4.63 (m, 11 H, CHα Met), δ 4.48−4.41 (m, 80 H, CHα Val and Pro, VPGXG), 4.37-4.28 (m, 11H, CHOH Met, signal β), 4.19-4.17 (d, 30 H, CHα Val, VPGVG), 3.59-3.39 (m, 22H, CHCH_2S Met, signal α), 3.01-2.98 (dd, 33 H, SCH_3 Met), 1.38-1.36 (dd, 33 H, CH_3CHOH Met, signal γ), 1.00−0.93 (br m, 420 H, CH_3 Val). Yield= 88 %.

Compound 2B. Alkylation with glycidyl propargyl ether, procedure B. ^{1}H NMR (400 MHz, D_2O, 25°C): (main peaks) δ 4.66−4.62 (m, 11 H, CHα Met), δ 4.47−4.41 (m, 80 H, CHα Val and Pro, VPGXG), 4.38-4.36 (m, 11 H, CHOH Met, signal β), 4.29-4.28 (d, 22 H, CH_2 Met,

signal δ), 4.18-4.16 (d, 30 H, CHα Val, VPGVG), 3.63-3.52 (m, 22 H, $CHCH_2S$ Met, signal α), 3.03-3.00 (dd, 33 H, SCH_3 Met), 2.95 (t, 3 H, CH alkyne), 1.38-1.36 (dd, 33 H, CH_3CHOH Met), 1.00−0.94 (br m, 420 H, CH_3 Val). Yield= 86 %.

Compound 3B. Alkylation with allyl glycidyl ether, procedure B. ^{1}H NMR (400 MHz, D_2O, 25 ℃): (main peaks) δ 6.01-5.91 (m, 11 H, CH alkene, signal ε), δ 5.37-5.27 (m, 22 H, CH_2 alkene, signal #), 4.64−4.62 (m, 11 H, CHα Met), δ 4.47−4.40 (m, 80 H, CHα Val and Pro, VPGXG), 4.37-4.35 (m, 11 H, CHOH Met, signal β), 4.18-4.16 (d, 30 H, CHα Val, VPGVG), 4.11-4.10 (d, 22 H, CH_2 Met, signal δ), 3.02-2.99 (dd, 33 H, SCH_3 Met), 1.00−0.93 (br m, 420 H, CH_3 Val). Yield= 89 %, functionalization 95 %.

2.2.3 Alkylation of ELP[V_3M_1-*40*] with oxaziridine derivatives

General procedure. To a solution of ELP[V_3M_1-*40*] (50 mg, 2.9 μM) in degassed water (50 mL) under Ar. atmosphere was added a solution of oxaziridine derivative synthesized as described by Lin and co-workers (Supporting information) (6 equiv. per Met) in DMF (200 μL). After stirring for 30-60 mins, DCM (20 mL) was added and the mixture was extracted with DCM for two times to remove the benzaldehyde. The combined water layer were then dialyzed (MWCO 3k) against Milli-Q water for 12h (changing water every 4 h). The final product was obtained by lyophilization.

Compound 1C. Alkylation with Ox-ethyl. ^{1}H NMR (400 MHz, D_2O, 25 ℃): (main peaks) δ 4.47−4.40 (m, 80 H, CHα Val and Pro, VPGXG), 4.18-4.17 (d, 30 H, CHα Val, VPGVG), 3.14-3.09 (q, 22 H, CH_2 Met signal α), 3.07-2.95 (m, 22 H, CH_2S Met, signal l), 2.70 (s, 33 H, SCH_3 Met), 1.09-1.05 (dt, 33 H, CH_3CH_2 Met, signal β), 1.00−0.93 (br m, 420 H, CH_3 Val). Yield = 63 %.

Compound 2C. Alkylation with Ox-alkyne. ^{1}H NMR (400 MHz, D_2O, 25°C): (main peaks) δ 4.47−4.40 (m, 80 H, CHα Val and Pro, VPGXG), 4.18-4.17 (d, 30 H, CHα Val, VPGVG), 3.13-3.01 (m, 22 H, CH_2 Met signal l), 2.73 (s, 33 H, SCH_3 Met), 2.58 (t, 11 H, CH-Alkyne, signal β), 1.00-0.93 (br m, 420 H, CH_3 Val). Yield = 94 %.

Compound 3C. Alkylation with Ox-N_3. ^{1}H NMR (400 MHz, D_2O, 25°C): (main peaks) δ 4.47−4.41 (m, 80 H, CHα Val and Pro, VPGXG), 4.19-4.17 (d, 30 H, CHα Val, VPGVG), 6.40-3.36 36 (t, 22 H, CH_2-N_3, signal γ), 3.24-3.20 (t, 22 H, CH_2-NH Met signal α), 3.13-3.03 (m,

22 H, CH_2S Met, signal l), 2.75 (bs, 33 H, SCH_3 Met), 1.80-1.73 (q, 22 H, -CH_2-$\underline{CH_2}$-CH_2-Met, signal β), 1.00−0.93 (br m, 420 H, CH_3 Val). Yield = 85 %

2.2.4 Demethylation of modified-ELP

General procedure. To a solution of modified- ELP[V_3M_1-*40*] (50 mg, 10 mM) in 75% EtOH(aq) was added ammonium pyrrolidinedithiocarbamate (APDC) (5.0 equiv per Met residue). The solution was stirred under Ar. for 24 h at room temperature. The obtained mixture was transferred to a 1 kDa MWCO dialysis bag and dialyzed against 50% MeOH(aq) during 24 h with 3 solvent changes followed by 8 h dialysis against Milli-Q water with 3 changes. The dialysis bag contents were then lyophilized to provide demethylated ELPs.

Compound 1D. Demethylation of compound 1B (propylene oxide). ^{1}H NMR (400 MHz, D_2O, 25°C): (main peaks) δ 4.58−4.55 (m, 11 H, CHα Met), δ 4.47−4.40 (m, 80 H, CHα Val and Pro, $\underline{VP}$GXG), 4.19-4.17 (d, 30 H, CHα Val, VPG$\underline{V}$G), 2.70-2.55 (m, 22 H, $\underline{CH_2}$S, signal l), 1.25-1.23 (d, 33 H, $\underline{CH3}$CHOH), 1.00−0.93 (br m, 420 H, CH_3 Val). Yield= 44 %.

2.2.4 Click reaction

General procedure. To a solution of ELP[V_3M_1-*40*] derivative in degassed water (5 mg/mL) under Ar. Atmosphere, the desired azido-functionalized monosaccharide (1.5 equiv. per alkyne) was added. A solution of Cu(I) was prepared by addition of sodium ascorbate (1.3 equiv. per alkyne) to a degassed solution of Cu(II)SO_4 (0.26 equiv. per alkyne) and pentamethyldiethylenetriamine (0.26 equiv. per alkyne) in Milli-Q water. The fresh Cu(I) solution was then transferred to the reaction mixture with a syringe. The reaction was stirred under Ar. at room temperature for 72 hrs. Cuprisorb was added to remove cupper by shaking overnight. Few drops of an aqueous solution of EDTA (0.15 M) were added and the solution was purified by ultracentrifugation with Amicon® 3000 MWCO ultra-centrifugal filter tube against Milli-Q water (40 mL). The remaining mixture was lyophilized.

Compound 4B. Click-reaction of compound 2B with β-D-galactopyranosyl azide. ^{1}H NMR (400 MHz, D_2O, 25°C): (main peaks) δ 8.34 (s, 11 H, CH triazole proton), δ 5.74-5.72 (d, 11 H, $CH_{1'}$), δ 4.65−4.61 (m, 11 H, CHα Met), δ 4.47−4.42 (m, 80 H, CHα Val and Pro, $\underline{VP}$GXG), 4.40-4.36 (m, 11 H, CHOH Met, signal β), 4.18-4.16 (d, 30 H, CHα Val, VPG$\underline{V}$G), 3.81-3.80

(d, 11 H, $CH_{6'}$), 299-2.97 (m, 33 H, SCH_3 Met), 1.00−0.92 (br m, 420 H, CH_3 Val). Yield= 71 %.

2.3 Characterization methods

NMR spectrometry analysis

^{1}H NMR analyses were performed in D_2O at 298 K on a Bruker AVANCE III HD 400 apparatus equipped with a 5 mm Bruker multinuclear z-gradient direct probe operating at 400.2 MHz. The solvent signal was used as the reference signal (δ = 4.79 ppm). HSQC analyses were performed on a Bruker AVANCE NEO 400 spectrometer operating at 100.7 MHz, equipped with a 5 mm Bruker multinuclear z-gradient direct cryoprobe-head operating at 298 K. Data processing was performed using Bruker Topspin Software.

Transition temperature measurements

Turbidity assays were performed on a Cary 100 Bio UV-visible spectrometer equipped with a multi-cell thermoelectric temperature controller from Varian (Palo Alto, CA) operating at 600 nm between 20 ℃ and 80 ℃ at a 1 ℃.min-1 scan rate for ELP[V_3M_1-*40*], compound 1A, 1B, 1C and 1D in Tris buffer at four different concentrations (25 µM, 50 µM, 125M and 250 µM).

Size-exclusion chromatography (SEC)

Measurements in water were performed on an Ultimate 3000 system from Thermoscientific equipped with diode array detector DAD. The system also include a multi-angles light scattering detector MALS and differential refractive index detector dRI from Wyatt technology. Polymers were separated on two TOSOH successive columns (one G4000PWXL (7.8*300) column with exclusion limits from 2 000 Da to 300 000 Da and one G3000PWXL (7.8*300) column with exclusion limit bellow 40 000 Da). Measurements were performed at a flowrate of 0.6 mL/min and columns temperature was held at 26 ℃. Aqueous solvent composed by Acetic Acid (AcOH) 0.3 M, Ammonium Acetate 0.2 M and ACN (6.5/3.5, v/v) was used as the eluent. Ethylene glycol was used as flow marker.

3. RESULTS AND DISCUSSION

We specifically focused on a forty repeat unit-ELP containing periodically spaced methionine residues namely ELP[V_3M_1-*40*] following established nomenclature.[33] ELP[V_3M_1-*40*] was

produced recombinantly in *Esherichia coli* bacteria and purified by *inverse transition cycling* as described previously.[31] This particular ELP was chosen for its intermediate methionine content (one Met every four pentapeptide units, corresponding to a total of 10 methionine in addition to the *N*-terminal Met residue) and T_t in a suitable temperature range for further turbidimetry studies (*i.e.*, 32 ℃ at 250 μM in water). ELP[V_3M_1-*40*] was chemoselectively modified on methionine residues using either the alkyl halide method (Figure 1, route A), epoxide chemistry, (Figure 1, route B), or the recently reported ReACT method[28] (Figure 1, route C).

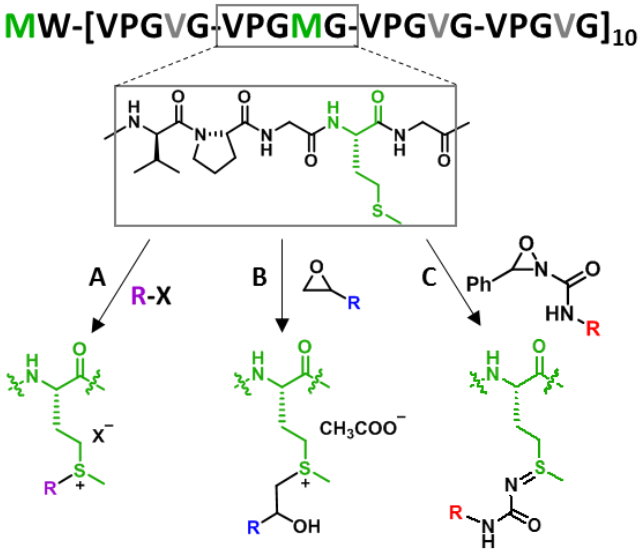

Figure 1. Primary structure of ELP[V_3M_1-*40*] and chemoselective modifications at methionine residues using alkyl halide (A), epoxide (B) or oxaziridine (C) reagents.

A small series of ELP derivatives was synthesized following each of the three synthetic routes so as to introduce various pendant groups (R groups in Figure 1) onto methionine residues' side chain. (Table 1) Short alkyl chains, such as methyl or ethyl, were introduced (compounds 1A, 1B[29] and 1C) in order to compare within similar conditions. The thermo-responsive properties of the resulting ELP derivatives from different type of modification methods were compared to the pristine ELP. ELP derivatives containing functional reactive groups such as alkyne, alkene, or azido groups were also designed with the aim of further investigating post-modification reactions.

3.1 Chemoselective modifications at methionine residues using alkyl halide

In route A, ELP[V_3M_1-*40*] was dissolved in aqueous formic acid before to add a large excess of the corresponding alkyl halide and the mixture was stirred for 5 days under argon atmosphere, as already published for both ELP[M-*20*][30] and ELP[V_3M_1-*40*].[31] Using these conditions, ELP[V_3M_1-*40*] was chemoselectively modified with iodomethane and compound 1A was obtained after purification by dialysis using ultra-centrifugal filter tube against Milli-Q water. With the goal to incorporate functional group to ELP[V_3M_1-*40*] and inspired by the work of Kramer and co-workers[26], propargyl bromide was used in the same conditions as compound 1A however the reaction was not completed. Even after trying different reaction conditions such as increasing the alkyl halide equivalents or the reaction time and changing the organic co-solvent and/or the aqueous conditions, the functionalization rate was only 40% (compound 2A).

3.2 Chemoselective modifications at methionine residues using epoxide

New batches of compound 1B, 2B and 3B were synthesized following pathway B and according to previously established procedure[31,34] in order to perform complementary analysis. Considering the high molecular weight of ELP[V_3M_1-*40*] and as already reported, a mixture of AcOH/HFIP (9/1, v/v) was necessary to access all the Met and therefore perform a complete functionalization within 2 days of reaction. It's worth noting that in these conditions, Met is highly sensitive to oxidation, careful attention should be paid to maintain all the reagents and the reaction mixture under argon atmosphere in order to avoid sulfoxide side product formation.

3.3 Chemoselective modifications at methionine residues using ReACT

Finally, the newest ReACT strategy was explored to turn ELP[V_3M_1-*40*] into sulfimide through an oxidative sulfur imidation reaction and introduce different functionalities. In this way, three oxaziridines derivatives substituted with a weak electron-withdrawing urea linkage allowing high selectivity for the NTP were prepared following procedure optimized by Lin, Yang and co-workers.[28] The imidation reaction was performed under argon atmosphere in aqueous conditions containing 1% of DMF within 30-60 minutes after the addition of the corresponding oxaziridine derivative. After extraction of the excess oxaziridine and benzaldehyde side product through extraction with DCM, the aqueous phase was purified by dialysis to give compounds 1C, 2C or 3C.

3.4 NMR analysis of chemoselective modified ELPs at methionine residues

All compounds were synthesized and isolated in good purity as evidenced by size-exclusion chromatography (Figure S1), and obtained with isolated yields ranging from 75 % to 90 % (Table 1). Functionalization rates corresponding to the percentage of modified methionine were determined by ^{1}H NMR spectroscopy by precise integration of the shifted signal resulting from the resonance of the methyl protons of the thioether as compare to the reference peak corresponding to the asymmetric protons signal of the guest residue valine (signal i) integrating for 30 H (not affected after any of the modifications). NMR spectra of all derivatives are provided in Figures S8-S18. Small alkyl chains were introduced quantitatively whatever the route used, derivatives 1A, 1B, and 1C (Figure S8, S9 and S13, respectively) being obtained with complete functionalization rates (100%). Regarding the modification of ELP[V_3M_1-*40*] with functional groups, the ReACT method have shown excellent results with total incorporation of either alkyne or azide handle in less than one hour yielding, respectively, compounds 2C and 3C (Figure S14-S15). Owing to minor methionine oxidation into sulfoxide (0.5 Met over 11 total), compounds 2B and 3B were synthesized with slightly lower functionalization rate (>95%) using the epoxide chemistry strategy (Figure S11-S12). However, introduction of an alkyne group using propargyl bromide proved more difficult and a maximum functionalization rate of 40 % was obtained for compound 2A. Attempts to increase this functionalization rate by increasing the equivalence of propargyl bromide, prolonging the reaction time or playing with different solvents, did not lead to any improvement.

	Compound	Reagent	MW (g.mol^{-1})	Funct.[a]	Yield[b]	Tt (125 µM)[c]
A) Alkyl halide	1A[d]	R =  X = I	18,597	100 %	75 %	> 70 °C
R-X	2A	R = X = Br	18,344	ca. 40 %	81 %	n.d.
B) Epoxide	1B[d]	R =	18,335	100 %	88 %	> 70 °C
	2B[d]	R = 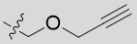	18,929	> 95 %	90 %	> 70°C
	3B[d]	R = 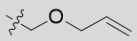	18,952	> 95 %	89 %	n.d.
C) Oxaziridine	1C	R = 	17,982	100 %	88 %	57 °C
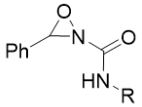	2C	R = 	18,092	100 %	92%	54 °C
	3C	R = 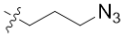	18,588	100 %	85 %	48 °C

Table 1. *Characteristics of modified ELP[V_3M_1-40] derivatives. Solvent conditions: A) THF/0.2 M aqu. formic acid; B) AcOH/HFIP (9:1); and C) H_2O/DMF (99.5:0.5).* [a]

Functionalization rate determined by [1]H NMR, [b] Yield of reaction, [c] Transition temperature in Tris buffer determined by DLS, [d] Synthesized following previous published procedure.[31]

Overall, with a longer reaction time (5 days) and a lower functionalization rate for compound 2A, the alkyl halide route (A) did not prove as efficient as the epoxide (B) or oxaziridine (C) routes. As previously reported,[31,34] we noted that epoxide chemistry is also more versatile than the use of alkyl halides for the thioalkylation of ELP[V_3M_1-*40*]. Specific care is however needed to avoid oxidation of the sensitive thioether group. The ReACT approach[28] based the use of oxazidine derivatives was found very efficient with short reaction times (1 hour) and quantitative functionalization rates. One drawback of this strategy is however the tedious synthesis and purification of oxaziridine derivatives obtained in poor yields (30 % - 40 %) as already mentioned by Lin *et al*.[28]

3.5 Tuning T_t by chemoselective modification at methionine residues

In order to evidence the impact of each type of modification onto the thermo-responsive properties, turbidity experiments were performed on derivatives with similar alkyl R groups, namely compounds 1A, 1B and 1C. Transition temperature measurements were performed at different ELP concentrations in Tris buffer using light absorption at 600 nm (Figure 2, Figures S3-S6). The T_t values were determined as the temperature corresponding to the onset of turbidity (Figure 2C and Table S1). As shown in Figure 2A, thioalkylated derivatives 1A and 1B presented none or very weak thermo-responsive properties in the temperature and concentration ranges studied. As already reported by our group, this can be directly attributed to the increased hydrophilicity and solubility afforded by the sulfonium groups present along the polypeptide chain.[31] Besides, strong effect of the nature of the counterion on the thermo-responsive behavior of ELP[V_3M_1-*40*] has been previously demonstrated with iodine and acetate anions resulted in samples with weak thermos-responsive properties. This is consistent with the current observed results where acetate counterion involved a slightly higher thermo-responsiveness as compare to iodine counterion (Figure 2C).

Compound 1C obtained from the modification of ELP[V_3M_1-*40*] through the ReACT strategy surprisingly presented very high T_ts in the 25–250 µM concentration range despite a higher molecular weight than ELP[V_3M_1-*40*] and the uncharged linkage between the ethyl R group and the methionine side chain (Figure S4, S6). We may also suspect the keto-enol equilibrium of the sulfimide-urea structure and possible H-bonds formation to be responsible for an

increased overall hydrophilicity of 1C as compared to the pristine ELP. In order to confirm these hypotheses and have access to a synthetic strategy leading to chemoselectively modified methionine side chains while retaining the thermo-responsive properties of the ELP, we have performed a demethylation of compound 1B (Scheme S1). The resulting uncharged compound 1D (^{1}H NMR Figure S10) was indeed found to recover its thermal responsiveness with a range of T_ts closer to those of ELP[V_3M_1-*40*] (Figure 2B). The presence of the hydroxyl group in the S-alkyl-L-homocysteine-containing derivative is however likely attributed to the slightly higher T_ts of 1D (31-43 ℃) than those of ELP[V_3M_1-*40*] (30-37 ℃). T_t versus concentration curves were measured for uncharged derivatives 1C and 1D for comparison with ELP[V_3M_1-*40*] (Figure 2B) and fitted plots obtained using the empirical equation (eq 1) established by Chilkotti and co-workers (Figures S2).[35] For both 1C and 1D, the slope of the fits were found steeper than the one observed with the pristine ELP[V_3M_1-*40*] confirming their greater hydrophilic character. Importantly, additional studies confirmed the maintained reversibility of the thermal transition for both 1C and 1D derivatives (Figure S4-S5).

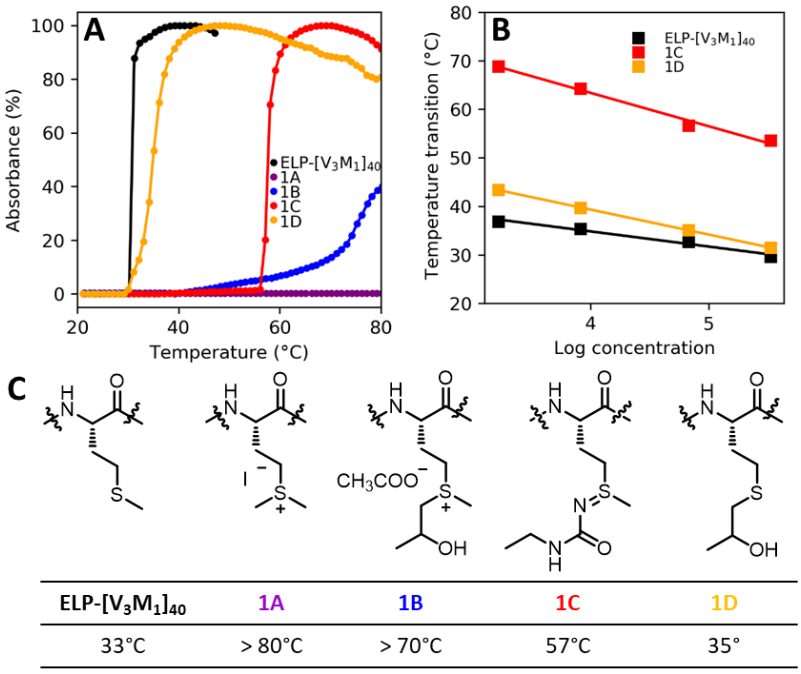

ELP-[V_3M_1]$_{40}$	1A	1B	1C	1D
33°C	> 80°C	> 70°C	57°C	35°

Figure 2. *(A) Relative absorbance at 600 nm of ELP[V_3M_1-40], 1A, 1B, 1C and 1D at 125 µM in Tris buffer as a function of temperature. (B) T_t values of ELP[V_3M_1-40], 1C and 1D as functions of concentration in Tris buffer. Lines correspond to the fits of the data using eq1. (C) Chemical structures of the methionine residues' side chain for each derivative and their corresponding onset transition temperature (T_t) at 125 µM in Tris buffer.*

3.6 Chemoselective grafting payloads onto modified ELPs at methionine residues

In this study, we were also particularly interested in exploring subsequent orthogonal post-modifications using "click chemistry" to allow the grafting of a wide variety of relevant molecules onto ELPs such as bioactive moities, active drugs, contrast agents, *etc*. With potentially three strategies in hand to chemoselectively modify ELPs at methionine residues, we wished to investigate the functionalization of ELP[V_3M_1-*40*] with azido-galactose as illustrated on Scheme 1. As unsatisfying functionalization was obtained for compound 2A, this strategy was no further continued. Functionalization of compound 2B with azido-galactose in aqueous conditions gave compound 4B with full conversion. This result was confirmed by ^{1}H and HSQC NMR spectroscopy (Figure S16-S18), in particular thanks to the resonance peak of the triazole proton at 8.34 ppm integrating as 11 ^{1}H, indicating a full bioconjugation. We also noticed that the original resonance of the methylene in α position of the alkyne function shifted from 4.29 ppm to 4.79 ppm, this being the result of the deshielding induced by the increased electron density of the triazole as compared to the alkyne bond (Figure S17). Surprisingly, the functionalization of compound 2C with azido-galactose performed using similar reaction conditions (0.26 equiv. $CuSO_4$ per alkyne, 1.3 equiv. sodium ascorbate per alkyne and 0.26 equiv. PMDETA per alkyne in Milli-Q water) yielding in incomplete bioconjugation. Despite many attempts to solve this issue, especially playing with catalytic conditions, for example using tris((1-benzyl-4-triazolyl)methyl)amine (TBTA) as a catalyst, the highest conversion only reached 65 % corresponding to an average of 7 galactose units onto the ELP using catalytic conditions in aqueous copper sulfate system. Although we do not completely explain this result, we suspect the nitrogen atoms of the sulfimide bond and ELP backbone to participate to the competitive coordination of copper(I) therefore reducing its catalytic activity towards the adjacent alkyne bond and resulting in incomplete functionalization.

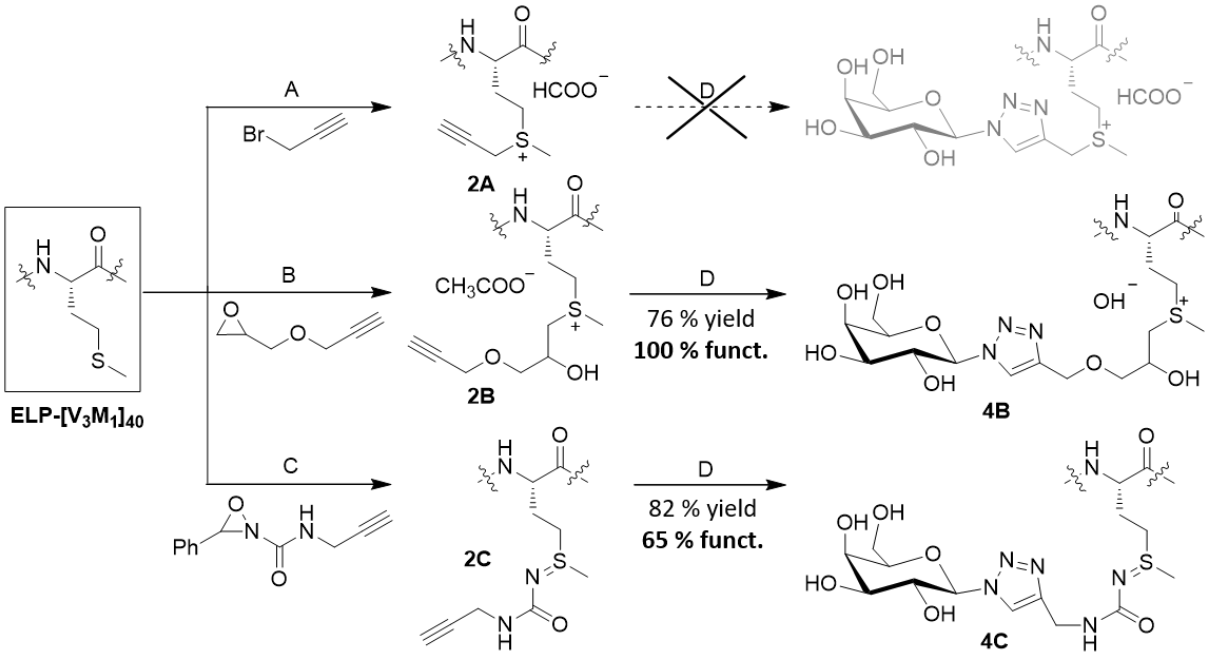

Scheme. 1. Synthetic strategies to chemoselectively graft galactose units onto ELP[V_3M_1-*40*].

CONCLUSION

To conclude, we have herein explored a new route for chemoselectively modifying methionine-containing ELPs using oxaziridine-based reagents, providing an additional means for easily tuning the thermo-responsive properties of recombinant ELPs. This enlarges the variety of accessible ELP derivatives through sulfonium, thioether or sulfimide linkages. Still, with commercially available reagents, reasonable reaction times and high efficiency, the epoxide-based route is highly favorable. The possibility to recover a thioether bond by sulfonium demethylation adds on to the list of advantages of this chemical route. Altogether, the set of reactions used in this study opens up a whole range of new possibilities to functionalize ELPs with a large variety of molecules for the design of new ELP bioconjugates.

REFERENCES

(1) Abascal, N. C.; Regan, L. The Past, Present and Future of Protein-Based Materials. *Open Biol.* **2018**, *8* (10), 180113. https://doi.org/10.1098/rsob.180113.
(2) van Hest, J. C. M.; Tirrell, D. A. Protein-Based Materials, toward a New Level of Structural Control. *Chem. Commun.* **2001**, No. 19, 1897–1904. https://doi.org/10.1039/b105185g.
(3) Capezza, A. J.; Newson, W. R.; Olsson, R. T.; Hedenqvist, M. S.; Johansson, E. Advances in the Use of Protein-Based Materials: Toward Sustainable Naturally Sourced Absorbent Materials. *ACS Sustain. Chem. Eng.* **2019**, *7* (5), 4532–4547. https://doi.org/10.1021/acssuschemeng.8b05400.
(4) Silva, N. H. C. S.; Vilela, C.; Marrucho, I. M.; Freire, C. S. R.; Pascoal Neto, C.; Silvestre, A. J. D. Protein-Based Materials: From Sources to Innovative Sustainable Materials for Biomedical Applications. *J. Mater. Chem. B* **2014**, *2* (24), 3715. https://doi.org/10.1039/c4tb00168k.
(5) Urry, D. W.; Urry, K. D.; Szaflarski, W.; Nowicki, M. Elastic-Contractile Model Proteins: Physical Chemistry, Protein Function and Drug Design and Delivery. *Adv. Drug Deliv. Rev.* **2010**, *62* (15), 1404–1455. https://doi.org/10.1016/j.addr.2010.07.001.
(6) Kowalczyk, T.; Hnatuszko-Konka, K.; Gerszberg, A.; Kononowicz, A. K. Elastin-like Polypeptides as a Promising Family of Genetically-Engineered Protein Based Polymers. *World J. Microbiol. Biotechnol.* **2014**, *30* (8), 2141–2152. https://doi.org/10.1007/s11274-014-1649-5.
(7) Urry, D. W. Physical Chemistry of Biological Free Energy Transduction As Demonstrated by Elastic Protein-Based Polymers. *J. Phys. Chem. B* **1997**, *101* (51), 11007–11028. https://doi.org/10.1021/jp972167t.
(8) Rauscher, S.; Pomès, R. The liquid structure of elastin https://elifesciences.org/articles/26526 (accessed Jul 26, 2019). https://doi.org/10.7554/eLife.26526.
(9) MacEwan, S. R.; Chilkoti, A. Elastin-like Polypeptides: Biomedical Applications of Tunable Biopolymers. *Biopolymers* **2010**, *94* (1), 60–77. https://doi.org/10.1002/bip.21327.
(10) Garanger, E.; MacEwan, S. R.; Sandre, O.; Brûlet, A.; Bataille, L.; Chilkoti, A.; Lecommandoux, S. Structural Evolution of a Stimulus-Responsive Diblock Polypeptide Micelle by Temperature Tunable Compaction of Its Core. *Macromolecules* **2015**, *48* (18), 6617–6627. https://doi.org/10.1021/acs.macromol.5b01371.
(11) Walsh, C. T.; Garneau-Tsodikova, S.; Gatto, G. J. Protein Posttranslational Modifications: The Chemistry of Proteome Diversifications. *Angew. Chem. Int. Ed.* **2005**, *44* (45), 7342–7372. https://doi.org/10.1002/anie.200501023.
(12) van Kasteren, S. I.; Kramer, H. B.; Jensen, H. H.; Campbell, S. J.; Kirkpatrick, J.; Oldham, N. J.; Anthony, D. C.; Davis, B. G. Expanding the Diversity of Chemical Protein Modification Allows Post-Translational Mimicry. *Nature* **2007**, *446* (7139), 1105–1109. https://doi.org/10.1038/nature05757.
(13) Davis, B. G. Mimicking Posttranslational Modifications of Proteins. *Science* **2004**, *303* (5657), 480–482. https://doi.org/10.1126/science.1093449.
(14) Amiram, M.; Haimovich, A. D.; Fan, C.; Wang, Y.-S.; Aerni, H.-R.; Ntai, I.; Moonan, D. W.; Ma, N. J.; Rovner, A. J.; Hong, S. H.; et al. Evolution of Translation Machinery in Recoded Bacteria Enables Multi-Site Incorporation of Nonstandard Amino Acids. *Nat. Biotechnol.* **2015**, *33* (12), 1272–1279. https://doi.org/10.1038/nbt.3372.
(15) Kim, W.; George, A.; Evans, M.; Conticello, V. P. Cotranslational Incorporation of a Structurally Diverse Series of Proline Analogues in an Escherichia Coli Expression System. *ChemBioChem* **2004**, *5* (7), 928–936. https://doi.org/10.1002/cbic.200400052.
(16) Catherine, C.; Oh, S. J.; Lee, K.-H.; Min, S.-E.; Won, J.-I.; Yun, H.; Kim, D.-M. Engineering Thermal Properties of Elastin-like Polypeptides by Incorporation of Unnatural Amino Acids in a Cell-Free Protein Synthesis System. *Biotechnol. Bioprocess Eng.* **2015**, *20* (3), 417–422. https://doi.org/10.1007/s12257-015-0190-1.
(17) Johnson, J. A.; Lu, Y. Y.; Van Deventer, J. A.; Tirrell, D. A. Residue-Specific Incorporation of Non-Canonical Amino Acids into Proteins: Recent Developments and Applications. *Curr. Opin. Chem. Biol.* **2010**, *14* (6), 774–780. https://doi.org/10.1016/j.cbpa.2010.09.013.
(18) Sletten, E. M.; Bertozzi, C. R. Bioorthogonal Chemistry: Fishing for Selectivity in a Sea of Functionality. *Angew. Chem. Int. Ed.* **2009**, *48* (38), 6974–6998. https://doi.org/10.1002/anie.200900942.
(19) Baslé, E.; Joubert, N.; Pucheault, M. Protein Chemical Modification on Endogenous Amino Acids. *Chem. Biol.* **2010**, *17* (3), 213–227. https://doi.org/10.1016/j.chembiol.2010.02.008.
(20) King, M.; Wagner, A. Developments in the Field of Bioorthogonal Bond Forming Reactions—Past and Present Trends. *Bioconjug. Chem.* **2014**, *25* (5), 825–839. https://doi.org/10.1021/bc500028d.

(21) Spicer, C. D.; Davis, B. G. Selective Chemical Protein Modification. *Nat. Commun.* **2014**, *5* (1). https://doi.org/10.1038/ncomms5740.
(22) Toennies, G. Sulfonium Reactions of Methionine and Their Possible Metabolic Significance. *J. Biol. Chem.* **1940**, *132* (1), 455–456.
(23) Toennies, G.; Kolb, J. J. Methionine Studies. VIII. Regeneration of Sulfides from Sulfonium Derivatives1. *J. Am. Chem. Soc.* **1945**, *67* (7), 1141–1144. https://doi.org/10.1021/ja01223a031.
(24) Perlmann, G. E.; Katchalski, Ephraim. Conformation of Poly-L-Methionine and Some of Its Derivatives in Solution. *J. Am. Chem. Soc.* **1962**, *84* (3), 452–457. https://doi.org/10.1021/ja00862a026.
(25) Kramer, J. R.; Deming, T. J. Reversible Chemoselective Tagging and Functionalization of Methionine Containing Peptides. *Chem. Commun.* **2013**, *49* (45), 5144. https://doi.org/10.1039/c3cc42214c.
(26) Kramer, J. R.; Deming, T. J. Preparation of Multifunctional and Multireactive Polypeptides via Methionine Alkylation. *Biomacromolecules* **2012**, *13* (6), 1719–1723. https://doi.org/10.1021/bm300807b.
(27) Deming, T. J. Functional Modification of Thioether Groups in Peptides, Polypeptides, and Proteins. *Bioconjug. Chem.* **2017**, *28* (3), 691–700. https://doi.org/10.1021/acs.bioconjchem.6b00696.
(28) Lin, S.; Yang, X.; Jia, S.; Weeks, A. M.; Hornsby, M.; Lee, P. S.; Nichiporuk, R. V.; Iavarone, A. T.; Wells, J. A.; Toste, F. D.; et al. Redox-Based Reagents for Chemoselective Methionine Bioconjugation. *Science* **2017**, *355* (6325), 597–602. https://doi.org/10.1126/science.aal3316.
(29) Christian, A. H.; Jia, S.; Cao, W.; Zhang, P.; Meza, A. T.; Sigman, M. S.; Chang, C. J.; Toste, F. D. A Physical Organic Approach to Tuning Reagents for Selective and Stable Methionine Bioconjugation. *J. Am. Chem. Soc.* **2019**, *141* (32), 12657–12662. https://doi.org/10.1021/jacs.9b04744.
(30) Kramer, J. R.; Petitdemange, R.; Bataille, L.; Bathany, K.; Wirotius, A.-L.; Garbay, B.; Deming, T. J.; Garanger, E.; Lecommandoux, S. Quantitative Side-Chain Modifications of Methionine-Containing Elastin-Like Polypeptides as a Versatile Tool to Tune Their Properties. *ACS Macro Lett.* **2015**, *4* (11), 1283–1286. https://doi.org/10.1021/acsmacrolett.5b00651.
(31) Petitdemange, R.; Garanger, E.; Bataille, L.; Bathany, K.; Garbay, B.; Deming, T. J.; Lecommandoux, S. Tuning Thermoresponsive Properties of Cationic Elastin-like Polypeptides by Varying Counterions and Side-Chains. *Bioconjug. Chem.* **2017**, *28* (5), 1403–1412. https://doi.org/10.1021/acs.bioconjchem.7b00082.
(32) Petitdemange, R.; Garanger, E.; Bataille, L.; Dieryck, W.; Bathany, K.; Garbay, B.; Deming, T. J.; Lecommandoux, S. Selective Tuning of Elastin-like Polypeptide Properties via Methionine Oxidation. *Biomacromolecules* **2017**, *18* (2), 544–550. https://doi.org/10.1021/acs.biomac.6b01696.
(33) Meyer, D. E.; Chilkoti, A. Genetically Encoded Synthesis of Protein-Based Polymers with Precisely Specified Molecular Weight and Sequence by Recursive Directional Ligation: Examples from the Elastin-like Polypeptide System. *Biomacromolecules* **2002**, *3* (2), 357–367. https://doi.org/10.1021/bm015630n.
(34) Gharakhanian, E. G.; Deming, T. J. Versatile Synthesis of Stable, Functional Polypeptides via Reaction with Epoxides. *Biomacromolecules* **2015**, *16* (6), 1802–1806. https://doi.org/10.1021/acs.biomac.5b00372.
(35) Meyer, D. E.; Chilkoti, A. Quantification of the Effects of Chain Length and Concentration on the Thermal Behavior of Elastin-like Polypeptides. *Biomacromolecules* **2004**, *5* (3), 846–851. https://doi.org/10.1021/bm034215n.

SUPPORTING INFORMATION

Synthesis of oxaziridine derivatives

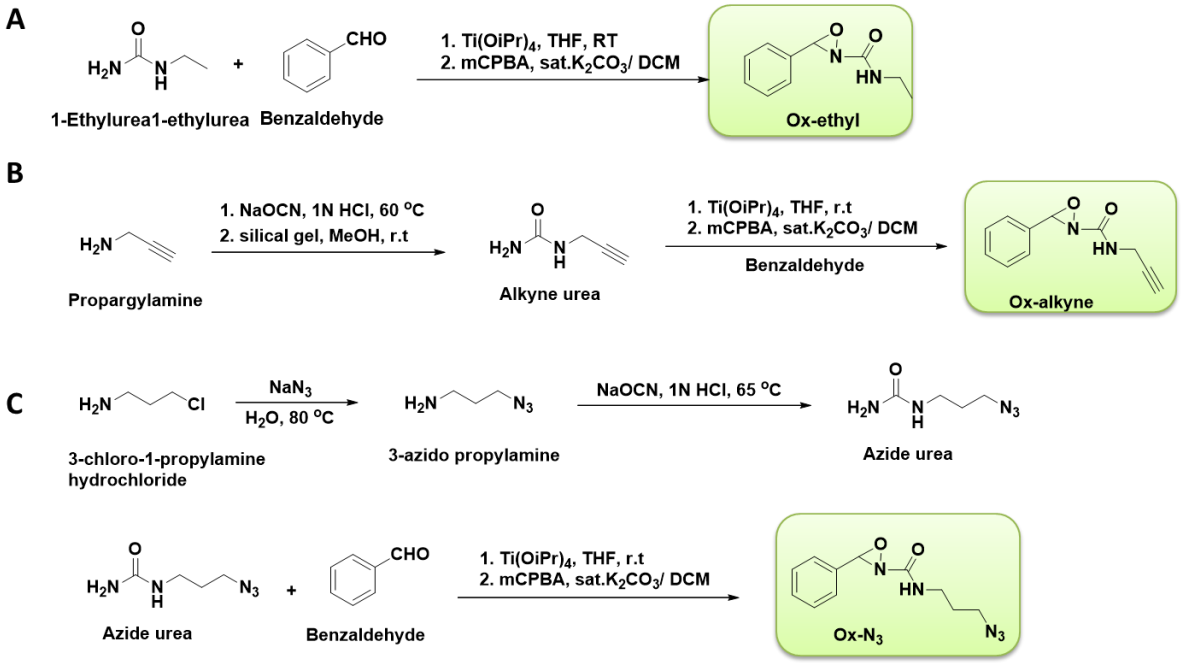

Oxaziridine derivatives were synthesized follow the procedure reported by Lin and co-coworkers.[28] Breifly, the synthetic strategy were based on the amination of benzaldehyde by urea to generate imine and the imine was subsequently oxidized by mCPBA, forming oxzaridine derivatives. The chemical shift of the only proton on oxaziridine ring was found 4.92 ppm in ^{1}H NMR spectra of ox-ethyl, ox-alkyne, ox-N_3, which in agreement with the literature data.

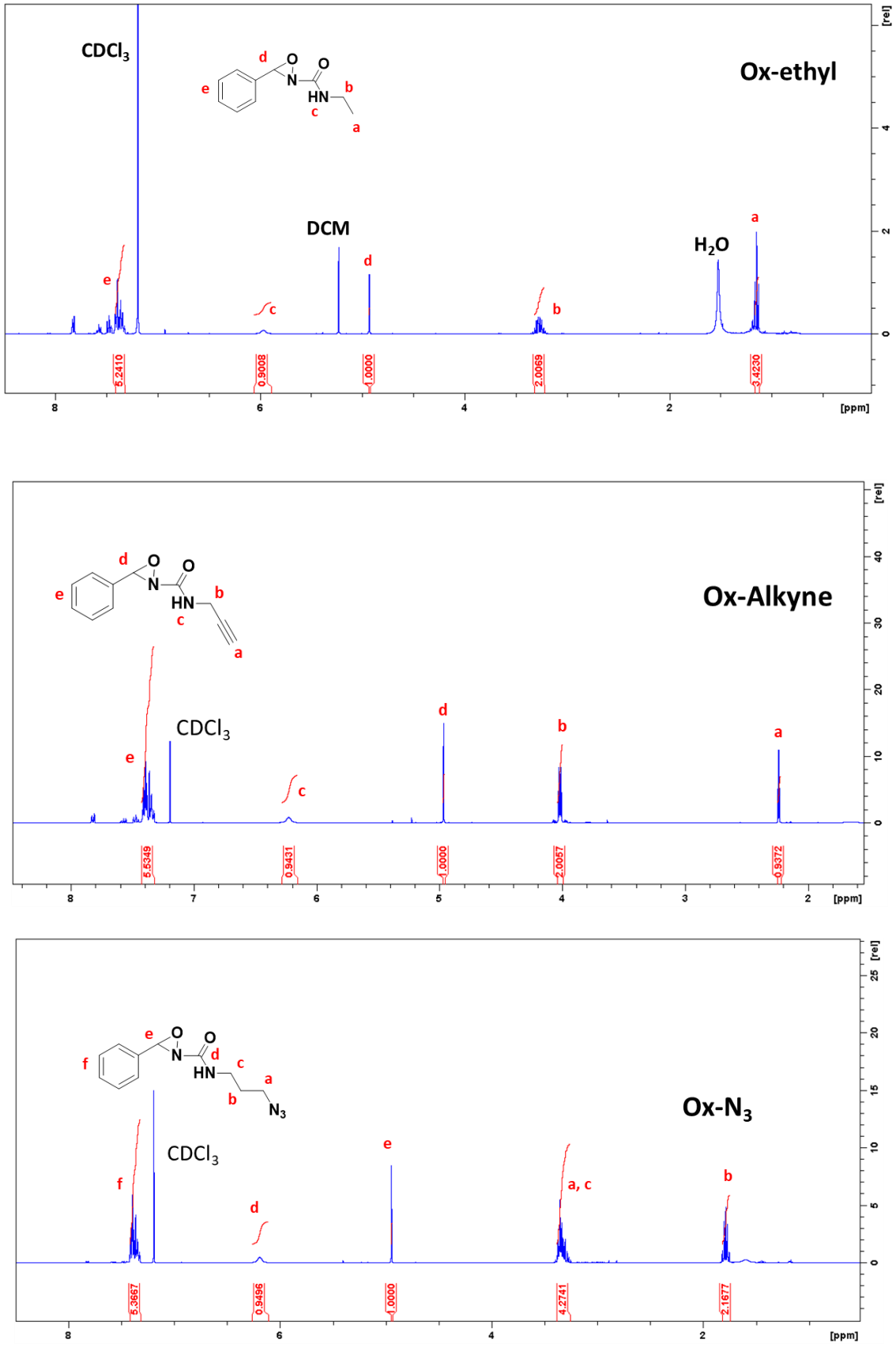

^{1}H NMR spectra of Ox-ethyl, Ox-alkyne, Ox-N_3

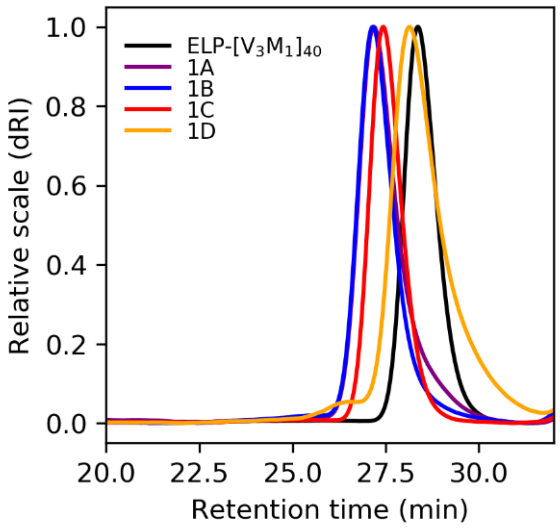

Figure S1. Size exclusion chromatography of ELP[V_3M_1-*40*], compound 1A, 1B, 1C and 1D in AcOH/Ammonium Acetate/CAN eluent.

Concentrations	ELP-$[V_3M_1]_{40}$	1A	1B	1C	1D
25 µM	37°C	> 80°C	> 70°C	69°C	43°C
50 µM	35°C	> 80°C	> 70°C	64°C	40°C
125 µM	33°C	> 80°C	> 70°C	57°C	35°
250 µM	30°C	> 80°C	> 70°C	54°C	31°C

Table S1. Table summarizing the onset temperature of aggregation (T_t) of the derivatives at 125 µM in Tris buffer.

$$T_t = T_{t,c} + \frac{k}{L} ln(\frac{C_c}{C}) \qquad \text{(eq 1)}$$

Figure S2. Empirical equation established by Chilokotti and c-workers.

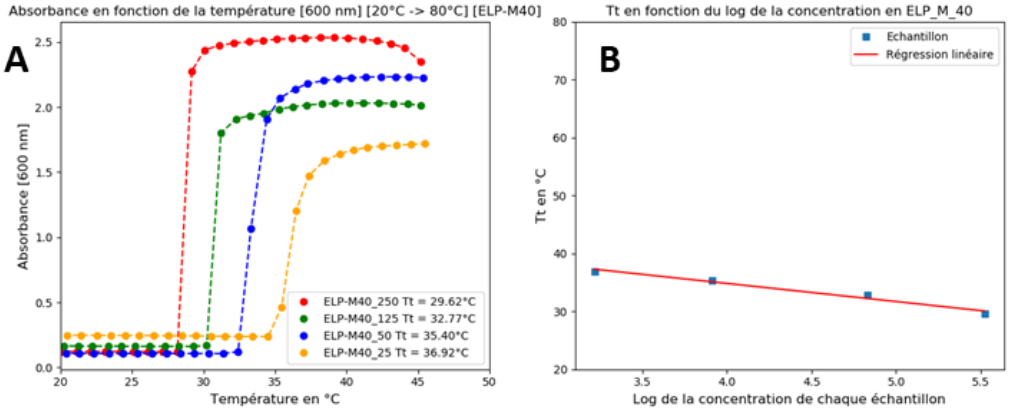

Figure S3. (A) Absorbance of 125 µM solutions of ELP[V_3M_1-*40*] in Tris buffer as function of temperature. (B) T_t values of ELP[V_3M_1-*40*], plotted as functions of sample concentration in Tris buffer; data fitted using eq 1.

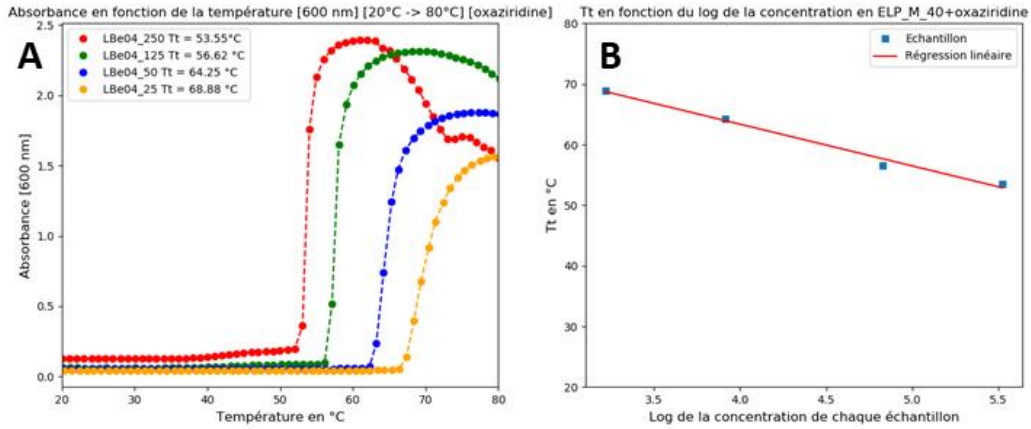

Figure S4. (A) Absorbance of 125 µM solutions of compound 1C in Tris buffer as function of temperature. (B) T_t values of compound 1C, plotted as functions of sample concentration in Tris buffer; data fitted using eq 1.

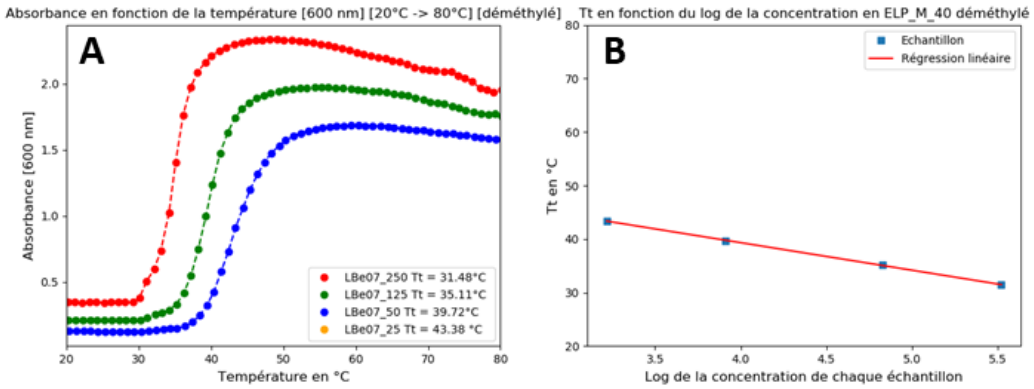

Figure S5. (A) Absorbance of 125 µM solutions of compound 1D in Tris buffer as function of temperature. (B) T_t values of compound 1D, plotted as functions of sample concentration in Tris buffer; data fitted using eq 1.

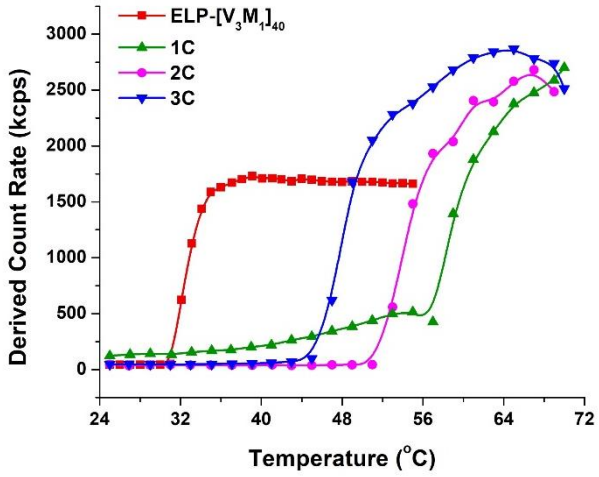

Figure S6. Scattered light intensity of ELP[V_3M_1-*40*], compound 1C, 2C and 3C at 125 µM in Mili-Q water as function of temperature.

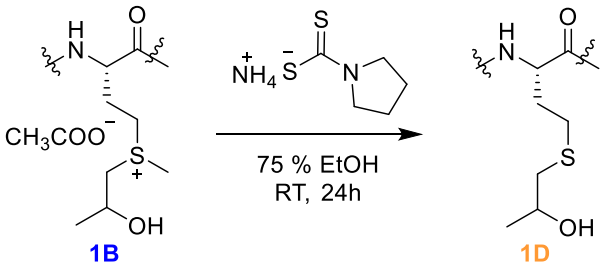

Scheme S1. Demethylation reaction conditions of compound 1B to obtain compound 1D.

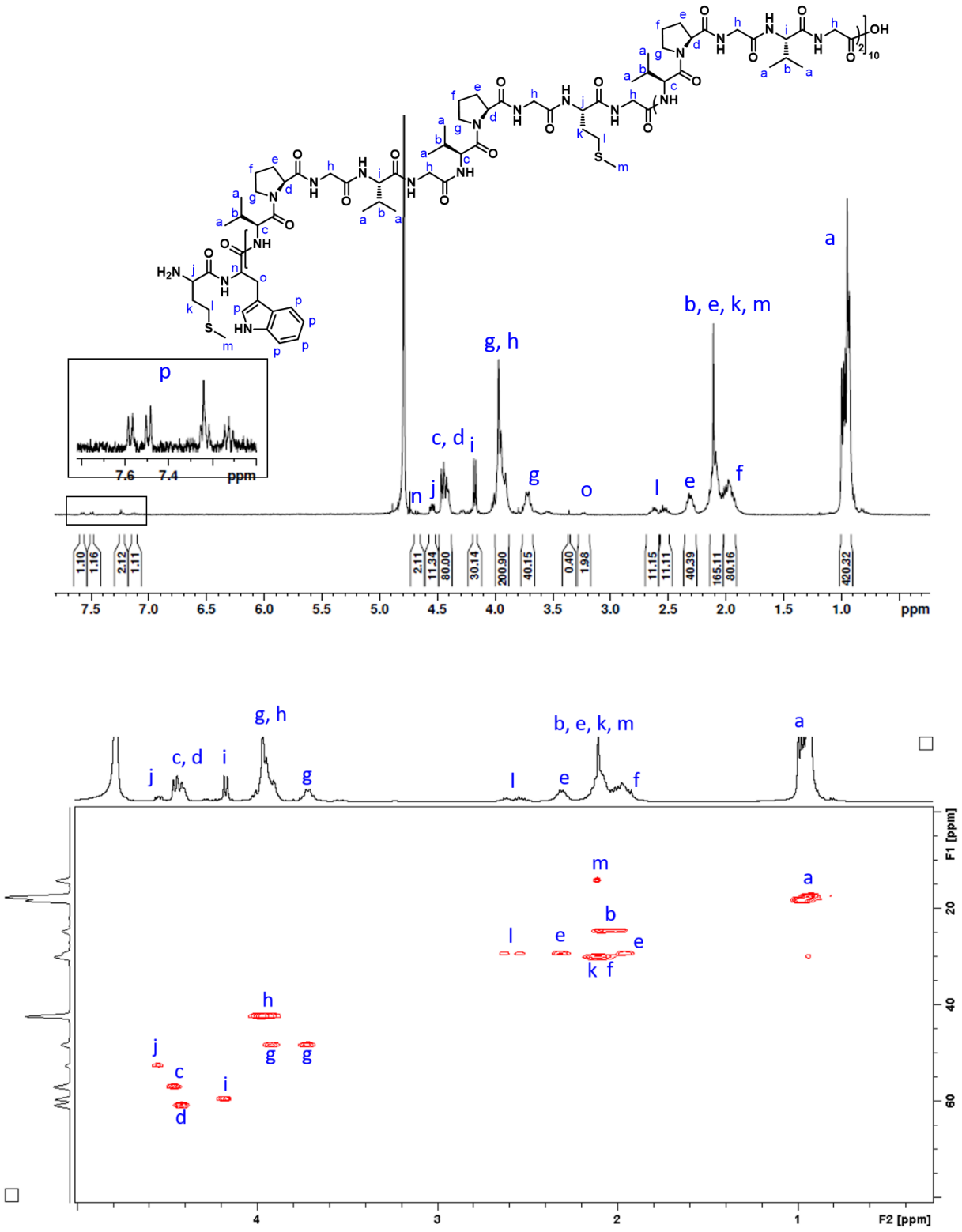

Figure S7. ^{1}H and HSQC NMR spectra of ELP[V_3M_1-*40*] in D_2O

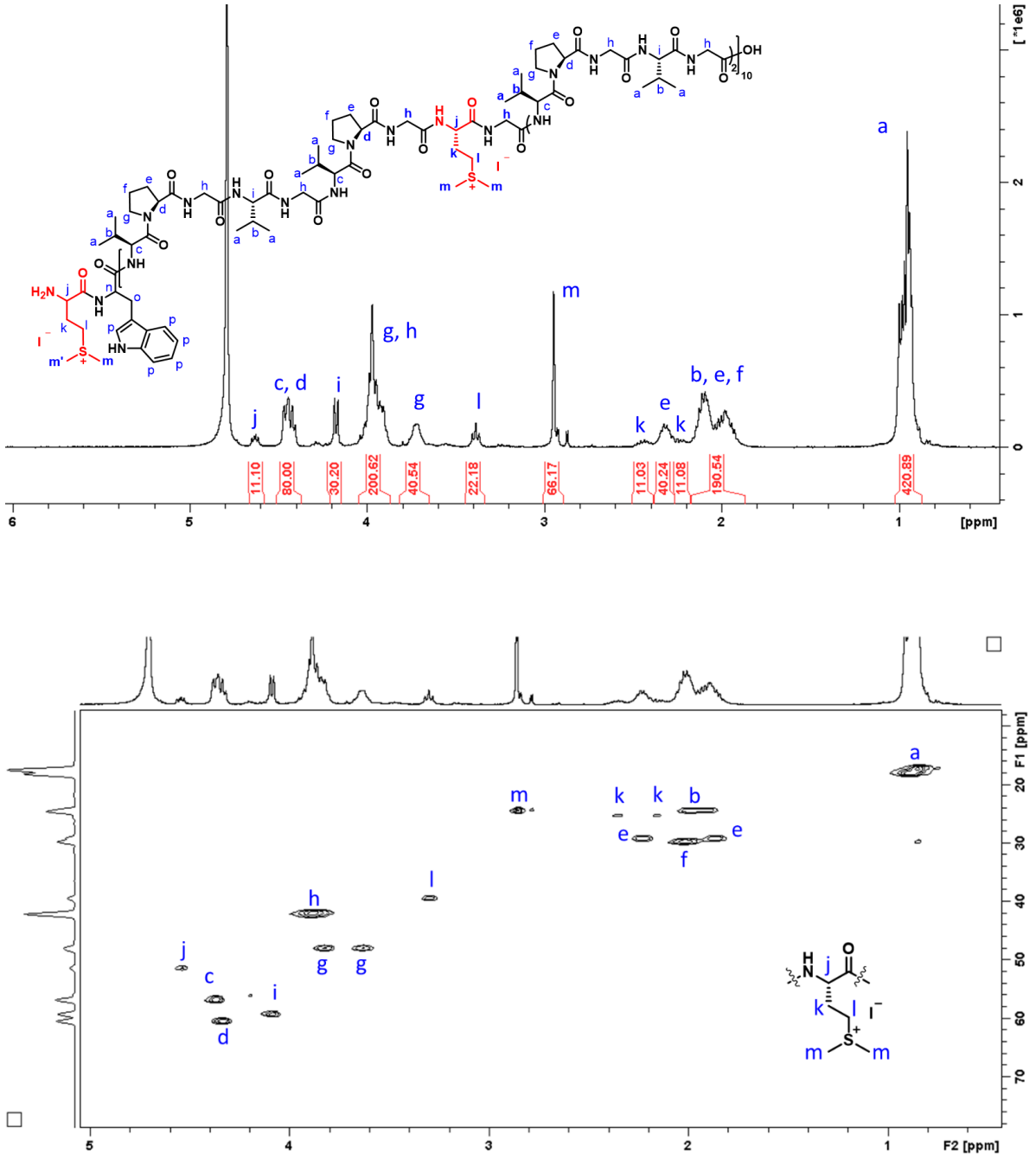

Figure S8. ^{1}H and HSQC NMR spectra of compound 1A in D_2O

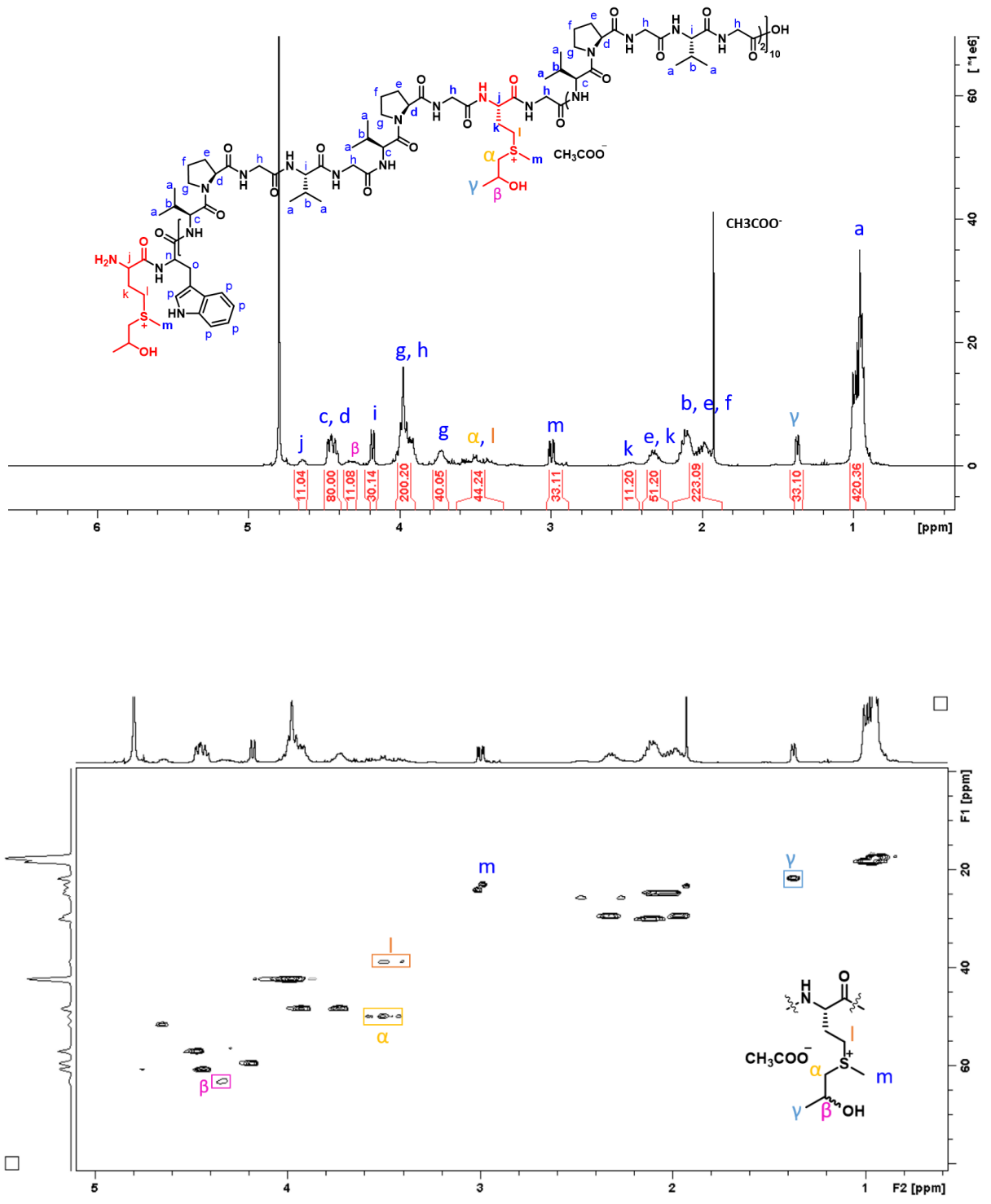

Figure S9. ^{1}H and HSQC NMR spectra of compound 1B in D_2O

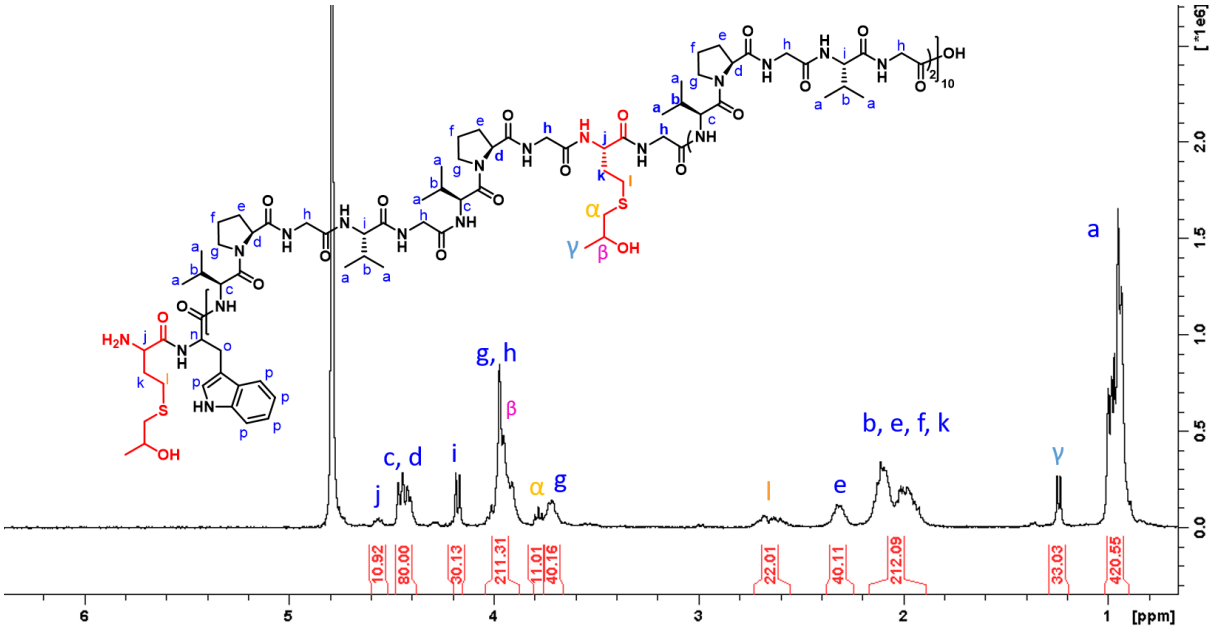

Figure S10. ^{1}H NMR spectra of compound 1D in D_2O

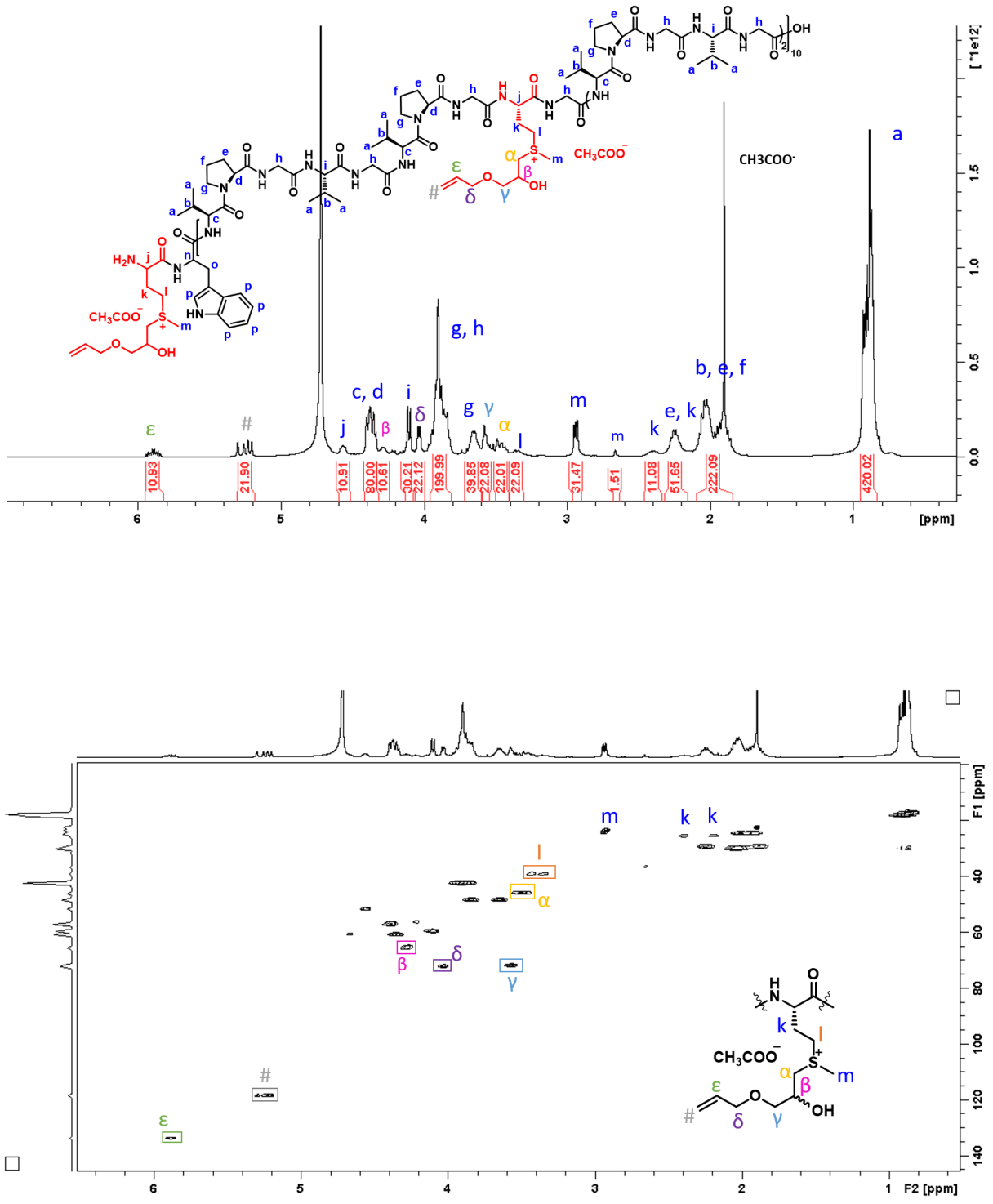

Figure S11. ^{1}H and HSQC NMR spectra of compound 3B in D_2O

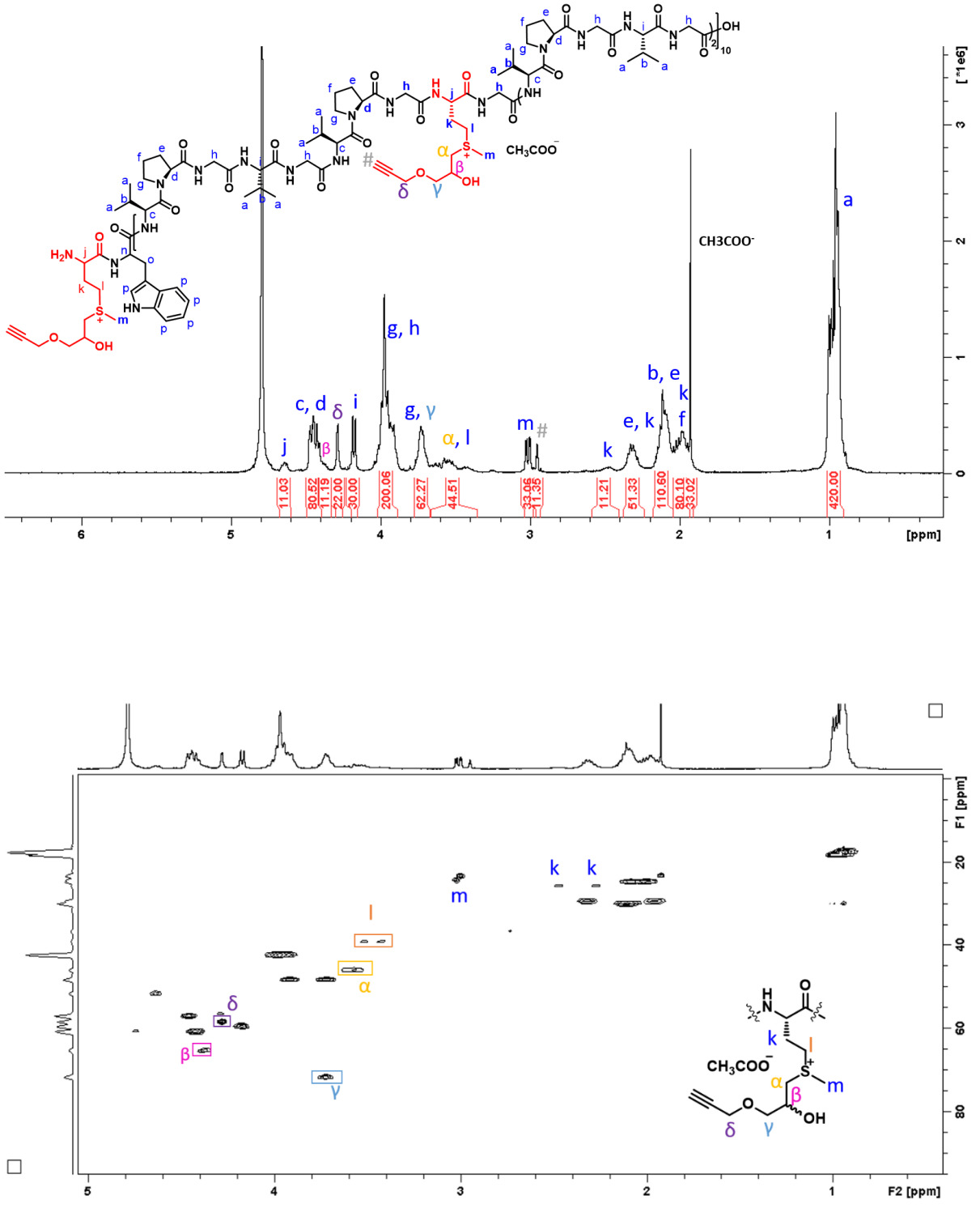

Figure S12. ^{1}H and HSQC NMR spectra of compound 2B in D_2O

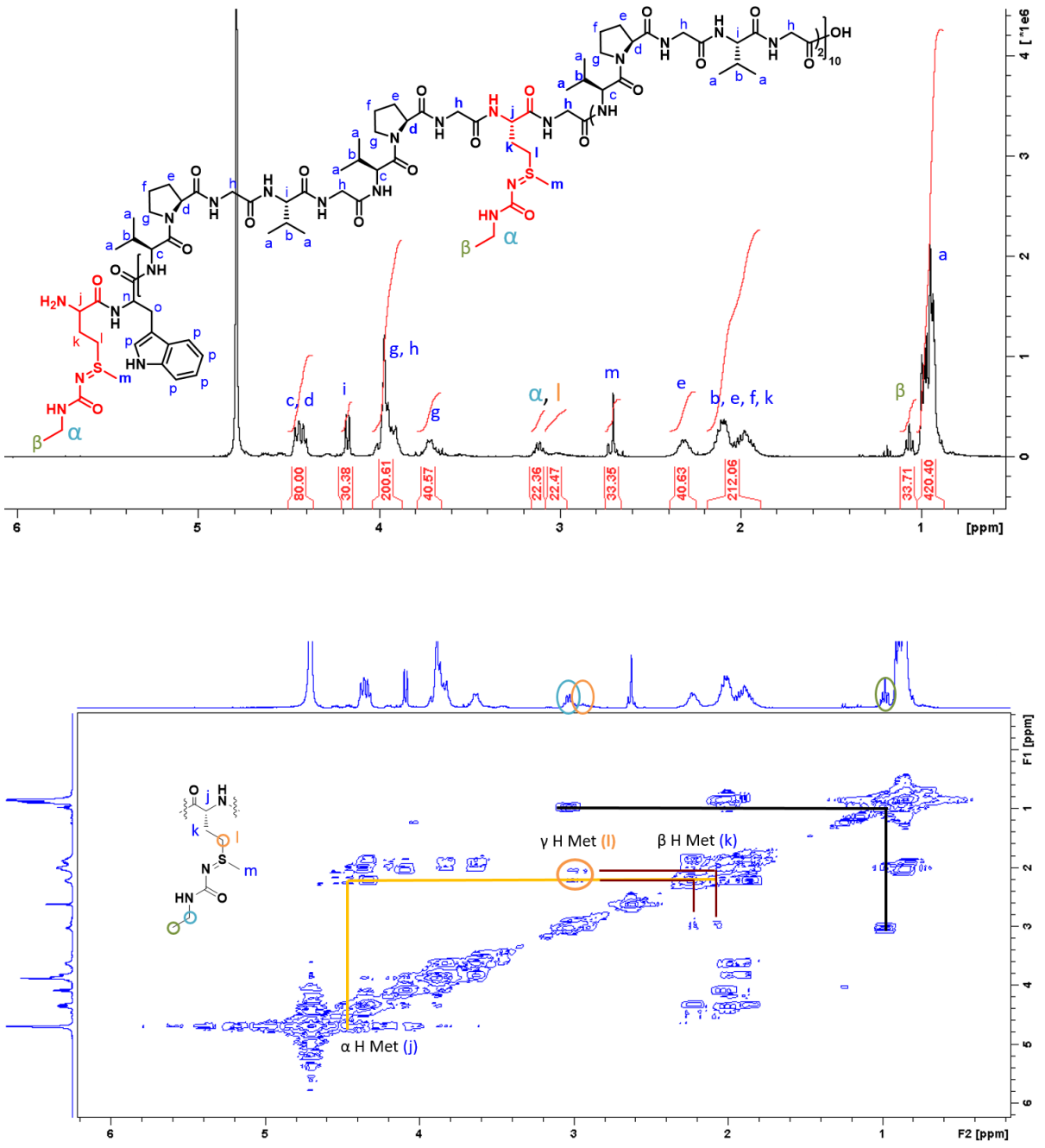

Figure S13. ^{1}H and HSQC NMR spectrum of compound 1C in D_2O.

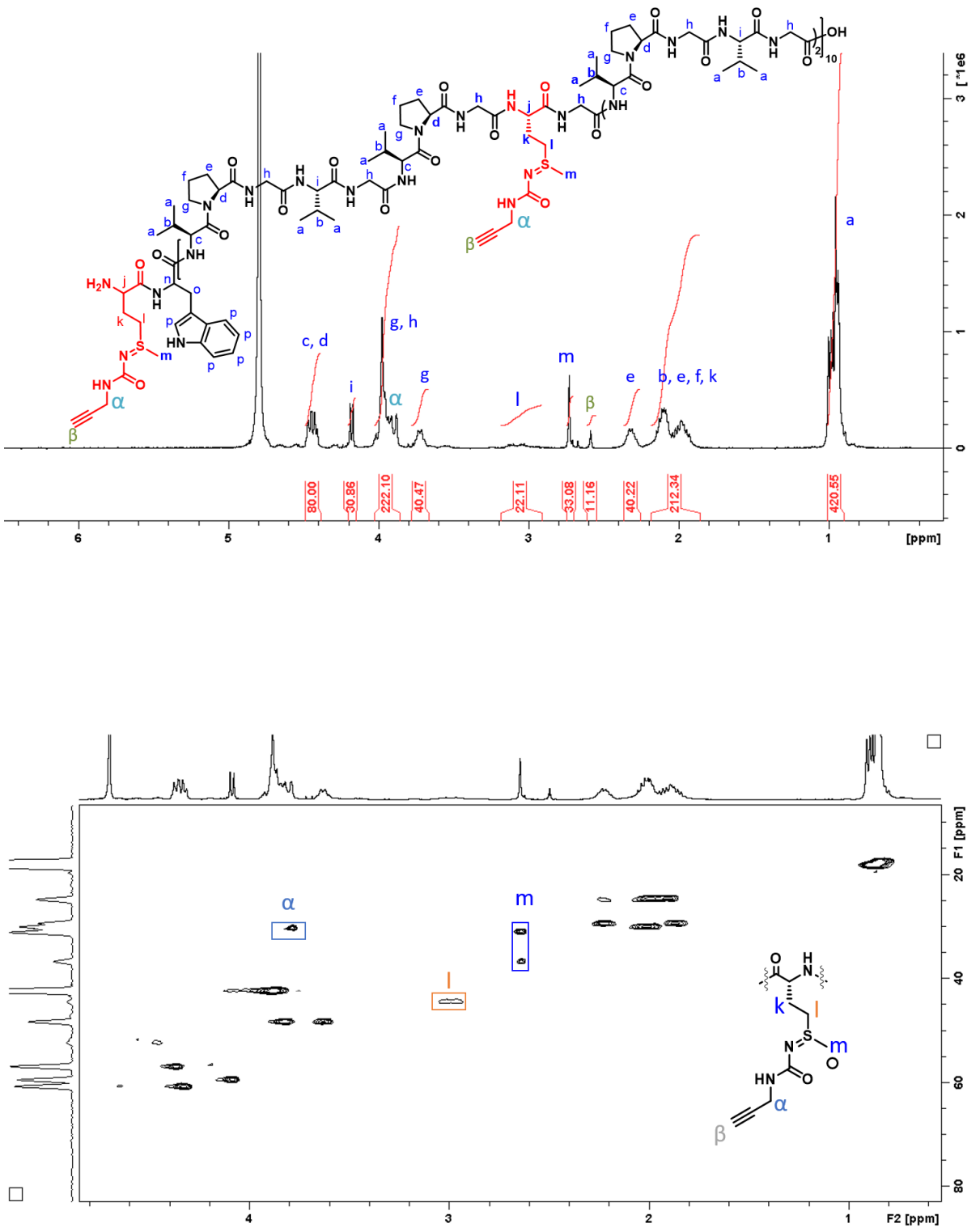

Figure S14. ^{1}H and HSQC NMR spectra of compound 2C in D_2O.

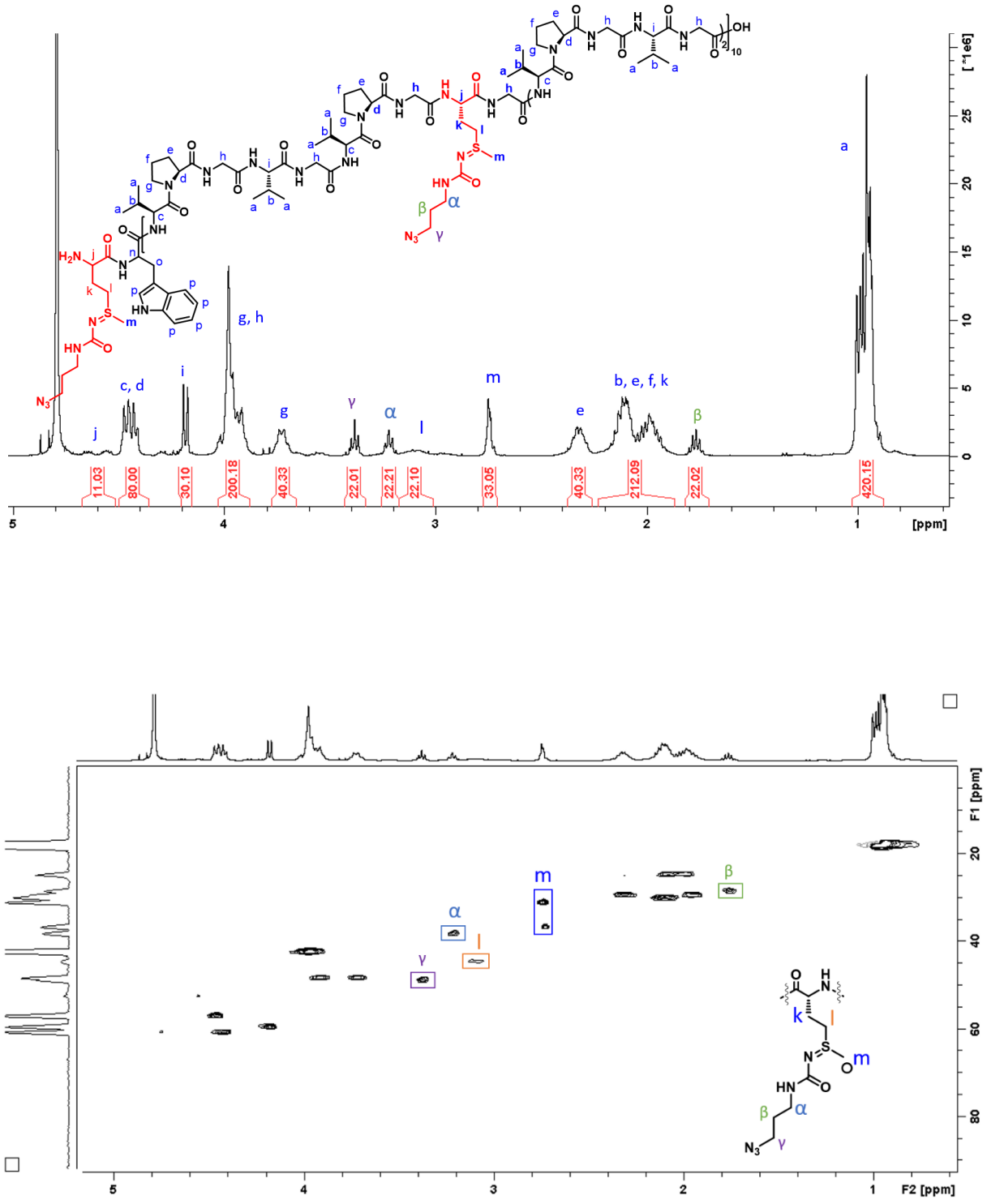

Figure S15. ^{1}H and HSQC NMR spectra of compound 3C in D_2O

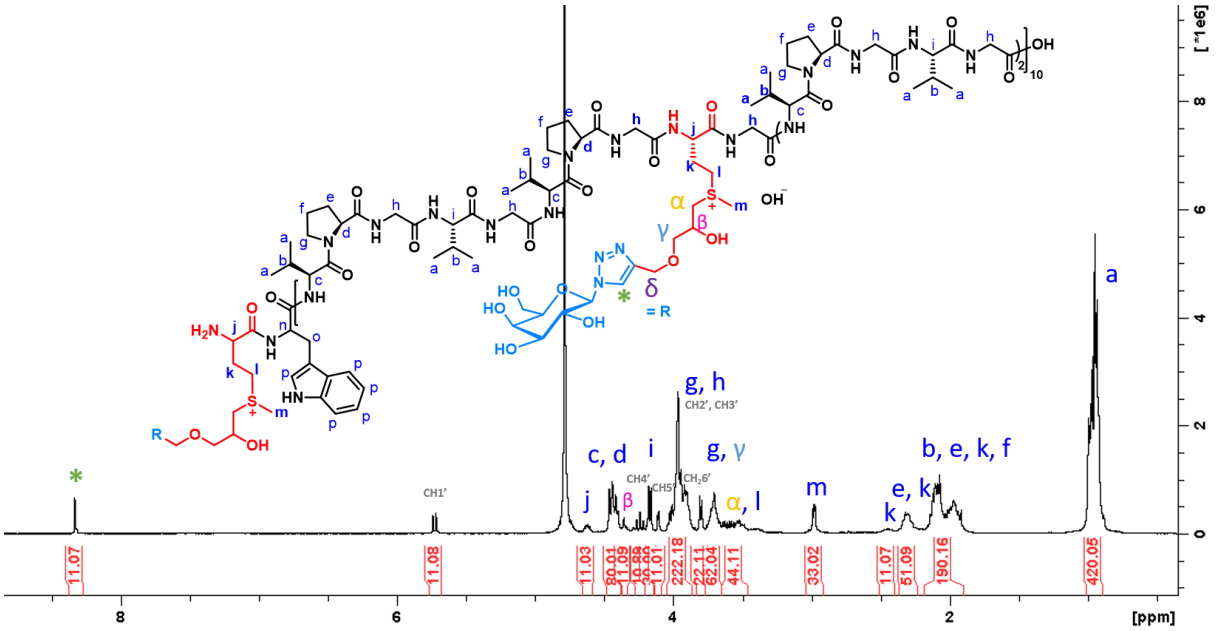

Figure S16. ^{1}H NMR spectra of compound 4B in D_2O

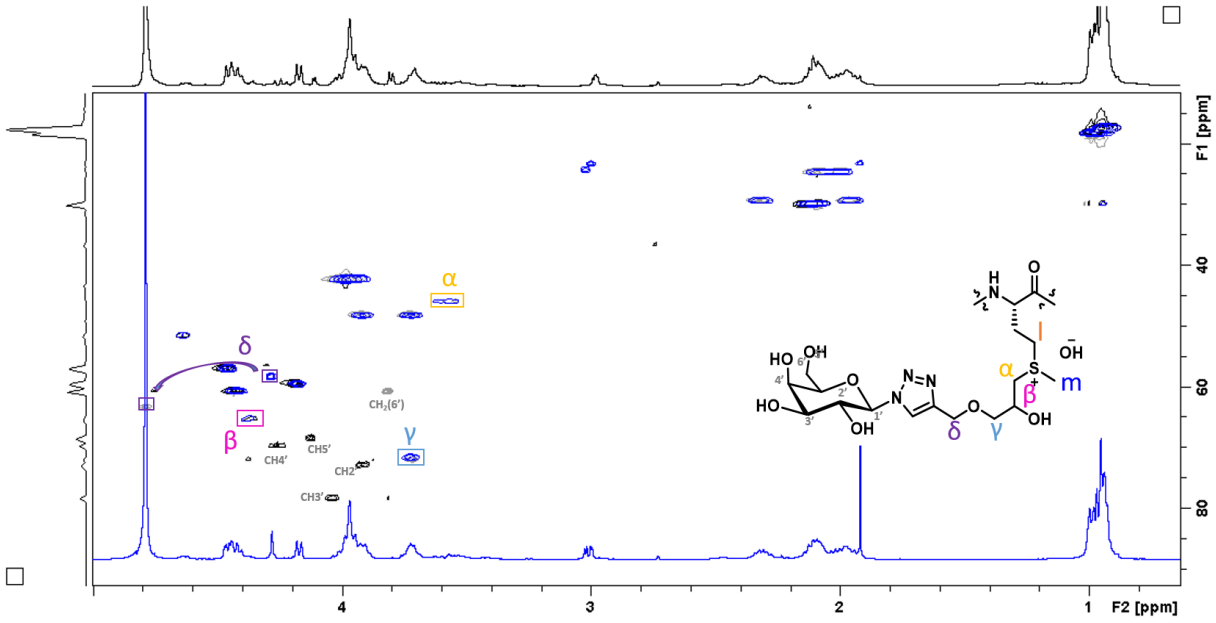

Figure S17. HSQC NMR spectra of compound 4B (in black) and compound 2B (in blue) in D_2O.

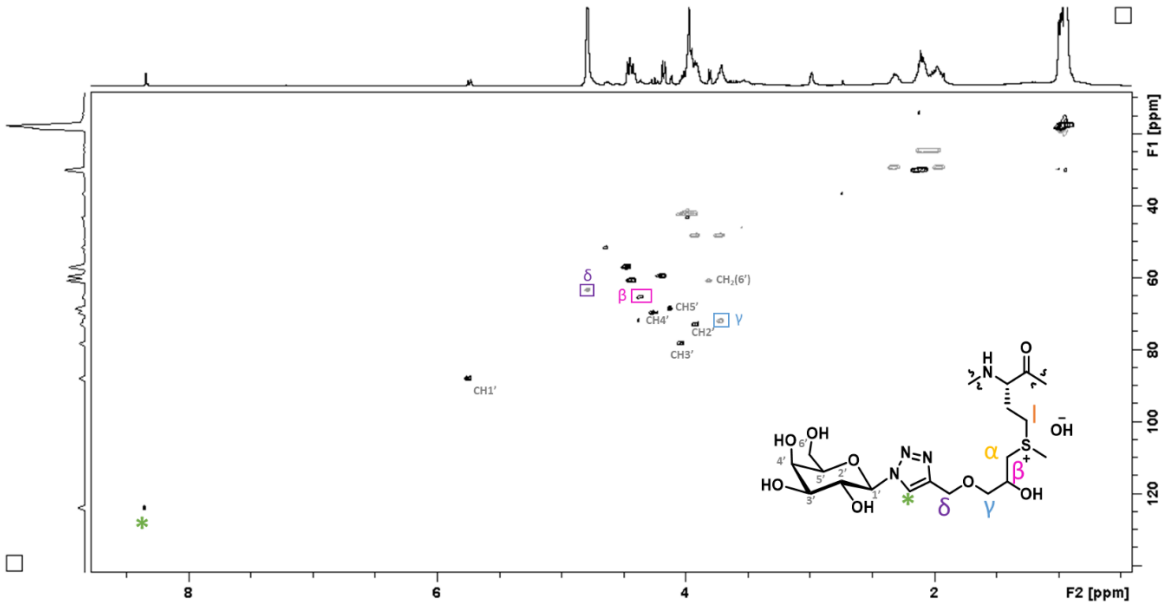

Figure S18. HSQC NMR spectra of compound 4B in D_2O.

CHAPTER 5

CHEMOSELECTIVE POST-MODIFICATIONS AT METHIONINE IN POLYSACCHARIDE-*b*-ELP BIOCONJUGATES

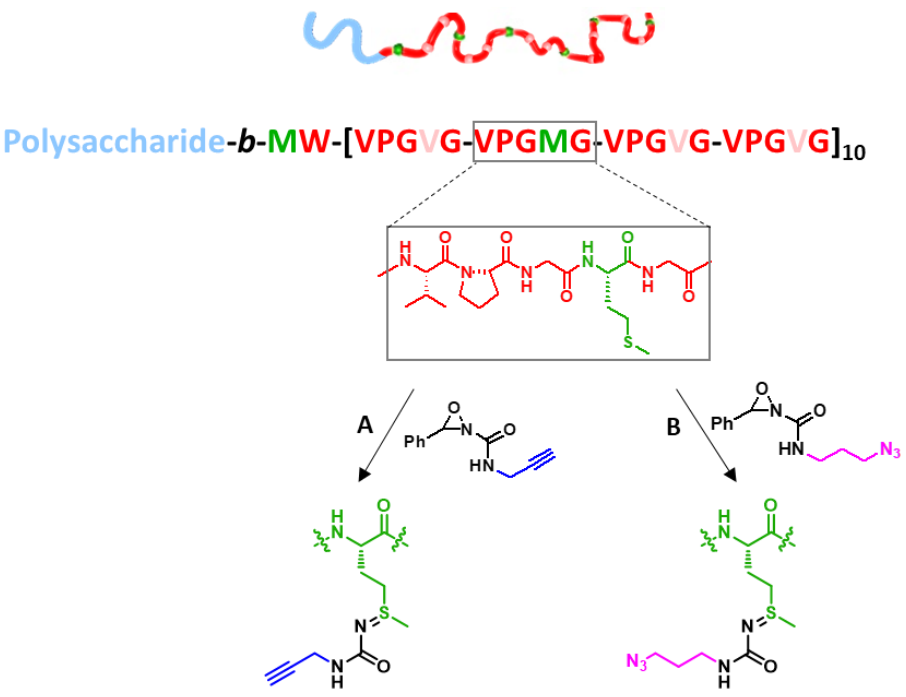

ABSTRACT

Oxaziridine-based redox-activated chemical tagging (ReACT) provides an attractive strategy for chemoselective modification of methionine in proteins under physiological conditions. ReACT has been reported to be high selective towards methionine over the whole range of canonical amino acid residues. However, the selectivity and compatibility of ReACT in the presence of other natural macromolecules such as polysaccharides are still unknown. Herein, we have explored the possibility of applying ReACT on our previously described polysaccharide-*b*-ELP bioconjugates for selective modification of the ELP block at methionine residues. Two polysaccharide-*b*-ELP bioconjugates, namely Dex-*b*-ELP and HA-*b*-ELP, were successfully chemoselectively functionalized with alkyne or azido group, using appropriate oxaziridine-based reagents, with a conversion higher than 95% in 1 hour. The resulting modified polysaccharide-*b*-ELP bioconjugates were characterized by ^{1}H, COSY and HSQC NMR, and their T_t were determined by DLS. Coumarin was subsequently grafted onto Dex-*b*-ELP^{ox}, providing insights into applications of ReACT for selective methionine labeling of polysaccharide-containing bioconjugates.

1. INTRODUCTION

Post-translational modifications of proteins and synthesis of protein bioconjugates have attracted considerable interests in recent decades for the development of protein therapeutics.[1–6] The modification of proteins usually involves their terminal ends or the side chain of specific residues *via* chemoselective reactions. Among sulfur-containing amino acids, cysteine is the most commonly exploited residue regarding selective reactions involving thiols and therefore has been comprehensively studied as target site for bioconjugation.[7–13] In contrast to cysteine, the other sulfur-containing amino acid methionine has long lacked available modification strategies due to its relatively weak nucleophilicity. Revisiting thioether chemistry described in the 40's,[14,15] the group of T. Deming however showed that low pH conditions enhanced the nucleophilicity of thioether as compared to thiol or amine, thus enabling chemoselective modification of methionine in synthetic polypeptides using alkyl halides[16,17] or epoxides.[18–20] Recently Lin and Yang reported an attractive strategy for chemoselective modification of methionine in proteins by using a "Redox-Activated Chemical Tagging" (ReACT) method based on oxaziridine chemistry.[21,22] They found that urea-derived oxaziridines can chemoselectively label methionine residues in proteins and proteomes under aqueous conditions at neutral pH. This method was found very efficient with reactions completed in few

minutes and fully chemoselective to methionine, other amino acid residues being unaffected. They also proposed that two possible pathways are involved in ReACT: the *N*-transfer pathway (NTP) leading to sulfimide and the *O*-transfer pathway resulting in sulfoxide (Figure 1).[21,23] Solvent systems and electron effects in oxaziridine reagents mainly were found to favor one or the other pathway. *N*-substituted urea as a weak electronic withdrawing group on oxaziridine was found to enhance selectivity of NTP path.[21] Various applications of ReACT including precise protein functionalization, antibody–drug conjugation, and chemoproteomic methionine identification, reveal the broad utility of this method.

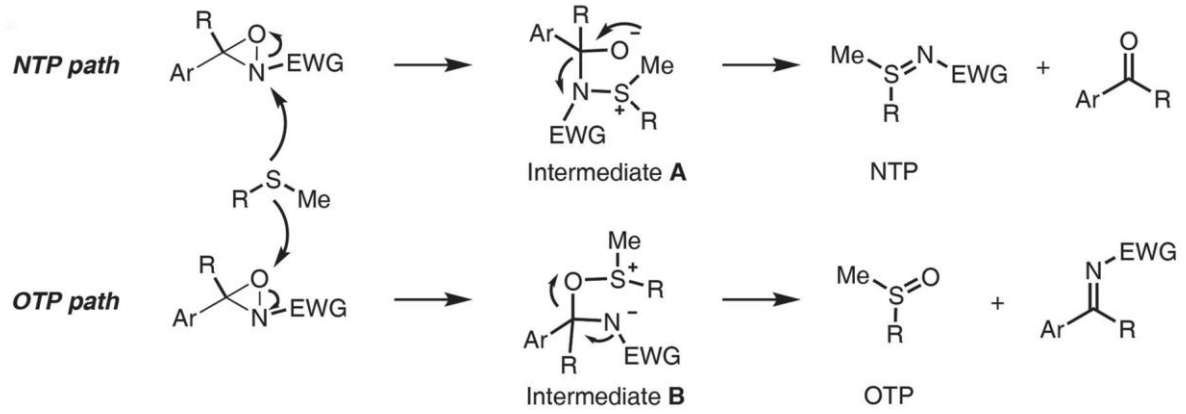

Figure 1. *The proposed reaction mechanism between methionine and oxaziridine compound proceeds by nucleophilic attack of sulfide at N atom or O atom of oxaziridine ring, followed by N–O bond cleavage to generate reaction intermediate A or B, respectively. The NTP or OTP is generated, along with the corresponding aldehyde or imine as side product, through an intramolecular rearrangement.*[21]

In the previous chapter, we have explored ReACT for chemoselective modification of methionine-containing ELP[V_3M_1-40][24] and compared it with alkyl halide- and epoxide-based approaches. ELP[V_3M_1-40] was successfully modified by oxaziridine chemistry under mild reaction conditions with high selectivity. ReACT showed high selectivity to methionine with regards to other amino acid residues and to the ELP *N*-terminal end. However, the selectivity and compatibility of ReACT in the presence of other natural macromolecules such as polysaccharides are still unknown. In this study, we explore the possibility of applying ReACT on polysaccharide-*b*-ELP bioconjugates for the chemoselective modification of the ELP segment at methionine residues. Selective introduction of alkyne or azido groups onto methionine residues allow subsequent orthogonal biofunctionalization of polysaccharide-*b*-ELP bioconjugates with small molecules such as fluorescent dyes or inter-chain cross-linking,

providing insights into applications of ReACT for selective methionine labeling of polysaccharide-containing bioconjugates.

2. EXPERIMENTAL SECTION

2.1 Materials

Dichloromethane (DCM, 99.9%), *N*,*N*-dimethylformamide (DMF, 99.8%), dimethyl sulfoxide (DMSO, 99.7%) were purchased from Sigma-Aldrich. Water was purified using an ELGA PURELAB Classic system. Solvent was purified using PureSolv MD-5 solvent purification system from Innovative Technology. Dialysis was conducted using a Spectra/Por®6 dialysis membrane. Synthesis of fuctional oxaziridines and alkyne functionalized ELP were prepared as previously chapter.

2.2 Synthetic Procedure

Pretest reactions in deuterated solvents

Oxaziridine Alkyne or N_3 derivative (Ox-Alkyne or Ox-N_3) (2 μM) in deuterated dimethylformamide DMF (40 μL) was added to a solution of polysaccharide-*b*-ELP (0.2 μM) in D_2O (1 mL) under N_2 atmosphere. After stirring for 60 mins and 90mins, mixture of 0.5 mL was directly analyzed by ^{1}H NMR.

Modification of Dex-b-ELP via Ox-N₃ (Dex-b-ELP^{ox}-N₃). Ox-N_3 (45 mg, 223 μM) in DMF (400 μL) was added to a solution of Dex-*b*-ELP (50 mg, 2.0 μM) in degassed water (50 mL) under N_2 atmosphere. After stirring for 60 mins, DCM (20 mL) was added and the mixture was extracted with DCM (2 × 20 mL) to remove the byproduct benzaldehyde. The combined water layer was then dialyzed (MWCO cut 15kDa) against Milli Q water for 24h (changing water 3 times per day). The final product was obtained by lyophilization (51 mg, 96% yield). ^{1}H NMR (400 MHz, D_2O): δ 7.75 (s, triazole H), 7.63–7.09 (br, indole *H* Trp), 4.99 (d, Dex H-1), 4.55 (m, CH_α Met), 4.44 (m, CH_α Val, Pro), 4.17 (d, CH_α Val$_{Xaa}$), 4.06–3.87 (br m, C$H_{2\alpha}$ Gly, C$H_{2\delta}$ Pro, Dex H-6,H-5), 3.82-3.67 (m, C$H_{2',\delta}$ Pro, Dex H-6',H-3), 3.62–3.49 (Dex H-2,H-4), 3.29 (t, $N_3CH_2CH_2CH_2$ Ox), 3.12 (t, $N_3CH_2CH_2CH_2$ Ox), 3.15–2.85 (br m, C$H_{2\gamma}$ Met), 2.64 (C$H_{3\varepsilon}$ Met), 2.31–2.18 (m, C$H_{2\beta}$ Pro), 2.17–1.89 (m, C$H_{2\beta}$ Met, C$H_{2',\beta}$ Pro, C$H_{2\gamma}$ Pro, CH_β Val), 1.63 (m, $N_3CH_2CH_2CH_2$ Ox), 1.03–0.88 (m, C$H_{3\gamma}$ Val). FT-IR (ATR): 3332, 2929, 2101, 1653, 1527, 1444, 1340, 1152, 1107, 1019, 917, 546 cm^{-1}

Modification of HA-b-ELP via Ox-N_3 (HA-b-ELP^{ox}-N_3). HA-*b*-ELP^{ox}-N_3 was synthesized with the same procedure in 92% yield. ^{1}H NMR (400 MHz, D_2O): δ 7.75 (s, triazole H), 7.60–7.09 (br, indole *H* Trp), 4.62–4.37 (br, C*H*$_\alpha$ Met, Val, Pro, GlcUA H-1, GlcNAc H-1), 4.17 (d, C*H*$_\alpha$ Val$_{Xaa}$), 4.04–3.66 (br, C*H*$_{2\alpha}$ Gly, C*H*$_{2\delta}$ Pro, C*H*$_{2',\delta}$ Pro, GlcUA H-4, GlcNAc H-2, H-3, H-5, H-6), 3.65–3.42 (GlcUA H-3, H-5), 3.33–3.23 (t, GlcUA H-2, $N_3CH_2CH_2CH_2$ Ox), 3.12 (t, $N_3CH_2CH_2CH_2$ Ox), 3.15–2.98 (br m, C*H*$_{2\gamma}$ Met), 2.78–2.62 (m, C*H*$_{3\varepsilon}$ Met), 2.41–2.25 (m, C*H*$_{2\beta}$ Pro), 2.20–1.89 (m, C*H*$_{2\beta}$ Met, C*H*$_{2',\beta}$ Pro C*H*$_{2\gamma}$ Pro, C*H*$_\beta$ Val), 1.65 (m, $N_3CH_2CH_2CH_2$ Ox), 1.06–0.88 (m, C*H*$_{3\gamma}$ Val). FT-IR (ATR): 3298, 2964, 2099, 1631, 1528, 1440, 1236, 1154, 1047, 545 cm^{-1}.

Modification of Dex-b-ELP via Ox-Alkyne (Dex-b-ELP^{ox}-Alkyne). Dex-*b*-ELP^{ox}-Alkyne was synthesized with the same procedure in 93% yield. ^{1}H NMR (400 MHz, D_2O): δ 7.75 (s, triazole H), 7.63–7.09 (br, indole *H* Trp), 4.99 (d, Dex H-1), 4.55 (m, C*H*$_\alpha$ Met), 4.44 (m, C*H*$_\alpha$ Val, Pro), 4.17 (d, C*H*$_\alpha$ Val$_{Xaa}$), 4.06–3.78 (br m, C*H*$_{2\alpha}$ Gly, C*H*$_{2\delta}$ Pro, Dex H-6,H-5, C*H*$_2$C≡CH Ox), 3.82-3.67 (m, C*H*$_{2',\delta}$ Pro, Dex H-6',H-3), 3.62–3.49 (Dex H-2,H-4), 3.15–2.85 (br m, C*H*$_{2\gamma}$ Met), 2.64 (C*H*$_{3\varepsilon}$ Met), 2.50 ($CH_2C{\equiv}CH$ Ox), 2.31–2.18 (m, C*H*$_{2\beta}$ Pro), 2.17–1.89 (m, C*H*$_{2\beta}$ Met, C*H*$_{2',\beta}$ Pro, C*H*$_{2\gamma}$ Pro, C*H*$_\beta$ Val), 1.03–0.88 (m, C*H*$_{3\gamma}$ Val).

Modification of HA-b-ELP via Ox-Alkyne (HA-b-ELP^{ox}-Alkyne). HA-*b*-ELP^{ox}-Alkyne was synthesized with the same procedure in 90% yield. ^{1}H NMR (400 MHz, D_2O): δ 7.75 (s, triazole H), 7.60–7.09 (br, indole *H* Trp), 4.62–4.37 (br, C*H*$_\alpha$ Met, Val, Pro, GlcUA H-1, GlcNAc H-1), 4.17 (d, C*H*$_\alpha$ Val$_{Xaa}$), 4.04–3.66 (br, C*H*$_{2\alpha}$ Gly, C*H*$_{2\delta}$ Pro, C*H*$_{2',\delta}$ Pro, GlcUA H-4, GlcNAc H-2, H-3, H-5, H-6, C*H*$_2$C≡CH Ox), 3.65–3.42 (GlcUA H-3, H-5), 3.41–3.30 (t, GlcUA H-2), 3.15–2.98 (br m, C*H*$_{2\gamma}$ Met), 2.78–2.62 (m, C*H*$_{3\varepsilon}$ Met),2.51 ($CH_2C{\equiv}CH$ Ox), 2.41–2.25 (m, C*H*$_{2\beta}$ Pro), 2.20–1.89 (m, C*H*$_{2\beta}$ Met, C*H*$_{2',\beta}$ Pro C*H*$_{2\gamma}$ Pro, C*H*$_\beta$ Val), 1.06–0.88 (m, C*H*$_{3\gamma}$ Val).

2.3 Characterization Methods

Nuclear Magnetic Resonance Spectrometry Analysis (NMR)

NMR spectra were acquired in D_2O or $CDCl_3$ at 298 K either on a Bruker Avance I NMR spectrometer or Bruker Avance III HD operating at 400.2 MHz. The relaxation time was fixed to 3 seconds for COSY measurements. Data processing was performed using Bruker TopSpin software.

Fourier Transform Infrared Spectroscopy (FT-IR)

FT-IR spectra were recorded using a Bruker Vertex 70 spectrometer with a GladiATR diamond. Spectra were recorded directly on a powder samples at 400-4000 cm^{-1} (resolution of 4 wavenumber) range by using attenuated total reflection mode.

Dynamic light Scattering Measurements (DLS)

Dynamic light scattering measurements were performed on NanoZS instrument (Malvern, U.K.) at a 90 ° angle at a constant position in the cuvette (constant scattering volume). The derived count rate (DCR) was defined as the mean scattered intensity normalized by the attenuation factor. The DCR was plotted against temperature and the T_t is defined as the temperature corresponding to the point where the DCR starts increasing on this plot.

3. RESULTS AND DISSCUSSION

In the previous chapter, we have summarized synthetic methods to chemoselectively modify the methionine side chain in ELPs. Nucleophilic addition using alkyl halides or epoxides yields a sulfonium group with a positive charge strongly affecting ELPs' physico-chemical properties, in particular their thermal responsiveness. Chemoselectivity at methionine thioether group also requires the reaction to be performed at low pH to enhance its nucleophilicity over other nucleophilic groups (*e.g.*, *N*-terminal amine in the case of ELP[V_3M_1-40]). These stringent reaction conditions are however a strong limitation for some acid-sensitive polymers, such as polysaccharides, especially in the case of our polysaccharide-*b*-ELP bioconjugates.[25] We also explored the recently reported ReACT method based on the use of oxaziridine derivative, a redox-based reaction yielding a sulfimide derivative as an alternative route for chemoselective modification of methionine-containing ELPs in aqueous solution at neutral pH with high efficiency. Inspired by these results, we assumed that oxaziridine chemistry could also be used to modify our polysaccharide-*b*-ELP bioconjugates. One need to note that hydroxyl groups as well as carboxyl groups frequently present in polysaccharide structures were reported non-reactive within 1 hour upon ReACT.[21]

3.1 Pretest reactions in deuterated solvents

In order to test this hypothesis, pretest reactions were carried out in deuterated solvents and rapidly analyzed by NMR. Three polysaccharide-*b*-ELP bioconjugates (Dex-*b*-ELP, Lam-*b*-ELP and HA-*b*-ELP) as well as PEG-*b*-ELP were reacted with oxaziridine-N_3 (Ox-N_3) and oxaziridine-alkyne (Ox-alkyne) derivatives in D_2O/ Deuterated DMF at r.t (Scheme 1).

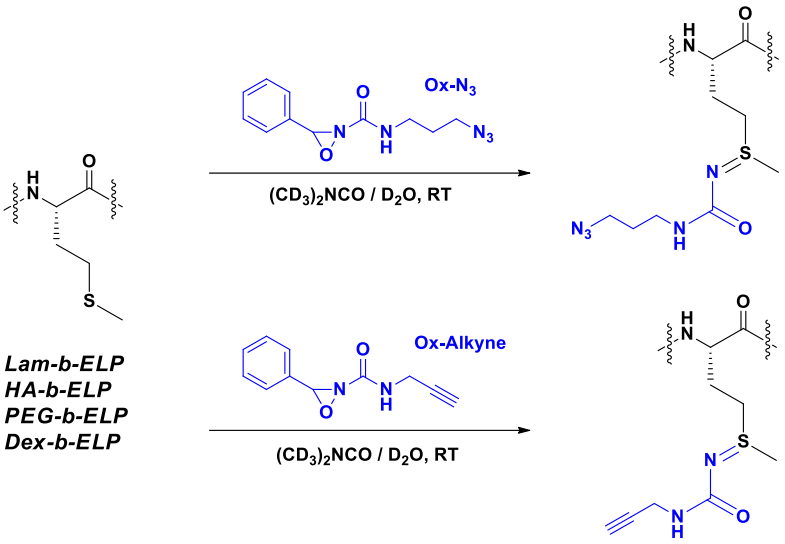

Scheme 1. *Pretest reactions in deuterated solvents.*

The reactions were monitored by following the chemical shift of the methionine methyl group with ^{1}H NMR. Full conversion of methionine was observed in all bioconjugates as methyl group totally shifted from 2.02 to 2.62 ppm (Figure S1, S2) after 1 hour. However, it still needed to be confirmed that methionine residues were converted into the desired sulfimide *via the* N-transfer pathway and not into the unwanted sulfoxide *via* the O-transfer pathway, since sulfoxide may also result in similar shift of methionine methyl. One has also to mention that methionine sulfoxide was found not reactive with oxaziridine.[21] To verify the success of expected modifications, the reaction mixtures required to be purified and the products isolated for full characterization by NMR. We selected Dex-*b*-ELP and HA-*b*-ELP bioconjugates among our series of polysaccharide-*b*-ELP block copolymers for further synthetic studies due to their chemical structures, bioactivity (HA) and favorable self-assembly properties.

3.2 Modification of polysaccharide-b-ELP via Ox-N$_3$/Alkyne

The Dex-*b*-ELP block copolymer was first reacted with Ox-N$_3$ or Ox-alkyne in a cosolvent (H_2O/DMF 125:1) (Scheme 2). Excess water (99.2%) was used to increase stabilization of the transition state of NTP by solvation and hydrogen bonding of the alkoxy anion intermediate leading to high conversion to sulfimide.[21] The reaction was stirred for 60 min regarding the results of the pretest reactions. Regarding the purification of the reaction mixtures, as the oxaziridine derivatives used in excess and benzaldehyde byproduct easily dissolved in organic solvents such as DMF and DCM, it was possible to remove them by simple extraction using

DCM as water immiscible organic solvent. After extraction with DCM for two times, the combined water phase were dialyzed against MilliQ water to remove the residual DMF. The final product was obtained by lyophilization and subsequently analyzed by NMR.

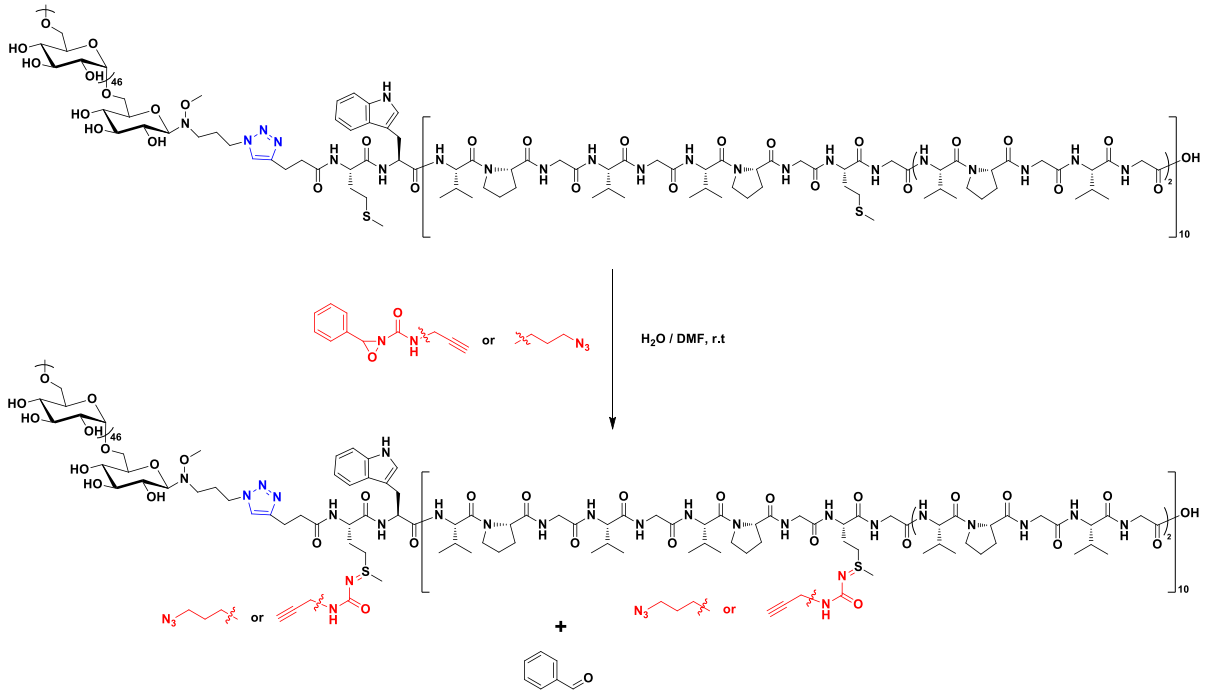

Scheme 2. *Modification of polysaccharide-b-ELP via Ox-N_3 or Ox-Alkyne*

As observed on proton NMR spectra, the chemical shift of added methylene groups on Dex-*b*-ELP^{ox} derivatives were found at nearly identical positions as compared to the ones of modified ELP^{ox} derivatives (Figure 2). All peaks in the ^{1}H NMR spectra were assigned with the help of corresponding 2D NMR analyses (HSQC, COSY) (Figure 3, S3). In all cases, the methyl group of methionine was shifted to relatively low field due to the electronic withdrawing effect of the sulfimide. The alkyne proton in Dex-*b*-ELP^{ox}-Alkyne was recorded at 2.5 ppm, while the methylene group (Alk-H2) adjacent to the alkyne bond was found at 3.8 ppm, both similarly than in ELP^{ox}-alkyne. The chemical shift of the three additional methylene groups (N_3-H1, H2, H3) of Dex-*b*-ELP^{ox}-N_3 were at 1.63, 3.12, 3.29 ppm (1.63 ppm for N_3-H2, 3.12 and 3.29 for H1 and H3) and their ^{1}H-^{1}H correlations were confirmed by COSY (Figure 2B). More than 94% conversions for Dex-*b*-ELP^{ox}-alkyne and Dex-*b*-ELP^{ox}-N_3 were determined by comparing the integral of the peak at 4.1 ppm corresponding to the resonance of the α proton of valine at the guest residue position (-VPG**V**G- repeat units) with the integral of the alkyne proton (Alk-H1) of Dex-*b*-ELP^{ox}-alkyne (Figure S3), and the integral of the methylene protons of Dex-*b*-ELP^{ox}-N_3 (Figure 3). The presence of the characteristic peak of the azido function in Dex-*b*-ELP^{ox}-N_3

was also verified by FTIR (Figure S6-7). The polysaccharide structure of dextran showed no change after ReACT, which indicated polysaccharides having similar structure to dextran may also well tolerate this type of reaction.

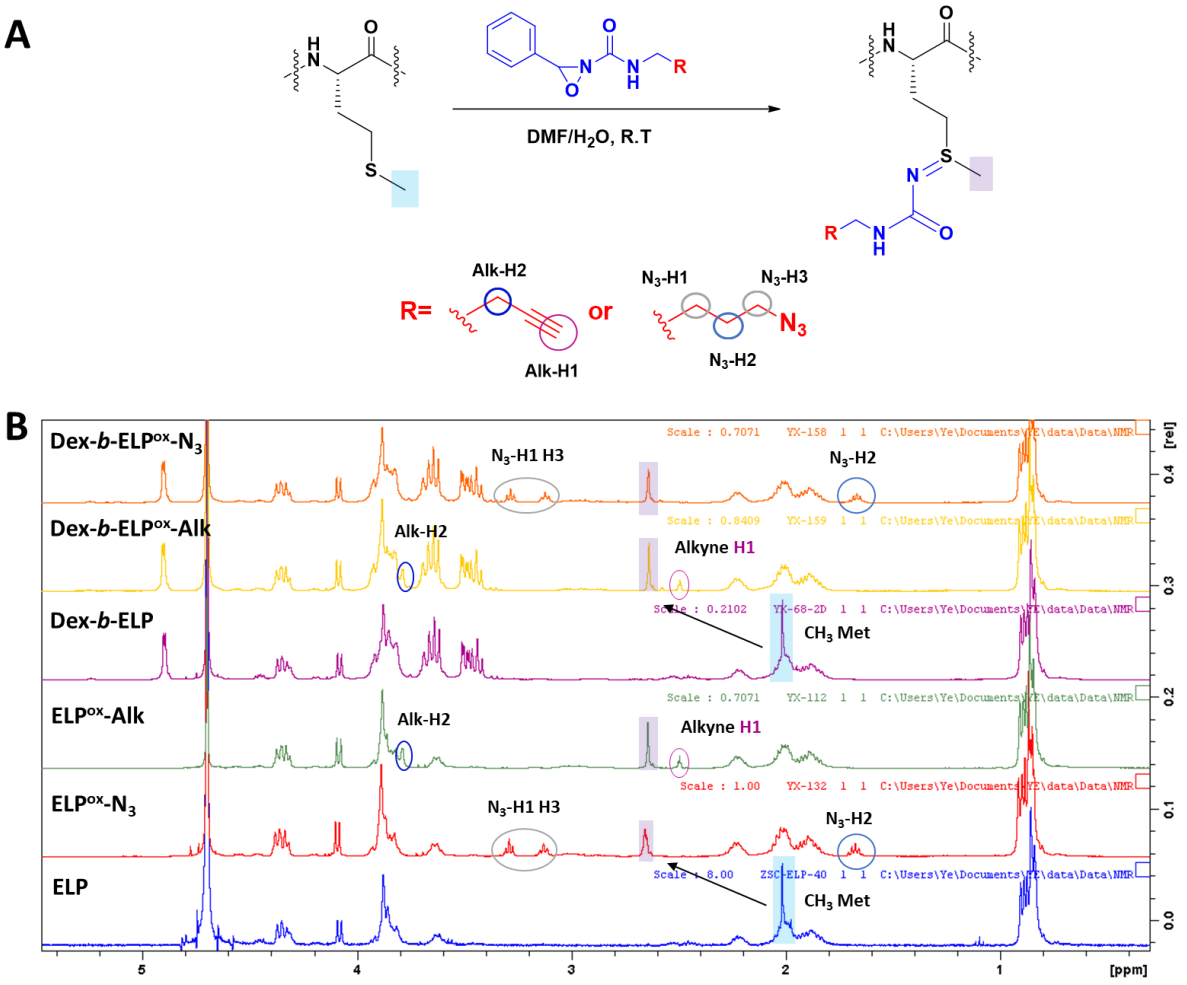

Figure 2. (A) Synthetic scheme of the modification of methionine by oxaziridine reagents. (B) Comparison of ^{1}H NMR spectra between pristine ELP, oxaziridine-modified ELP^{ox}-N_3 and, ELP^{ox}-alkyne, Dex-*b*-ELP, and oxaziridine-modified Dex-*b*-ELP^{ox}-alkyne and Dex-*b*-ELP^{ox}-N_3.

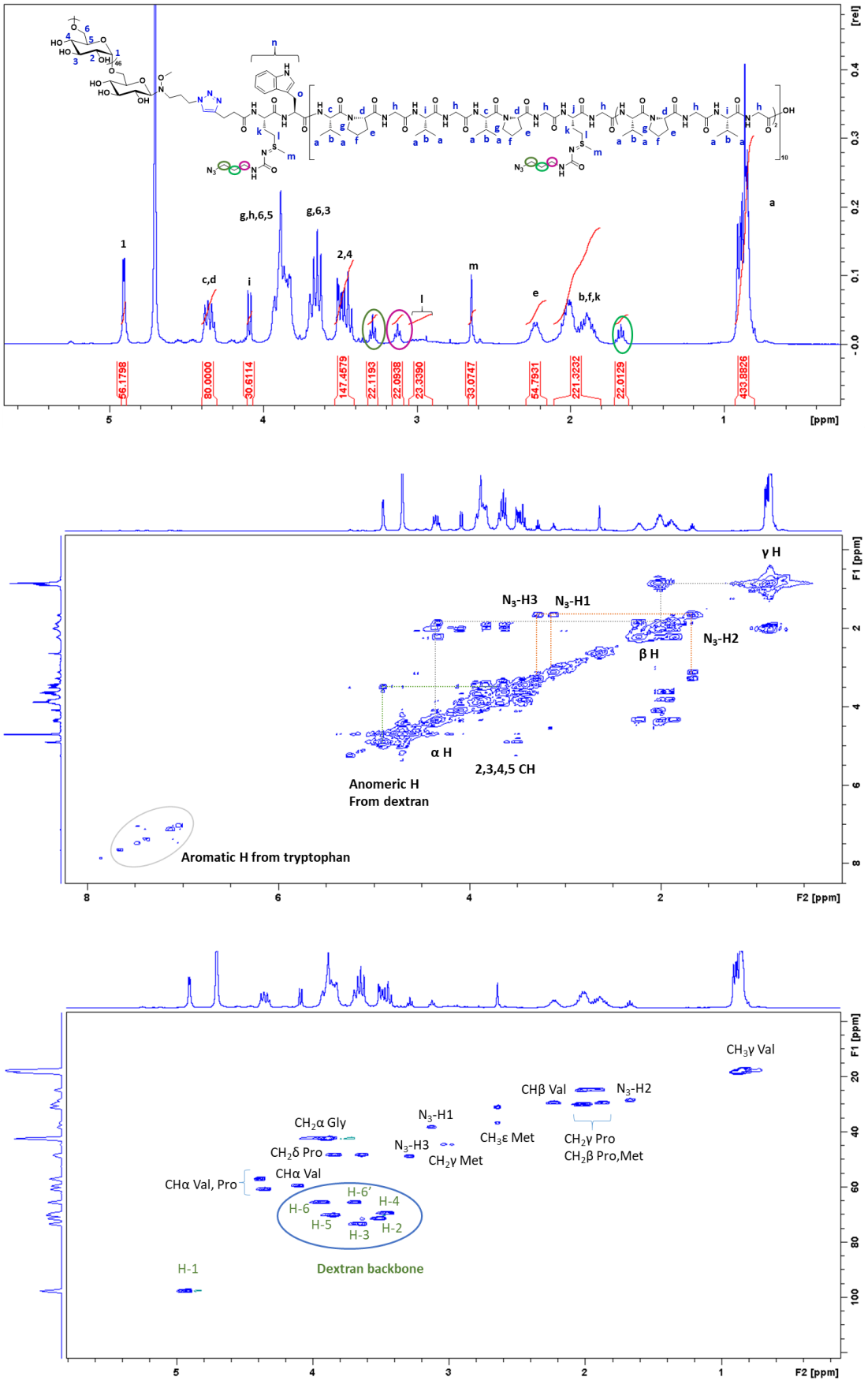

Figure 3. ^{1}H, COSY and HSQC NMR spectra of Dex-*b*-ELP^{ox}-N_3 in D_2O at 25 ℃.

A similar study was achieved on the HA-*b*-ELP bioconjugate. HA additionally presenting carboxylic acid groups, we wanted to assess the possibility of using ReACT with the HA-*b*-ELP bioconjugate. HA-*b*-ELP was therefore modified with functional oxaziridine derivatives Ox-N_3 and Ox-alkyne using a similar procedure to the one used for Dex-*b*-ELP. ^{1}H NMR spectra were fully assigned with the help of corresponding HSQC and COSY spectra (Figure S4, S5). Consistent with Dex-*b*-ELP^{ox}, HA-*b*-ELP^{ox} demonstrated a methionine conversion superior to 95% and no significant structural change of HA, revealing the full compatibility of ReACT with polysaccharides such as dextran and hyluronan.

3.3 Effect of methionine modification by ReACT on the thermal responsiveness of polysaccharide-b-ELP bioconjugates

The effect of different modifications of Dex-*b*-ELP by the ReACT strategy onto the thermal responsiveness of the resulting bioconjugates was studied by DLS. (Figure 4) As previously mentioned in chapter 4, the modification of methionine with oxaziridine derivatives yielded ELP derivatives with increased T_t as compared to the pristine ELP as a consequence of the polar sulfimide-urea structure that contributes to raise the hydrophilicity (Figure 4A). Similarly, the transition temperature of Dex-*b*-ELP^{ox}-alkyne and Dex-*b*-ELP^{ox}-N3 was significantly raised as compared to the one of Dex-*b*-ELP at similar molar concentration (Figure 4B).

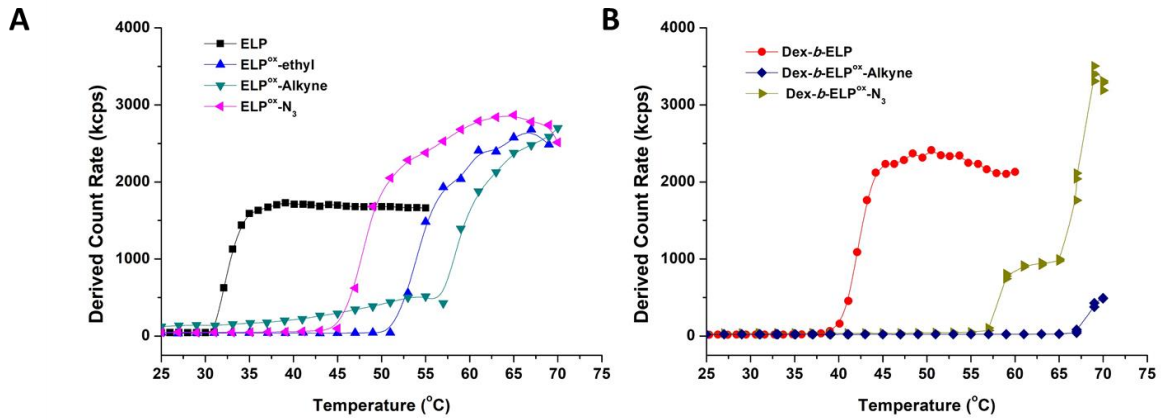

Figure 4. Temperature-responsiveness of (A) ELP and ELP^{ox} derivatives and (B) Dex-*b*-ELP and Dex-*b*-ELP^{ox} as measured by DLS upon the application of a temperature heating ramp from 25 to 70 ℃.

3.4 Dye loading onto Polysaccharide-b-ELP^{ox} bioconjugates

Polysaccharide-*b*-ELP^{ox} bioconjugates bearing a functional alkyne or azido group allow for subsequent orthogonal functionalization with various molecules as well as inter-chain cross-linking. We therefore did a preliminary reaction test to graft coumarin, a small fluorescent dye onto Dex-*b*-ELP^{ox}-N_3 *via* click chemistry (see supporting information). Although we did not check the grafting ratio of dye, grafting of coumarin moieties resulted in a strong decrease of T_t (below 25 ℃) on DLS and to the formation of nano-sized particles above the T_t (Figure 5A). Above 30 ℃, Dex-*b*-ELP^{ox}-Coumarin was able to self-assemble into stable nanoparticles around 100 nm in diameter (Figure 5B). The grafting ratio needed to further check by spectrofluorometer.

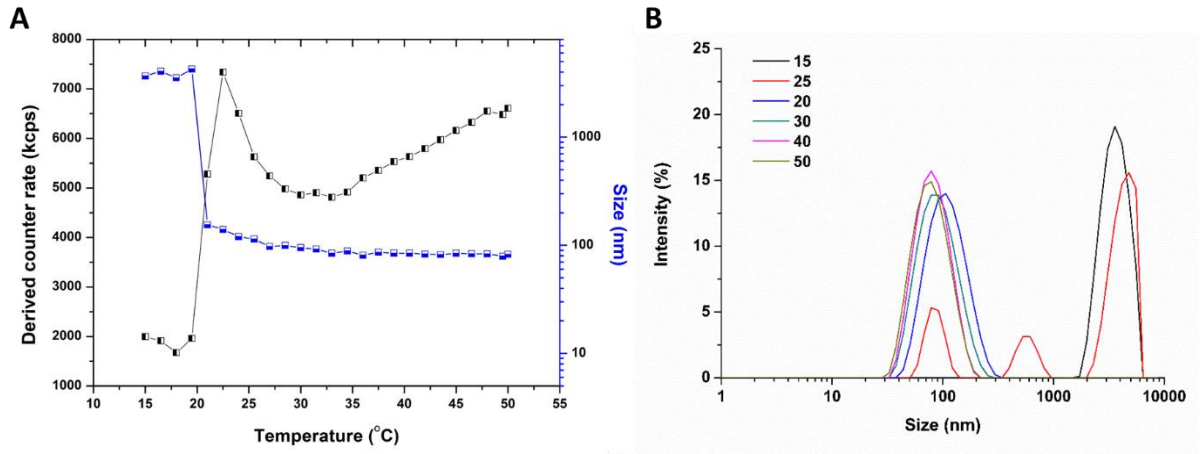

Figure 5. DLS study of Dex-*b*-ELP^{ox}-Coumarin upon heating ramp. (A) Scattering intensity (DCR, black curve) and Z-average size (Size, blue curve) as a function of temperature. (B) Size distribution in intensity at selected temperatures.

CONCLUSION

Herein, we explored the possibility of applying the ReACT strategy using oxaziridine derivatives on polysaccharide-*b*-ELP bioconjugates for chemoselective introduction of azido and alkyne groups. Two polysaccharide-*b*-ELP bioconjugates, Dex-*b*-ELP and HA-*b*-ELP, were successfully quantitatively functionalized (conversion > 95%) in relatively short reaction times (1 hour). The resulting polysaccharide-*b*-ELP bioconjugate derivatives were characterized by ^{1}H, COSY and HSQC NMR, and the effect of the different modifications on their thermal responsiveness measured. Consistently with our previous observations, the modification of Dex-*b*-ELP with oxaziridine derivaties drastically increased their T_t. A small organic molecule, namely coumarin, was subsequently grafted onto Dex-*b*-ELP^{ox}-N_3 by copper-catalyzed azide-alkyne cycloaddition allowing for possible fluorescent detection of the bioconjugate or resulting self-assembled nanoparticles, as well as possible inter-chain cross-linking. Very importantly, oxaziridine-based chemistry on Dex-*b*-ELP and HA-*b*-ELP showed overall no significant structural influence on dextran and hyaluronan blocks, revealing the compatibility of the ReACT method with polysaccharide-containing bioconjuagtes.

REFERENCES

(1) Müller, M. M. Post-Translational Modifications of Protein Backbones: Unique Functions, Mechanisms, and Challenges. *Biochemistry* **2018**, *57* (2), 177–185. https://doi.org/10.1021/acs.biochem.7b00861.

(2) He, W.; Wei, L.; Zou, Q. Research Progress in Protein Posttranslational Modification Site Prediction. *Brief. Funct. Genomics* **2019**, *18* (4), 220–229. https://doi.org/10.1093/bfgp/ely039.

(3) Kumar, G. K.; Prabhakar, N. R. Post-Translational Modification of Proteins during Intermittent Hypoxia. *Respir. Physiol. Neurobiol.* **2008**, *164* (1–2), 272–276. https://doi.org/10.1016/j.resp.2008.05.017.

(4) Santos, A. L.; Lindner, A. B. Protein Posttranslational Modifications: Roles in Aging and Age-Related Disease. *Oxid. Med. Cell. Longev.* **2017**, *2017*, 1–19. https://doi.org/10.1155/2017/5716409.

(5) Karve, T. M.; Cheema, A. K. Small Changes Huge Impact: The Role of Protein Posttranslational Modifications in Cellular Homeostasis and Disease. *J. Amino Acids* **2011**, *2011*, 1–13. https://doi.org/10.4061/2011/207691.

(6) Wang, Y.-C.; Peterson, S. E.; Loring, J. F. Protein Post-Translational Modifications and Regulation of Pluripotency in Human Stem Cells. *Cell Res.* **2014**, *24* (2), 143–160. https://doi.org/10.1038/cr.2013.151.

(7) Kundu, R.; Ball, Z. T. Rhodium-Catalyzed Cysteine Modification with Diazo Reagents. *Chem. Commun.* **2013**, *49* (39), 4166–4168. https://doi.org/10.1039/C2CC37323H.

(8) Chung, H. S.; Wang, S.-B.; Venkatraman, V.; Murray, C. I.; Van Eyk, J. E. Cysteine Oxidative Posttranslational Modifications. *Circ. Res.* **2013**, *112* (2), 382–392. https://doi.org/10.1161/CIRCRESAHA.112.268680.

(9) Sechi, S.; Chait, B. T. Modification of Cysteine Residues by Alkylation. A Tool in Peptide Mapping and Protein Identification. *Anal. Chem.* **1998**, *70* (24), 5150–5158. https://doi.org/10.1021/ac9806005.

(10) Leesnitzer, L. M.; Parks, D. J.; Bledsoe, R. K.; Cobb, J. E.; Collins, J. L.; Consler, T. G.; Davis, R. G.; Hull-Ryde, E. A.; Lenhard, J. M.; Patel, L.; et al. Functional Consequences of Cysteine Modification in the Ligand Binding Sites of Peroxisome Proliferator Activated Receptors by GW9662. *Biochemistry* **2002**, *41* (21), 6640–6650. https://doi.org/10.1021/bi0159581.

(11) Spicer, C. D.; Davis, B. G. Selective Chemical Protein Modification. *Nat. Commun.* **2014**, *5* (1), 4740. https://doi.org/10.1038/ncomms5740.

(12) Wobbe, L.; Blifernez, O.; Schwarz, C.; Mussgnug, J. H.; Nickelsen, J.; Kruse, O. Cysteine Modification of a Specific Repressor Protein Controls the Translational Status of Nucleus-Encoded LHCII MRNAs in Chlamydomonas. *Proc. Natl. Acad. Sci.* **2009**, *106* (32), 13290–13295. https://doi.org/10.1073/pnas.0900670106.

(13) Gunnoo, S. B.; Madder, A. Chemical Protein Modification through Cysteine. *ChemBioChem* **2016**, *17* (7), 529–553. https://doi.org/10.1002/cbic.201500667.

(14) Toennies, G.; Kolb, J. J. Methionine Studies. VII. Sulfonium Derivatives 1. *J. Am. Chem. Soc.* **1945**, *67* (5), 849–851. https://doi.org/10.1021/ja01221a046.

(15) Toennies, G. Sulfonium Reactions of Methionine and Their Possible Metabolic Significance. *J. Biol. Chem.* **1940**, *132* (1), 455–456.

(16) Kramer, J. R.; Deming, T. J. Preparation of Multifunctional and Multireactive Polypeptides via Methionine Alkylation. *Biomacromolecules* **2012**, *13* (6), 1719–1723. https://doi.org/10.1021/bm300807b.

(17) Deming, T. J. Synthesis of Side-Chain Modified Polypeptides. *Chem. Rev.* **2016**, *116* (3), 786–808. https://doi.org/10.1021/acs.chemrev.5b00292.

(18) Kramer, J. R.; Petitdemange, R.; Bataille, L.; Bathany, K.; Wirotius, A. L.; Garbay, B.; Deming, T. J.; Garanger, E.; Lecommandoux, S. Quantitative Side-Chain Modifications of Methionine-Containing Elastin-Like Polypeptides as a Versatile Tool to Tune Their Properties. *ACS Macro Lett.* **2015**, *4* (11), 1283–1286. https://doi.org/10.1021/acsmacrolett.5b00651.

(19) Petitdemange, R.; Garanger, E.; Bataille, L.; Bathany, K.; Garbay, B.; Deming, T. J.; Lecommandoux, S. Tuning Thermoresponsive Properties of Cationic Elastin-like Polypeptides by Varying Counterions and Side-Chains. *Bioconjug. Chem.* **2017**, *28* (5), 1403–1412. https://doi.org/10.1021/acs.bioconjchem.7b00082.

(20) Gharakhanian, E. G.; Deming, T. J. Versatile Synthesis of Stable, Functional Polypeptides via Reaction with Epoxides. *Biomacromolecules* **2015**, *16* (6), 1802–1806. https://doi.org/10.1021/acs.biomac.5b00372.

(21) Lin, S.; Yang, X.; Jia, S.; Weeks, A. M.; Hornsby, M.; Lee, P. S.; Nichiporuk, R. V.; Iavarone, A. T.; Wells, J. A.; Toste, F. D.; et al. Redox-Based Reagents for Chemoselective Methionine Bioconjugation. *Science (80-.).* **2017**, *355* (6325), 597–602. https://doi.org/10.1126/science.aal3316.

(22) Christian, A. H.; Jia, S.; Cao, W.; Zhang, P.; Meza, A. T.; Sigman, M. S.; Chang, C. J.; Toste, F. D. A Physical Organic Approach to Tuning Reagents for Selective and Stable Methionine Bioconjugation. *J. Am. Chem. Soc.* **2019**, *141* (32), 12657–12662. https://doi.org/10.1021/jacs.9b04744.

(23) Wang, C.; Jiang, Y.-Y.; Qi, C.-Z. Mechanism and Origin of Chemical Selectivity in Oxaziridine-Based Methionine Modification: A Computational Study. *J. Org. Chem.* **2017**, *82* (18), 9765–9772. https://doi.org/10.1021/acs.joc.7b02026.

(24) Petitdemange, R.; Garanger, E.; Bataille, L.; Dieryck, W.; Bathany, K.; Garbay, B.; Deming, T. J.; Lecommandoux, S.; Dieryck, W.; Petitdemange, R.; et al. Selective Tuning of Elastin-like Polypeptide Properties via Methionine Oxidation. *Biomacromolecules* **2017**, *18* (2), 544–550. https://doi.org/10.1021/acs.biomac.6b01696.

(25) Munneke, S.; Prevost, J. R. C.; Painter, G. F.; Stocker, B. L.; Timmer, M. S. M. The Rapid and Facile Synthesis of Oxyamine Linkers for the Preparation of Hydrolytically Stable Glycoconjugates. *Org. Lett.* **2015**, *17* (3), 624–627. https://doi.org/10.1021/ol503634j.

SUPPORTING INFORMATION

Pretest reactions of ox-N_3 in deuterated solvents

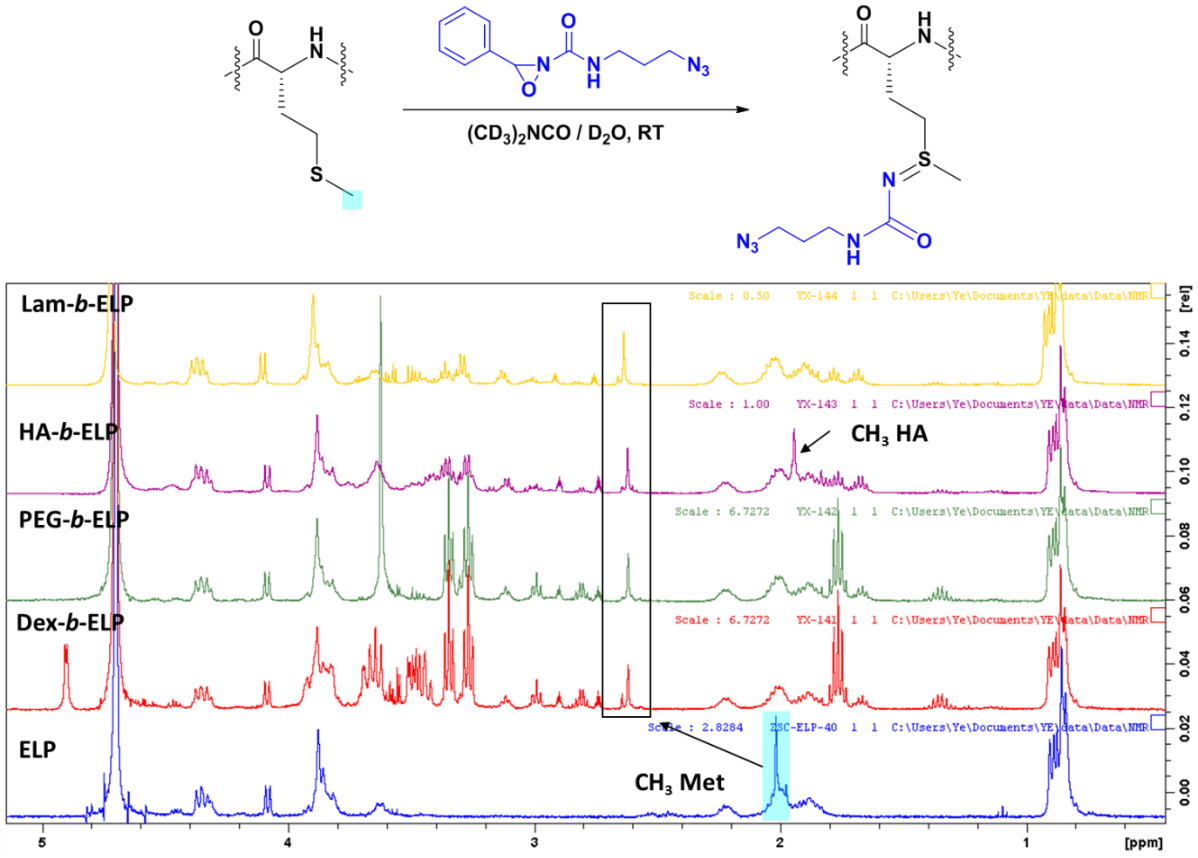

Figure S1. Pretest reactions of ox-N_3 on polysaccharide-*b*-ELP block copolymers in deuterated solvents. ^{1}H NMR spectra was recorded after stirring for 60 mins.

Pretest reactions of ox-alkyne in deuterated solvents

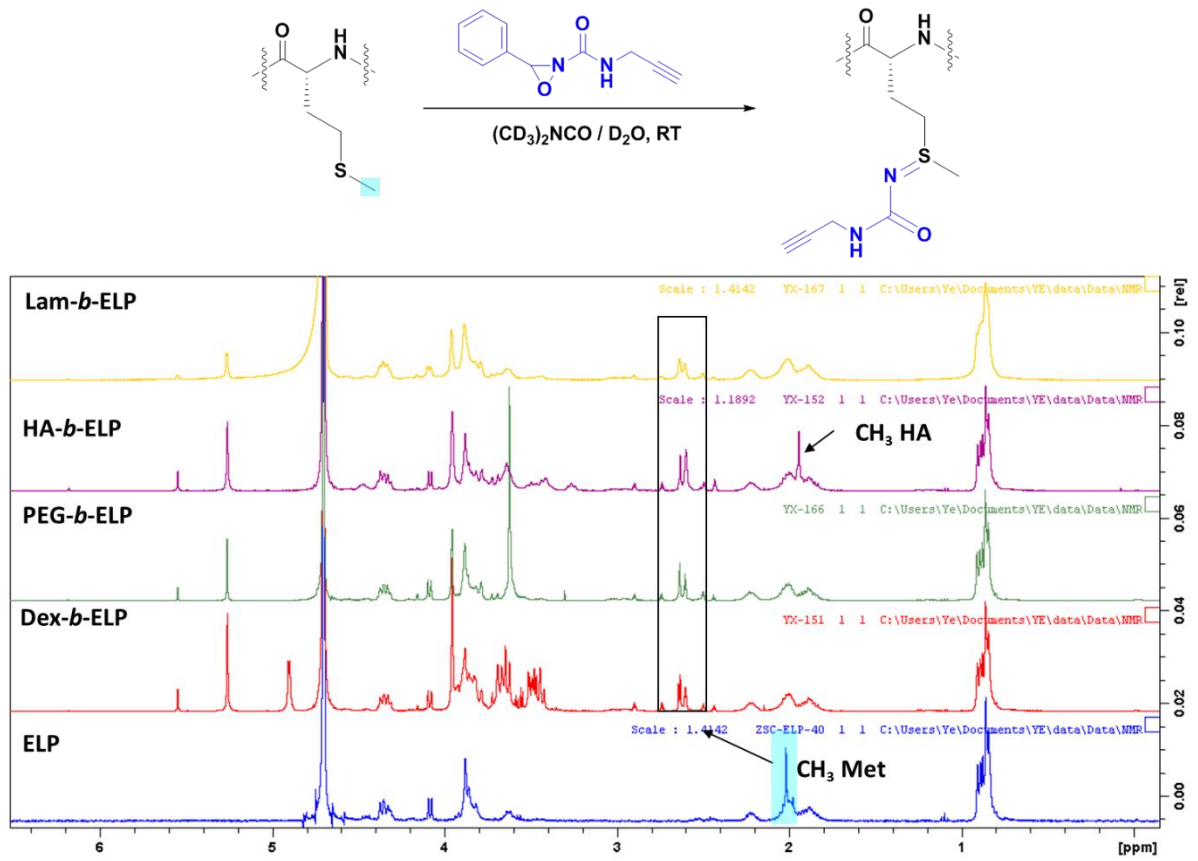

Figure S2. Pretest reactions of ox-alkyne on polysaccharide-*b*-ELP block copolymers in deuterated solvents. ^{1}H NMR spectra was recorded after stirring for 60 mins.

NMR Spectra of Dex-b-ELP^{ox}-Alkyne

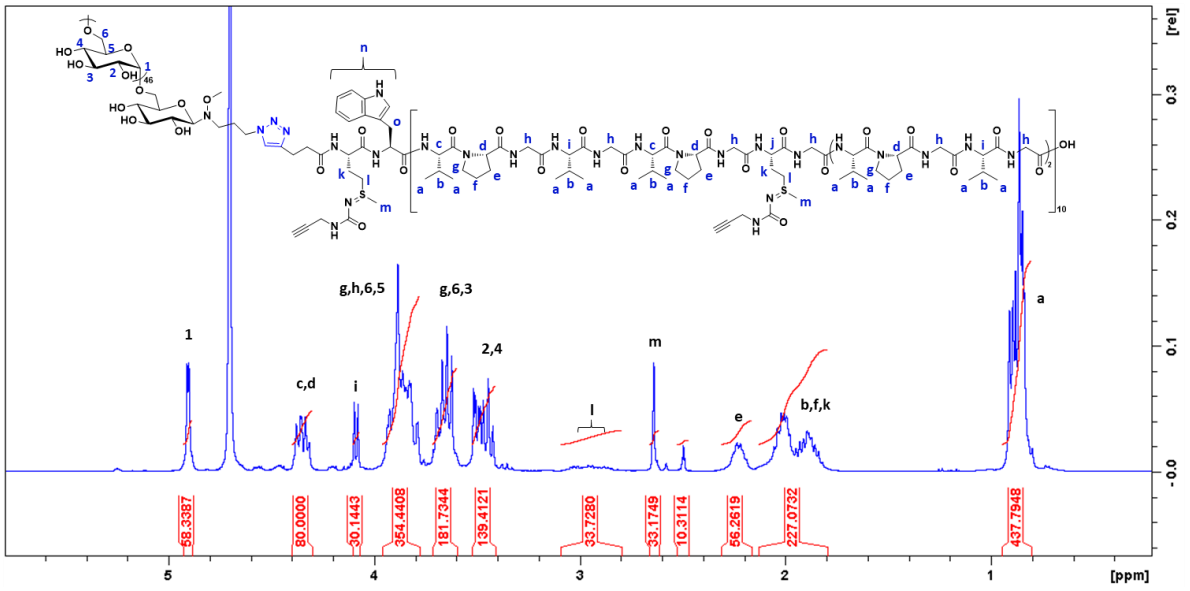

^{1}H NMR

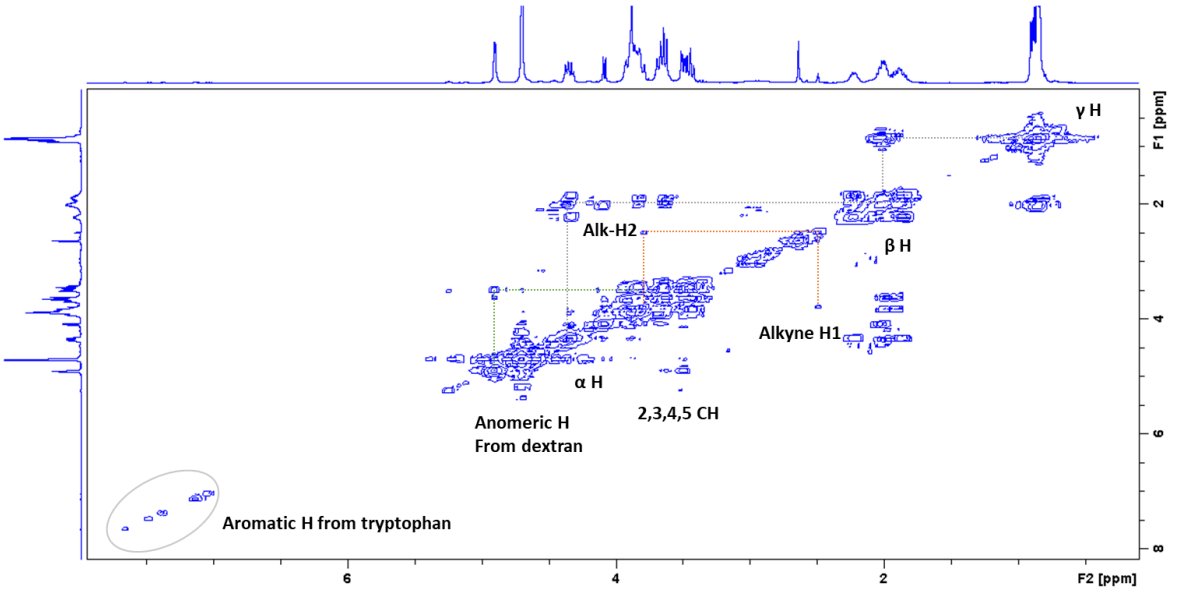

COSY

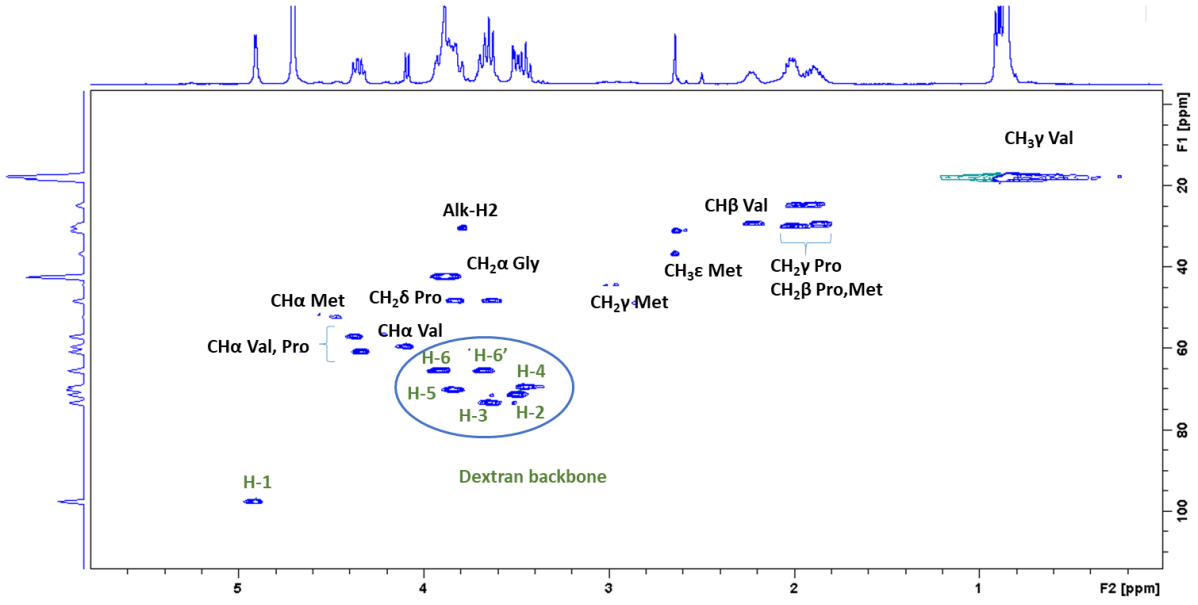

Figure S3. ^{1}H and HSQC NMR Spectra of Dex-*b*-ELP^{ox}-Alk in D_2O at 25 ℃.

NMR Spectra of HA-b-ELP^{ox}-N_3

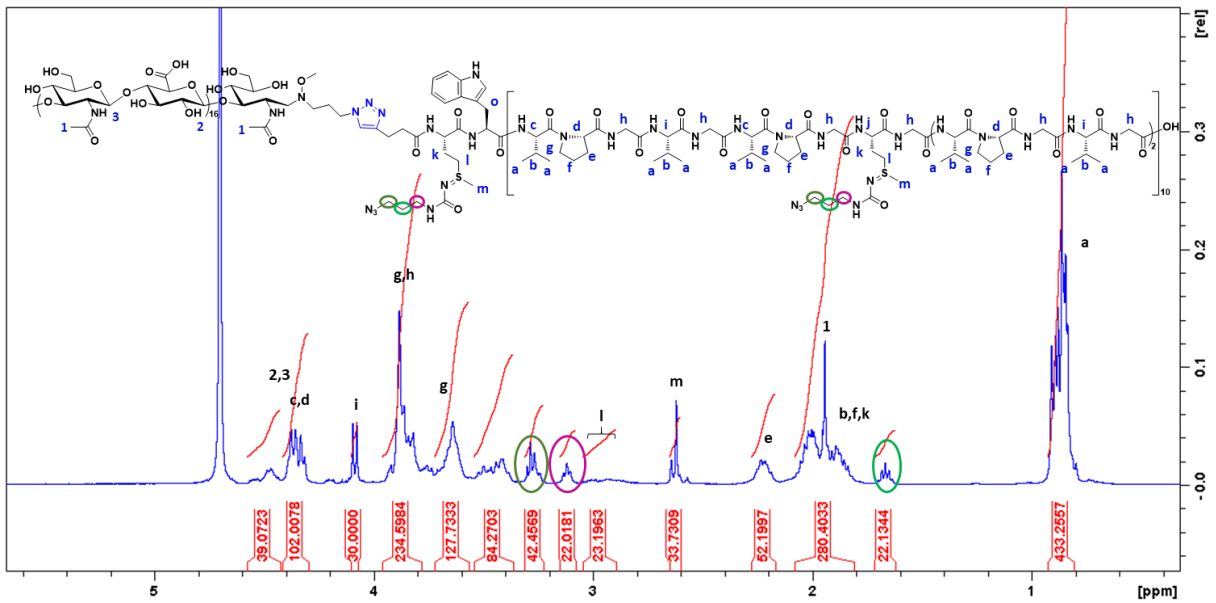

^{1}H NMR

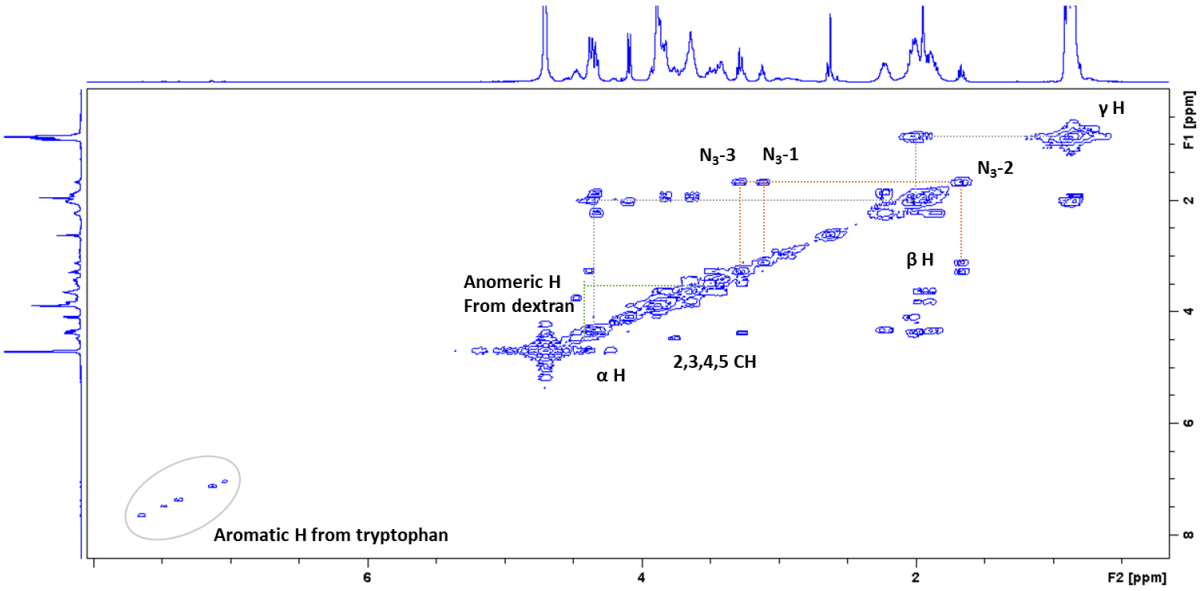

COSY

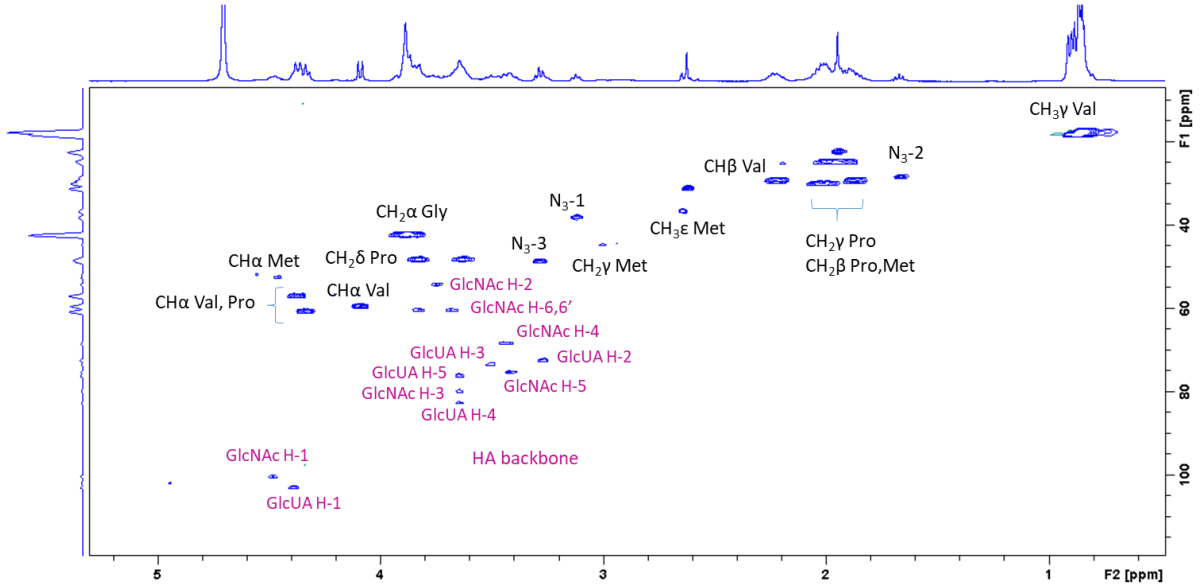

HSQC

Figure S4. ^{1}H, COSY, HSQC NMR spectra of HA-*b*-ELP^{ox}-N_3 in D_2O at 25 ℃.

NMR Spectra of HA-b-ELP^{ox}-Alkyne

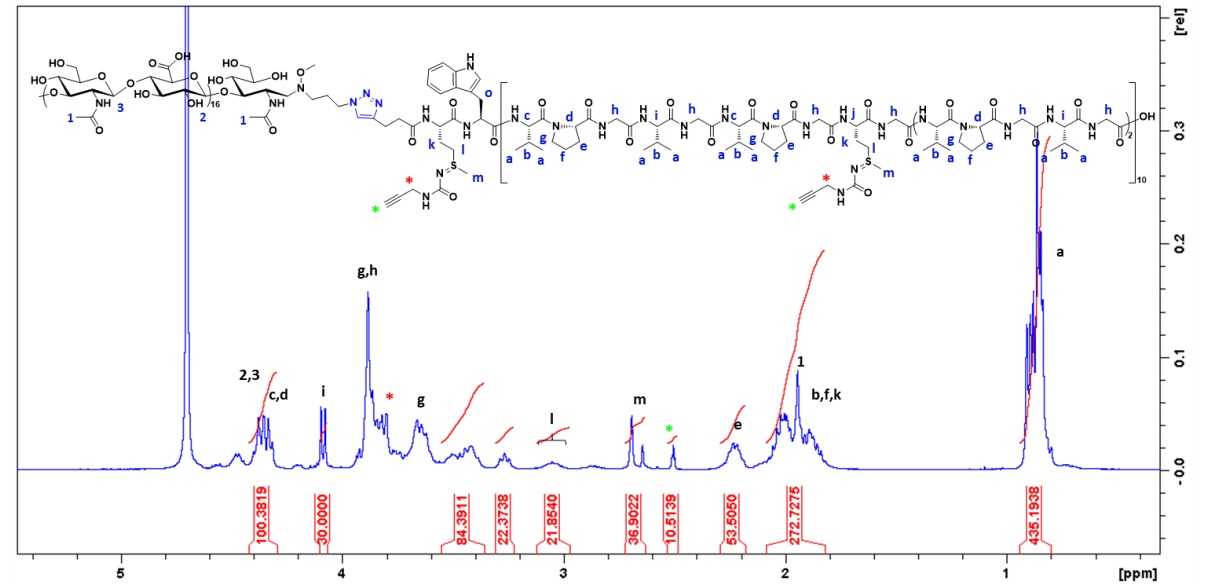

^{1}H NMR

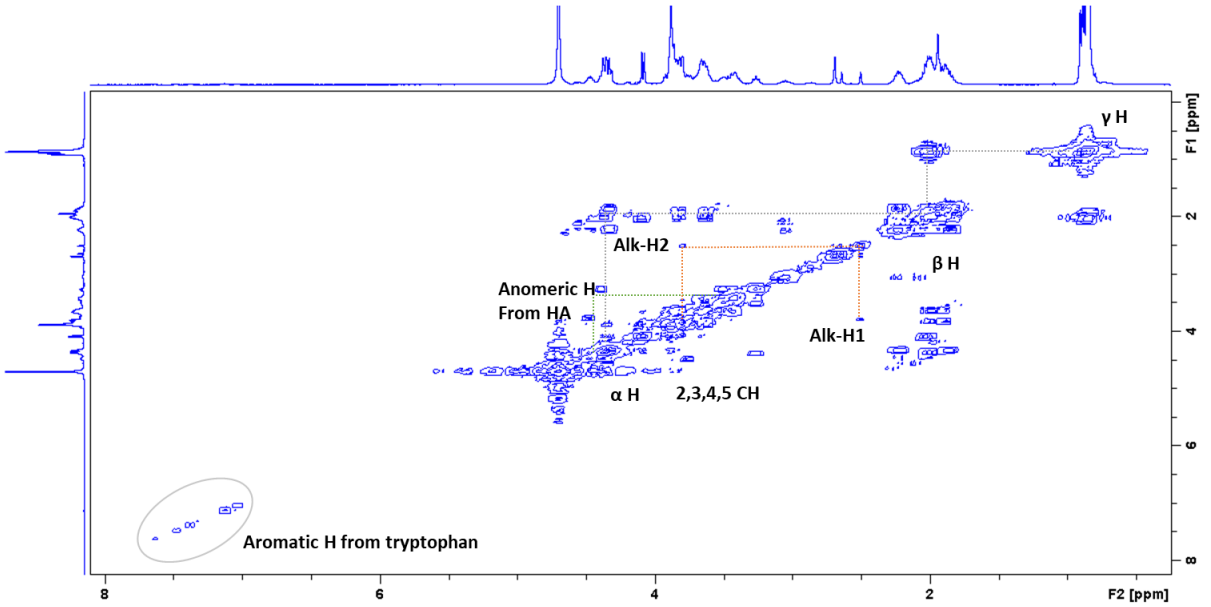

COSY

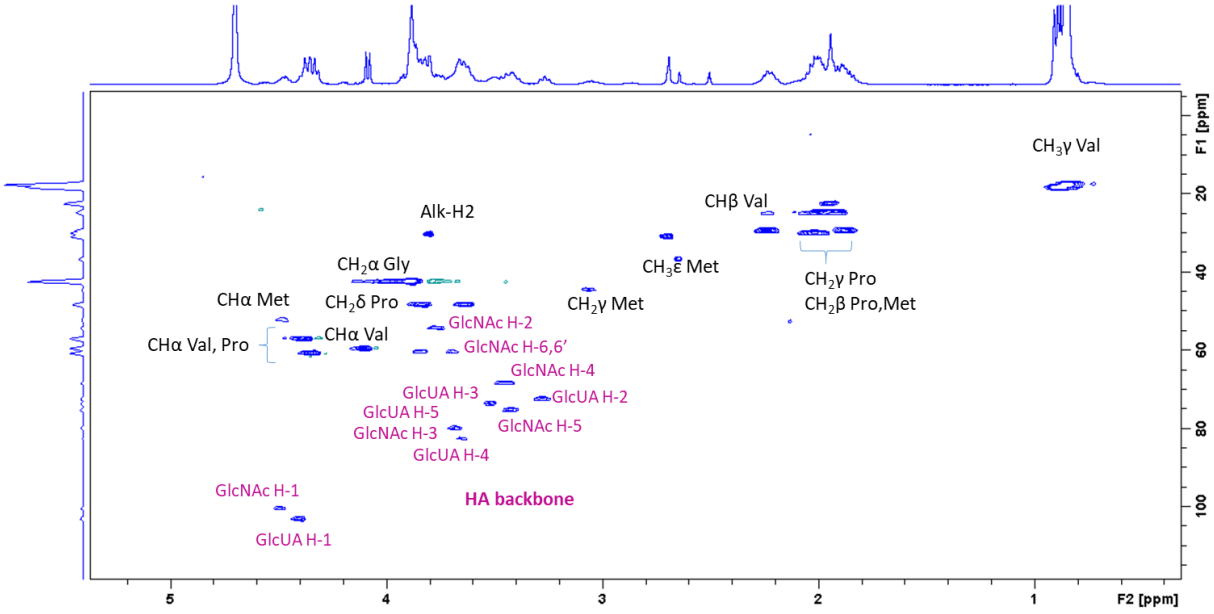

HSQC

Figure S5. ^{1}H, COSY and HSQC NMR spectra of HA-*b*-ELP^{ox}-Alk.

FTIR spectroscopy of polysaccharide-b-ELP^{ox}-N_3

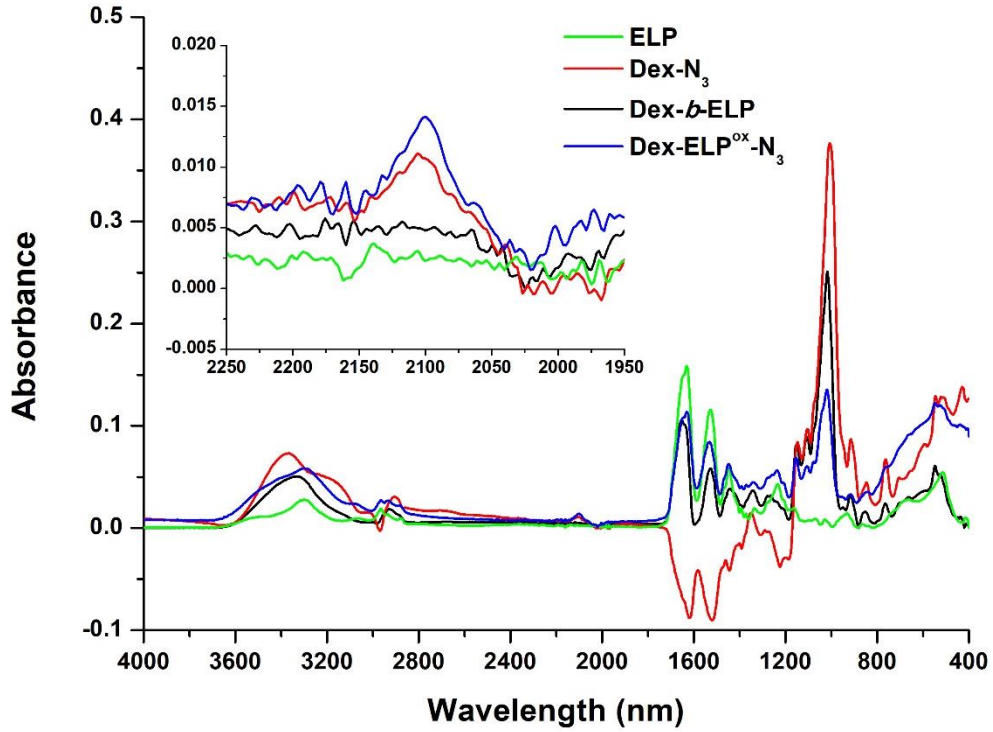

Figure S6. FTIR spectroscopy of Dex-*b*-ELP^{ox}-N_3

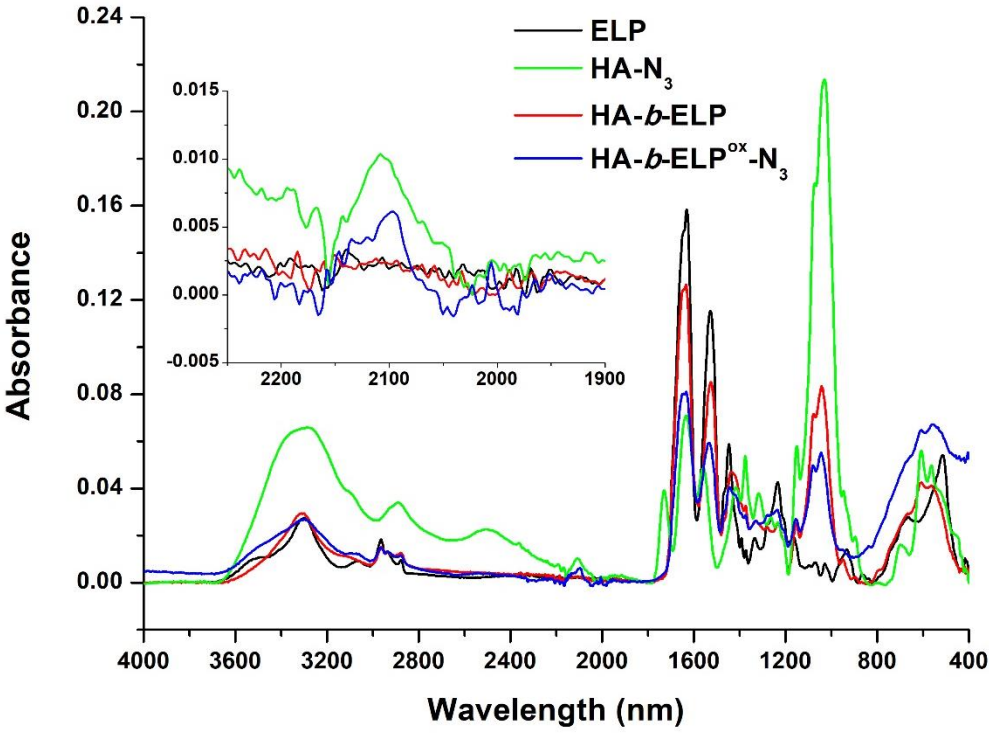

Figure S7. FTIR spectroscopy of HA-*b*-ELP^{ox}-N_3

Synthesis of Coumarin-grafted polysaccharide-b-ELP^{ox} bioconjugates

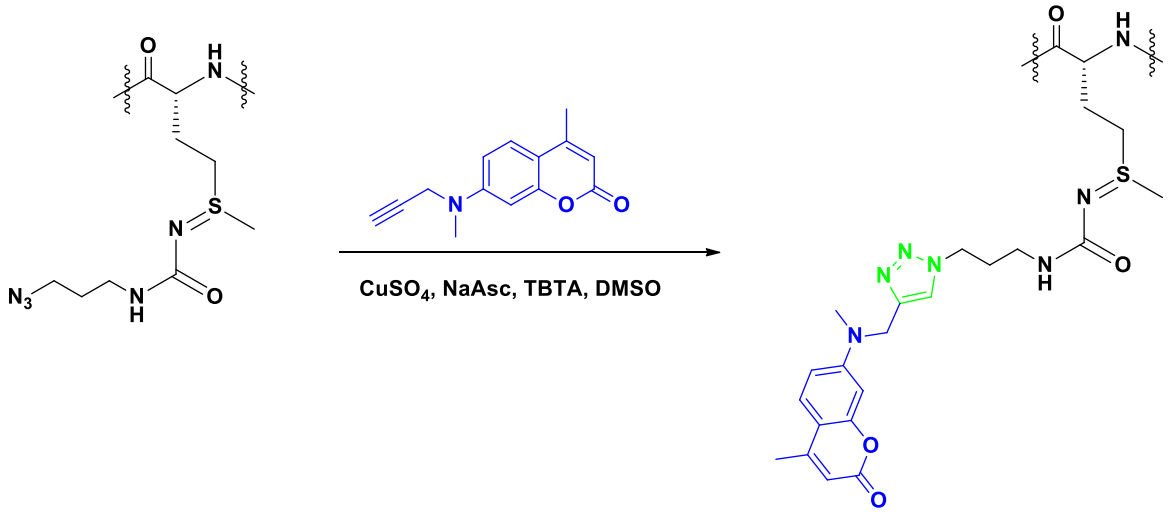

Precedure

Copper sulfate (2 mg, 8.3 μmol), sodium ascorbate (4 mg, 20 μmol) and TBTA (12 mg, 22.8 μmol) were added to a solution of Coumarine-alkyne (3 mg, 15 μmol) and Dex-*b*-ELP^{ox}-N_3 (10 mg, 0.38 μmol) in anhydrous DMSO (3 mL) under argon atmosphere and the reaction mixture was stirred at r.t for 3 days. It was then diluted with cold water (20 mL) and cooled in a refrigerator at 4 ℃ for 20 min. TBTA was precipitated and removed by centrifugation. Cuprisorb (120 mg) was added to the resulting solution and it was then incubated at r.t with shaking, for 18 h to remove the copper. The solution containing cuprisorb was centrifuged and the supernatant was purified by dialysis (dialysis bag 15 kDa) against pure water for 5 days (changing water 3 times per day), followed by lyophilization to obtain the product as a off-yellowe powder (8.2 mg, 76 % yield).

GENERAL CONCLUSION AND OUTLOOK

The natural properties of polysaccharides and stimuli-responsive feature of ELPs are attracting great attention for designing “bioactive” or “smart” polymeric nanocarriers. The combination of polysaccharides and ELPs into block copolymers may lead to materials with unique properties especially interesting for biomedical applications. The aim of this PhD project was thus to have a pioneer study of polysaccharide-*b*-ELP bioconjugates, including synthesis and characterizations, self-assembly study, and chemoselective post-modification and functionalization.

Firstly, a modular “end-to-end” approach was exploited to combine inert (Dex) and bioactive (Lam and HA) polysaccharides with a stimuli-responsive ELP-[V_3M_1-40] into well-defined block copolymers. Polysaccharides were successfully functionalized with an azide moiety at the reducing end using a bifunctional *N*-methoxyoxyamine linker. NHS-ester coupling chemistry was utilized to modify the *N*-terminal primary amine of ELP with an alkyne group. Thereafter, smart polysaccharide-*b*-ELP block copolymers were produced by CuAAC, and their thermal responsiveness was studied by turbidity measurements. Increasing temperature above the phase transition of ELP bioconjugates resulted in the formation of amphiphiles, which self-assembled into well-defined and stable nano-objects.

We then carried out a comprehensive structural analysis of a series of polysaccharide-*b*-ELP bioconjugates to understand the thermally-triggered self-assembly process of polysaccharide-*b*-ELP bioconjugates. Light scattering studies demonstrated a fully reversible self-assembly/disassembly process by controlling the temperature above/below the T_t. Below the T_t, polysaccharide-*b*-ELP chains behave as unimer with little aggregation. Although HA showed an attractive interaction with ELP, mixing HA-*b*-ELP with Dex-*b*-ELP or PEG-*b*-ELP presented independent nature. Above the T_t, ELP chains of polysaccharide-*b*-ELP bioconjugates hydrophobically collapsed, leading to structural evolution of polysaccharide-*b*-ELP from unimer to self-assembled nanostructure. Insufficient hydrophilicity of Lam-*b*-ELP led to aggregation. Mixing Dex-*b*-ELP with HA-*b*-ELP or PEG-*b*-ELP also showed similarly structural evolution from unimer to self-assembled spherical particles. However, mixture of HA/PEG-*b*-ELP indicated a more complex behavior, with a three regimes of particle distribution, which might due to the structural interaction of these two bioconjugates.

In order to further functionalize ELP backbones and introduce various functionalities and tune their properties, we explored a new route "ReACT" based on redox reactivity of methionine for chemoselectively modifying methionine-containing ELPs using oxaziridine-based reagents, providing an additional means for easily tuning the thermo-responsive properties of recombinant ELPs. This enlarges the variety of accessible ELP derivatives through sulfonium, thioether or sulfimide linkages. With commercially available reagents, reasonable reaction times and high efficiency, the epoxide-based route is highly favorable in acidic conditions. In terms of neutral conditions, ReACT demonstrated to be a viable tool for highly efficient post-modifications of ELPs. Altogether, the set of strategy opens up a whole range of new possibilities to functionalize ELPs with a large variety of molecules for the design of new ELP bioconjugates.

Accordingly, in the last chapter we explored the possibility of applying the ReACT strategy using oxaziridine derivatives on polysaccharide-*b*-ELP bioconjugates for chemoselective selective introduction of azido and alkyne groups. Two polysaccharide-*b*-ELP bioconjugates, Dex-*b*-ELP and HA-*b*-ELP, were successfully quantitatively functionalized (conversion > 95%) in relatively short reaction times (1 hour). The resulting polysaccharide-*b*-ELP bioconjugate derivatives were characterized by ^{1}H, COSY and HSQC NMR, and the effect of the different modifications on their thermal responsiveness measured. Consistently with our previous observations, the modification of Dex-*b*-ELP with oxaziridine derivaties drastically increased their T_t. A small organic molecule, namely coumarin, was subsequently grafted onto Dex-*b*-ELP^{ox}N$_3$ by copper-catalyzed azide-alkyne cycloaddition allowing for possible fluorescent detection of the bioconjugate or resulting self-assembled nanoparticles, as well as possible inter-chain cross-linking. Very importantly, oxaziridine-based chemistry on Dex-*b*-ELP and HA-*b*-ELP showed overall no significant structural influence on dextran and hyaluronan blocks, revealing the compatibility of the ReACT method with polysaccharide-containing bioconjuagtes.

To conclude, (i) four polysaccharide-*b*-ELP bioconjugates were successfully synthesized by click chemistry. Other bioactive polysaccharides, for example, galactan and fucoidan, are also interesting polysaccharide blocks for constructing polysaccharide-*b*-ELP block copolymers. (ii) These bioconjugates were well-characterized and their thermally-triggered self-assembly behavior were investigated by light scattering and neutron scattering. Regarding the self-assembly study of different ELP bioconjugates mixtures, additional experiments using

fluorescently labeled bioconjugates or electron microscopy experiments may provide a better understanding to the formation of individual micelles or mixed micelles. (iii) Post-modification of methionine on ELP and polysaccharide-*b*-ELP bioconjugates via ReACT was proved highly selective and efficient. Functional oxaziridine derivatives, for example, fluorescent or crosslinking-based derivatives, would be promising to develop as highly selective dye-attaching or crosslinking agents. Regarding the biological application, it would be interesting to firstly test the binding affinity of the stable polysaccharide-*b*-ELP nanoparticles, followed by investigation of controlling payload loading or release with a temperature trigger.

Titre : Synthèse et auto-assemblage de bioconjugués polysaccharide-*b*-polypeptide d'élastine

Résumé : L'association de polysaccharides naturels et de polypeptides recombinants de type élastine (ELP) dans des structures de copolymères à blocs doit permettre d'accéder à des matériaux possédant des propriétés d'auto-assemblage sous l'action de stimuli et potentiellement bioactifs. Nous avons réalisé et présentons ici la synthèse d'une série de bioconjugués polysaccharide-b-ELP, dans lesquels 4 polysaccharides hydrophiles différents ont été couplés à l'extrémité *N*-terminale de l'ELP par "chimie clic".Ces bioconjugués ont été caractérisés par RMN 1D et 2D, SEC et FTIR. Leur thermo-sensibilité et leur auto-assemblage induit par la température ont été étudiés par spectroscopie UV-Visible, DLS, SLS, SANS et AFM liquide à température contrôlée. Cette étude a démontré que les bioconjugués polysaccharide-*b*-ELP peuvent s'auto-assembler en milieu aqueux en nanoparticules bien définies au-dessus d'une température de transition spécifique et modulable (T_t) et se désassembler de façon réversible sous la T_t, ce qui les rend particulièrement prometteurs pour la conception de vecteurs de principes actifs à libération contrôlée. La fonctionnalisation chimiosélective des résidus méthionine du segment ELP par chimie de l'oxaziridine a également été exploitée pour moduler les propriétés des bioconjugués.

Mots clés: polysaccharide, polypeptide d'élastine, thermosensibilté, modification chimiosélective, auto-assemblage

---

Title: Synthesis and self-assembly of polysaccharide-*b*-elastin-like polypeptide bioconjugates

Abstract: The combination of natural polysaccharides and recombinant elastin-like polypeptides (ELPs) into block copolymers is expected to lead to materials with precise stimuli-responsive self-assembly properties and bioactivities. Herein, we report the synthesis of a series of polysaccharide-*b*-ELP bioconjugates, in which 4 different hydrophilic polysaccharides were coupled to the *N*-terminal end of an ELP *via* "click chemistry". The resulting bioconjugates were characterized by 1D and 2D NMR, SEC and FTIR. Their thermal sensitivity and temperature-triggered self-assembly in aqueous solution was investigated by UV-Vis spectrometry, DLS, SLS, SANS and temperature-controlled liquid AFM. This study demonstrated that polysaccharide-*b*-ELP bioconjugates can self-assemble into well-defined nanoparticles in aqueous condition above a specific and tunable transition temperature (T_t) and reversibly disassemble below the T_t, which make them particularly promising candidates for the design of controlled drug delivery nanocarriers. Chemoselective functionnalizations of the ELP segment at methionine residues using oxaziridine chemistry were additionally applied for further tuning of bioconjugates' properties.

Keywords: polysaccharide, elastin-like polypeptide, thermosensitivity, chemoselective modification, self-assembly

---

Laboratoire de Chimie des Polymères Organiques, UMR 5629
16 Avenue Pey-Berland, F-33607 PESSAC